Evaluation of a Step-Recovery Diode in a Broad-Band Frequency Multiplier.

Saul, Peter Henry.

P.H. SAUL

EVALUATION OF A STEP-RECOVERY DIODE IN A BROAD-BAND FREQUENCY MULTIPLIER

Ph.D. Thesis 1976

CONTENTS

CONTENTS OF APPENDIX

LIST OF ILLUSTRATIONS

In the Appendix

A6.2.2 to 6.2.12 Diode C-V plots
A6.3.1 to 6.3.3 Fourier Series
A6.3.4 The Half-wave rectifier a_n coefficients
A6.3.5 The Half-wave rectifier-predicted spectra
A6.3.6 to 6.3.10 Practical rectifier spectra

A6.5.2 $\frac{\text{The } \sin x}{x}$ curve

A6.5.4 Spectral Assessment at 23 MHz

A7.3.9
A7.3.10 Directional Coupler

LIST OF PHOTOGRAPHS (11 plates)

ACKNOWLEDGEMENTS

The author is indebted to Dr. B.L.J. Kulesza for his supervision, advice, consultation and encouragement throughout this project.

The help of other members of the Solid State Research Group at Durham is also gratefully acknowledged, especially Mr. J. Emmett, and the late Mr. J. Gregory.

Thanks are also extended to Professor D. A. Wright, head of the Department of Applied Physics and Electronics at the University of Durham, for placing the facilities of the department at the author's disposal, and to the U.K. Science Research Council for supporting the project.

ABSTRACT

In the first chapter, the history and principles of harmonic generators are reviewed. Some analyses presented by earlier authors are considered, including the Manley-Rowe equations.

The available types of nonlinear solid state devices are discussed in chapter two. The Manley-Rowe equations show that nonlinear reactive devices are better harmonic generators than nonlinear resistors. In particular, the operation of charge storage diodes (step-recovery diodes, or S.R.D.s) is described in detail.

Extending the work of chapter two, chapter three illustrates practical harmonic generating circuits. Outputs of 25 mW at 8.8GHz in an octupler and 400 mW at 4.68GHz in a tripler were achieved. The fundamental limits to the fractional bandwidth possible for an 'n' times multiplier was shown to be

$$\phi = \frac{2}{2n+1} \qquad \phi = \text{fractional bandwidth}$$

or $$\phi = \frac{2}{n+1}$$ if alternate harmonics are suppressed.

Much of the initial work was concentrated on hyperabrupt frequency multipliers. The theory of this class of devices is presented in chapter four. The basic elastance equation is

$$S(\upsilon) = S_{max} \cdot \left(\frac{\upsilon + \phi}{V_b + \phi} \right)$$

where υ = instantaneous voltage

V_b = reverse bias maximum

ϕ = forward bias potential

γ = nonlinearity factor.

It is shown that generation of the 'nth' harmonic requires a diode of nonlinearity

$$1 > \gamma > \left(\frac{n-1}{n}\right)$$

A fundamental new equation for the optimum operating conditions was derived i.e.

$$\underline{\tan(n\theta+\phi) = -n\tan\theta}$$

From this equation the optimum bias and power flow equations are derived. It is shown that the efficiency increases as γ approaches unity, but an optimum power handling condition occurs when

$$n = \frac{3}{2} \cdot \frac{1}{(1-\gamma)}$$

Hence, where γ can be manipulated in manufacture, the diode can be designed for the generation of a specific harmonic. Alternatively, tuning diodes can be designed for the best tuning range consistent with low harmonic generation.

When it became clear that hyperabrupt diodes would not be available for study, the step-recovery diode was selected as an alternative (Chapter five). The same optimum current equation

$$\tan(n\theta+\phi) = -n\tan\theta$$

was shown to apply, although the voltage series is different. The analysis derives the optimum operating conditions, and predicts the parameters

required for the design of a practical multiplier. The selection of a suitable diode is shown to depend on the recombination time, transit time, stored charge and permissible voltage swing of the diode.

In order to assess the practical diode parameters, measurements were made over a range of frequencies (chapter six). In addition, a comparison with low frequency measurements was made to confirm the mathematical model of the device operation. The most significant part of this chapter was the series of photographs of the operation of a diode over a range of input frequencies. The effects of recombination and transit time were demonstrated, a comparison technique for microwave measurements was established, and was used to determine the transit time of the diodes in use, i.e. t_p = 160 ps. for the Hewlett-Packard 5082-0386.

The development of a practical broadband frequency multiplier is the subject of chapter seven. It is shown that, in a balanced quintupler design, a bandwidth of 25% can be achieved, (theoretical maximum 33%) three times wider than the best previously reported figures. The techniques of filter design and construction are discussed. Photographs of individual filter components are shown. The whole multiplier was integrated into a single package, with no adjustable components included. It is believed that this is the first frequency multiplier to be designed along these lines, i.e. a single microwave integrated circuit, in which the realization of the components is accurate enough to allow correct operation without 'trimming'. The suppression of unwanted harmonic products was shown to be as good as many equivalent narrow band multipliers, due to the balanced arrangement, and the very high quality multi-element filters.

In the final chapter the work is reviewed and the conclusions drawn on the effects of this work in the future design of frequency multipliers.

An appendix is included in which the bulk of mathematical deviations is included, and some of the practical constructional aspects are described.

1. PRINCIPLES OF HARMONIC GENERATION

1.1 Introduction

This chapter is concerned with harmonic generation, in which power is fed to non-linear device at a frequency $f_o n$ and is delivered to a load at one or more frequencies which are integral multiples of f_o. The factor n has unity value for frequency multipliers, or small integral value to cover dividers and rational-fraction multipliers. A non-linear device is essential to the multiplying process; by the principle of superposition, the application of any number of frequencies to a linear time-variant device never results in additional beat or harmonic frequencies. If, however, the device is non-linear, it will generate sum, difference and multiples of the frequencies applied to it, and the sums and differences of the multiples. Although not necessary to the multiplication process, energy storing elements, (L and C) are usually required for frequency conversion and extraction. Since a non-linearity is necessary for any generation or mixing process, it follows that harmonic generation may be also regarded as the fundamental process underlying mixers. Applications for harmonic generators are found across the spectrum from very low to microwave frequencies. Telephony systems rely on a harmonic generator driven by a crystal-controlled master oscillator, which produces a group of integral-multiple frequencies with high stability. In radio systems, harmonic generators are used to prevent instability and are often used with a crystal source. Where reliable communication links are essential, it is usual to make both transmitter and receiver crystal controlled. The crystal oscillators feed multipliers up to the frequency in use. At microwave frequencies, signal noise and drift are important factors. Harmonics of a crystal-controlled

source are the most stable and noise free oscillations economically available. Similarly, when high powers and efficiencies are specified, as in space projects, oscillator/multiplier chains are often the best sources.

1.2 Non-linear Element as a Source of Harmonics

A periodic waveform may be represented by a Fourier series. Any device non-linearity can be expanded as a Taylor series. The solution of a particular problem partially rests in a sound correlation between the two series. A device achieves harmonic generation by means of its non-linear characteristic. A number of analyses have appeared which derive the efficiency of harmonic generators under various conditions. Two duality-related types of generator are distinguished, in one case, only selected currents are allowed, while harmonic voltages are unrestricted, and, in the other, restrictions are put on the voltages, while all harmonic currents flow through the device. In either case, it may be desirable, or necessary, to allow the presence of harmonic currents or voltages, respectively, at frequencies other than the fundamental and output; these are known as idlers. Penfield and Rafuse[66] have analysed the abrupt junction varactors extensively, showing that, for harmonics other than the second, idlers are essential. The general varactor analyses have been presented by Lesson and Weinreb[29] for the idlerless circuit and by Utsonomya and Yuan[31] for the circuit with idlers. In each case the approximation involved was that only a limited number of terms in the power-series expansion of the non-linearity were used. These were small signal analyses. Scanlan and Laybourn,[51] and

Markard and Yuan,[34] have introduced large signal analyses which required numerical methods. It will be shown here by the author that, by introducing a new class of restrictions, analytical solutions are possible for most frequency multiplier problems.

In both the current restricted and voltage restricted cases, it is usually found that the non-restricted parameter has a complex time-domain waveform, which, by Fourier's theorem contains many harmonics. A frequency domain analysis often leads to a better understanding of the problem and a closer correlation with the practical results.

There are many electronic and electro-mechanical non-linear devices available. The simplest is the switch which, ideally, has the perfect non-linearity. Much of the early practical work was on magnetic amplifiers, using the non-linearity of saturated chokes and transformers for parametric amplification and harmonic generation. Valves and transistors have been used as harmonic generators with gain in addition to frequency multiplication. More recently, however, the varactor and step-recovery diode have been used to produce the fastest pulses and highest frequencies yet available.

1.3 Linear Network Representation of a Non-linear Element

When dealing with non-linear capacitors it is usual to define the incremental capacitance, which is a derivative of charge with respect to voltage

$$C = \frac{dq}{dv}$$

The analogous definition of the incremental inductance is

$$L = \frac{d\phi}{di} \qquad \phi = \text{flux}$$

and resistance

$$R = \frac{dv}{di}$$

If the relation between the parameters is linear e.g.

$$q = c.\ v$$

but the coefficient c is a function of time, the resulting capacitance is said to be linear, but time-varying. Mathematically, there is a difference between circuits containing non-linear reactances and those containing time-varying linear reactances. In the latter case, the principle of superposition holds, and powerful analytical tools are available. Superposition fails for non-linear circuits, and the difficulty of analysis is increased; however, both circuits cause frequency mixing and are capable of transferring power from one frequency to another.

A form of equivalent circuit which does apply to non-linear elements is that due to Leeson and Weinreb. The non-linear device is replaced by harmonic generators and linear impedances which are dependent on drive level. In the linear circuit thus obtained, some of the linear network laws are obeyed, at a given drive level, and the small signal analysis can be applied. Kirchoff's laws must be satisfied at each instant of time. The conditions of reciprocity, however, do not, in general, apply to harmonic generators. The reciprocity theorem may be stated:-

The transfer impedance from branch m to branch n of a reciprocal network is identical to that from branch n to branch m.

This property is intrinsic with linear systems containing passive elements. Non-linear networks containing elements which display hysteresis or unilateral characteristics are not, in general, reciprocal.

1.4 Historical Background

The first known calculations of the reactions of currents on one another in a non-linear system were made by R.V.L. Hartley in 1916, although the non-linear properties of iron-cored transformers and induction machines were observed before the turn of the century. As a result of this early work, magnetic amplifiers, modulators and harmonic generators were developed, mainly for telephony. A comprehensive treatment by Peterson, Manley and Wrathall of the then widely used harmonic generator circuit utilising a non-linear coil, appeared in 1937. A number of workers successfully generated harmonics using vacuum tubes, led by Terman (1931, 1938), Everitt (1934) and Black and Scott (1938). The techniques used rapidly became standardized in the 'Class C amplifier' circuit which in transistor form still predominates at frequencies up to the microwave region today.

Rapid development of small 'crystal' rectifiers during 1942/46 period encouraged the use of these non-linear resistors in harmonic generating circuits. However, in 1956, Page showed analytically that the maximum efficiency obtainable, with non-linear resistors cannot exceed $1/n^2$, where n is the harmonic order. At about the same time, in the paper 'General Properties of Non linear elements' Manley and Rowe showed that non-linear reactive elements were potentially 100% efficient. With the work of Bakanowski, Cranna and Uhlir (1959) microwave generation by non-linear capacitance became a practical proposition. More recently, the step-recovery effect, a nuisance in early rectifiers, has been applied successfully to harmonic generators, and this process currently leads the field.

Low noise levels are a fundamental property of reactive devices,

and it has been observed that this characteristic is also inherent in some non-linear reactive devices. Non-linear resistors are usually more noisy in use than their reactive counterparts.

The stability of oscillators, particularly at high frequencies, is often a problem. The most stable oscillators available are crystal-controlled. It is possible to achieve good stability at higher frequencies by harmonic multiplication from a crystal oscillator, or by phase-locking a higher frequency oscillation to the crystal source.

1.5 The Manley-Rowe Equations

Manley and Rowe have derived a very general set of equations for power transfer in non-linear reactive elements. The relations apply to parametric amplifiers, harmonic generators and frequency up and down converters and can be used to predict the ultimate conversion gain.

The Manley Rowe power relations for any single-valued, non-linear, lossless reactance which is excited so that the current and voltage have frequency components of the form $(mf_1 + nf_2)$ where m and n are integers, are given by:-

$$\sum_{m=0}^{\infty} \sum_{n=-\infty}^{\infty} \frac{m P_{m,n}}{m f_1 + n f_2} = 0$$

$$\sum_{n=0}^{\infty} \sum_{m=-\infty}^{\infty} \frac{n P_{m,n}}{m f_1 + n f_2} = 0$$

where Pmn is the average power at the frequencies $\pm [mf_1 + nf_2]$. Since the reactance is considered lossless the sum of powers must be zero. Pantell has extended these equations to cover the non-linear resistance.

Following the work by Manley and Rowe, a number of analyses of reactance harmonic generators were produced. Two closely related small signal analyses are recognised; the 'parametric amplifier' type, where only the fundamental can switch the device, and the harmonic is considered as a small perturbation, and the Taylor series type, in which input and output are considered commensurate, but cause only small excursions of voltage.

Hyltin and Kotzebue have used the second technique in a series-type harmonic generator. The fundamental equations were:-

$$i = C(v) \cdot \frac{dv}{dt}$$

$$C(v) = C(v_1) + \left.\frac{dC}{dv}\right|_{v=v_1}$$

$$C(v_1) = C_0 \sum_{n=-\infty}^{\infty} \gamma_n e^{jn\omega t}$$

(γ_n is a non-linearity coefficient)

The optimum transducer gain was given as:-

$$g_t = \frac{\gamma_{n-1} - \gamma_{n+1}}{\gamma_{n-1}} \cdot \frac{\bar{\gamma}^2 \cdot Q_n^2}{\left[1 + \sqrt{1 + \bar{\gamma}^2 Q_n^2}\right]^2}$$

where $\bar{\gamma}$ = average value

$$Q_n = \frac{1}{n\omega C_0 R_s}$$

It may be seen that the capacitance is assumed to vary at the drive frequency only; computed Fourier coefficients are fed into the equation. Similar expressions under the 'Parametric Amplifier' approximations derive from the 1st and Nth terms only.

1.6 Large Signal Analysis

The first large signal analytical treatment of the reactance harmonic generator was published by Scanlan and Laybourn in 1965. Subsequent papers by the same authors covered most aspects of the linearised large signal theory, and are considered in Appendix 1. The type of relationship assumed between capacitance and voltage was:-

$$C(v) = \frac{C_o}{(1 - v/\phi)^{\gamma}} = \frac{dq}{dv} \qquad 1.6.1$$

This leads to the equation

$$v + V_L = V_o \left\{ 1 - \left(\frac{Q}{Q_R}\right)^m \right\} \qquad 1.6.2$$

$$m = \frac{1}{1-\gamma}$$

V_R and Q_R are respectively the maximum reverse voltage and charge, both negative in sign.

If either the charge or voltage at the varactor is constrained to a finite number of sinusoidal components, then, from 1.6.2 above, it is evident that the unrestricted component must be complex. As an example, if the charge is constrained to two harmonically related sinusoids,

$$Q = Q_B + Q_1 \cos \omega t + Q_n \cos (N\omega t + \phi)$$

then

$$\frac{v + V_R}{V_o} = 1 - \left(\frac{Q_B}{Q_R}\right)^m \left\{ \begin{matrix} a_o + a_1 \cos \omega t + a_2 \cos 2\omega t \text{----} \\ + b_1 \sin \omega t + b_2 \sin 2\omega t \text{----} \end{matrix} \right.$$

In general, all frequencies may be present.

We may write the Fourier series as

$$\frac{v + V_R}{V_o} = 1 + \left(\frac{Q_B}{Q_R}\right)^m \left\{ a_o + \sum_{n=1}^{\infty} (a_n \cos n\omega t + b_n \sin n\omega t) \right\}$$

where

$$a_n = -\frac{1}{\pi} \int_{-\pi}^{\pi} \left\{ 1 + q_1 \cos \omega t + q_n \cos (N\omega t + \phi) \right\}^m \cdot \cos n\omega t \cdot d(\omega t)$$

$$b_n = -\frac{1}{\pi} \int_{-\pi}^{\pi} \left\{ 1 + q_1 \cos \omega t + q_n \cos (N\omega t + \phi) \right\}^m \cdot \sin n\omega t \cdot d\omega t$$

In a general case every term of this series must be included. The addition of idlers further increases the complexity.

POWER

The power relations may be written for the multiplier in general terms.

Input power

$$= V_1 I_1$$

and

Output power

$$= V_n I_n$$

When a solution for the V_n is available, the equations may be made specific.

In the simple case where all the loss in the multiplier may be represented by a single, fixed series loss resistance, the power dissipated may be shown to be

$$(I^2 + I_n^2) \times Rs$$

and hence

$$V_1 I_1 = V_n I_n + (I_1^2 + I_n^2) \times Rs.$$

1.7 Efficiency of Energy Transfer

The calculation of efficiency in harmonic generators may be made under various constraints. The available power, the input current, output power, dissipation, or reverse voltage swing may be specified. Because the generator is essentially non-linear, the specifications are unlikely to be equivalent. The maximum efficiency is different under each constraint, although the variation may be small; a major theme of the following chapters will be the derivation of the conditions for optimum operation.

The subject of efficiency is concerned mainly with losses in the circuit. Losses can arise from two main sources; resistive losses in the

Fig. 1.7.1. Varactor Equivalent cct.

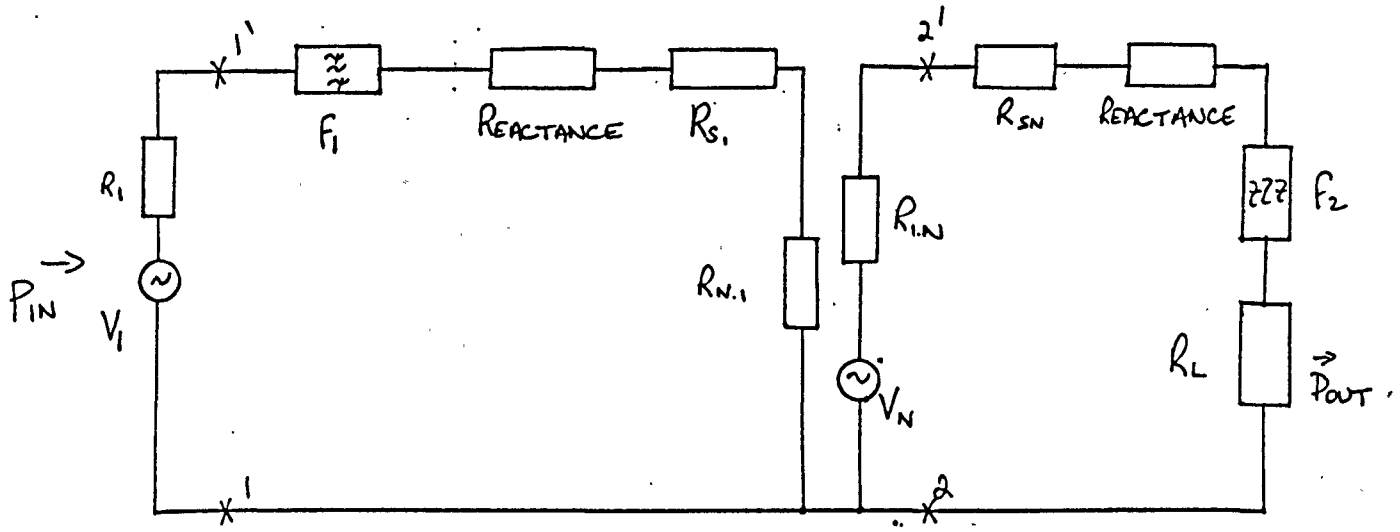

R_1 = Source Resistance

R_{S1} = Filter and Varactor loss - input

R_{SN} = " " " " output

R_{N1} = Equivalent load in input cct.

R_{IN} = " Resistance of generator V_N

P_{IN} = Power in at 1-1'

P_1 = Power transferred at 2-2'

P_{OUT} = Power in Load.

non-linear element and associated filters, and losses in the source, load and idlers (if any) at unwanted frequencies. The non-ideal element losses usually predominate in a well-constructed system. The equivalent circuit of fig. (1.7.1) applies; the series case is derived from the dual analysis. The parameters $R_{N.1}$, $R_{1.N}$, and V_N (and hence R_1 and R_N if these are matched) are strongly drive dependent. The loss resistance of the varactor is often non-linear also, so that general solutions are not readily available. However, at a particular drive level, we may write the circuit relations

$$\frac{P_{IN}}{P_I} = 1 + \frac{R_{S.1}}{R_{N.1}}$$

and

$$\frac{P_I}{P_{OUT}} = 1 + \frac{R_{S.N}}{R_L}$$

$$\therefore \quad \frac{P_{IN}}{P_{OUT}} = \left\{1 + \frac{R_{S.1}}{R_{N.1}}\right\} \cdot \left\{1 + \frac{R_{S.N}}{R_L}\right\}$$

When the maximum power transfer conditions are imposed.

$$R_1 = R_{S.2} + R_{N.1}$$

$$R_L = R_{1.N} + R_{s.N}$$

The efficiency, η, is usually expressed as the ratio $\left\{\frac{P_{out}}{P_{in}}\right\}$, and is quoted as a decimal or a percentage.

It is often necessary to work at the maximum efficiency obtainable both to conserve power and to limit device dissipation.

1.8 Conclusions

This chapter has dealt with some of the principles and history of harmonic generation, and has tried to show the importance of harmonic generators in general, and varactor devices in particular at microwave frequencies. Mention has been made of the literature available on the subject, with reference to analyses existing of varactor multipliers. The following chapters are intended to cover, analytically and experimentally, the harmonic generation problem in more specific terms.

Many attempts have been made to define 'ideal' non-linearities for harmonic generators. Without defining a device, it is possible to deduce from the Fourier waveforms (in tables) the best harmonic generation pattern. Theoretical and practical studies of available devices may be compared with the mathematical optimum. In the microwave case, it may be shown that the step-recovery diode is the best harmonic generator presently available.

2. NON-LINEAR SOLID STATE DEVICES

2.1 Device Classification.

2.1 This chapter is intended as a review of the physics and functional properties of some nonlinear devices.

The technology of all the devices, although well documented, has been developed primarily from an empirical approach. With the advent of planar diffusion technology, in silicon, germanium and gallium arsenide, many new devices have appeared. An approximate classification was introduced grouping together devices with similar properties, although some devices may well belong to two classes, or may not clearly belong to any. Non-linear resistors are discussed in para. 2.2. This group contains point-contact, metal-semiconductor, and backward diode rectifiers. The p.i.n. structure, in 'plasma diode' form is also included. Negative resistance devices and the tunnel, Gunn and Impatt (Impact Ionisation and transit time) effects are considered in para. 2.3. The group comprising non-linear capacitors has been split into conventional variable capacitance devices and step-recovery diodes, and is the subject of para. 2.4.

Any classification scheme must rest on the primary microwave characteristics of the devices considered; in some cases a device may enter a different class when the operating conditions are changed.

All the main semiconductor materials (Si, Ge, GaAs) have been used at microwave frequencies. Silicon has technological advantages, and is likely to continue to predominate. The theoretical advantages of Ge, and particularly of Ga As are offset by the more complex and costly

technology, except for those devices which rely on the particular band structure. The continued development of the technology is likely to bring in new devices, reduce prices and improve device specifications.

2.2 Resistive devices and applications

The point contact diode has been of great importance in the microwave field. The main advantage is the low capacitance compared with conventional junction devices. The rectifying contact is easily made and has a low turn-on voltage. The junction is usually a miniature metal-semiconductor type, which departs from ideality due to the forming processes.

Recently, metal-semiconductor (Schottky-barrier, or hot-carrier) diodes have been made by an evaporation process, which leads to more predictable and useful parameters. The theory is well documented; only a brief description is necessary.

The hot-carrier diode is a metal-semiconductor rectifying (non-ohmic) contact. When the metal and semiconductor are brought together, equilibrium is established between the materials, and it can be shown that the Fermi levels become coincident. At its maximum height, the barrier seen by the carriers is given by

$$\psi_{ms} = \psi_m - \chi - \Delta$$

where

ψ_{ms} = barrier height (eV)

ψ_m = Fermi level energy in metal

χ = " " " " semiconductor

Δ = Correction for surface states

The maximum width of the barrier is that of the depletion layer, usually of the order of thousands of angstroms. 'Hot-carrier' refers to

the high energy electrons injected into the metal from the semiconductor; the conduction is a majority carrier effect.

Practical hot-carrier diodes have a low turn-on voltage and a characteristically low forward resistance. A great deal of design effort has gone into producing diodes with low fringing and overlay capacitances and minimal lead inductance. Recently, gallium arsenide has begun to take over from silicon in critical applications; the more mature silicon technology is now moving into the volume market.

As detectors, tunnel diodes with low, or non-existent, peak currents (often referred to as backward diodes) have significant advantages over conventional types. The I-V characteristics have a strong curvature in the zero bias region, especially at low currents. Detection or mixing in the zero bias state ensures a low level of shot and I/F noise.

Recently, many forms of p.i.n. type of diode structure have been fabfabricated. These devices can operate as varactors, impatts, trapatts, variable resistances or modulators; design optimization differs in each case. For example, the p.i.n. structure designed for use as a variable microwave resistance is usually a poor rectifier at frequencies above a few megahertz. Under reverse bias, the diode has a high impedance at microwave frequencies; a forward current reduces the impedance to a low value, hence the device can be used as an electronically controlled microwave switch, with a response time, which depends on the diode and is determined by its construction, of the order of microseconds or less. In this form the diode has applications as a variable attenuator or amplitude or pulse modulator.

Fig. 2.2.1

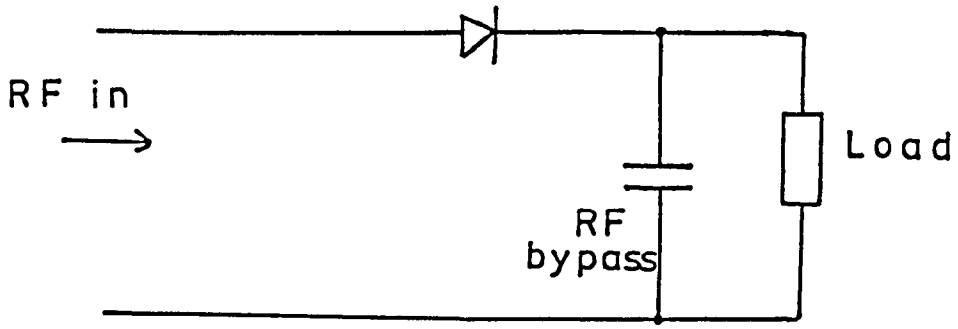

Simple detector

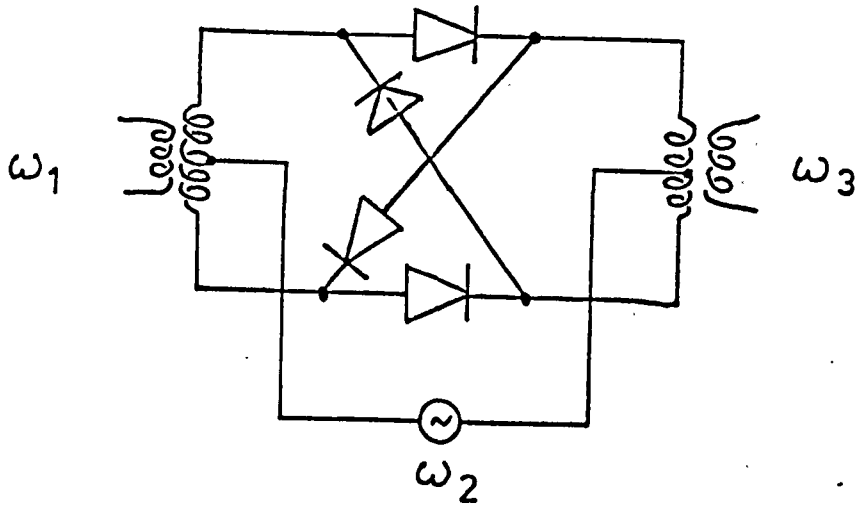

Modulator

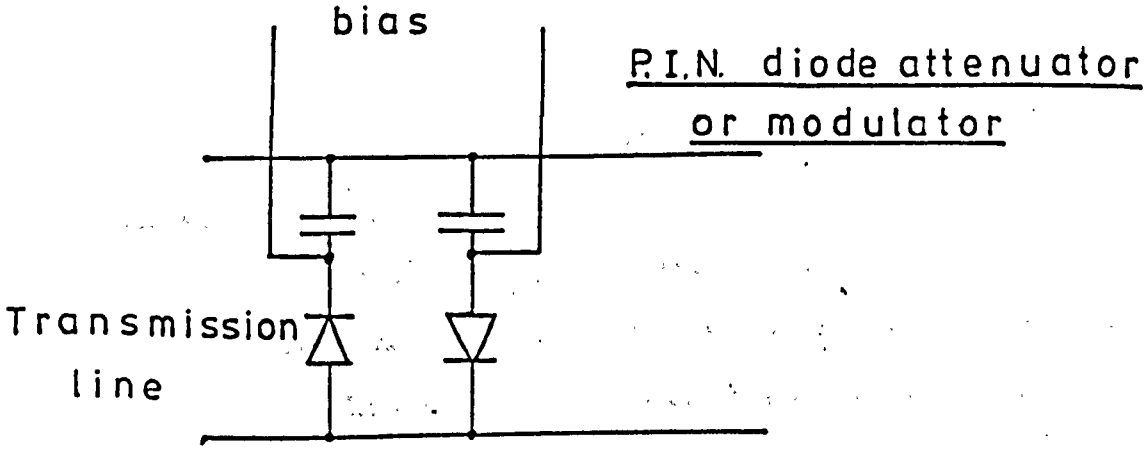

The varistors discussed are used primarily in modulator, detector, or mixer circuits, or in some instances as variable attenuators. Typical circuits are shown in fig. 2.2.1. The generation of unwanted harmonics is inherent. These can very often be minimised by employing filtering methods.

Point-contact diodes were used before the advent of varactors as frequency multipliers. It has been shown by Page that the efficiency can never exceed $1/n^2$ (n is the harmonic number). The circuit equations have been analysed by Page, Pantell and Belevitch (see Chapter 6).

Recently, however, possible fundamental limitations on varactor performance at high frequencies have been suggested, which could have serious effects above 100 GHz (Brand). The limitations are caused by the physical requirements of the semiconductor processing, in particular in the photographic techniques. Consequently, miniaturised Schottky or point contact diodes are likely to remain in the lead for the extreme frequency ranges, although Gunn and Impatt devices have recently moved into the millimetre wave field.

2.3 Negative resistance devices and applications

Negative resistance devices available at present include tunnel diodes, impatts, trappatts (trapped plasma avalanche transit time) Gunn and Limited space charge (LSA) devices. A summary of the properties of each will be given.

A tunnel diode is a p.n. junction device with extremely heavy doping on both sides of the junction, and a very abrupt transistion from p to n type. In the appropriate bias range, electrons can

quantum-mechanically tunnel through the potential energy barrier. With the energy band structure, the tunnelling results in a negative resistance region over a part of the forward bias characteristic. The tunnelling phenomenon, a majority carrier effect, is very fast, and useful devices can be constructed well into the millimeter-wave region. The negative resistance is used in simple low noise mixers, amplifiers and oscillators. The chief disadvantage of the diode is the small power handling capability; the negative resistance region is only a few hundred mv. wide, and the peak current about 100 mA max. per diode.

In 1958 Read predicted the existence of microwave oscillations in diodes of certain structures under breakdown conditions. Although the original theory called for p.n.i.p. or n.p.i.p. fabrication, Read (or Impatt) type oscillations may be observed in many diodes. It was shown that if a high field existed in a small region of the diode, avalanche multiplication of carriers would occur. The carriers then drifted from the avalanche region to the electrodes. When the applied field and the drift time were appropriate the device presented a negative resistance, and sustained oscillations occurred.

Impatt diodes may be used for amplification; they are suitable for power amplification, but in general, the noise levels are prohibitive for receiver applications.

The trapped plasma avalanche transit time diode (trapatt) a development of the impatt, was introduced by Johnston et al in 1968. They found that high efficiency oscillations occurred at half the predicted Impatt frequency; the explanation postulated was trapping of the plasma avalanche in the drift region by the subharmonic field. The trapatt is still largely experimental.

The devices considered up to this point have been related to non-ohmic contacts or junctions in semiconductor materials. In contrast, Gunn discovered in 1963 that microwave oscillations could be produced in a wafer of 'n' type GaAs with ohmic contacts. This device exhibits a lower conductance at high electric fields than it does at low fields, and, in the intermediate zone, a negative differential conductance. When biased into this stage, and in the presence of a suitable L-C circuit, cyclic high field domain formation occurs and oscillations result. An alternative mode, the limited space-charge accumulation mode (LSA) permits higher power, as it is not transit-time limited as is the Gunn mode. Consequently, the field interaction distance can be longer, the capacitance lower, and the heat-sinking problem alleviated. The mode may be compared to the trappatt, in terms of interaction space, and, like the other devices, mentioned above, it is largely experimental at present.

The tunnel diode has been used in simple circulator-coupled amplifiers as fig (2.3.1) Separation of the input and output parts is usually a desirable feature. Oscillators need only a bias supply and a frequency determining network; it is often difficult to prevent the devices oscillating under D.C. testing conditions.

Impatts are currently used in small radar systems especially where high pulse power and small size are required. High Q cavities, for noise bandwidth reduction, are often made from silver-plated brass or copper. The lower noise Gunn diodes can be operated in stripline conditions with acceptable noise performance and are currently used in small Doppler radars, mainly C.W., in such applications as spacecraft docking, tanker berthing and intruder alarms.

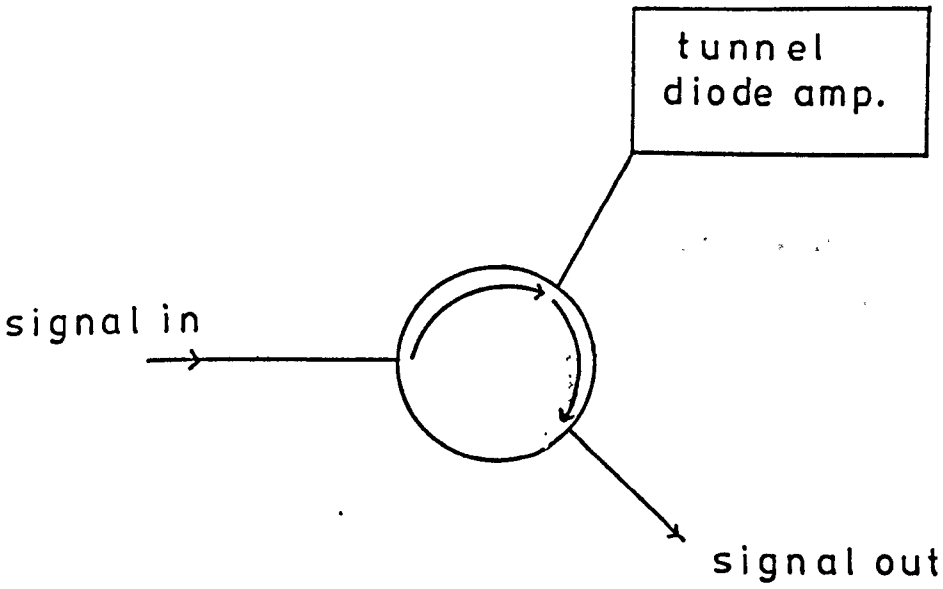

Fig. 23.1 Circulator coupled Amplifier

In the context of the work in hand, the negative resistance devices have not been considered. Use of a negative resistance in conjunction with a varactor multiplier has been reported. (Isobe,[19] Furukawa[13,14]). It is possible that such a device might be capable of slightly greater power handling than the negative resistance alone, and this could lead to highly efficient harmonic generators; however, the limitations of the devices currently available preclude their use at present. The negative resistance region is very narrow and occurs at a low forward voltage, which is not suitable for currently available varactors.

2.4 Capacitance devices and applications

This section deals with the devices usually referred to as varactors, varicaps or voltage variable capacitors. Charge storage devices are considered separately.

The varactor diode is a semiconductor device which may be used as a voltage controlled reactance element. Circuits are available for electronic tuning, modulators, harmonic generators and parametric amplifiers. The first usable high frequency varactors were produced by Bakanowski, Cranna and Uhlir[1] (1959). The capacitance of a junction as a function of depletion layer width may be approximated to:-

$$C = \frac{A}{w(V)}$$

where $w(V)$ is the width of the depletion layer, and is voltage dependant.

$$w = Wo \left(1 - \frac{V}{\phi}\right)^{\gamma}$$

For an abrupt junction

$$\gamma = \tfrac{1}{2}.$$

Most varactors lie between this and the graded junction, where

$$\gamma = 1/3$$

Later work will show the theoretical advantages of γ's between 0.5 and 1.0.

The diode is constructed, usually by epitaxy/diffusion in silicon or gallium arsenide. If the heat dissipation is likely to be high the chip is bonded into an encapsulation which must have acceptable thermal properties in conjunction with low parasitics. Doping profiles depend on the applications. Provided the diode package is small compared with the wavelength, the elements may be considered lumped.

In an attempt to define the device quality, a number of figures of merit were introduced by research workers and manufacturers.

1. Cutoff frequency at a specified bias, usually 6V

$$f_{cv} = \frac{1}{2\pi R_s C_{jv}}$$

2. Quality factor at specified bias and frequency

$$Q_v = f_{cv}/f$$

3. Dynamic cut-off frequency

$$f_c = \left(\frac{1}{C_{jb}} - \frac{1}{C_{jf}}\right) \Big/ 2\pi R_s .$$

C_{jb} @ breakdown
C_{jf} @ fwd. cond.

4. Dynamic Quality factor Q

Defined as $Q = Si/WR_s$

where Si is the first component of the Fourier series of time-dependent elastance.

The latter two figures of merit take into account part of the non-linearity of the device. A further figure-of-merit usually applied to parametric amplifier diodes is $\{\gamma . Q_v\}$. Hyltin and Kotzebue have pointed out the relevance in assessing diodes of the device nonlinearity factor γ.

Recently, it has been shown that almost any doping profile can be achieved, over a restricted range (Nishizawa). With no limit to the value of γ, a number of useful devices may be constructed. Capacitance ratios of 100:1 are possible, of particular use as tuning diodes for wide ranges. Some of the advantages of hyperabrupt ($\gamma > .5$) diodes in frequency multipliers and dividers have been pointed out (Kulesza, McConnell). It is thus necessary to define, for a particular varactor, the equivalent circuit (when in use), the quality factor, and the degree of non-linearity.

The Manley-Rowe equations predict the useful frequency, power and harmonic ranges and high conversion gains available from parametric devices. Varactor diodes are often used as up-converters (modulators); instability conditions indicate that down conversion is less useful. Small signal lower sideband up-conversion is a negative resistance effect; the operation is very similar to non-degenerate parametric amplification, with the advantage that for operation at frequencies below 1 GHz the up-converter is more stable.

Large signal up-converters are used as modulators. Usually, the lower frequency input is FM and the microwave signal is a carrier; reversal of the roles, or carrier-carrier operation may be used in frequency shifting operations.

A great deal of work has been done on parametric amplifiers, in industry, so that they have become a standard product. The desirable features which govern the choice of varactor for parametric amplifiers are:-

1. High dynamic quality factor
2. High self-resonant frequency
3. Large non-linearity factor, compatible with (1)
4. Stable characteristics over the full operating ranges of signal and pump source and, temperature.

Harmonic generators using varactor diodes have become a practical source of microwaves in the medium power range. The noise levels are inherently low, and the C.W. output power is comparable to other solid state oscillators. Frequently, the overall system efficiency is better than that of an alternative system.

The elastance equation

$$\frac{S}{S_{max}} = \left(\frac{\phi - v}{\phi - V_b}\right)$$

is a good approximation in the reverse direction. Alternatively, forward bias may be allowed, so that charge storage and step-recovery take place; this is the usual mode of operation. Typical circuits are shown in fig. 2.4.1. Idlers are commonly included to improve efficiency, even in step-recovery multipliers where they are not theoretically necessary, because it is not yet possible to produce theoretically perfect step recovery diodes.

Penfield and Refuse have shown that the abrupt junction requires idlers to function as a multiplier for harmonics higher than the second. Work on hyperabrupt diodes (Kannam, Leonard, Saito, Change et al) has been reported, and theoretical considerations (Chapter 5) show that this class of diodes may have several advantages over the conventional types. As yet, practical work in this area has not been reported.

2.5 Charge Storage Devices

Charge storage capacitance is produced by the injection of minority carriers during the forward-bias excursion of the varactor drive voltage, and the subsequent withdrawal of this charge during the first part of the reverse bias cycle. The effective capacitance change may be very large, i.e. the device may have a high dynamic Q.

Fig. 2.4.1

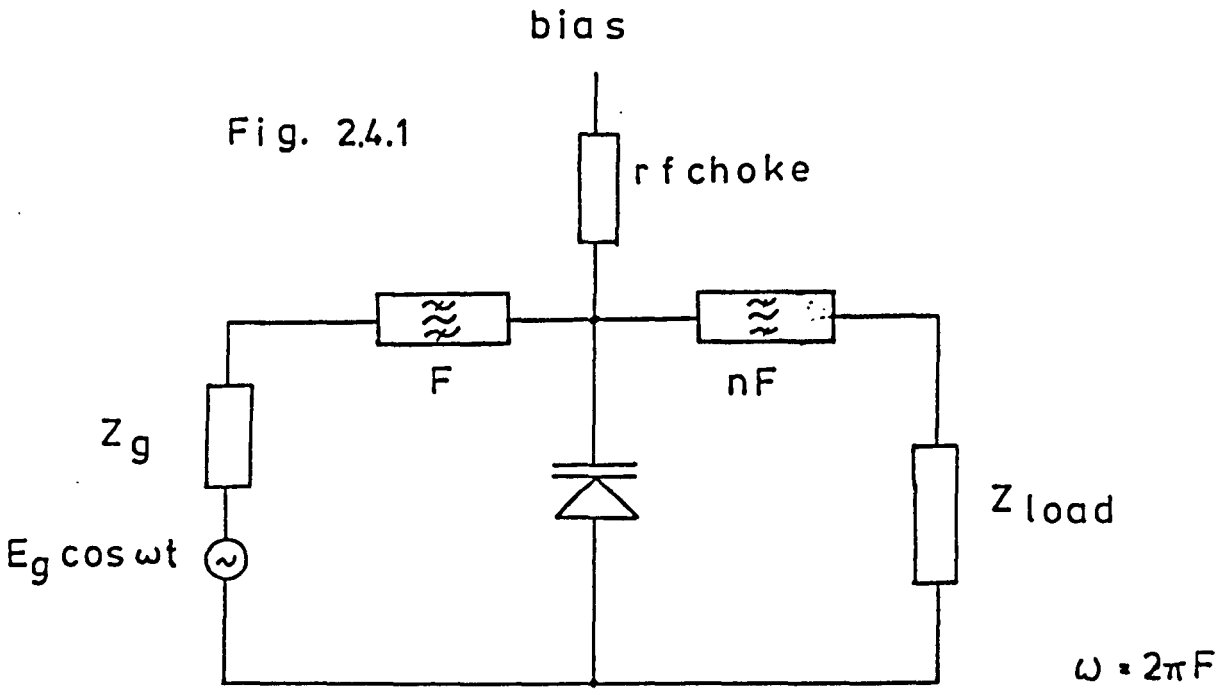

Current mode Multiplier

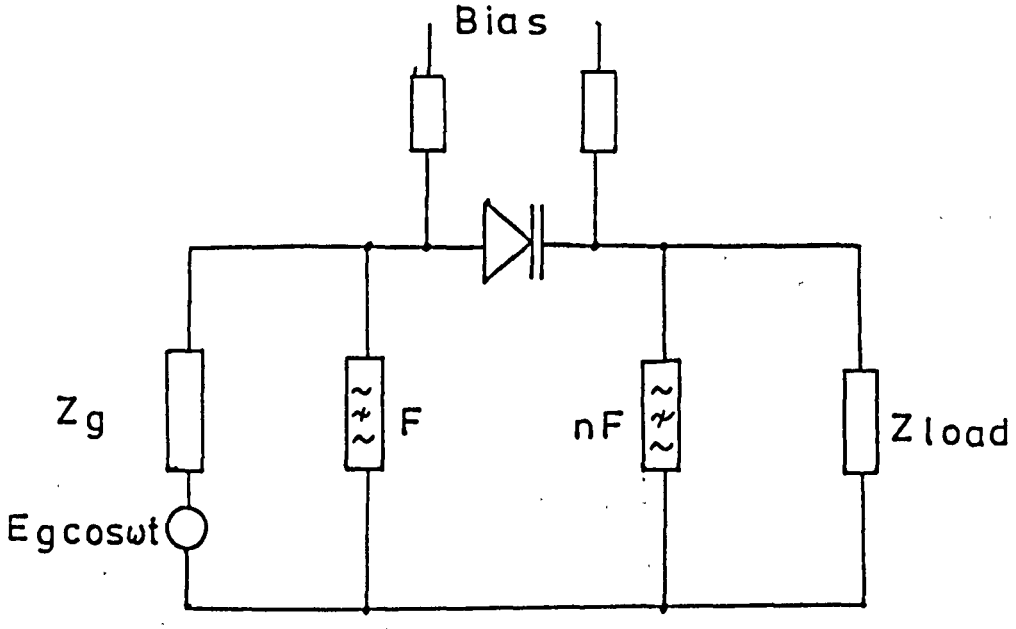

Voltage mode Multiplier

The charge storage effect is a dynamic property. Analyses performed in terms of d.c. parameters of non-linear capacitance or resistance are not valid; fully dynamic solutions are required. It is possible to analyse the charge storage diode as either a switching capacitance (Burckhardt et al) or as a switched R-C combination (Bozic and Stinchcombe). An exponential model of the capacitance variation, similar to that of Jungmeister and Schmidt has shown good correlation with the experimental results obtained by the author. One form of charge storage device, the step-recovery diode, has led to the fabrication of high-order, high efficiency frequency multipliers at microwave frequencies; at present most production quantity microwave solid state sources are based on step-recovery multipliers.

Charge storage effect in semiconductor rectifiers was observed in the earliest junction devices (Schottky) and as it led to the loss of rectification efficiency, attempts were made to eliminate it (Steele). Mains frequency rectifiers today are free from charge storage.

In 1959, Leenov and Uhlir discussed harmonic generation using the concept of an ideal non-linear capacitor. Boff produced the step-recovery effect empirically in 1959, and, in 1960, put forward a theoretical basis. Advances in silicon technology, coupled with theoretical considerations or the fast transient phenomena have produced a silicon p-i-n structure for the modern SRD.

The requirements for a charge-storage capacitance are that minority carrier injection into the junction region is possible, and that most of the injected charge is recoverable. Carrier recombination or drift from the junction region is detrimental to step-recovery action. The p-i-n structure has evolved to prevent carrier drift by large intrinsic fields, and it is usual to operate the device in a region where recombination is small.

The effect of recombination can be calculated from the continuity equation.

$$\frac{dQ}{dt} = I - \frac{Q}{\tau_R}$$

τ_R - Effective minority lifetime.

Q - Stored charge.

The short lifetimes available in GaAs normally preclude its use as an SRD (Moll, Hamilton).

The main time constant associated with the step-recovery diode is the transition time t_t. This is the time taken for the carriers to be extracted from the junction. Intuitively, the storage of minority carriers at or near the metallurgical junction shortens the transition time; this is enhanced in the p-i-n structure. Carriers are stored in the i-layer, confined by potential barriers at the p+-i and i-n+ junction. Practical diodes do allow some charge storage outside the i-region; the ideal step junctions are not possible with the present technology.

The diode cycle may be described as follows. During the forward bias period, the i-layer is flooded with carriers, electrons and holes, evenly distributed. The voltage passes the forward peak and moves into the reverse region. Negative current flow extracts charge although the diode incremental resistance is low, so the voltage drop is small. As the mobile carrier extraction proceeds uncompensated mobile charges at the boundaries show a voltage drop. The centre of the i-region, with a relatively high conductivity, shows little voltage drop. The edges, depleted of mobile charge, conduct only space-charge-limited current.

The effect of the reverse current is to produce a voltage such that the space charge barriers are overcome, and the current is maintained in the circuit. As the centre region loses charge, the space charge layers widen and the voltage increases. When all the mobile carriers are

depleted the transition to the reverse bias state occurs; the transition time is limited by

$$t = \pi\sqrt{L.C_{Vr}}$$

L - Circuit total L

C_{Vr} - Reverse bias C

Clearly, C_{VR} should be replaced by a variable quantity to develop full mathematical rigour for the whole transition this will be treated in a later chapter. A voltage spike is induced in an external resistive load; reactive loads may modify the output waveform. A good diode punches through at a low reverse voltage i.e. the mobile carriers are entirely depleted, and the capacitance variation is that of the depletion layer. In a diode with a p-i-n structure, this is substantially constant. The reverse capacitance variation can be used to get some idea of the doping profile. (Coerver).

Depletion of the mobile charge layer constitutes a turn-off transient in the form of a voltage ramp before the main spike. Similarly, a turn-on transient occurs at the end of the spike, as the reverse capacitance is discharged in preparation for forward charging in the next cycle.

However, the turn-on transient is usually much faster than the turn-off as the capacitance involved is at least an order of magnitude smaller.

Figure (2.5.1) illustrates the (idealized) current and voltage waveform expected in the diode. The origin of the turn-off ramp is traced to the finite transition time. The turn-on ramp is related to the reverse-bias capacitance charging and discharging. In a later section, a mathematical model will be approximated to the practical case, to predict the Fourier spectrum. Practical time-domain waveforms are shown for low frequencies and frequency domain plots at high frequencies in chapter 6.

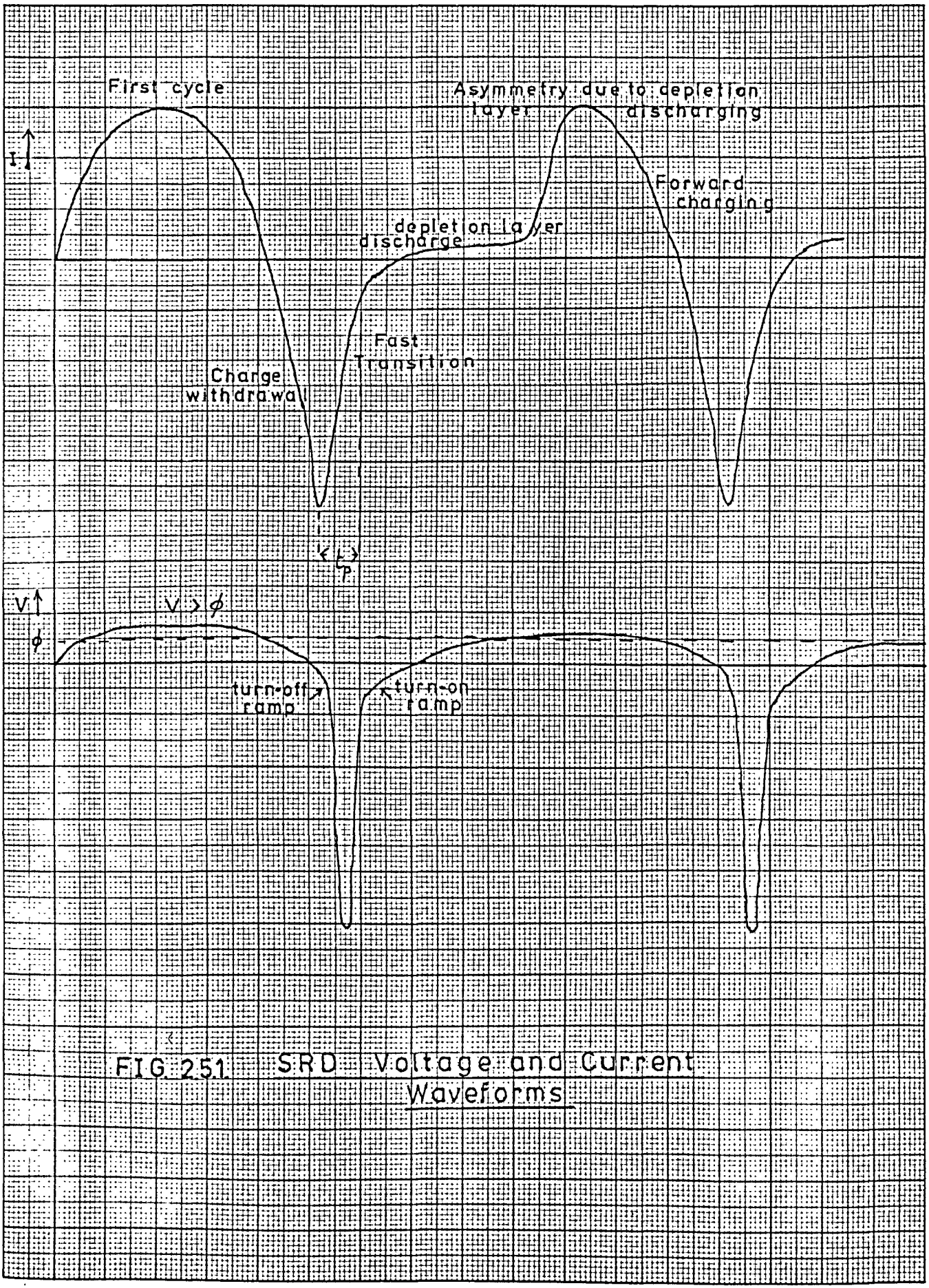

FIG 251 SRD Voltage and Current Waveforms

The width of the voltage pulse, tp is

$$t_p \simeq \left(\frac{\pi \sqrt{L.C_{VR}}}{1 - \sigma^2} \right)$$

where σ is a damping factor

$$\sigma = \frac{1}{2 R_L} \cdot \sqrt{\frac{L}{C_{VR}}}$$

Ultimately, the performance limit of the diode is set by the varactor package inductance, i.e. the minimum possible circuit inductance, and by the varactor loss resistance. The pulse height depends on the driving charge and the circuit loading; assuming that all the energy is recoverable (which is not strictly true) the impulse voltage is

$$V_p = I_p' . \left(\sqrt{L/C_{VR}} \right) . \exp . \frac{-\pi\sigma}{2\sqrt{1 - \sigma^2}}$$

Some advantage at extreme frequencies may be gained by the use of the series mode (fig. 2.4.1) and include the package inductance as the driving impedance matching inductance.

It may be possible to approximate the current step to an impulse, at least to determine the orders of magnitude of the circuit parameters.

In the forward half cycle the energy stored is

$$\tfrac{1}{2} . L . I_p'^2$$

(The exact value of Ip may be difficult to determine in practice.

The energy appears in C_{VR} after switching as an impulse of approximately half sine form of height V_p' and width t_p.

where

$$\frac{1}{2} . I_p'^2 . L^2 \simeq \frac{1}{2} . C_{VR} . V_p'^2$$

and $V_p' = I_p' \sqrt{L / C_{VR}}$ for light loading.

The impulse width is determined by the LC circuit i.e.

$$t_p' \simeq \sqrt{L . C_{VR}}$$

With the load R_L, the impulse height becomes

$$V_p = V_p' . \exp \frac{-\pi\sigma}{2\sqrt{1-\sigma^2}}$$

and the width

$$t_p = \frac{\pi \sqrt{L . C_{VR}}}{\sqrt{1-\sigma^2}}$$

where σ is a damping factor

$$\sigma = \frac{1}{2 R_L} \sqrt{\frac{L}{C_{VR}}}$$

The equations involve the assumption that all the energy is recoverable. In practice, the loss resistance, which is also nonlinear, absorbs power. Hence, the equations represent only an outline of the true situation.

3. HARMONIC GENERATING CIRCUITS AND SYSTEMS

In this chapter, some of the existing harmonic generating circuits are reviewed and results of experimental models discussed. Although not comprehensive, this early work led to the decision to aim for broad-band multipliers, and a section on the maximum theoretical bandwidth is included. The design considerations for a varactor multiplier are discussed in general terms, and some consideration of alternative multipliers is made.

3.1 The 'State-of-the-Art'

In the course of this project, there has been a considerable advance in the state-of-the-art, and, to a certain extent, a change of the priorities in the development of frequency multipliers and chains.

When the project commenced, in 1969, frequency multiplier chains were coming into use as high stability local oscillators for microwave receivers, parametric amplifiers and low power ($< 5w$) transmitters. In general, R.F. power was provided at or below 100 MHz, and a number of frequency multiplier stages employed to take the output to typically, X-band. The technique was costly in varactors, materials, and man-hours of design, construction and tuning time. However, the advantages of microwave power, with crystal controlled stability, still command respect in many applications, in particular satellite ground stations, and, increasingly, the L-band inter-aircraft communication systems.

Recently, other more advanced devices have become available which modify the requirement for frequency multipliers. Gunn diodes, at the cost of increased complexity, may be phase-locked to crystals or high stability

cavities for local oscillators. Impatts, and some Gunn devices, can operate at pulse powers much higher than varactors with comparable efficiencies. Impatt-mode oscillators have achieved d.c. to microwave efficiencies of 65%. Transistors are becoming available at 2GHz with 5w power capability.

The effect of this work on the field of frequency multipliers in general, and this project in particular, has been to shape the objectives towards a useful and viable role in future communication applications. At an early stage, it was decided to consider broadband frequency multipliers this was included in the initial terms of reference. Consideration of spurii was to be made, and means of reducing them evolved. In addition it was hoped that high-order multipliers would be developed. Ultimately, the two design philosophies of broadband and high-order were united in a general approach.

At the suggestion of Dr. Kulesza, the initial theoretical effort was directed towards the hyperabrupt junction. The theory shows (Chapter 4) that inherent output filtoring exists in this device. Coupled with, say, the high-pass property of a waveguide, this could lead to extremely simple frequency multipliers. At present, hyperabrupt devices of a specific non-linearity are not available, although some experimental work has been done on them in the U.S.

The step-recovery diode has been in use for several years as a high order frequency multiplier. Several theories of operation have been suggested (Burckhardt, Moll and Hamilton). In particular, the work of Jungmeister and Schmidt, and Moll and Hamilton, was found particularly useful. Certain equations due to the former group, with the optimisation

conditions as derived in Chapter 4 led to a new and a useful analysis of the step-recovery diode (Chapter 5). Further theoretical and practical work resulted in a conclusion that a pulse spectral analysis technique had a valuable contribution to make in harmonic generation and related fields (Chapter 6). Finally, the multiple diode approach was used, and it soon became clear that a theoretical model of a multiplier circuit become unnecessarily complicated compared with the spectral analysis technique.

3.2 Transistor Multipliers

The Class C amplifier was devised independently by a number of workers (Terman et al.) in the 1930's, using valve circuits. Any three terminal active device (valve, transistor, F.E.T.) can operate in a Class C mode. The bias applied is such that amplification of the signal occurs only on a small part of the input cycle. The waveforms are shown in fig. A (3.2.1) (Appendix 3.1).

By making the approximation of the device linearity, it may be shown that an optimum condition exists for the relative bias and signal levels.

The input and the load are usually resonant circuits which are resistive when correctly tuned. The power drawn from the generator and the power delivered, at the nth harmonic, are readily calculated. Hence the efficiency is shown to be

$$\eta = \frac{4}{(n^2-1)^2} \cdot \frac{\sin^2 \pi/n}{(\sin \pi/n - \pi/n \cos \pi/n)^2}$$

where π/n is the optimum conduction angle for the nth harmonic.

In practical circuits, losses associated with the circuit

elements lead to efficiencies below the theoretical maximum. Typical circuits are shown in fig. (3.2.2).

Certain modern transistors, in particular the overlay types which contain many transistors strapped together, have a large swing of output capacitance in the same way as a varactor. The junctions are effectively nearly abrupt. It is possible to take advantage of this effect by introducing idlers into the output circuit (fig. (3.2.2)). The transistor is driven at frequencies up to the cutoff frequency, f_t. The varactor action, which is in the collector circuit, then multiplies the input frequency. The manufacturers of these devices claim high efficiencies.

Simple practical circuits were constructed in the early part of the project. Harmonics of a Hewlett-Packard oscillator were generated by an RCA 2N3866. The results were comparable to those published by the transistor manufacturers i.e.

f_T = 800 MHz

P_{in} = 200 mW @ 370 MHz

P_{OUT} = 550 mW @ 1.1GHz

While it was felt that this technique has considerable advantages in the frequency range up to 2 GHz, the need for high powers at frequencies well beyond the f_T of the present transistors pointed to the use of more conventional frequency multiplying devices.

3.3 Non-linear Capacitance Multipliers

The existing technology of varactor multipliers, in theory and practice, was reviewed at the beginning of the project. In early 1970, it appeared that single or two-stage frequency multipliers were becoming commercially available. More common were oscillator-multiplier packages,

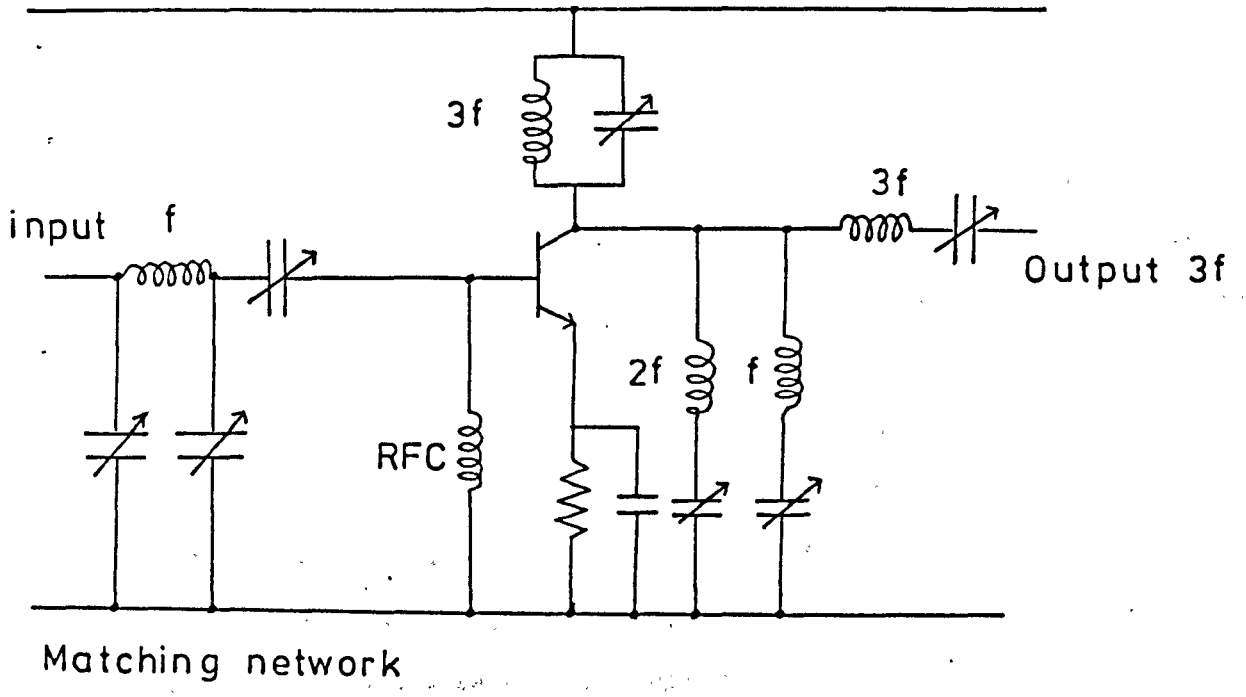

Class 'C' Amplifier with Idlers fig. 3.2.2

which gave the user fewer degrees of freedom in choice of frequency and rate of change of frequency. Theoretical studies by many authors contributed to the initial steps of the analysis developed here; in particular Penfield and Rafuse, Burckhardt, and Scanlan and Laybourn may be quoted. An encouraging practical paper on hyperabrupt junction was written by Markard and Yuan.

Several practical circuits were constructed, (by the author) relying for their design on manufacturer's information or intuition. It was found that empirical designs gave reasonable results when accurately tuned, but were limited by narrow ($\sim$ 1%) instantaneous bandwidths. Examples will be given showing the results obtained.

3.3.1 Triplers 1.1GHz - 3.3GHz

These designs were direct interpretations of the general circuit (fig. 2.4.1). The first model employed dielectric screw tuning, a very satisfactory method provided the line lengths were correct. An idler was included, and the multiplier performed resonably well. Fig. 3.3.1 is an alternative tunable over a wider range, but having the disadvantage of metal-to-metal contacts. At the time of construction, the equipment available was not very sophisticated, a power meter and tunable filters only were available. The oscillator was a free-running single transistor in a Clapp-derived cavity. It was found that when the multipliers loaded the oscillator, the power output changed (a change in the D.C. input was evidence of this) and so the efficiencies, often measured at 60%, were probably deceptively high. Input powers up to 400 mW were available but strong 'moding' prevented linearity checks. The oscillator and the multiplier were strongly interactive, and it was found that tuning

3.3.1.

Tripler 1·1 / 3·3 GHz

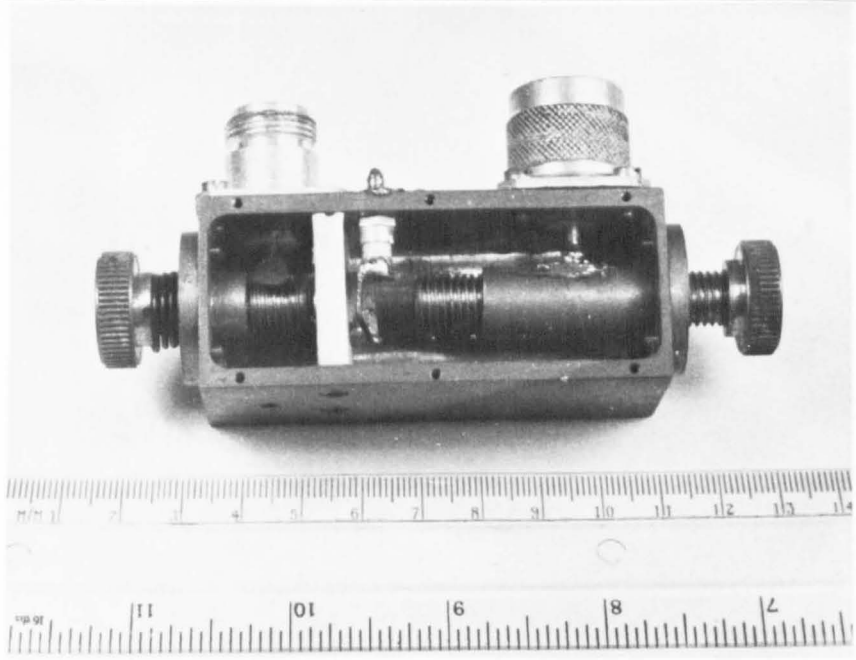

3.3.2.

Tripler 1·5 / 4·5GHz

3W input

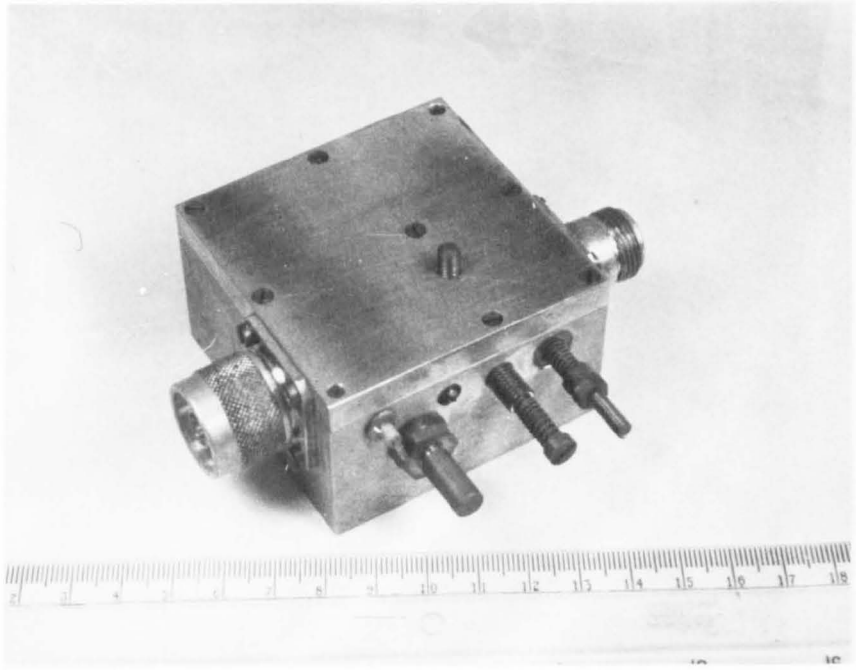

3 3 3

OSCILLATOR /

MULTIPLIER

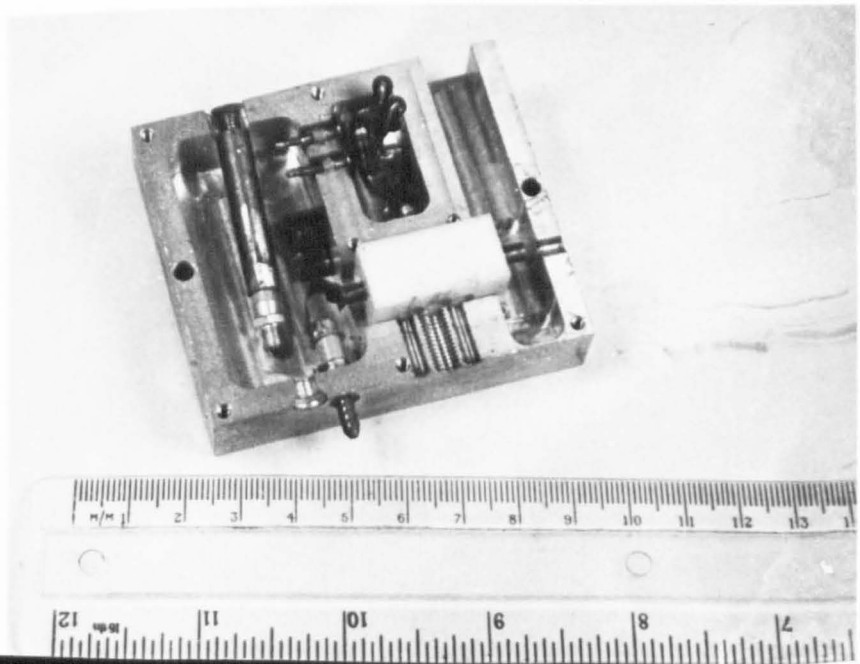

the multiplier produced changes in the oscillator output power, and, to a lesser degree, the oscillator frequency. When changes in output power occurred due to tuning, they were often abrupt, which indicated rapid impedance changes known as 'moding', i.e. the cavities used were capable of sustaining oscillations in several different electromagnetic modes.

3.3.2 Octupler 1.1 GHz - 8.8 GHz.

An initial attempt at high-order multiplication was made with the design of fig. 3.3.3. An integral oscillator provided an estimated 200mW of power at the fundamental. The circuit used was that of fig. 3.3.3a. Idlers were used, placed symmetrically about the varactor. A Ferranti ZC50C proved marginally superior to a Mullard BXY 27 in this application. Tuning was fairly critical, but experience showed that it was reproducible. Re-starting proved no problem. Power output was typically 25mW with spurii, on the high frequency side, 10 db down or better.

3.3.3 High Power Tripler 1.56 - 4.68 GHz

A crystal-controlled source of 3 Watts output at 1.56 GHz was available. Spurii were present in the output, in particular at 1.95 GHz, but were about 20 db down.

The tripler was constructed in the form (fig. 3.3.2) of an add-on unit. The efficiency was about 50%, using a Ferranti IN5155 diode. Spurii were troublesome; the fourth harmonic was only 13 db. down. An external filter reduced the overall efficiency, due to the high insertion loss, but some 400 mW was available, with spurii 30 db or more below the output level. Such conditions, with the stability of crystal control, provide a near-ideal source for a narrowband mixer, or parametric amplifier.

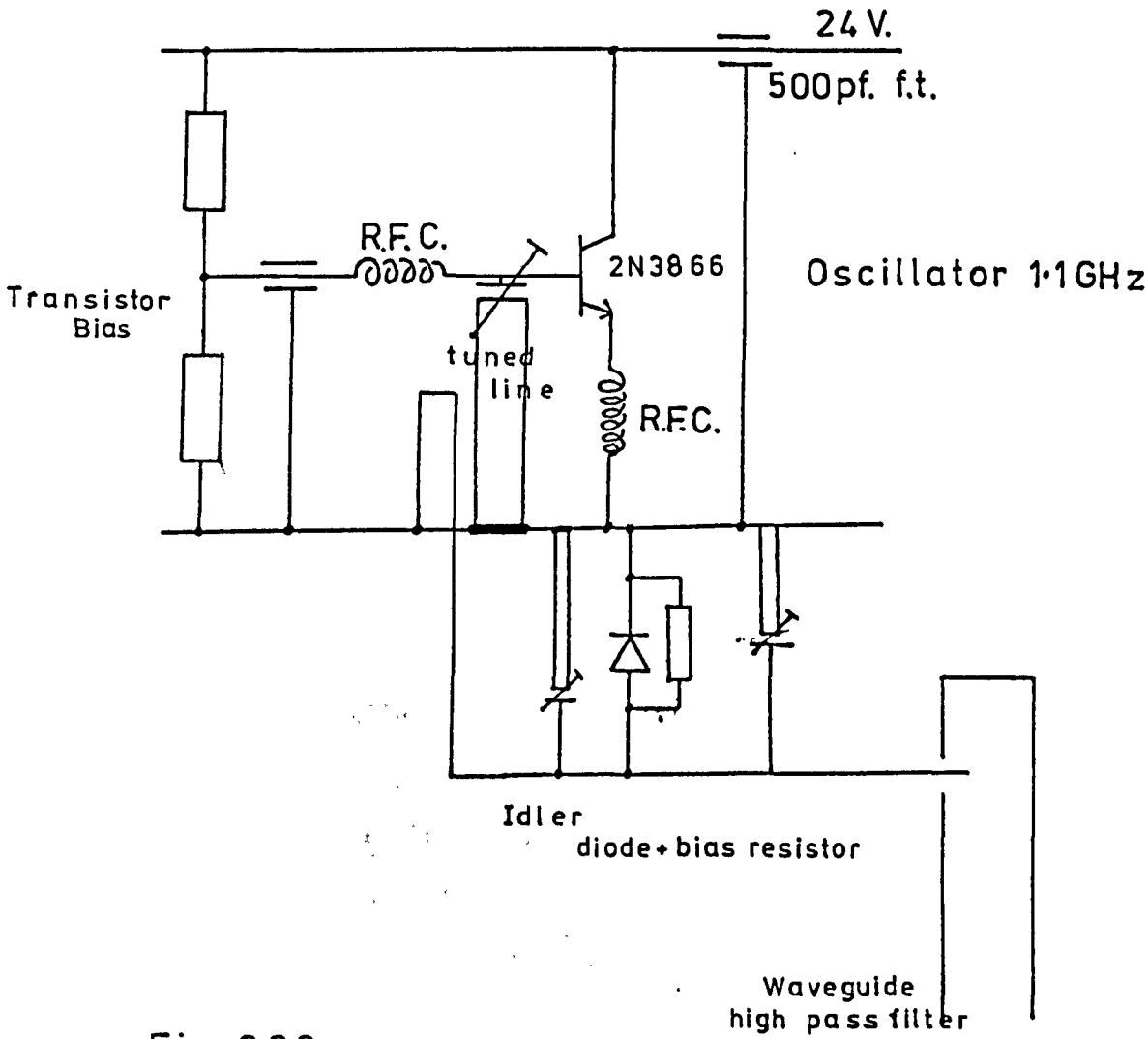

Fig. 3.33.a.

Oscillator and multiplier

3.4 Fundamental Theoretical Bandwidth Limitations

Limitations to the bandwidth of varactor harmonic generators have been discussed by Penfield and Rafuse, Scanlan and Laybourn and Grayzel. It was concluded that the bandwidth of abrupt and graded junction multipliers depends largely on the quality factor. In general, high Q factors lead to high efficiency and narrow bandwidth; a practical realization of this is the extreme difficulty found in tuning a multiplier with a high Q diode. A lower Q device peaks , to a lower efficiency, more easily. Typically, in the references mentioned, 3 db bandwidth limits of 4%, at 1% efficiency, were predicted. Most multipliers designed using varactors have conformed to these results, although step-recovery multipliers showed a marked improvement.

Recent papers by Redd and Kotzebue, and Kotzebue and Matthaei have shown that, with the application of good circuit design, wideband multipliers may be constructed. The former group produced a 70% efficient tripler circuit, with 45% 3db bandwidth. In this example, the balanced diode technique, which will be referred to later, was used.

The ultimate limitations to step-recovery multipliers are the speed of the transition and the elimination of unwanted harmonics.

The speed of the transition pulse is a complex subject, related to the diode structure and the external circuit, the analysis is presented in Chapter 5.

Balanced systems may be used to cancel odd or even components; it is shown in Appendix 3. 2 that the fundamental limitations of any harmonic generation system are:-

$$\phi = \frac{2}{2n+1}$$ all harmonics generated

$$\phi = \frac{2}{n+1}$$ alternate harmonics suppressed.

Where ϕ is the fractional bandwidth, and n the harmonic number.

Filters with infinitely sharp cutoffs are not realizable so these limits may be regarded as extreme upper bands.

3.5 Design Considerations for Multiplier Chains

Frequency multipliers are used in a very wide range of applications so that generalizations of the requirements are difficult to make. However, for the proposed objective of local oscillators in microwave systems, the fundamental requirements may be summarised as follows:-

(1) Adequate stability - 1 part in 10^7 or better - this depends on the drive oscillator, which is usually crystal controlled.

(2) Low noise - amplitude and phase noise can be introduced by the multiplier, so care in construction is required.

(3) Freedom from Spurii - particularly in a chain, spurious generation can lead to operation on frequencies often close to the desired frequency, but distinct from it, with possible disastrous results.

(4) Power output and efficiency - provided these remain adequate, they may be traded to some extent for other desirable characteristics.

As later chapters will show, the multipliers developed are ideal for chain operation, in particular because of very low spurious output levels, and wide instantaneous bandwidths to accommodate rapid frequency changes.

Several alternative types of frequency 'multiplier' were considered. It is possible that Y.I.G. filters could be suitably constructed and driven so that the passbands would track on the input and output of a multiplier. Such a technique could lead to a high-efficiency, high order multiplier, with a potential of wide band limits but narrow instantaneous bandwidth. The drive oscillator could be a Y.I.G. or a varactor tuned device. Very often, however, only a small relative bandwidth is required (say 25%). Two alternative systems are possible, either the simple frequency multiplier is developed to handle the bandwidth, or a heterodyne system . The first method was ultimately adopted, as it involved the solution of the non-linear circuit problems in detail, and is the subject of the later chapters. The heterodyne technique has a number of disadvantages, primarily in the generation of spurii, but could be usefully developed. The system would consist of a mixer-varactor, fed with two large signals; a fixed-frequency microwave power source, and a lower-frequency tunable source, which need not delivery quite as much power. The Manley-Rowe equations dictate this choice of pump sources, as the full power of the microwave frequency source cannot be extracted at an increased frequency. Although basically attractive, the circuit sophistication required to provide good operating characteristics would probably be prohibitively costly.

3.6 Conclusions

From the investigations included in this chapter it was decided that a good solution to the local oscillator problem would be a frequency multiplier capable of operating over a wide band, possibly in a chain of multipliers, and having minimal generation of spurious frequencies.

Practical consideration of cost and reproducibility indicated stripline construction while the non-availability of hyperabrupt diodes forced the use of step-recovery devices. Before the final multiplier could be designed however, theoretical and practical characterisation of the devices had to be carried out.

4. ANALYSIS OF A HYPERABRUPT FREQUENCY MULTIPLIER STAGE

4.1 The hyperabrupt device

It is first necessary to define the term 'hyperabrupt'. In general, any diode whose elastance-voltage relationship is more than abrupt (see fig. 4.1.1a) is classified as hyperabrupt. Many diodes can be represented, at least for part of their characteristic, by the equation

$$S(v) = S_{MAX}\left(\frac{v+\phi}{V_b+\phi}\right)^{\gamma}$$

v = reverse voltage
V_b = breakdown
S_{MAX} = S at V_b.

All diodes with $\gamma > 0.5$ are described as hyperabrupt. Since a discontinuity can be deduced from figs. 4.1.1b and 1c at $\gamma = 1$ two classes of hyperabrupt diodes are distinguished i.e.

$$(\tfrac{1}{2} < \gamma < 1) \text{ and } (1 < \gamma).$$

The theory of abrupt junction varactors has been extensively treated by many authors. (Penfield & Rafuse, Scanlan & Laybourn, Leeson & Weinreb et. al.) In particular, it has been pointed out that, using an abrupt junction without idlers, only the second harmonic may be produced. This apparent disadvantage is significant in that it implies an inherent filtering in the device. It will be shown that a more general rule can be derived, that any harmonic up to 'n' may be produced by the varactor having:

$$\gamma = \frac{(n-1)}{n}$$

The interest in hyperabrupt junctions has recently been revived with the introduction of the ion-implantation process, with which precise profiles may be synthesised. The hyperabrupt diode requires a retrograded doping

Fig 411 The s-v-q Curves

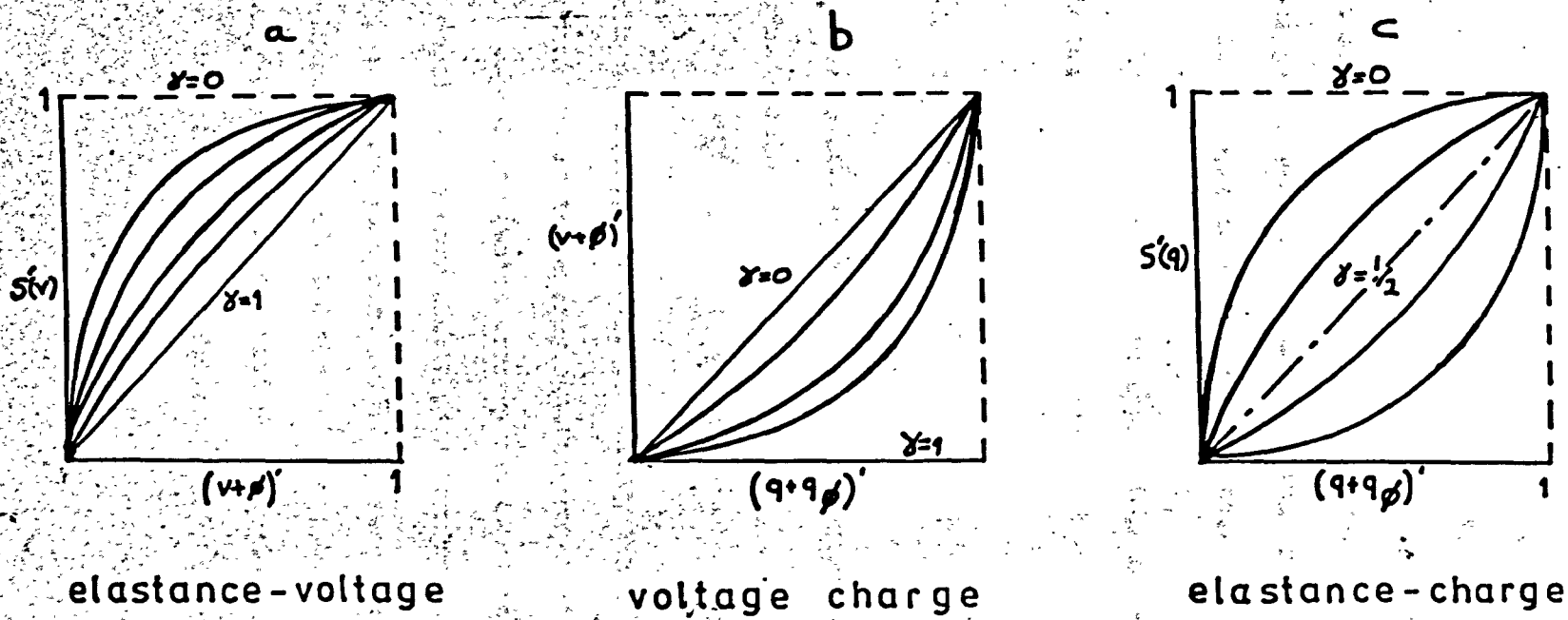

Fig. 4.1.1.

profile (fig. 4.1.1d), which has only recently been readily achievable to the required precision (Kannam).

A number of workers have considered hyperabrupt diodes as frequency multipliers. In particular, Markard and Yuan reported experimental results of 25% efficiency (narrow-band) in a X8 frequency multiplier. The theoretical predictions were less satisfactory, however, and it is possible that step-recovery effects could have modified the results. More theoretical papers were due to Leonard, and Chang, Foster and Ryder. Reference will also be made to the work of Kulesza and Saito.

Leonard, in 1963, pointed out the apparent anomaly in the c-V and q-V characteristics of hyperabrupt varactors. The expression for the stored energy is:

$$W(t) = \frac{(1-\gamma)}{(2-\gamma)} \cdot v_T \cdot q_T$$

which shows asymptotic behaviour. As γ approaches zero, the capacitance tends to a constant, and

$$W \rightarrow \tfrac{1}{2} Q.V.$$

As γ approaches unity, however, the energy tends to zero. This is significant in that, while the energy handling capability falls, the power conversion capability (which corresponds to efficiency) improved. The same paper continues to show that closed form solutions are possible for γ's of $\frac{1}{2}$, 2/3, $\frac{3}{4}$ etc., provided certain assumptions are made. However, the maximum power relations adopted are not considered accurate, and so a γ - efficiency curve was drawn which demonstrates an optimum value. It will be shown that the maximum efficiency, as indicated in part of

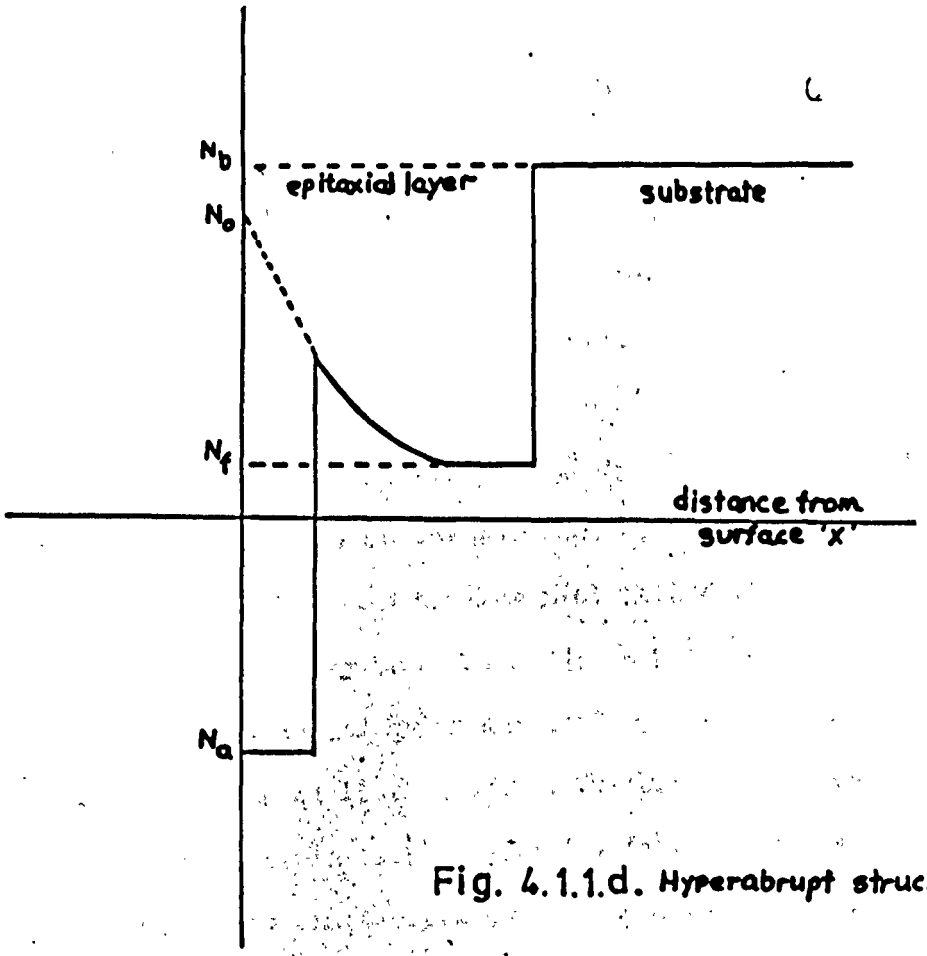

Fig. 4.1.1.d. Hyperabrupt structure

Fig.4.1.1.e Abrupt structure

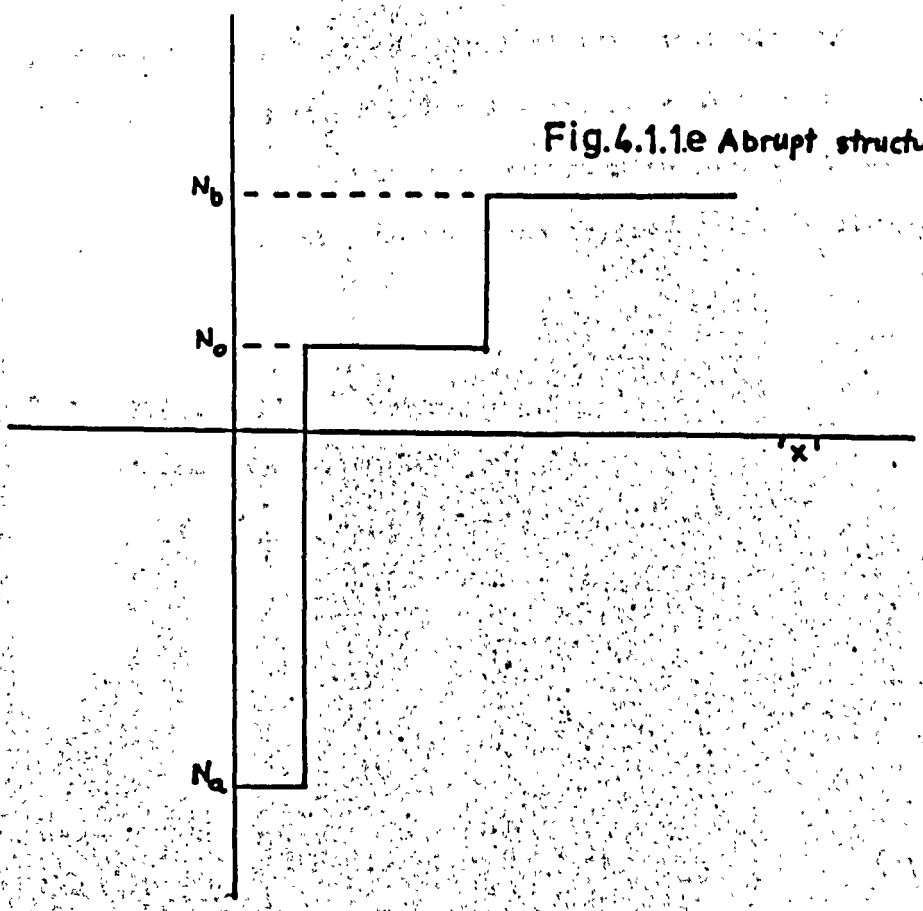

Leonard's paper, occurs when $\gamma = 1$; unfortunately, this is a zero-power transfer condition, so that a compromise solution must be determined. Plots of $S'(v)$, $(v+\phi)'$ and $S'(q)$ are given in fig. (4.1.1), corresponding to Leonard's graphs.

A similar form of the $\gamma = 1$ discontinuity has been commented on by Kulesza (q.v.). In this context, fig. (4.1.2) is an extension of Kulesza's work to include $\gamma > 1$ and $\gamma < 0$.

The latter case has been considered theoretically by Grayzel. At the zero crossings on the harmonic coefficient curves, the $A(\gamma)$ are zero (see appendix). A similar plot with dual assumptions of circuitry, i.e. voltage-fed, may be made. (fig. 4.1.3.)

Chang, Foster and Ryder assessed hyperabrupt junctions by two standards. The quality factor of Kurokawa and Uenohara, $\tilde{Q}$, was shown to be rather poorer, in general, for the hyperabrupt device, due to the practical device considerations. The transducer gain of Hyltin and Kotzebue, g_T, was also shown to be lower than that of conventional diodes; the small signal basis of this analysis was, however, cast into some doubt. It was concluded that, in some circumstances, particularly when contact, bulk or circuit resistances contribute most to the circuit losses, hyperabrupt junctions may be preferable to conventional devices.

4.2 The Power Series

It has been shown that

$$[\,1 + v'(t)\,] = [\,1 + Q'(t)\,]^{\frac{1}{1-\gamma}} \qquad 4.2.1$$

Fig. 4.1.2

Harmonic Coeficient

A(γ) vs. γ

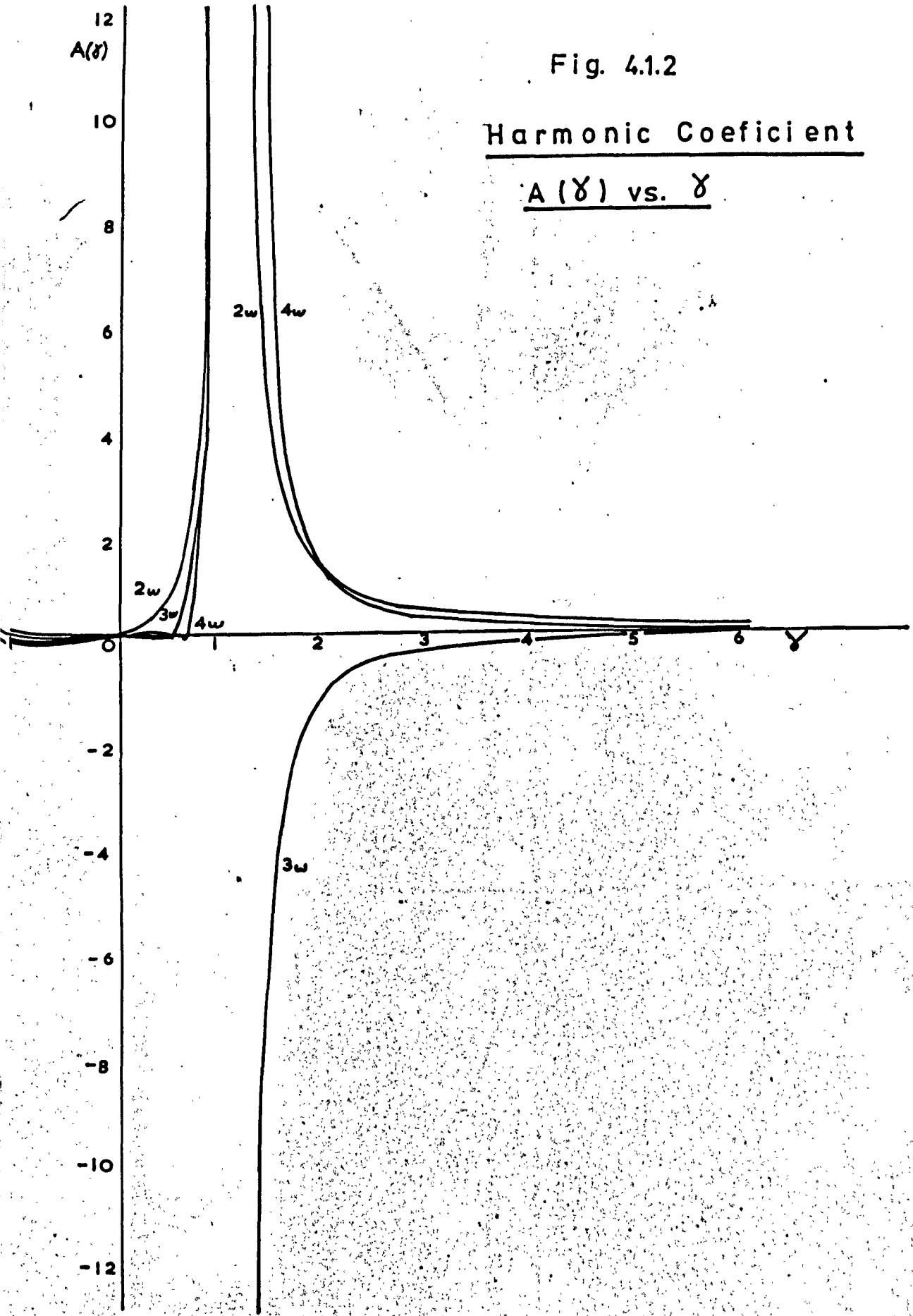

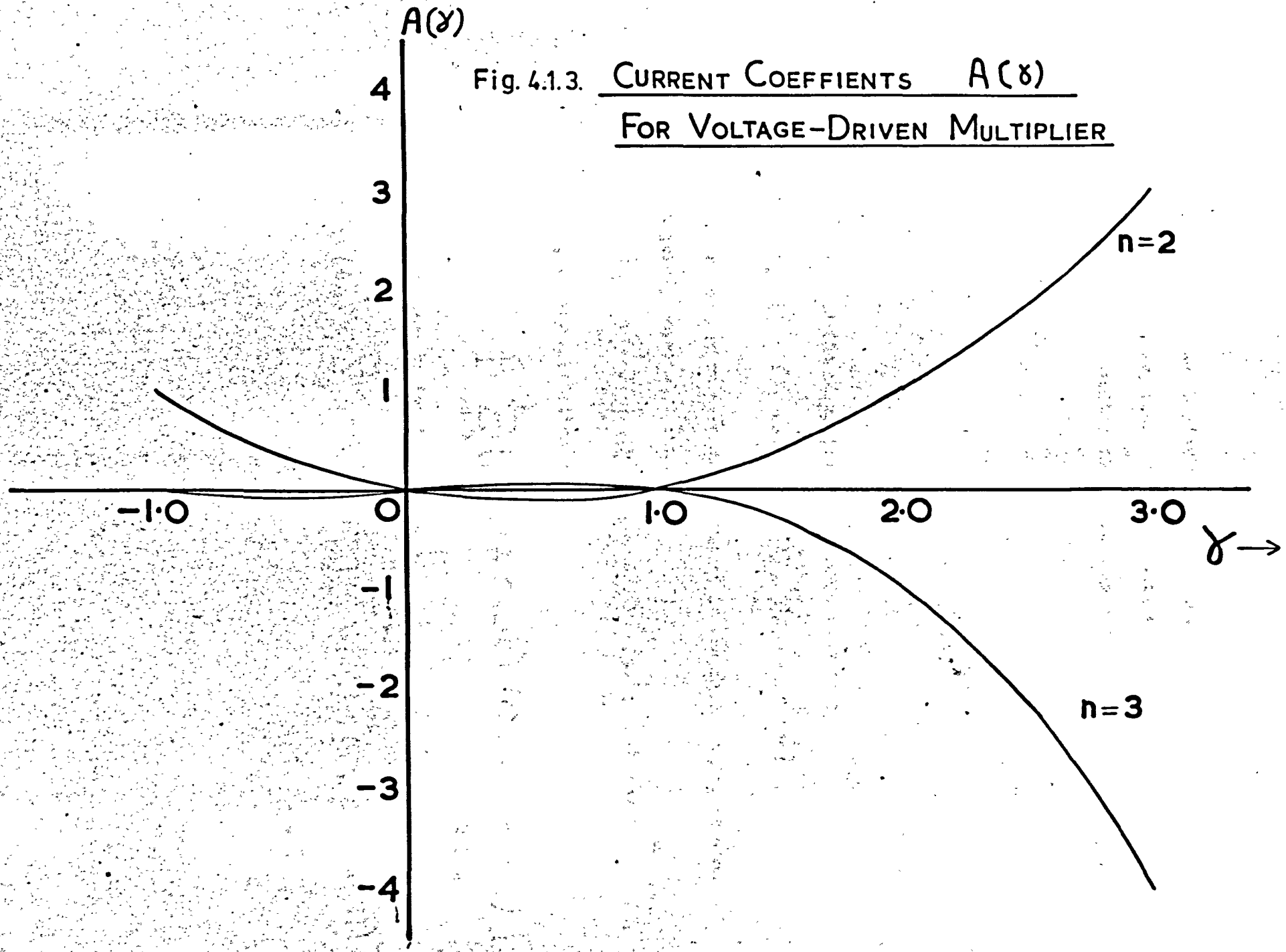

Fig. 4.1.3. CURRENT COEFFIENTS A(γ) FOR VOLTAGE-DRIVEN MULTIPLIER

The general case Fourier series will now be derived, making only the two current assumption. This is justified in that the search is for simple and efficient multipliers with high orders of multiplication.

Rewriting 4.2.1

$$[1 + v'(t)] = [1 + Q'(t)]^m \qquad 4.2.2$$

$$= \sum_{K=0}^{m} \binom{m}{K} . [Q'(t)]^K \qquad 4.2.3$$

$Q'(t)$ is the normalized a.c. charge component,

i.e. $$Q'(t) = Q_1' \cos \omega t + Q_n' \cos (n\omega t + \phi) \qquad 4.2.4$$

n is the harmonic required, and ϕ is the phase angle, at some defined point, between ωt and $n\omega t$.

$$\therefore [Q'(t)]^K = [Q_1' . \cos \omega t + Q_n' \cos (n\omega t + \phi)]^K \qquad 4.2.5$$

or, in sigma notation,

$$[Q'(t)]^K = \left[\sum_{L=0}^{K} \binom{K}{L} . (Q_1' . \cos \omega t)^{K-L} . (Q_n' \cos (n\omega t + \phi))^L \right] \qquad 4.2.6$$

The voltage series is seen to be

$$(1 + v'(t)) = \sum_{K=0}^{M} \binom{m}{K} . \sum_{L=0}^{K} \binom{K}{L} . (Q_1' \cos \omega t)^{K-L} . (Q_n' \cos (n\omega t + \phi))^L \qquad 4.2.7$$

The most important parameter in most frequency multipliers is the efficiency, or the closely related power transfer factor. In the present calculation, it is convenient to consider the varactor loss component lumped with the loss of the external circuit, and deal only with the non-linear capacitive element.

The input current, I_1' is

$$I_1' = \frac{d[Q_1']}{dt} = -\omega . Q_1' \sin \omega t \qquad 4.2.8.$$

and the output,

$$I_n' = \frac{d[Q_n']}{dt} = -n\omega Q_n' \sin (n\omega t + \phi) \qquad 4.2.9$$

The powers involved in the diode derived from 4.2.6 to 4.2.9 are:-

$$P_1 = \frac{1}{2\pi} \int_{-\pi}^{\pi} \sum_{K=0}^{m} \binom{m}{K} . \sum_{L=0}^{K} \binom{K}{L} . (Q_1' . \cos \omega t)^{K-L} . (Q_n' . \cos (n\omega t + \phi))^{L} . (-\omega . Q_1' \sin \omega t) d(\omega t)$$

4.2.10

and

$$P_n = \frac{1}{2\pi} \int_{-\pi}^{\pi} \sum_{K=0}^{m} \binom{m}{K} . \sum_{L=0}^{K} \binom{K}{L} . (Q_1' \cos \omega t)^{K-L} . (Q_n' \cos (n\omega t + \phi))^{L} . (-n\omega . Q_n' . \sin (n\omega t + \phi)) . d(\omega t)$$

4.2.11.

Up to this point, no assumption other than the constancy of the diode non-linearity has been made. One possible approach to the solution at this stage would be to programme the equations onto a computer; in fact, simple hand calculations on a desk machine show that most terms in the power series are redundant or very small. A set of simplifying assumptions

will be made which make an analytical solution possible. The increased awareness of the physical problem and the 'feel' for the mathematical operations justify the slight loss of absolute accuracy.

The assumptions are:-

1. That the input power is transferred to the load, or dissipated. This condition should be valid if the reflected power is subtracted from the incident, although, ideally, a match should be made.
2. The magnitude of the output charge coefficient is small compared to the input charge coefficient.

   i.e.

$$\frac{Q_n'}{Q_1'} \leqslant \frac{1}{n} \qquad 4.2.12.$$

This is, in all practical multipliers, true, so that by neglecting $(Q_n')^2$ terms, and higher, very little error is incurred. This is not a small signal assumption, since the output current, $(n.Q_n')$ can have a magnitude approaching that of the fundamental without seriously violating the conditions.

In the expansion of $(Q_n' \cos(n\omega t+\phi))^L$, the first two terms only are required. Hence, from 4.2.11, the general power term is

$$P = \frac{-n\omega}{2\pi} \sum_{k=0}^{m} \binom{m}{k} \cdot \left\{ Q_1'^{k} \cdot \int_{-\pi}^{\pi} (\cos\omega t)^k \cdot \sin(\omega t+\phi) \cdot d\omega t \right.$$

$$\left. + k \cdot Q_1'^{k-1} \cdot Q_n' \int_{-\pi}^{\pi} (\cos\omega t)^{k-1} \cdot (\cos n\omega t+\phi) \cdot (\sin n\omega t+\phi) d\omega t \right\}^{\frac{1}{2}}$$

4.2.13

The expression is integrable by conventional methods. For convenience, two integrals are considered:

$$P_\alpha = -\frac{n\omega}{2\pi} \sum_{k=0}^{m} \binom{m}{k} \cdot \left\{ Q_1'^{k} \cdot Q_n' \int_{-\pi}^{\pi} (\cos \omega t)^k \cdot \sin(\omega t + \phi) \cdot d.\omega t \right.$$

and

4.2.14

$$P_\beta = -\frac{n\omega}{2\pi} \sum_{k=0}^{m} \binom{m}{k} \cdot Q_1'^{k-1} \cdot Q_n'^{2} \cdot \frac{k}{2} \int_{-\pi}^{\pi} (\cos \omega t)^{k-1} \cdot \sin 2(n\omega t + \phi)\, d\omega t$$

4.2.15

The method of solution of these equations is shown in Appendix 4.2.1. It is shown that the dominant term is:-

$$P_\alpha = -\frac{n\omega}{2} \sum_{j=0}^{\frac{1}{2}(m-n)} \binom{m}{n+2j} \cdot \frac{(n+2j)!}{(n+j)!} \cdot \frac{Q_1'^{n+2j} \cdot Q_n'}{2^{n+2j-1}} \cdot \frac{1}{j!} \cdot \sin\phi$$

The variables in this equation are clearly defined; if this term is considered alone. $\sin\phi$ is set equal to unity. This makes the P_β term identically zero. P_ψ and further odd terms contain factors of the form $\left\{ \frac{Q_n'^2}{4} \right\}$, and so are ignored; the assumption that $(Q_n'^2)$ is small is justified.

(The limit of the summation, $\frac{1}{2}(m-n)$ can lead to half-integral values; in this case the integral limit is interpreted as $(\frac{1}{2}(m-n) - \frac{1}{2})$.

4.3 General Theory of the Hyperabrupt Frequency Multiplier

4.3.1 The Limiting Curve

The limiting curve concept was introduced by Penfield and Rafuse. It was shown that, because limitations of current or voltage excursions must be imposed in a practical circuit only a limited area of operation is available to the diode. By defining an abrupt junction doubler case only, Penfield and Rafuse were able to draw a two-dimensional plot of allowed operating conditions. A more general set of conditions will be derived below, for the 'double-limited' case. In the usual varactor analysis, forward and reverse conduction regions are avoided, hence the 'double-limit'. Conditions may occur when only a single (reverse conduction) limit is necessary; this will be considered in a later chapter.

The operating level of the varactor is set by the current drive. Only two currents are allowed to flow, and the limits of charge swing are defined as 0 and $2Q_0$, an excursion of $\pm Q_0$ about a mean Q_0.

i.e.

$$|Q'(t)| \leq 1 \qquad 4.3.1.a$$

This condition represents a set of allowed values of Q_1' and Q_n'. The exact area of the set depends on θ, and ϕ, parameters which are defined below.

The operational region is defined by

$$|Q_1' \cos \omega t - Q_n' \cos (n\omega t + \phi)| \leq 1 \qquad 4.3.1.b$$

ϕ = Phase angle of 'n' th harmonic current

Initially, the full drive condition, which allows the equality to hold at certain points, is assumed.

Then, for any n, we can find an angle at which the equality holds.

$\therefore$

$$Q_1' \cos\theta - Q_n' \cos(n\theta + \phi) = \pm 1 \qquad 4.3.1.c$$

This point is also a maximum w.r.t. θ so, differentiating,

$$Q_1' \sin\theta - n Q_n' \sin(n\theta+\phi) = 0$$

$\therefore$

$$\frac{Q_n'}{Q_1'} = \frac{\sin\theta}{n \sin(n\theta+\phi)} \qquad 4.3.1.d$$

The equations 4.3.1.c and d are simultaneous equations with 4 independent variables. Earlier work of this chapter indicated that $\phi = \pi/2$, although other solutions will be considered. Hence, one further equation is needed to separate the variables Q_1', Q_n', and θ.

Appendix 4.3.1 shows the solution of the equations to be

$$\underline{\tan(n\theta+\phi) = -n \tan\theta.} \qquad 4.3.1.e$$

where n = harmonic number
θ = value of 'ωt' under the maximum power conditions
ϕ = phase angle of harmonic

This is a significant new equation, which implies that, given n, and calculating ϕ, the angles θ at which charge maximum and minimum occur may be found, independently of the device non-linearity. The only assumption made which leads to this conclusion is that only two currents are allowed flow.

From the tan θ expressions, the optimal values of Q_1' and Q_n' may be derived, for the general multiplier. The 'limiting curve' is described by equation 4.3.1 e with substitution of Q_1' and Q_n' from equation 4.3.1 c and d.

In the non-fully driven case, 4.3.1 d and e still apply, so that the optimum θ angle remains the same; other values of phase angle ϕ are permissible without violation of the boundary conditions, but the optimum values remain unchanged. The optimum Q_1' and Q_n' are derived from the drive level, and hence a variation in the power handling and efficiency will usually result from the change in drive.

4.3.2 The General Relations

Two fundamental equations have been derived. For any two-current parametric frequency multiplier,

$$\tan(n\theta+\phi) = -n\tan\theta \qquad 4.3.2.a$$

The power series for a simple γ-law varactor is

$$P = \frac{-n\omega}{2}\left\{\sum_{j=0}^{\frac{1}{2}(m-n)}\binom{m}{n+2j}\cdot\frac{(n+2j)!}{(n+j)!}\cdot\frac{Q_1'^{n+2j}\cdot Q_n'}{2^{n+2j-1}}\cdot\frac{1}{j!}\cdot\sin\phi\right\}$$

4.3.2. b

The approximation $\{Q_n'^2 = \text{small}\}$ is assumed. An examination of 4.3.2.a, shows that this assumption is correct in almost every example of this type of multiplier.

Equation 4.3.2.a is used to determine the optimum value of θ for a given n. The value of ϕ is determined graphically by considering the possible values and selecting those which provide the maximum output current. Alternatively, differentiation of P gives $\phi = \pm \pi/2$, which is in exact agreement with the graphical techniques.

4.3.3 The Optimum Bias Point

In the current driven mode, the bias point is the half-charge point, so that the variable part of the charge may change from 0 to 2Qo.

We have

$$Q_o = \frac{(v_o + \phi)}{(1-\gamma)} \cdot C_o \qquad 4.3.3.a$$

and

$$Q = Q_o\left(1 + v(t)\right)^{1-\gamma} \qquad 4.3.3.b$$

The maximum charge occurs when the voltage is at a maximum, provided γ is less than unity (see fig. 4.1.1.).

$$\therefore \quad Q_{max} = 2Q_o = Q_o\left(1 + v'_{max}\right)^{1-\gamma} \qquad 4.3.3.c$$

Hence

v_{max} = normalised max. reverse voltage.

$$v_{max} = \left(2^{\frac{1}{1-\gamma}} - 1\right) \qquad 4.3.3.d$$

The voltage is measured from the bias-point so that the reverse excursion is v' max., and the 'forward' (to zero volts) excursion is $(v_o + \phi)$. The total voltage swing is then

$$v_s' = 2^{\frac{1}{1-\gamma}}$$

In a practical multiplier, the maximum reverse voltage is the breakdown voltage, V_B, and this is equal to the maximum reverse voltage defined above.

i.e. $$V_B' = 2^{\frac{1}{1-\delta}} - 1$$

Hence, the bias voltage, $(v_o+\phi)$ can be found from the denormalization of this equation:

$$(v_o+\phi) = \frac{V_B}{2^{\frac{1}{1-\delta}} - 1}$$

4.3.3.e

Very often, it is found that negative values of v_o, representing slight forward bias, occur.

Although no practical measurements on this class of hyperabrupt varactor have been made, measurements on varactors in the graded and abrupt groups indicate similar trends. In practice, the achievement of the specified γ over a suitably wide range will be difficult. It is unlikely that devices will be produced to such perfection that high efficiencies will be achieved without allowing a certain amount of rectification to take place. The rectified current is the source of the popular 'self-bias'. Essentially, a controlled and measured forward current is a better guide to the bias conditions than is the D.C. voltage across the junction; the papers consulted by the author on this subject may be summarised by saying that, in almost every case, self-bias with effective current control established the best possible working conditions as predicted by the theory described. When this was not the case, it was evident that the drive power was insufficient, to produce the bias required,

so that external bias had to be applied. In this context, it is clear that any arbitrary figure may be introduced as a maximum reverse voltage, with bias varied accordingly. The effect is to reduce the power handled by the device and hence the output power available.

It is necessary to deduce, at this point, some 'general trends' in the way the hyperabrupt class of diodes will behave.

Equation 4.3.3.a shows that

$$Q_o = \frac{(v_o+\phi).C_o}{1-\gamma}$$

The bias-point capacitance could be expressed in terms of the reverse-bias capacitance; in general, this is an impossible measurement, masked by the package parameters. However, Co for any ;practical device is likely to be of the same order of magnitude as the zero bias capacitance.

In terms of the breakdown voltage,

$$(v_o+\phi) = \frac{V_B}{(2^{\frac{1}{1-\gamma}}-1)} \qquad 4.3.3.f$$

and so

$$Q_o = \frac{V_B.C_o}{(1-\gamma).(2^{\frac{1}{1-\gamma}}-1)}$$

$$\text{or } Q_o = \frac{m.V_B.C_o}{(2^m-1)} \qquad \text{where } m = \frac{1}{1-\gamma} \qquad 4.3.3.g$$

This equation shows that, as m tends to larger values (i.e. $\gamma \to 1$) then Qo tends to zero. Later work will show that the efficiency of the devices tend to 100% as γ tends to unity; however, the power transferred

approaches zero, so that all the equations are internally consistent.

The values of the parameter $\frac{m}{(2^m - 1)}$ are tabulated in fig. A4.3.3. (Appendix 4.3.1)

4.34. Efficiency

The efficiency formula is included in full in appendix 4.3.3. In general terms, it is stated:

$$\eta = \frac{P' - P'_{o/p\ loss}}{P' + P'_{i/p\ loss}}$$

where the primed quantities are the normalized values. The optimum currents are defined by the equation

$$\cot n\theta = n \tan \theta$$

so the loss quantities are fixed by r_s' and the optimum currents. However P' is a function of the device non linearity, i.e.

$$P' = \frac{n\omega}{2} \sum_{j=0}^{k_2(m-n)} \binom{m}{n+2j} \cdot \frac{(n+2j)!}{(n+j)!} \cdot \frac{Q_1'^{\,n+2j} \cdot Q_n'}{2^{n+2j-1}} \cdot \frac{1}{j!}$$

This function increases monotonically with m, at a rate illustrated by the examples of appendix 4.3.3. Hence, the efficiency increases with increasing m; as γ approaches unity, P' tends to infinity, but the loss component is fixed, so the expression for efficiency approaches 100%. However, the denormalization coefficient tends to the inverse of infinity, so that the power handled is zero, which overcomes the anomalous condition.

4.4 General trends evident in the Predicted output of the Hyperabrupt diode

It is evident from the tables and graphs that, for any harmonic number, there exists an optimum current input and output conditions which are independent of the γ factor. For a given γ, the power handled, and the efficiency of the diode itself, can be determined. In a broader view if it is necessary to select a diode γ for harmonic generation, two criteria should be considered:-

1. Efficiency.

   As γ tends to unity, the efficiency increases, for constant , r_s, V_B and C_o parameters.

2. Power handling

   For any harmonic number, there exists an optimum γ, which may be shown to obey the relation

$$n = \frac{3}{2}m = \frac{3}{2}\,\frac{1}{1-\gamma} \qquad \text{(See App. 4.3.3.)}$$

These conclusions are general to the whole class of hyperabrupt diodes, of which the simplest case is the abrupt junction. The predictions made in this chapter are in close agreement with those of Penfield and Rafuse for the abrupt junction multiplier and with Leonard on the subject of the optimum γ for a doubler. Complete generalization of the laws governing the hyperabrupt varactor for any n and m have been outlined. In practice, an n x m general set of solutions must be computed, although two single 'n' values (2 and 5) have been illustrated. (Fig. 4.4.1.)

The apparent discontinuity of $\gamma = 1$ is satisfactorily explained from the theory. The efficiency tends to 100%, but the power handled is zero;

Fig. 4.4.1. HYPERABRUPT FREQUENCY MULTIPLIER

Predicted P & η for n=2, n=5 [when $r_s = 1\Omega$ $V_B\omega.C_o = 1A$]

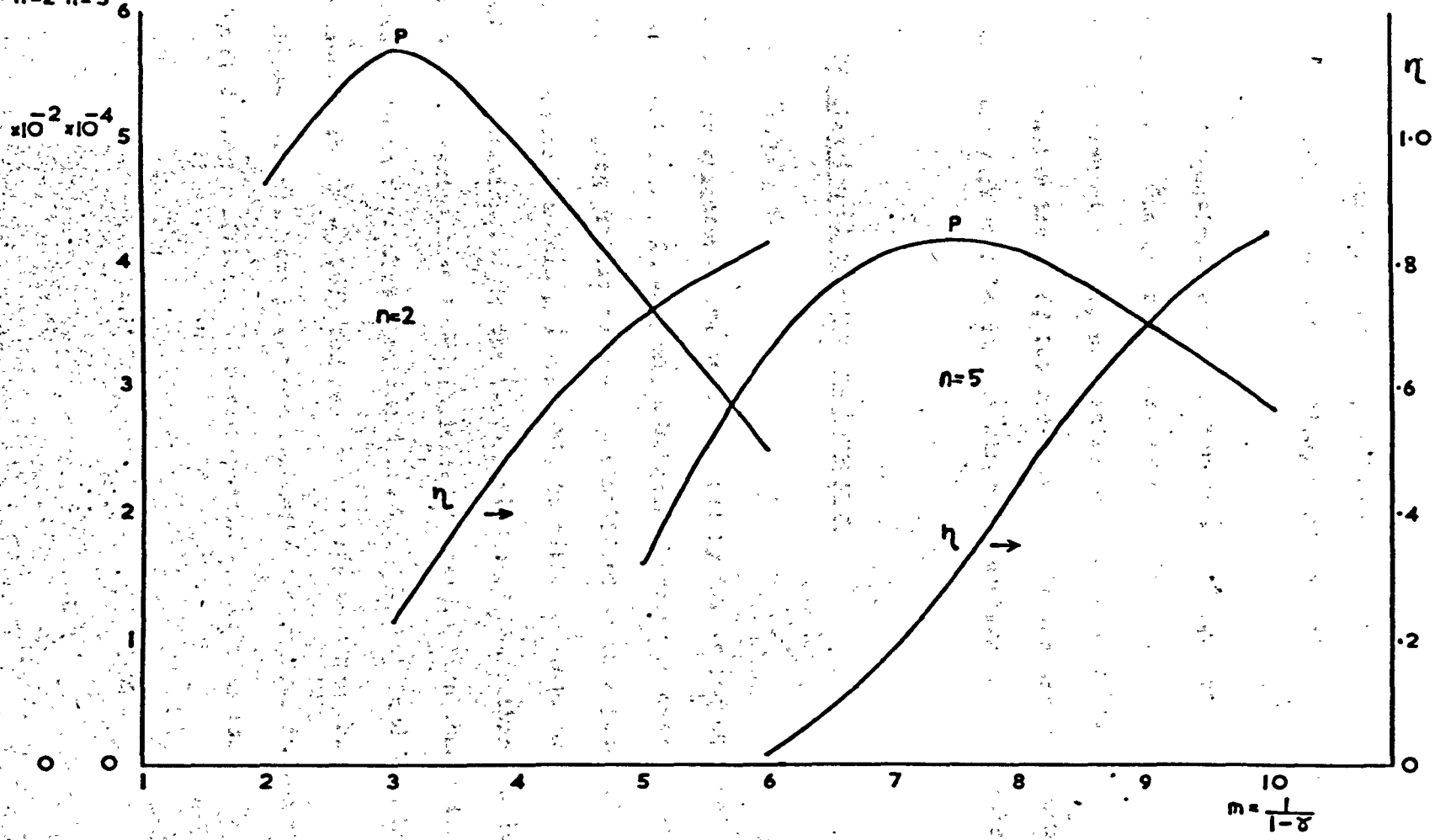

so no power is fed into or extracted from the device. Harmonics are produced by any diode up to

$$n = m$$

or, as a corollary, a diode must have $m \geq n$ in order to produce the nth harmonic. This explains the abrupt junction, which may only act as a doubler without idlers.

A similar set of equations, with some reversals of sign, apply to the values greater than 1. The general theory still holds.

The theory has predicted that, especially in high power multipliers, it may be advantageous to tailor the γ of the varactor to suit the harmonic required. It is hoped that such work will be done by other researchers in this field.

4.5 Practical Realization of Hyperabrupt Varactors

4.5.1 Diffusion Technique.

Hyperabrupt varactors have been produced by fairly conventional diffusion techniques. In general, a Schottky barrier is assumed, as the prediction of doping profile is greatly simplified by this generalization. Precise mathematical models are available to tailor devices to suit particular applications. To the best knowledge of the author, no devices in the $.5 < \gamma < 1$ region have been fabricated commercially although there is no reason to suppose that they could not be. Markard and Yuan have made devices with $\gamma = .875$ for reasonably wide bias ranges.

Nishizawa et. al. have given comprehensive design data information for hyperabrupt doping profiles, and have reported sample results.

Hyperabrupt diodes, for use as wide-range voltage-variable tuning elements, are commercially available (Motorola, I.T.T.). The γ values used appear to be in the range 2 to 5. McDonnell has reported the use of these diodes in a frequency divider. More recently, Kannam et. al.[24] have made diffused hyperabrupt devices with highly linear, wide range and repeatable characteristics. One extremely significant part of their findings was that the C.V. characteristics had negligible change over a temperature range of 25°C to 250°C. This could well indicate that hyperabrupt varactor multipliers may be operated over an unusually wide range of ambient temperatures.

4.5.2 Ion Implantation.

Recently, much attention has been focussed on the technique of ion implantation. It appears that ions may be implanted in such an accurate way that any desired device profile may be synthesized. In particular, talks with workers in this field revealed that hyperabrupt diodes are particularly easily fabricated. Moline and Foxhall[34] have reported extremely good results using several variations of the ion implantation process. It was hoped that engineering samples would be available for this project, but unfortunately this was not the case.

5. THEORETICAL ANALYSIS OF THE STEP RECOVERY DIODE

5.1 Introduction

A number of analyses of the step recover diode have been published in the past. This analysis differs from the work of others in that it brings together the concepts of the limiting curve and the C-V model, also it uses the basic analytical approach previously applied to a hyperabrupt device. In general, other authors selected a feature of the SRD and expanded it into a full analysis; usually it was the capacitance, but the resistance has also been used (Bozic).[3] An analysis is developed here which incorporates the practical device parameters, stored charge and voltage excursion. Most of the earlier analyses were concerned with the small-signal theory of the diode. Although the results were substantially correct for very high orders of multiplication without idlers, they were not general. Some analyses have used computer programmes to simulate the non-linearity of the device; inevitably, limitations on the understanding of the multiplying action were imposed by the numerical methods. Probably the most interesting group of analyses involved a true, if at some stage approximate mathematical solutions. Basically, a model for the diode is assumed, and then the restrictions are placed on the current and voltage conditions allowed in the device. Analyses of this type were due to Johnston and Boothroyd,[21] and Jungmeister and Schmidt.[23]

The analysis presented here contains ideas originating in the work of Scanlan and Laybourne,[54] Markard and Yuan,[34] Jungmeister and Schmidt,[23] and Penfield and Refuse ('Varactor Applications' M.I.T. Press). The most significant departure from the conventional analyses is in the use of the limiting curve conditions, which are derived in the same way as for the hyperabrupt device.

In the course of this work, it was found that the spectral assessment technique could also be used as a powerful tool.

5.2 The Predicted harmonic spectrum - General shape

In section 2.4, and the associated appendices, the general operation of the step-recovery diode, in relation to the solid state physics of the device, was discussed. It is evident that a complex model is required to describe the transition from C_{FWD} to C_{REV} (C_{FWD} is the capacitance under forward bias, C_{REV} under maximum reverse bias.) In fig. (2.4.1) the voltage can be interpreted as the in situ effect of the finite transition time. At first it would appear that the fastest possible diode is the most desirable; this is not necessarily so. The 'best' diode is that which is capable of transferring most energy to the desired frequency; generally, the fastest diodes handle only low powers. Three major loss mechanisms occur in the SRD:-

1. The I^2R loss. This is usually reduced in a high Q diode, although the transition time is not necessarily shorter.
2. The recombination loss. The time parameters t_t and τ_t are closely linked; the fastest diodes tend to have a short τ_t, and hence lose power by rectification (t_t = diode transition time; τ_t = diode recombination time)
3. The transition loss. Not all the energy in the junction before the transition is recoverable.

We can expect, therefore, in a reasonably well constructed untuned-circuit to see the characteristic 'pulse' spectrum of the high-speed transition, probably modified by other diode parameters(fig. 6.5.2).

In general, the approach applied to the hyperabrupt varactor is followed. Circuit equations in the limiting cases are set up with certain assumptions. With the aid of these circuit equations, and invoking the continuity conditions, a voltage-current series model of the diode is constructed. Using a range of typical device parameters, performance curves are derived according to the equations, and predictions are made of input and output impedances.

5.3 The Limiting Curve

For any varactor, a set of limiting curve conditions can be derived. In the series mode, with a two-current assumption, the currents are those defined in equations 4.3.1a-g i.e.

$$| Q_1' \cos \omega t - Q_n' \cos(n\omega t + \phi) | \leq 1$$

where $I_1 = \frac{d}{dt}(Q_1' \cdot Q_o)$ and $I_n = \frac{d}{dt}(Q_n' \cdot Q_o)$

The magnitude of the currents is determined by the bias-point charge, Qo, which is the key parameter.

The charge storage characteristic of the ideal step-recovery diode is shown in fig. 5.3.1. In a properly designed and applied device, the recombination time, τ_t, is long enough so that during one cycle of the drive frequency, the probability of recombination (which in the p.i.n. structure is equivalent to rectification) is low. If rectification does not occur, then the voltage range which is normally associated with forward conduction may be used as part of the operating zone, and hence one of the operating voltage boundaries can be removed. This is referred to as 'single-sided limiting' i.e. only the breakdown voltage limits the operating region.

Fig. 5.3.1.

IDEALIZED S.R.D.
Q-V CHARACTERISTIC

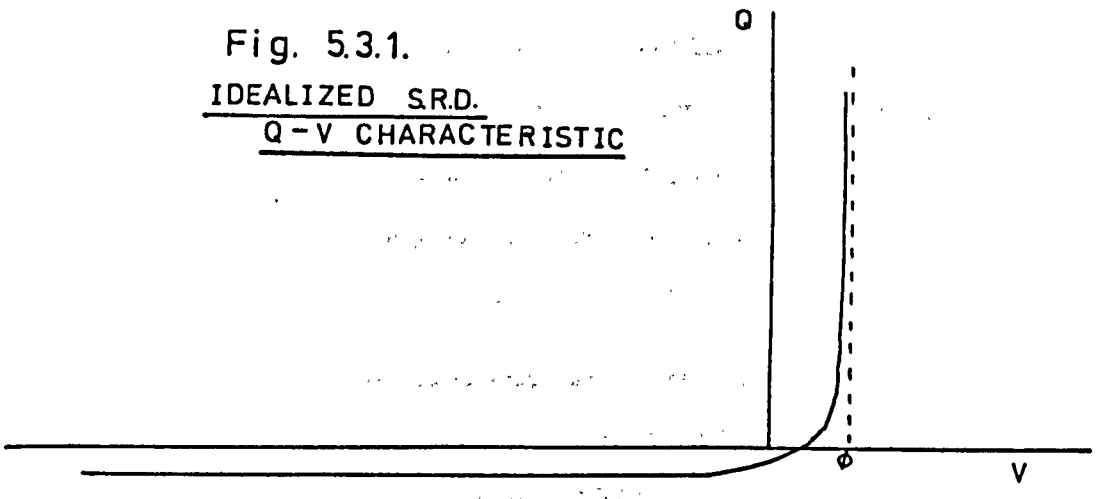

Fig. 5.3.2.

PRACTICAL S.R.D.

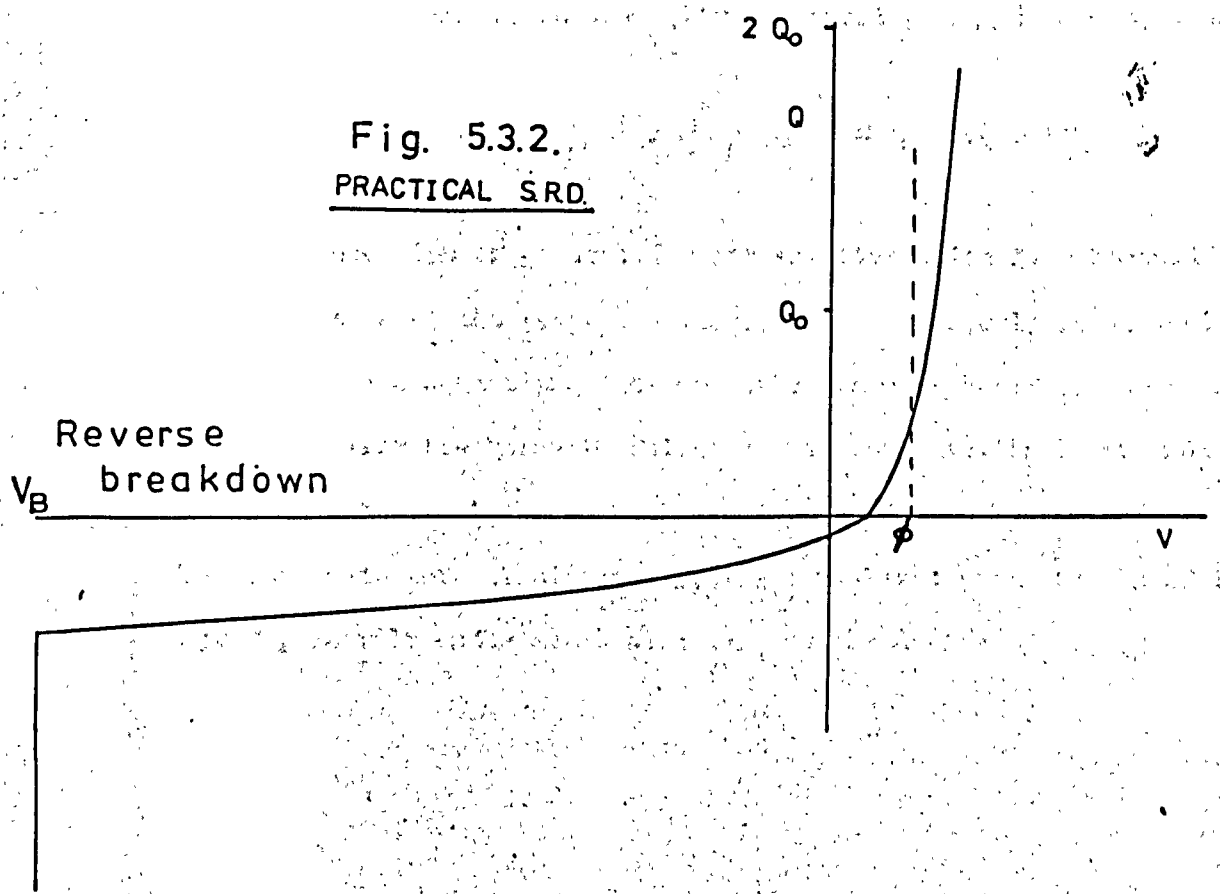

The maximum circuit 'Q' (dynamic quality factor) the reverse voltage should reach the point where the device capacitance is not voltage-variable (colloquially 'punch-through'), often, this means the reverse breakdown point V_B. For maximum charge storage, the diode should swing well into the forward bias region, although a compromise against rectification losses must be reached.

In the hyperabrupt analysis, the phase angle, ϕ, was adjusted so that the charge waveform was symmetrical, i.e. the voltage swings were equal. When only one constraint is applied, (the reverse voltage) alternative phase angles are possible.

Appendix 5.3.1 extends the analysis of Chapter 4 to derive the same equation for Θ, and hence the optimum currents, in a two-current series mod i.e.

$$\tan(n\Theta + \phi) = -n.\tan\Theta$$

This equation is general for any varactor which is subjected to only the limitation of the reverse voltage drive. The only other assumption is that forward conduction does not take place. However, the conclusions drawn regarding the harmonic voltages and powers available are not the same as in Chapter 4, because the voltage series to be derived is different and, more significantly, the normalized power levels of the SRD depend primarily on the exact structure of the device.

5.4 The exponential model of the Step-Recovery diode

5.4.1 The Mathematical Model

Conventional step-recovery diode analyses include a capacitive 'step' which is only a valid approximation at frequencies well below the 'transition frequency' i.e. t_t^{-1}. In pulse circuits, or where high-order harmonics are to be generated near the limit of the device's useful range, a more realistic approach is required.

It is known that the diffusion capacitance variation is exponential. Using this type of model, Jungmeister and Schmidt in 1969 produced pulse trains in very good agreement with the theoretically predicted forms. The exponential model as developed below, in conjunction with the limiting conditions, can be applied as a complete mathematical solution of the step-recovery diode multiplier. Such an approach removes the need to assume infinite forward capacitance or an infinitely short transition time.

For any voltage variable capacitance:

$$\text{static capacitance} \quad C_s = \frac{q}{v}$$

$$\text{dynamic} \quad " \quad C_d = \frac{dq}{dv}$$

The capacitive current is then

$$i_c = \frac{dq}{dt} = C_s \frac{dv}{dt} + v \cdot \frac{dC_s}{dt} = C_d \cdot \frac{dv}{dt}$$

Shockley, and others, have pointed out that the capacitance variation in the forward region is exponential, i.e.

$$C_s = C_o \exp\left(\frac{v_c}{V_{co}}\right) + C_c$$

C_c = Residual capacitance

$$V_{co} = a_c \cdot \frac{KT}{q}$$

The current through the resistive forward biassed diode is

$$i_r = I_o \left(\exp \left(\frac{v_c}{V_{co}} \right) - 1 \right)$$

However, we will, for the purposes of this analysis, neglect the resistive current. This is equivalent to assuming that we are operating the diode at a frequency much higher than the reciprocal recombination time. Some estimates of the errors involved in neglecting the resistive current are made in Chapter 6. The assumption is made that the storage time is short, as compared to the minority carrier lifetime in the junction.

The capacitive component of the current is

$$i_c = \frac{dv_c}{dt} \left[\left(1 + \frac{v_c}{V_{co}} \right) \cdot C_o \exp \left(\frac{v_c}{V_{co}} \right) + C_c \right]$$

The charge Q(t) is given by

$$Q(t) = \int i \cdot dt$$

$$Q(t) = \int \left\{ \left(1 + \frac{v_c}{V_{co}} \right) \cdot C_o \exp \left(\frac{v_c}{V_{co}} \right) + C_c \right\} \cdot dv_c$$

$$Q(t) = C_c \cdot v_c + C_o \left\{ v_c \cdot \exp \frac{v_c}{V_{co}} \right\}$$

We can say that, as the forward capacitance is many times the residual capacitance C_c, then the latter's charge is negligible in the forward region. Rationalization of the equation proceeds as in Chapter 4, i.e.

when $v_c = V_o$ bias voltage

$Q(t) = Q_o$ " charge

$$Q_o = C_o \left[V_o . \exp\left(\frac{V_o}{V_{co}}\right) \right]$$

$$\therefore \quad Q(t) = Q_o . \frac{v_c}{V_o} . \exp\left(\frac{v_c - V_o}{V_{co}} \right)$$

Now we introduce the normalized a.c. terms v_c' and $Q'(t)$

$$v_c = V_o(1 + v_c')$$

$$Q(t) = Q_o(1 + Q'(t))$$

$$\therefore \quad (1 + Q'(t)) = (1 + v_c') . \exp \frac{v_c'}{V_{co}'}$$

Rewriting the equation, gives

$$\frac{v_c'}{V_{co}'} + \log_e (1 + v_c') = \log_e (1 + Q'(t))$$

In the forward conduction region,

$$\frac{v_c'}{V_{co}'} \gg \log_e (1 + v_c')$$

so we can assume that the log. term is negligible and therefore

$$\frac{v_c'}{V_{co}'} = \log_e (1 + Q'(t))$$

The only assumptions made in this derivation were that the residual capacitance is small and that the storage time is much less than the recombination time. Both these parameters are controlled during the manufacture of the device.

The last equation above represents the voltage series produced by the varactor when the charge Q (t) is allowed to flow. Fourier analytical techniques are needed now to extract useful information; the major results are indicated in the following paragraphs.

5.4.2 The Analysis

The expression for the harmonic voltages of an exponential-model capacitor has been derived in the preceeding paragraph, i.e.

$$\frac{v_c'}{V_{co}'} = \log_e\left(1 + Q'(t)\right)$$

$$\therefore \frac{v_c'}{V_{co}'} = Q'(t) - \frac{Q'(t)^2}{2} + \frac{Q'(t)^3}{3} - \cdots$$

A general expression for the charge, in the two-current case, is

$$Q'(t) = Q_1' \cos \omega t - Q_n' \cos(n\omega t + \phi_n)$$

Step-recovery devices are usually operated without idlers, and, for the present, this condition will be assumed.

We have

$$\left[Q'(t)\right]^K = \left[Q_1' \cos \omega t - Q_n' \cos(n\omega t + \phi_n)\right]^K$$

$$= \sum_{L=0}^{K} \left(Q_1' \cos \omega t\right)^{K-L} \cdot \left(Q_n' \cos(n\omega t + \phi_n)\right)^L \cdot (-1)^L$$

Generally, we may assume that $\left(\frac{Q_n'}{Q_1'}\right)^2$ is negligible for $n \geqslant 4$,

$$\therefore \frac{v_c'}{V_{co}'} = \sum_{K=1}^{\infty} \frac{(-1)^{K+1}\left(Q'(t)\right)^K}{K} = \sum_{K=1}^{\infty} (-1)^{K+1} \cdot \frac{1}{K} \left\{ \left(Q_1' \cos \omega t\right)^K - \left(Q_1' \cos \omega t\right)^{K-1} \cdot \left(Q_n' \cos(n\omega t + \phi_n)\right) \right\}$$

The relevant harmonic voltages are

$$v_n' = a_n \cos n\omega t + b_n \sin n\omega t,$$

and

$$v_1' = a_1 \cos \omega t + b_1 \sin \omega t,$$

where:

$$a_1 = \frac{1}{\pi} \int_{-\pi}^{\pi} \frac{v_c'}{V_{co}'} \cdot \cos \omega t \cdot d\omega t$$

$$b_1 = \frac{1}{\pi} \int_{-\pi}^{\pi} \frac{v_c'}{V_{co}'} \cdot \sin \omega t \cdot d\omega t$$

and where

$$a_n = \frac{1}{\pi} \int_{-\pi}^{\pi} \frac{v_c'}{V_{co}'} \cdot \cos n\omega t \cdot d\omega t$$

$$b_n = \frac{1}{\pi} \int_{-\pi}^{\pi} \frac{v_c'}{V_{co}'} \cdot \sin n\omega t \cdot d\omega t$$

The work of Fourier (and others) shows that only the integrals of d.c. cross-products give non-zero integrands; therefore, only these terms need be considered. Similarly, when the power terms are calculated, only the voltage and current terms at the particular harmonic are required, and any other harmonic terms can be ignored.

The analysis of the exponential series is necessarily lengthy and is presented in full in appendix 5.4.2.

The approximations made for the step-recovery diode are:-

1. The exponential capacitance model
2. No forward conduction; if conduction does occur it can be introduced as a correction factor.
3. $(Q_n')^2$ is small; this is proved for $n \geq 4$
4. Certain simplifications are made to the series for terms greater than the nth order to obtain general results. Comparison with accurate values for specific examples shows that the errors are small.
5. $\sin \phi = 1$.

The major results of this part of the analysis are:- (See A.5.5.1)

$$P = n\omega Q_n' \sum_{\lambda=0}^{\infty} \frac{(-1)^{n+1}}{n+2\lambda} \cdot \frac{(n+2\lambda)!}{(n+\lambda)!} \cdot \frac{1}{\lambda!} \cdot \frac{1}{2^{n+2\lambda}} \cdot Q_1'^{\,n+2\lambda}$$

$$a_n = \sum_{\lambda=0}^{\infty} \frac{1}{n+2\lambda} \cdot \frac{(n+2\lambda)!}{(n+\lambda)!} \cdot \frac{1}{\lambda!} \cdot \frac{1}{2^{n+2\lambda-1}} \cdot Q_1'^{\,n+2\lambda}$$

$$Q_1 = \sum_{\lambda=0}^{\infty} \frac{1}{(2\lambda+1)} \cdot \frac{1}{2^{2\lambda+1}} \cdot \frac{(2\lambda+2)!}{(\lambda+1)!(\lambda+1)!} \cdot Q_1'^{\,2\lambda+2}$$

5.4.3 The Bias Point

Ideally, the bias point should be the point at which the charge is half the maximum permitted charge. In the step recovery diode, a number of factors are interrelated in defining this point. If the bias point is too near the forward region, excessive conduction current may flow. If the drive is too hard, reverse breakdown may occur giving rise to a noisy output spectrum. The diode should be operated at a point where the desired multiplication is achieved with the minimum of spurious responses, noise and thermal instability. Very often, a degree of amplitude linearity is also desired. Efficiency, once a major parameter, is becoming less important as advances in microwave power generation are made, although it remains vital in aerospace mobile applications.

Essentially, then, the bias point is a compromise. If the diode has a 'pure' step-recovery action (i.e. no account is made of the variable reverse capacitance) then the efficiency should not be substantially affected by the choice of bias point. In practice, automatic bias is preferred where the drive is sufficient, although external bias may be used at low drives.

It is important to realize that the charge storage capacitance is dynamic. When the diode is operating correctly, the set bias point will be satisfactory; if the operation is slightly off the optimum, the bias point will also shift, possibly causing difficulty in optimisation; again, this is less evident in practice, and the power input and bias can be adjusted with only a relatively small interaction, two or three repetitions of the optimisation of output with the two controls are usually sufficient.

5.4.4 The Normalization factor - Maximum power operation

The Q_o factor is defined at the bias point, so the remarks applying to V_o affect Q_o in the same way. Manufacturers charts for S.R.Ds show a variation in the transition and recombination times with stored charge, so that it is to be expected that an optimum Q_o will occur. If we take the manufacturers recommended maximum charge storage (under limiting conditions) then the Q should be half of this value. However two other limitations can occur. Under extreme drive conditions, the reverse voltage limit may be exceeded, or the dissipated power may cause burnout. In a correctly operated multiplier, the charge storage provides the limit.

5.5. Exponential Two Current Model Of The S.R.D.

5.5.1 Results of the Theoretical Work

The power handled by the diode is

$$P = \omega Q_n' \cdot \frac{1}{2^n} \cdot \frac{Q_1'.A.}{(1-Q_1'^2)}$$

Although the steady state current has been included in this expression, the voltage term was for a single cycle only so it would be more correct to write.

$$P = \omega^2 \cdot Q_n' \cdot \frac{1}{2^n} \cdot \frac{Q_1'^2.A}{(1-Q_1')^2}$$

Similarly, the voltage terms must be multiplied by ω

There is some difficulty in assigning practical values to the S.R.D., as different types have widely varying parameters. However, it is thought that, by remaining in normalized quantities as far as possible, meaningful results are produced. The main problem is the normalisation of the loss resistance, r_s .

In a typical diode,

$$r_s \sim 1\,\Omega$$

and the bias point dynamic capacitance is, say,

$$C_b = 1\,pf$$

If we now take the angular frequency to be

$$\omega = 10^{10} \qquad (1.59\ GHz)$$

$$\frac{1}{\omega C_b} = 100\Omega$$

Hence, at this point, r_s' has the value

(normalized ohms)

$$\underline{\underline{r_s' = .01}}$$

This is a convenient value for calculations, and is used throughout. If we wish to modify the frequency, the bias point capacitance, or the loss resistance for a specific case, then a suitable multiplier of r_s' must be applied; the graphs show the variation of efficiency and output power with r_s'.

The second problem is denormalization of power. It is not easy to estimate the actual charge stored, and, as the function is exponential, any attempts could be in serious error. Two methods to overcome this are available:-

1. Consult the manufacturers data; the possible limitations on the charge are wide.
2. Deduce the value by spectral means (Chapter 6); this is not easy, and again subject to error.

In this chapter we are concerned with general trends, and absolute values are less significant. However, anticipating the results of Chapter 7 it will be shown that the results derived correspond closely with the theoretical predictions.

The accompanying graphs (fig. 5.5.1 & 2) show the efficiency and power output under the specified conditions for harmonic numbers 4 to 10 and for a range of r_s' values. Plots for the input and output impedances are not included as the information should be directly related to specific examples.

Up to this point, the effects of excessive dissipation in the diode have not been considered. The analysis has been based on the limiting curve as the boundary condition, and normalized values have been employed.

Fig. 5.5.1. NORMALIZED OUTPUT POWER vs. NORMALIZED LOSS RESISTANCE 'n' as parameter

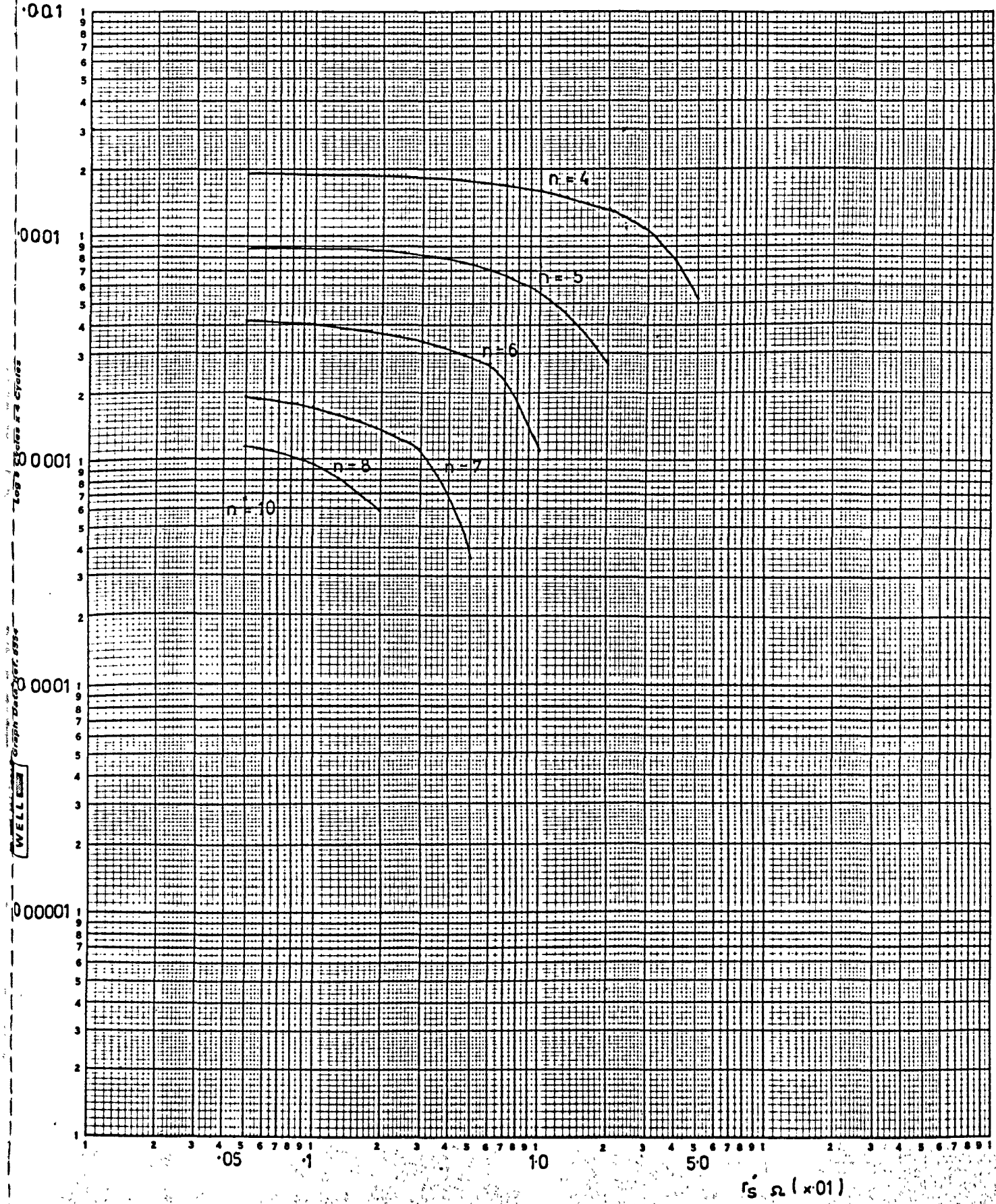

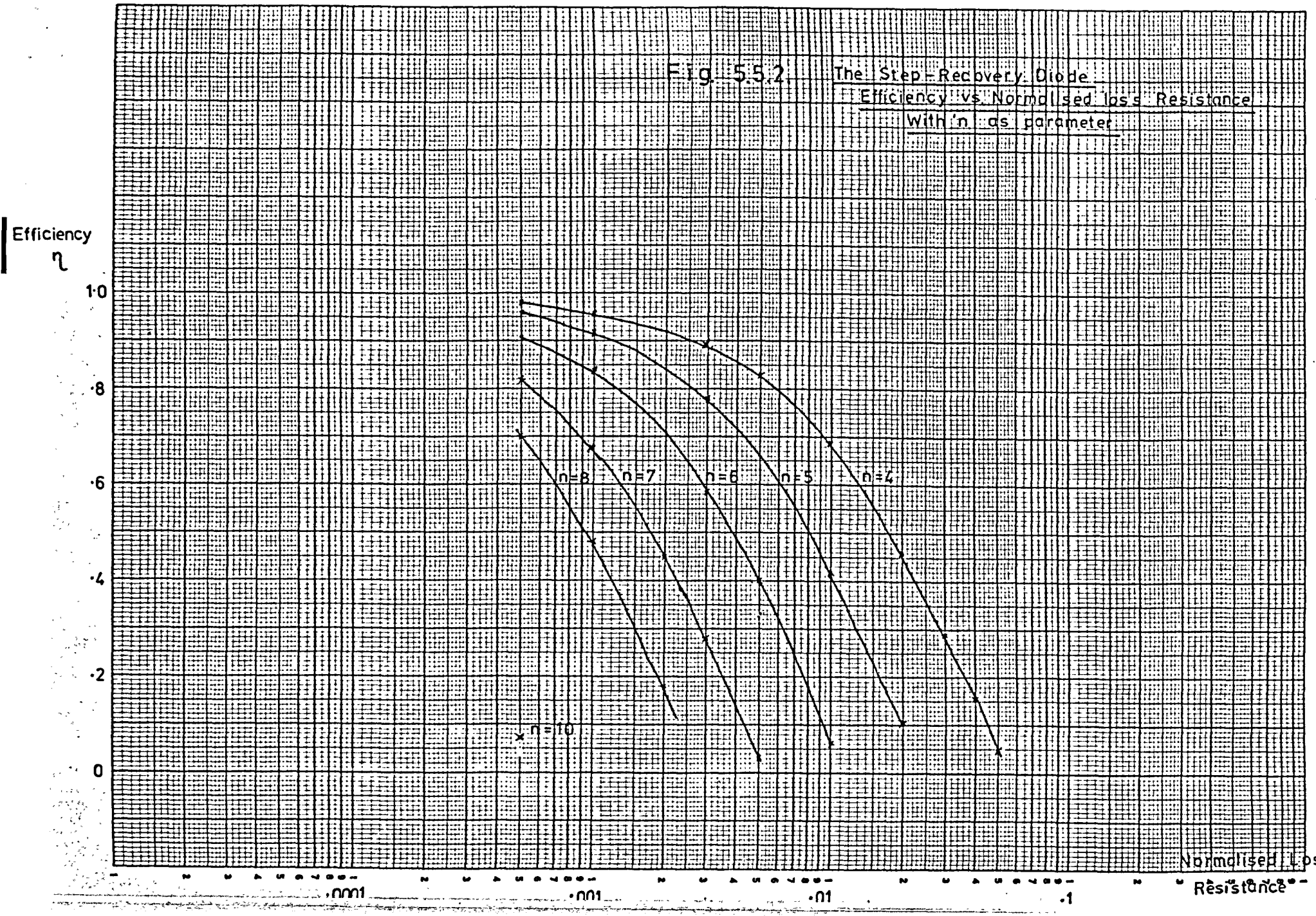

Fig. 5.5.2. The Step-Recovery Diode
Efficiency vs Normalised loss Resistance
With 'n' as parameter

In practice, the device may become dissipation limited, although experience shows that reverse breakdown conditions usually prevail before the dissipation becomes excessive.

5.5.2 Conclusions

1. The normalized results

The theory has produced normalized equations for the power handled by the device, the real and imaginary components of the voltage in the two-current case, and the efficiency. The variable parameter used in plotting the equations was

$$r_s^1 = r_s \omega . c_b$$

which is a modified form of the diode 'Q' factor.

The modification is in the definition of c_b, which is the bias point capacitance. It has been shown that the dynamic capacitance (i.e. the effect of the stored charge) is considerably larger than the static capacitance, and hence c_b is larger than the capacitances used in the usual definition of Q i.e.

$$Q = \frac{1}{\omega . r_s C}$$

The magnitude of c_b can be estimated from the total charge stored, and the forward voltage excursion, which is approximately equal to V_B.

Then: $$2Q_o = (2V_B).C_{max}$$

and

$$Q_o = V_b . C_b$$

$$C_{max} = C_b . \exp\left(\frac{2V_B}{V_b}\right)$$

$$\therefore \quad 2V_b . C_b = C_{max} . 2V_B$$

$$\therefore \quad \frac{V_B}{V_b} = \frac{C_b}{C_{max}}$$

$$\therefore \quad \frac{V_B}{V_b} = \exp\left(\frac{2V_B}{V_b}\right)$$

$$\therefore \quad \underline{\underline{V_b = 2 . V_B . (0.87)}}$$

V_B = Rev. breakdown limit
V_b = bias voltage
C_b = " capacitance

The bias point voltage, V_b, is determined from the boundary condition when the forward excursion is equal to the reverse breakdown; V_b is 1.74 x V_B above the reference point of - V_B, so it is evident that the bias point is at 0.74 x V_B volts above zero.

It is at this point that the practical results are likely to show greatest deviation from theory. The assumption of a forward voltage of equal magnitude to V_B is optimistic, and would usually lead to appreciable forward conduction. Most frequency multipliers are operated at an effective bias point between 0v and 5v. In the series of multipliers constructed, V_b was measured only as an incidental factor to the power output. The bias current, i.e. the forward conduction in the diodes due to rectification, was monitored and was not permitted to represent more than a small part ($< 5\%$) of the total power input.

It is necessary in the analysis to account for the charge stored, as a measure of the dynamic capacitance. The values were taken from the manufacturer's data sheets, as suitable measuring equipment was not available. The selection of a diode depended to a large extent on this stored charge, and the r_s and c_b of the junction,

2. It is evident that the efficiency and the power output improve for low orders of multiplication and for low r_s However, we have assumed that no rectification takes place, or that rectified power is subtracted from the input power. Rectification takes place when the switching time (i.e. the reciprocal of input frequency) is comparable to or greater than the diode lifetime τ_t.

At low frequencies the efficiency falls due to rectification. If attempts are made to reduce c_b, the tendency will be to reduce the stored charge. Finally, if the diode area is increased, to reduce r_s, then c_b will be increased, so that optimum diode structures can only be a compromise of potential advantages and faults. The equations derived would enable a diode designer to optimise the parameters of a device for specified operating conditions.
To support the theoretical work, a practical project was undertaken with commercial diodes, and a thorough study of their characteristics was made. A two-diode arrangement was selected, operating as a x5 multiplier, about a centre frequency of 1.56 GHz. The predicted results for this circuit are :-

Diode Type	HP 5082-0386	2 off
Bias point capacity	4 pf.	(combined - see Chap. 6)
Loss resistance (in parallel)	0.5	
Max. Power	3.6 W X 2	
Stored charge	200 pc - 1400 pc	(both)
D enormalization factor (see Chap. 7)	$\sim$ 50 Ω	

The $\pi r_s'$ (normalized loss resistance) is approximately .02 which corresponds to 30% efficiency, in reasonable agreement with previous predictions for these diodes (ref. Burckhardt, and application note AN920).

Therefore, in the ideal case, the bias point voltage would be 0.87 times the total voltage excursion. Practical considerations (of non-ideality) usually override this. Furthermore, the assumption of a maximum forward excursion of only ϕ volts does not fit with the previous statements about ϕ; it is merely a convenient reference, which indicates the magnitudes involved.

Typically, then, $V_B + \phi = 30v$, and hence $0.87 \times (V_B + \phi) =$ 26 volts. If the stored charge is 100 pC at V_b then

$$Q_b = C_b . V_b \quad \text{(dynamic)}$$
$$\therefore 100pC = C_pF \times 26$$
$$\therefore C = 4pF$$

Thus, very approximately, the dynamic capacitance has been calculated at the bias point from the knowledge of the stored charge only.

The normalized output power is

$$\omega \times 0.00028.$$

If we assume a bias point charge of 200 pc per diode (a relatively low drive) then

$$P = \omega \times 0.00028 \times 400\ pC$$

$$P = 10^{10} \quad 2.8 \times 10^{-4} \times 4.10^{-10} \qquad \text{at } w = 2\pi F$$

$$P = 1.12\ mW \qquad = 2\pi \times 1.56\ GHz$$

$$\sim 10^{10}\ Hz$$

The input and output impedances under the same conditions are:-

Rn'	= 0.258	$\therefore$	Rn	= 12.9 − 0.5	=	12.4 ohms
$I'mn$	= 2.050		Imn	= 102		102 ohms (capacitive)
R_1'	= 0.316	$\therefore$	R	= 15.8 + 0.5	=	16.3 ohms
$I\,m_1'$	= 1.164		Im_1	= 58	=	58 Ω (capacitive)

Details of the derivation of results are included in Chapter 7. The impedances predicted should be reasonably accurately matched. Without tabulating the results in detail, it may be said at this point that, at an output level of approximately 1 mW, i.e. ~ 1.5 mW at the diodes, the input impedance of 13 ohms was measured, and, on a later version using 50 ohm terminations, the power output peaked at 4 mW, which corresponds to twice the drive quoted in the example, i.e. for the input and output resistances of 63 Ω and 51 Ω . Hence, it may be said that the experimental results are in very good agreement,

within the limitations of the measuring techniques, with the theoretical predictions.

3. Variation of Efficiency with Drive.

There is a fundamental limitation imposed by the diode in the amount of charge it can store. Consequently, as the power levels in the diode approach this limit, the power output saturates, and the efficiency falls as the input power increases.

This is in agreement with the predictions of Burckhardt,[5] and with the experimental observations.

6. EXPERIMENTAL ASSESSMENT OF HARMONIC GENERATING DIODES

6.1 Introduction

It is essential in any experimental investigation to have a thorough knowledge of the physical parameters of the devices and the circuits used. Very often, some form of low-frequency simulation may also be helpful. Many research workers have characterised their devices using the S-parameters, usually obtained on a swept-frequency or an automatic instrument. Obtaining such information is costly in equipment, and is usually of limited value when the devices are to be driven at significantly higher powers ('S' parameters are usually measured at 1 mW or 10 mW). While high power impedance parameters could be measured on a point-by-point basis, it was felt that in many cases, a spectral technique would give more useful information.

In this chapter static measurements, low frequency simulations and microwave measurements of the diodes are discussed. The 'static' parameters of the diode are obtained from the capacitance-voltage and current-voltage plots. These are then used to compare the diodes and to identify the types and their doping profiles.

The dynamic, in-circuit measurements give a useful indication of the device parameters i.e. charge stored, charge storage time ('step' speed) and the breakdown point. A theoretical section and illustrations show the output signal levels expected. Few devices show spectra which can be characterized and explained by a single mechanism. In general, a step-recovery diode will show some small amount of rectification, which depends on the frequency of operation and the recombination time, and, conversely, one expects some charge storage to occur in rectifiers, especially when operated at frequencies above their normal range.

6.2 The Static Measurements

6.2.1 The Current-Voltage Characteristic

The normal type of diode transistor curve tracer is useful for this purpose. A typical characteristic is shown in fig. 6.2.1. Point-by-point plotting involves excessive dissipation in most diodes when high forward currents are applied. The slope resistance at high current may be taken as a measure of the diode loss resistance; obviously this is a variable factor at microwave frequencies, changing both with drive and frequency. Studies have shown (Motorola AN 920) that the loss resistance of a typical SRD changes over the cycle of operation.

A typical step-recovery diode, which was used in the final multiplier, was the HP5082-0386. The I-V plots for this diode are shown in fig. 6.2.2. The average loss resistance deduced was ($.75 \pm .05$).

6.2.2 The Capacitance-Voltage Characteristic

Variable capacitance devices were to be the main topic of this project, and it was soon considered essential that an accurate measurement instrument for the C-V characteristics was needed. A semi-automatic measurement system had been constructed by another member of the department, (P.G. Martin) and the principles of operation of this instrument were adapted to suit our particular application. The operation of the instrument and the circuits employed are discussed in appendix 6.2. A series of plots (in the appendix, A6.2.2/12) shows a range of diodes designed for different applications. Transistor junctions were also examined, and exhibited characteristics different

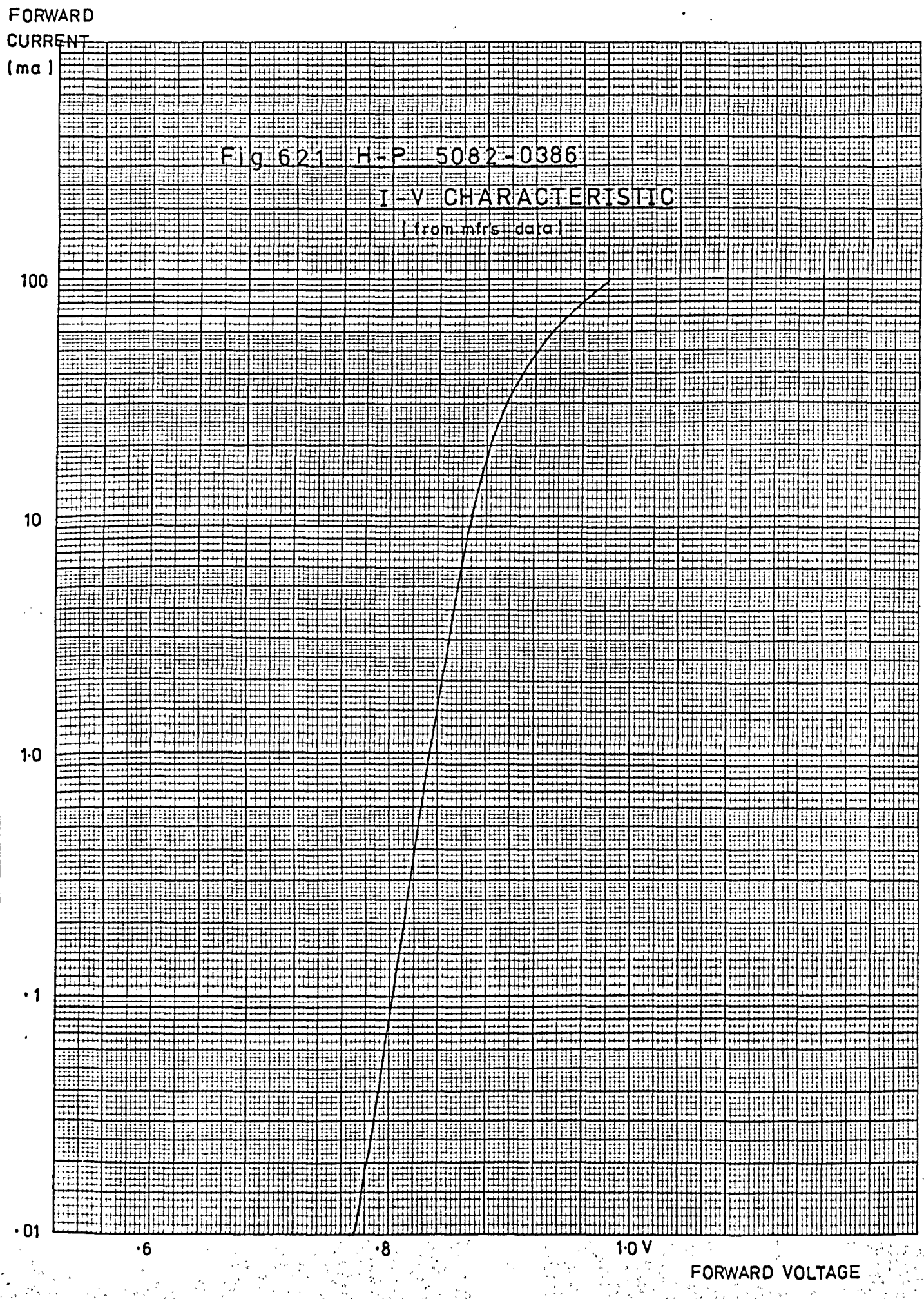

Fig 621 H-P 5082-0386
I-V CHARACTERISTIC
(from mfrs data)

from the usual diode law, due to their planar structure. Harmonic generation in planar devices shows properties similar to abrupt junctions at low drive levels and graded junctions at higher levels. Each type of diode, junction, point contact, transistor, zener, SRD has a characteristic C-V plot, which does not vary significantly between devices of the same type.

Several authors have shown that C-V plots can be used to determine the doping profile of the device (Coerver[7]), provided that a near Schottky barrier is assumed at the junction (i.e. one side of the junction is so heavily doped as not to effect the capacitance). When this assumption is valid, non-destructive diode tests may be carried out to check the doping process. The C-V plot can, with careful measurements, yield an accurate result for the diode static non-linearity factor, γ. Measurements of a wide range of production diodes were made, but only two types showed hyperabrupt ($\gamma > .5$) behaviour (ITT BA 141, 142). In both cases, the γ was approximately 0.6 for a part of the range, and it was not considered worthwhile to construct a multiplier with these relatively lossy devices. One manufacturer (Motorola) produces tuning varactors with γ of around 2.1; this is too far from the ideal value near unity to be of great use in a multiplier, though it has been used successfully in a divider, (McConnell).

6.3 Harmonic Spectra-Theoretical Background

A relevant selection of diode voltage or current waveforms, with the corresponding Fourier coefficients, are shown in figs.A 6.3.1 - 3), in the appendix.

The two most important waveforms in this context are the biassed half-wave rectifier and the triangular pulse.

6.3.1 The biassed half wave Rectifier

This analysis differs from that used in fig.A(6.3.2) in that a constant amplitude is assumed.

Let the maximum amplitude of the signal (voltage or current) be unity, and let the bias be A = Cos θ (See fig.A6.3.3.) (a)

The Fourier spectrum is

$$F(x) = a_0 + \sum_{n=1}^{\infty} a_n \cdot \cos nx$$

(even function)

where

$$a_0 = \frac{1}{2\pi} \int_{-\pi}^{\pi} F(x) \cdot dx$$

$$a_n = \frac{1}{\pi} \int_{-\pi}^{\pi} F(x) \cdot \cos nx \cdot dx$$

The solutions are found to be

$$a_0 = \frac{\cos\theta'}{\pi} \left\{ (\pi - \theta') \right\} + \left\{ \frac{\sin\theta'}{\pi} \right\}$$

$$a_n = \frac{1}{\pi} \left(\frac{-2\cos\theta' \cdot \sin\theta'}{n} + \frac{\sin(n+1)\theta'}{n+1} + \frac{\sin(n-1)\theta'}{n-1} \right)$$

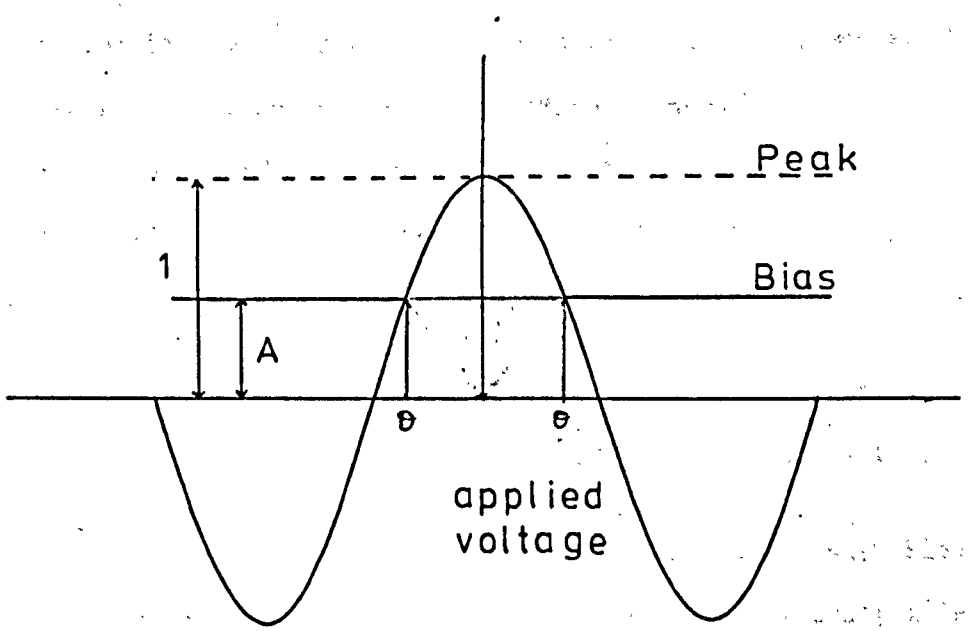

The biassed Half-wave Rectifier - time domain

fig. 6.3.3.a

The values of a_n show maxima and minima at $\theta = \pi/n, 2\pi/n$ etc. The solution $\theta' = \pi/2$ is a maximum for even harmonics and a minimum for odd harmonics. The spectrum analyser, or in the case of low-frequency measurements, the wave analyser can give no phase information, so that voltage maxima and minima both appear as peaks. Hence, there is some interest in the zeros of the expressions, the positions of which indicate whether the action is purely resistive or partly reactive in a given case. The coefficients a_n are tabulated for a range of θ' values in fig. A(6.3.4.). The same information is presented graphically in fig. A(6.3.5).

Practical measurements on a rectifier specified by the manufacturer for up to 50 KHz operation were made, (figs. A.6.3.6 - 10).

Three main parameters were considered as the variables, the drive, the bias and the frequency. These are not fully independent variables, but under chosen conditions their effects can be seen separately.

6.3.2 Interpretation of the Theoretical Predictions

The theory shows that, for a half-wave rectifier, the bias determines whether the odd harmonics are present or not. As the bias tends to zero ($A = \cos\theta'$ tends to $\cos\pi/2$), the amplitude envelope of the

harmonics is very wide. With an increasing bias, the envelope varies less rapidly until, at a conduction half angle of $\pi/6$, there is only a shallow dip in the curves at the 9th harmonic. In practice, few instruments can handle the dynamic range needed for this measurement, and so a limit was set at the 8th harmonic. The minima on the predicted amplitude plot occur in the region of the zeros of the $\cos n\theta$ function, so that, as phase information is lost in the measurements, careful interpretation is needed. Non-ideality, in the slowing down of the sharp transition from reverse to forward bias, is present in all diodes due to the junction capacitance, but in certain diodes actual step-recovery occurs. The presence of stored charge in the junction is the critical factor, for if this occurs, the diode exhibits 'step recovery'. A more involved theory is required to describe the process, as very often we are faced with a combination of rectification, multiplication and step-recovery action.

6.3.3 Measurements at low Frequencies-Rectification

A 1N4002 diode was chosen as an example of a rectifier with no measurable step-recovery action. The harmonic amplitudes are shown in figs. A636-10. These curves are included as references for comparison with later microwave measurements. The diode type used employs very heavy doping on one side of the junction, and is therefore similar to the Schottky microwave diodes. At a frequency of 1MHz, the diode was not suitable for harmonic generation, as the parasitic capacitance absorbed most of the switching power. Even at 100 KHz the harmonic content was low. The lowest frequency gave the highest harmonic content; this is characteristic of rectifier action.

6.4. The Step-Recovery Diode - Low Frequency Measurements

6.4.1. Introduction.

A number of authors have set up low frequency models of the SRD. An attempt was made by the author to repeat the experiment of Kotzebue (fig. 6.4.3). The switching device was a high speed read relay, driven by a transistor switch operated by the applied a.c. field. The output waveform was approximately correct, but the model made too many assumptions about the diode, in particular, the switching was just too good to compare to the real case. The circuit is not recommended as a useful model for theoretical considerations, and in addition contact bounce was a serious problem.

For a number of years after the introduction of solid state rectifiers, a major problem was the charge storage effect. Tests on a range of diodes showed that this effect had by no means been overcome, and about 30% of mains rectifiers exhibited charge storage to an appreciable degree at frequencies above their normal operating range. A particularly good example of such a diode was the IN4719, described by the manufacturer as a high surge current rectifier. A series of oscilloscope photographs was made which illustrated the step-recovery process in a single and two-diode arrays. Unfortunately, the wave analyser available at the time was limited to a minimum frequency of 1.5 KHz, so that corresponding frequency domain measurements could not be made over a useful range.

The two series of photographs presented in fig. (6.4.1) illustrate many of the salient features of the general broad-band step-recovery multiplier.

15 Hz

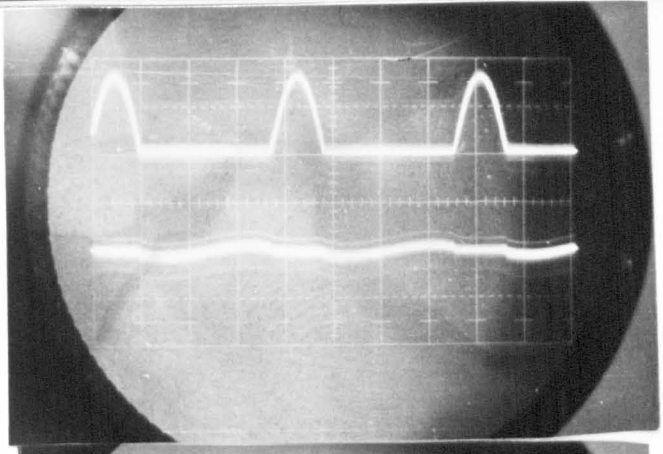

6.4.1. 50Hz

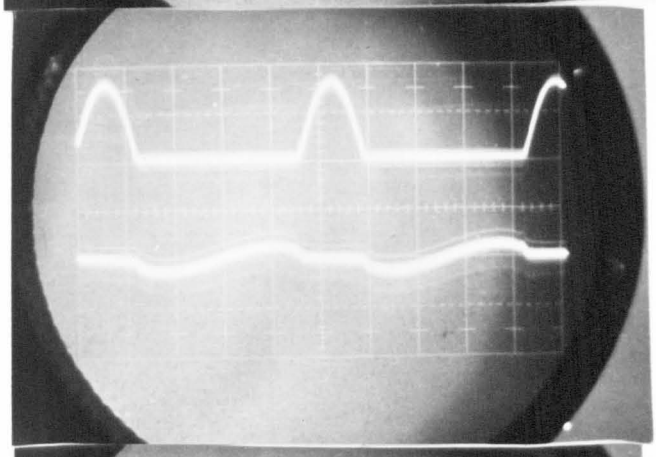

Step recovery diode

Frequency multiplier

(current upper trace,

voltage lower)

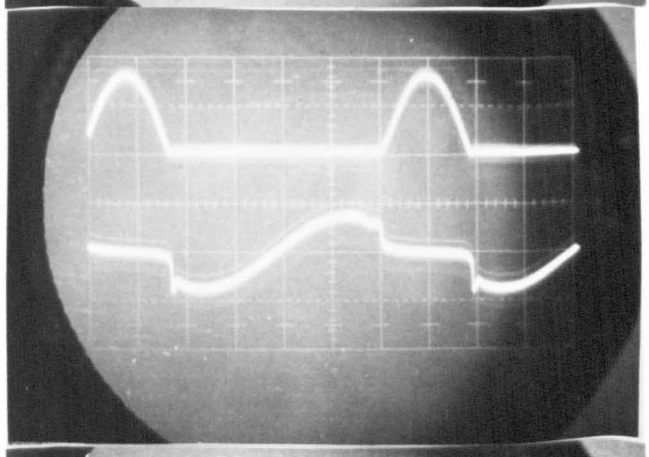

100 Hz

300 Hz

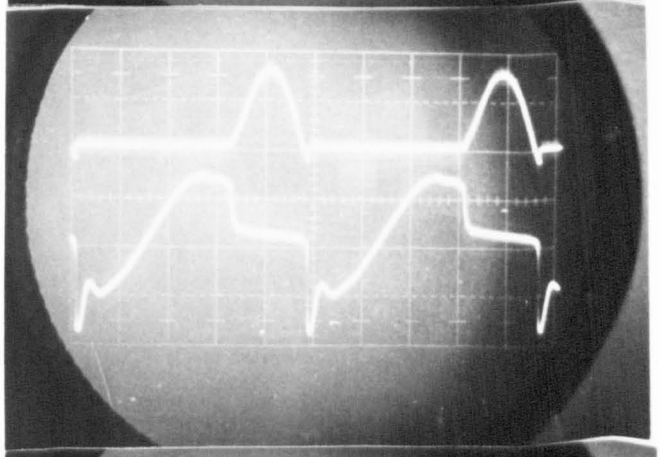

1 KHz

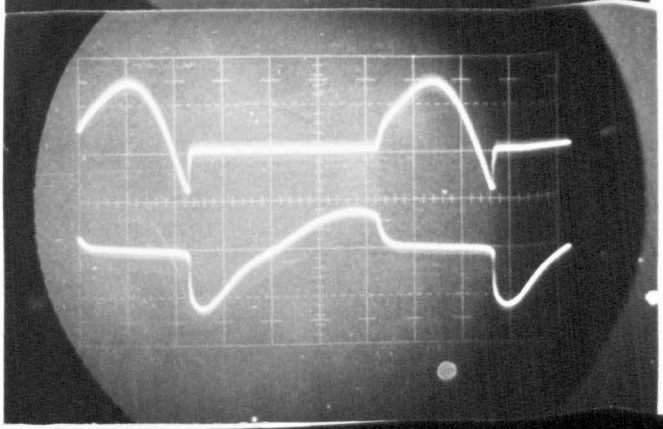

6.4.1.

3 KHz

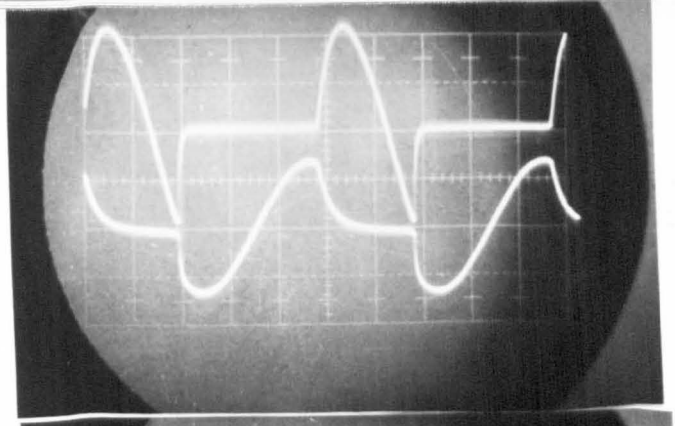

10 KHz

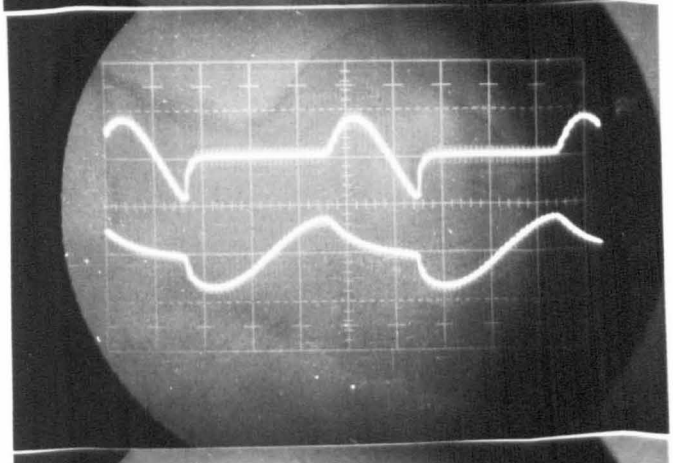

20 KHz

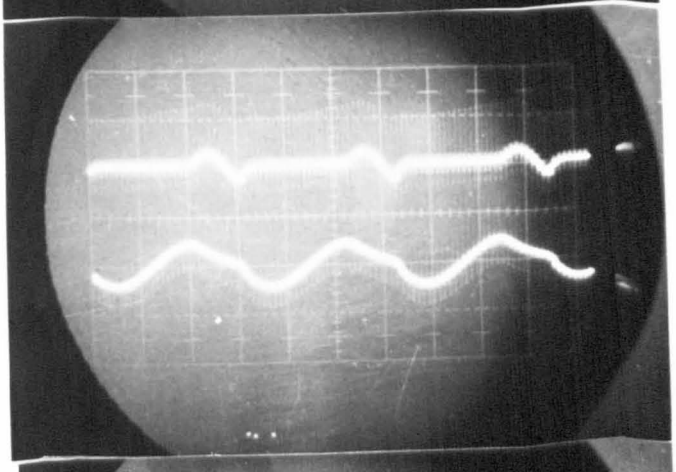

30KHz

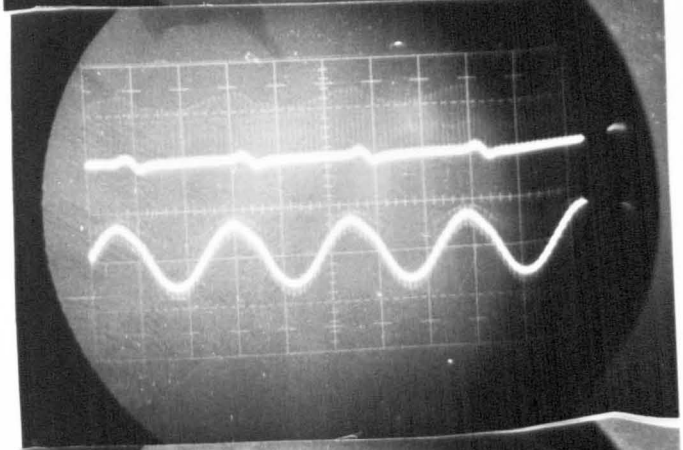

40KHz

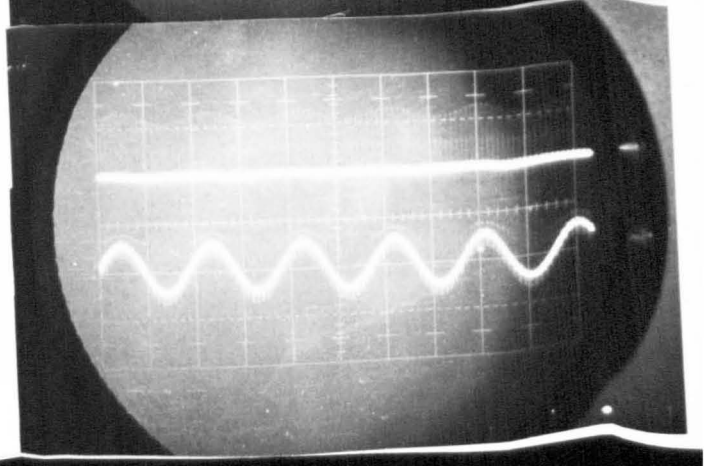

50Hz

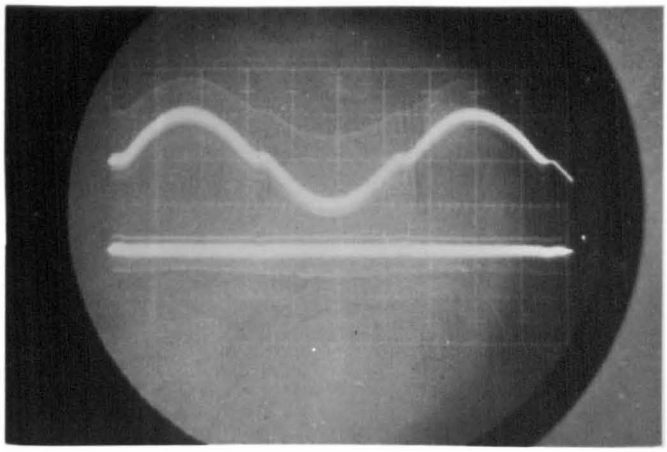

6.4.1.

Double Step-
Recovery diode
Frequency
multiplier

100Hz

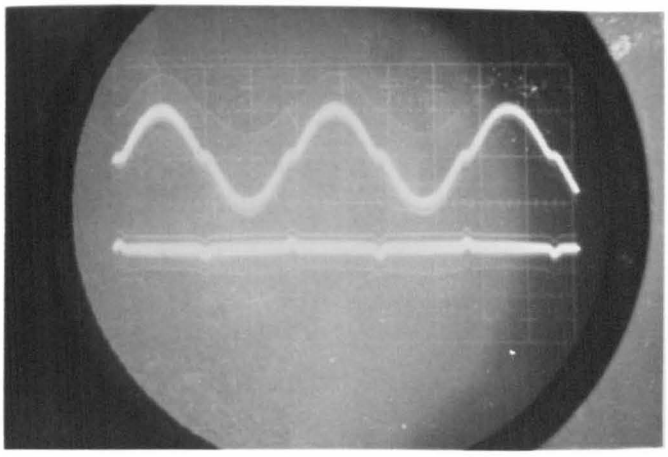

(current upper
trace, voltage
lower)

300Hz

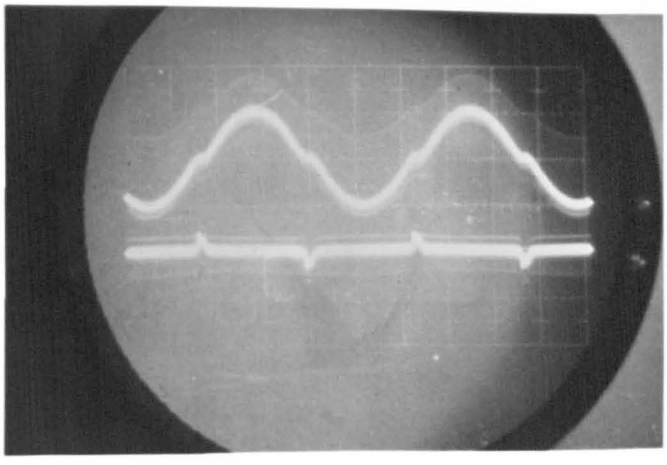

1KHz

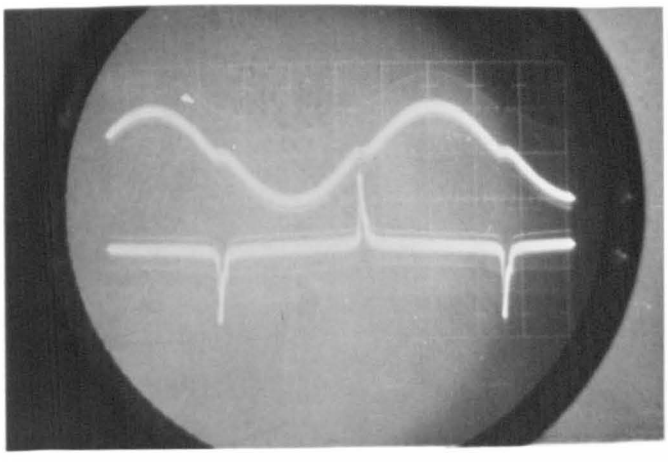

3 KHz

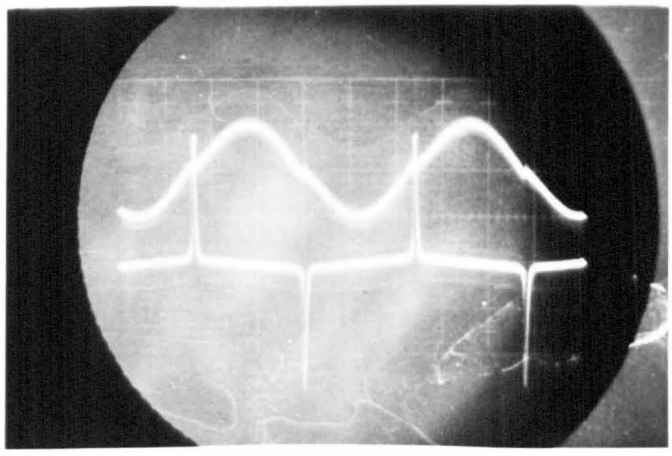

6.4.1.

10 KHz

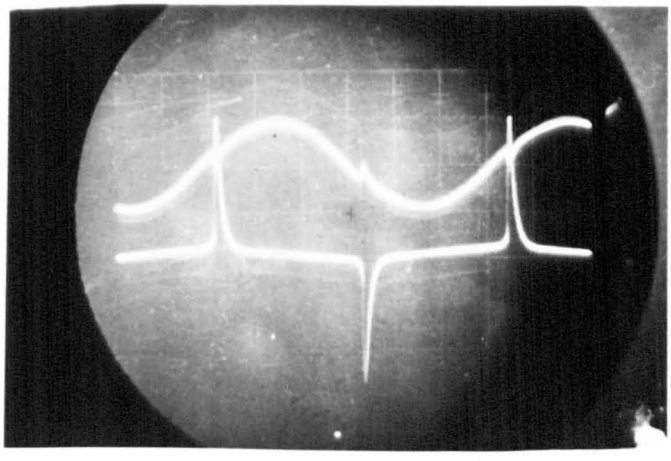

20 KHz

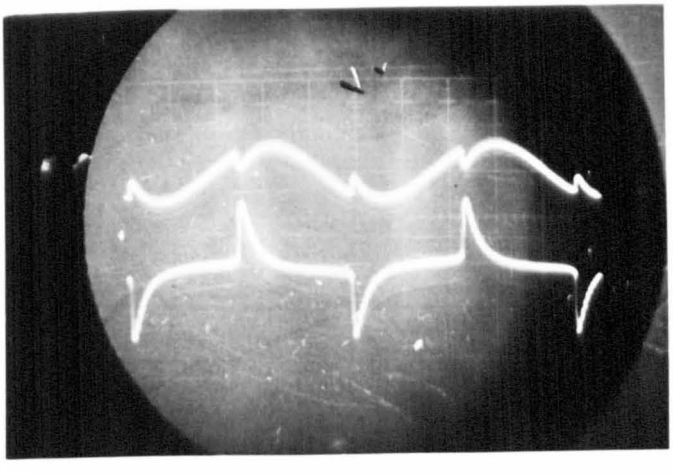

30 KHz

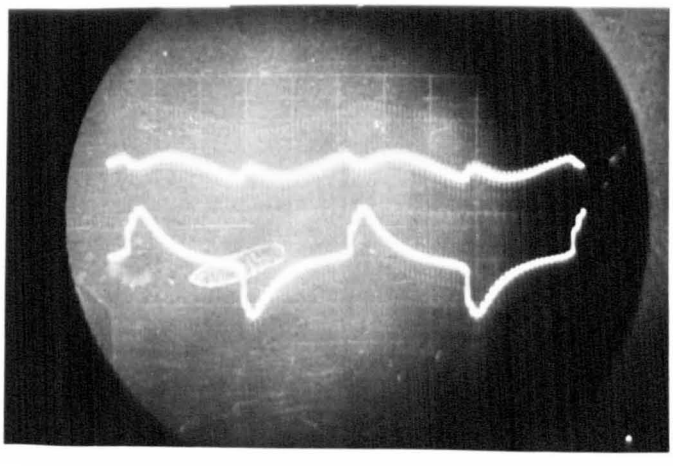

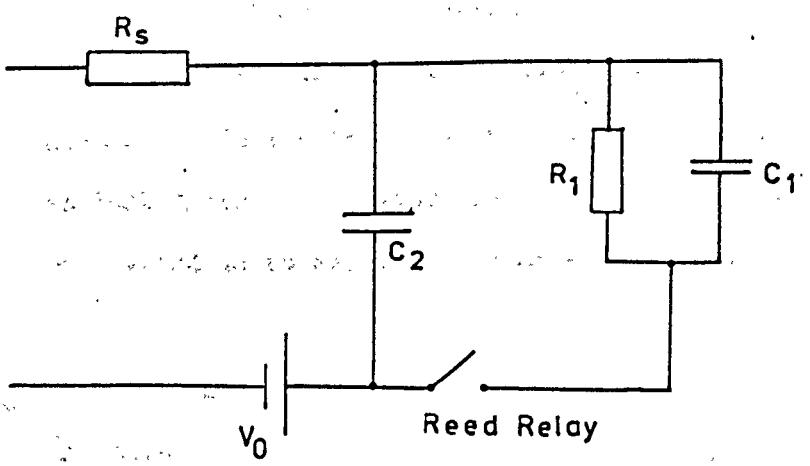

Fig. 6.4.3 Kotzebue's Simulator

The experimental arrangement is shown in fig. (6.4.2). The choke prevented high frequency effects from distorting the oscillator waveform; in practice it could be shorted with only a small amplitude change, and no apparent effect on the process. A capacitor of 0.1 uF blocked d.c. paths around the load and source, so that the bias was only due to diode leakage. External bias resistors reduced the amplitude of the output pulse. The 50 ohm load was chosen arbitrarily, as the impedance. The current measuring resistor, of 0.5 ohms, was a compromise between low circuit losses and reasonable sensitivity of measurement. In the two diode arrangement, the diodes were connected back to back directly. Later microwave measurements showed that isolation was needed as parasitic inductance could set up spurious resonances.

The analysis of the photographs is tabulated in the appendix. An input of approximately 8 volts peak-to-peak was applied, with the gain on the oscilloscope adjusted to produce reasonable displays.

6.4.2 The S.R.D. Spectral Analysis Model at low frequency

The photographs (fig. 6.4.1) show that the triangular pulse of fig.A(6.3.3) is a very good approximation for the untuned step recovery diode frequency multiplier. The voltage coefficients are:-

$$a_0 = \frac{E\,(y+z)}{4\pi}$$

$$a_n = \frac{E}{\pi n^2 yz}\left[(y+z)\cos ny - z - y.\cos(y+z)\right]$$

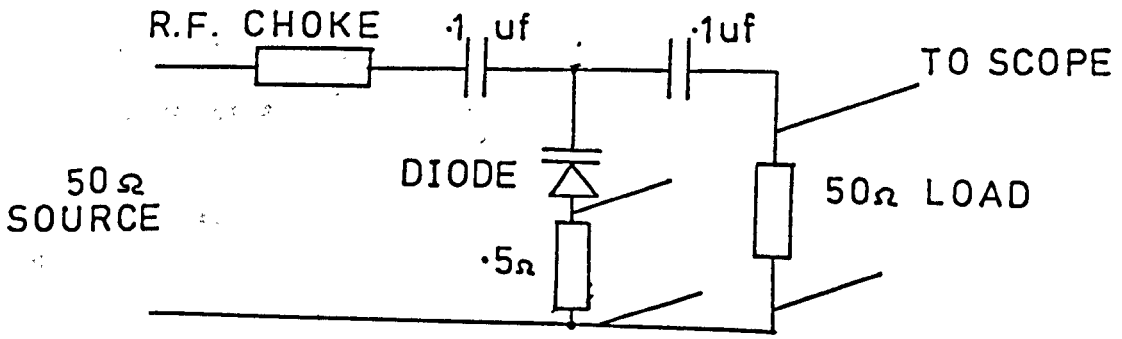

PULSE TEST CIRCUIT

Fig. 6.4.2.

$$b_n = \frac{E}{\pi n^2 y z} \cdot \left[(y+z) \sin ny - y \sin (y+z) \right]$$

for a single diode.

The parameters y and z are constants of the device and circuit, respectively, the transition time and the risetime of the L-C-R circuit formed by the driving inductance or resistance (50Ω) and the diode capacitance.

From the results obtained, we can put:-

$$y \sim 2\mu \text{ Sec}$$
$$z \sim 5\mu \text{ Sec}$$

for the IN4719.

The optimum frequency for multiplication was found to be between 3KHz and 10 KHz for the IN4719. It appears, then, that for multi-octave operation the transition time associated with the diode must be at least an order of magnitude faster than the highest frequency it is expected to generate. If the harmonic multiplication factor is greater than about 4, a speed of two orders of magnitude faster would be preferable.

6.5.1 The S.R.D. - Spectral Analysis Model at H.F.

The terms low and high frequency are related more to the diode and its associated circuitry than to the absolute frequency (Penfield and Rafuse). In the high frequency domain, a model more suited to the step-recovery transition is the periodic part-sinusoid, which is developed below.

When an instantaneous pulse is applied to a damped resonant circuit, the waveform is modified to a half-sinusoid of width

$$t = \pi\sqrt{L\,C_{VR}}$$

Usually, sufficient damping is present to suppress high amplitude ringing. The main deviation from the ideal impulse is the turn-off transient, which is due to the finite transition time. However, in many examples, it is reasonable to assume that the main effect is the half-sinusoidal pulse characterised below.

The assumed voltage waveform is illustrated in fig. (6.5.1).
The Fourier series is an even function, i.e.

$$F(x) = a_0 + \sum_{n=1}^{\infty} a_n \cos.nx$$

$$a_0 = \frac{1}{\pi}\int_0^{\pi} f(x).\,dx$$

$$a_n = \frac{2}{\pi}\int_0^{\pi} F(x).\cos nx.\,dx$$

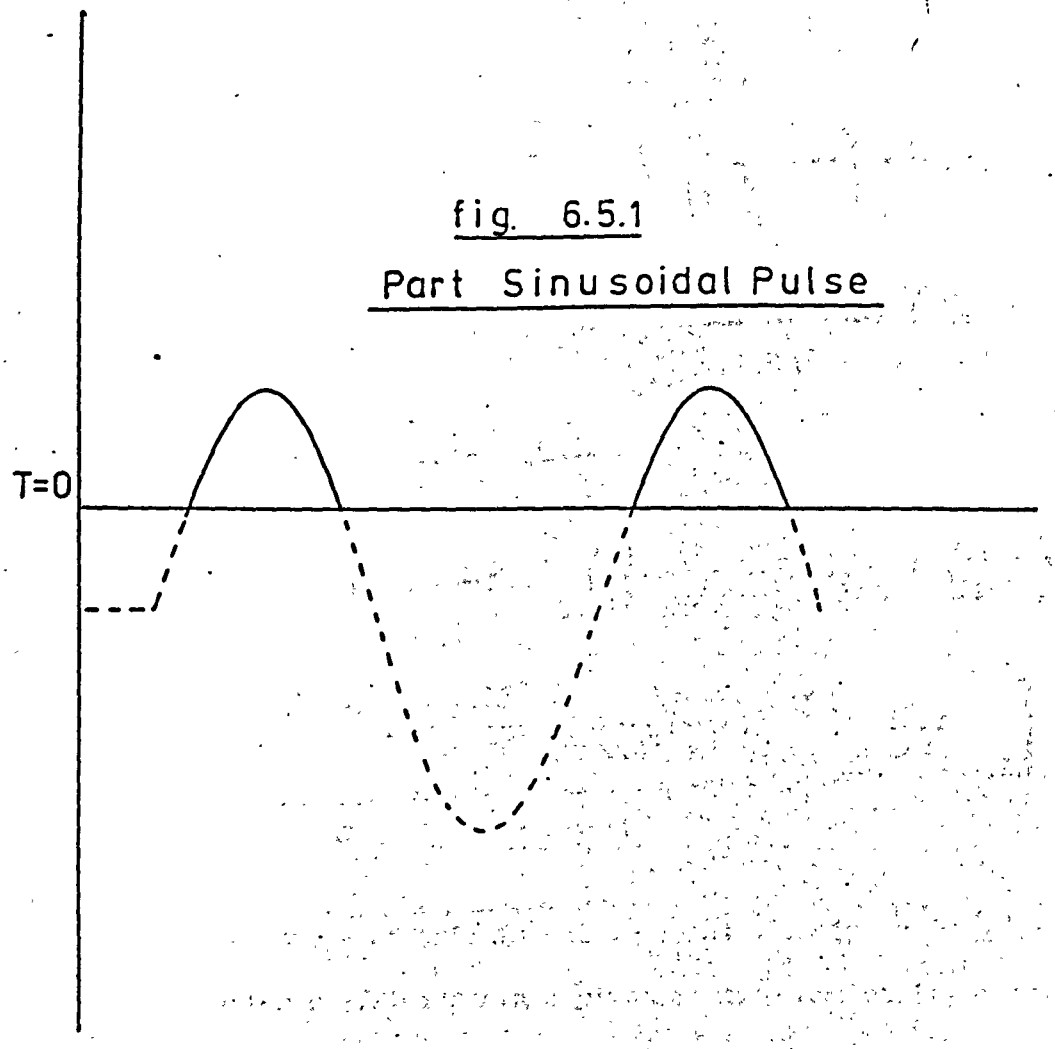

fig. 6.5.1

Part Sinusoidal Pulse

If the sinusoid has a period tp, and a repetition frequency f_i we have.

$$f(x) = -\cos \frac{1}{2t_p f_i} . x \qquad \frac{t_p}{2} > x > 0$$

$$f(x) = 0 \qquad x > |t_p/2|$$

Hence

$$a_o = \frac{-4\, t_p f_i}{\pi}$$

and

$$a_n = \frac{-2}{\pi}\left[\left(\frac{1}{\frac{1}{2t_p f_i} + n}\right) \sin\left(\frac{\pi}{2} + n\pi t_p f_i\right) + \frac{1}{\left(\frac{1}{2t_p f_i} + n\right)} \cdot \sin\left(\pi/2 - n\pi t_p f_i\right)\right]$$

or, if we put $N = \frac{1}{2 t_p f_i}$

$$a_n = \frac{-2}{\pi}\left[\left(\frac{1}{N+n}\right) \cdot \cos\frac{\pi n}{2N} + \left(\frac{1}{N-n}\right) \cdot \cos\frac{\pi n}{2N}\right]$$

$$\therefore a_n = \frac{-2}{\pi}\left[\left(\frac{2N}{N^2-n^2}\right) \cdot \cos\frac{\pi n}{2N}\right]$$

$$a_o = \frac{-2}{\pi} \cdot \frac{1}{N}$$

The shape of this function is the classic $\sin x/x$ curve, and the Fourier coefficients in a given example are easily computed.

The zeros of the a_n function occur at

$$n/N = 2y + 1 \qquad y = 0, 1, 2 \text{ etc}$$

The spectrum analyser is not phase sensitive, so that inversion of the negative going components, occurs. The curve predicted is then in a form similar to a pulse spectrum and consists of a series of minima,

separated by intervals where

$$^{n}/_{N} - 2_{y}$$

The general shape of this spectrum is illustrated in fig. A(6.5.2).

6.5.2 Spectral Analysis at Intermediate Frequencies

There are some advantages in driving a microwave diode at frequencies as low as 15 MHz, in particular because of the possibility of measuring accurately harmonics as high as the 20th. The application envisaged at this stage was the high-order 'comb' generator, reaching into the VHF and low microwave bands. The apparatus used is outlined in fig. (6.5.3. a, b). The simplest format (a), was very inefficient, with an insertion loss of more than 30 db. Fig. (6.5.3.b) had very low total insertion loss, around 5db, overall, and corresponded closely to the type of circuit often used. The diode used was a Ferranti ZC51E , a general purpose low-power SRD. An Airmec wave analyser was used as the detector, with an effective dynamic range of 55 db; in practice, signals of more than 40 db below the fundamental were rejected to avoid cross-modulation errors.

The harmonic spectra measured are illustrated fig. A(6.5.4). The input frequency was 22.8 MHz, tuned by the parallel circuit.

Several important features of the step-recovery operation were deduced from the plots. At the lowest level the drive was not sufficient to produce significant charge storage, and the harmonic spectrum was generated by rectification and varactor action.

Fig. 6.5.3. The SRD driven at 23 MHz

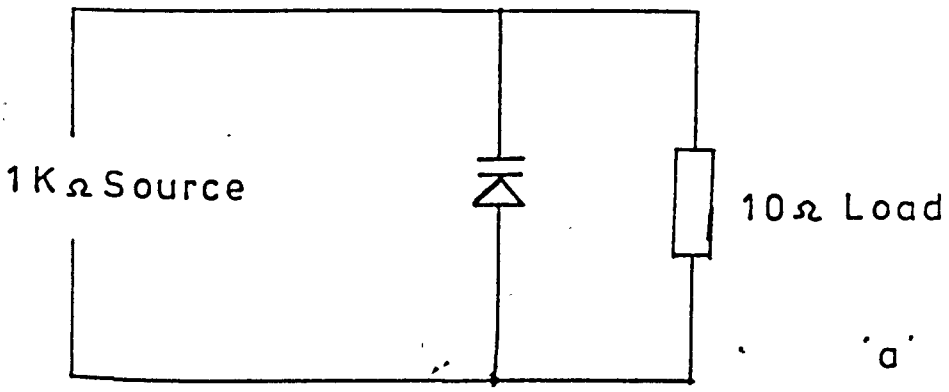

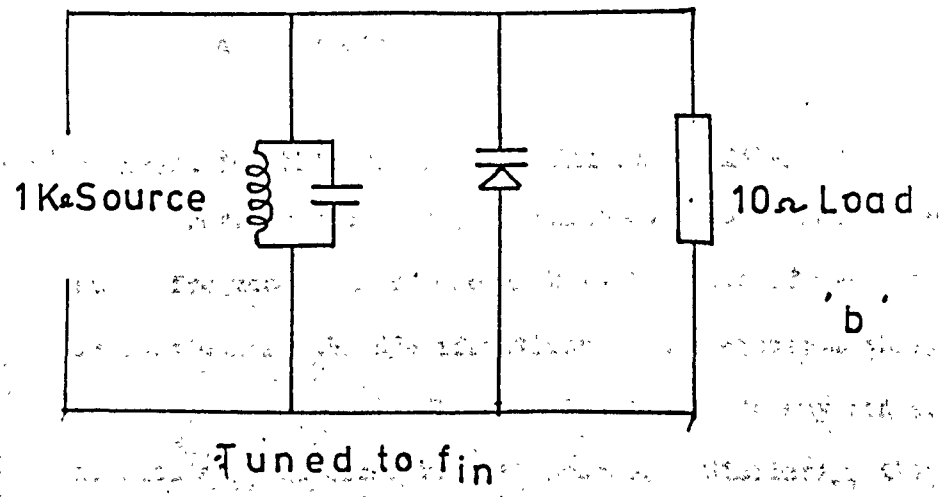

Although the spectrum was relatively flat, the efficiency of generation was low. At the 40 db drive level, the spectrum was characteristic of the step-recovery diode; the zeros occurred, at the 3rd, 5th, 7th, 9th and 11th harmonics, exactly as predicted by the theory when

$$n/N = 3, 5, 7 \text{ etc.}$$

According to the theory discussed in 6.5.1., we expect from these results that

$$N = 1$$

We have

$$N = \frac{1}{2\, t_p . f_i}$$

and

$$f_i = 23.10^6$$

$$\therefore \quad \underline{t_p = 22 \text{ nS}}$$

In the circuit used, this represented a very reasonable estimate of the pulse duration. This diode was capable of a fastest risetime of only about 1 nS. As the drive was increased, the spectrum was modified to longer pulse lengths, up to about 26 nS corresponding to more charge storage in the diode.

6.5.3 Spectral Analysis - Microwave Frequency Measurements

Spurious resonances or large changes of insertion loss over quite small frequency ranges are a characteristic of many instruments. In particular, the specifications of the Spectrum analyser showed that the response was only flat to within 3 db on any range, and there could be as much as 8 db error between ranges. Similarly, the directional couplers varied by $\pm$ 2db over each frequency range covered;

it was necessary to use two couplers, and at some frequencies, to operate in uncontrolled coupling regions. After a number of unsatisfactory attempts to calibrate the equipment, a comparative technique was evolved. A block diagram of the equipment is shown in fig. 6.5.5.

6.5.4. The Comparison Technique

The major concern in a spectral analysis must be the accuracy of each harmonic when other harmonics, and possibly spurious frequencies, are present at high levels. The main difficulties were the very low power levels involved, the limited dynamic range of the spectrum analyser, and the presence of the spurious outputs in the source. The Ferranti crystal controlled oscillator-multiplier was filtered and attenuated to provide a stable, clean output of easily adjustable level. The spectrum analyser was connected to position 1, to monitor the spectral purity of the source. The broadband directional coupler was calibrated at the source frequency (1.56 GHz).

The key element in the system was the 50Ω coaxial switch. A manually-operated 4-port Decca type, which was specified to 8 GHz, was used. The switch was mechanically symmetrical, and it was necessary to assume that this assured electrical symmetry. When a very small signal was to be measured in the presence of a set of much larger ones, a preselector, which ideally only passed the required signal, greatly improved the available sensitivity. The Tektronix 1L40 was specified for 46 db dynamic range; if this was exceeded, spurious responses were generated. The addition of a preselector protected the input to the

Fig. 6.5.5. Spectral Assessment-
The Comparison method

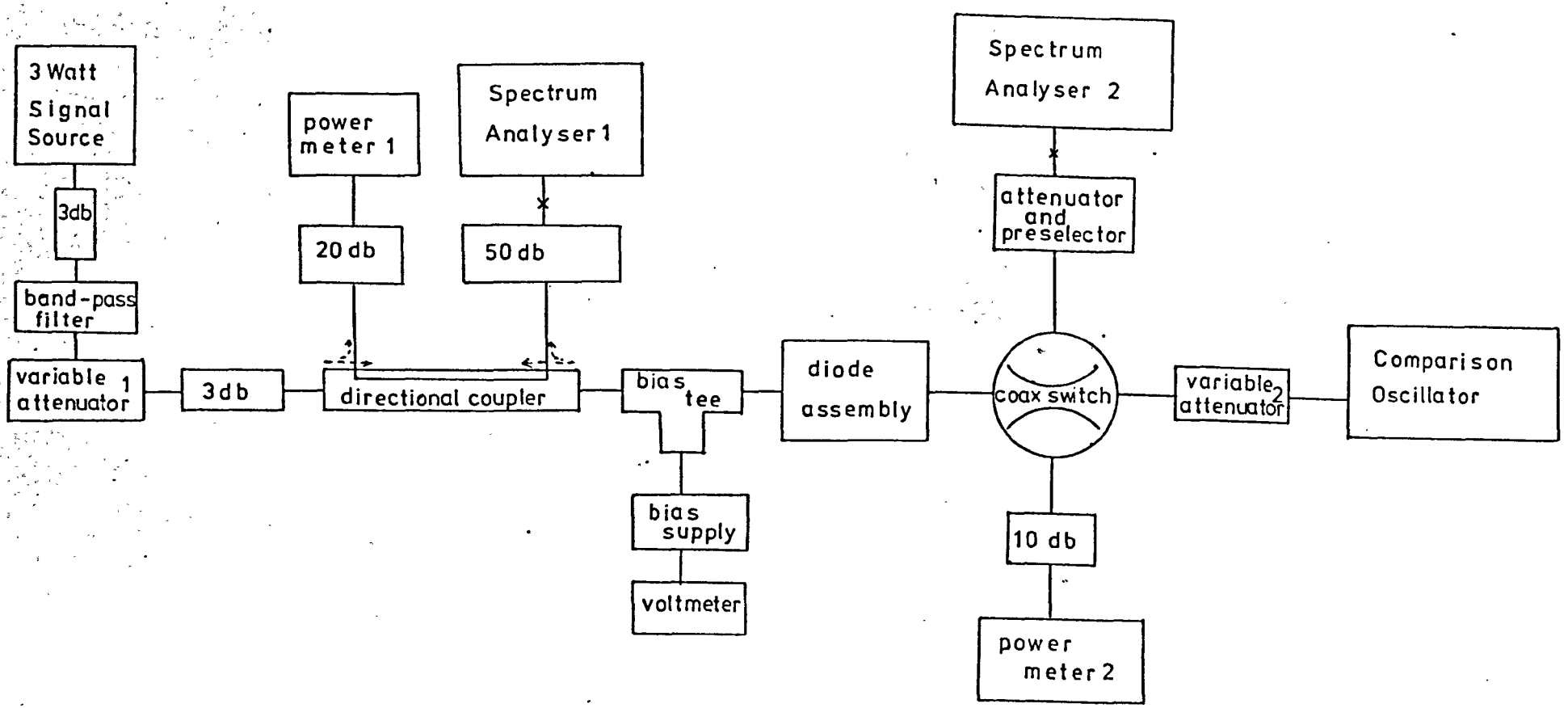

order of about 60 db against out-of-band signals. The spectrum analyser response to a particular harmonic was compared with a signal from the comparison oscillator at the same frequency. The comparison oscillator power was then measured on a power meter usually after the attenuation had been removed from the circuit. Hence, the technique used the extreme sensitivity of the spectrum analyser to compare accurately two signals which passed through the same switch, preselector and the analyser circuit.

The system was capable of 0.5 db resolution (the analyser limit) and all errors were effectively calibrated out. Very minor corrections were made for different cable connections from the diode and comparator to the switch, but no asymmetry in the switch itself could be detected.

6.55. The Diode Mounts

Several types of diode mount were employed (figs. 6.5.6/9). Simplicity of design was essential, to avoid as far as possible the influence of the mount on the measured parameters. The Schottky diodes available were wire-ended VHF and UHF types, and were used in mount 1. Most of the microwave varactors in use were in the S4 'pill-with-prongs' package, and were measured in the mounts 2 or 3. As the diagram implies, the measurements were performed in a series mode, so that 50 ohm lines could be maintained at the device.

6.5.6./ 8

Diode mounts

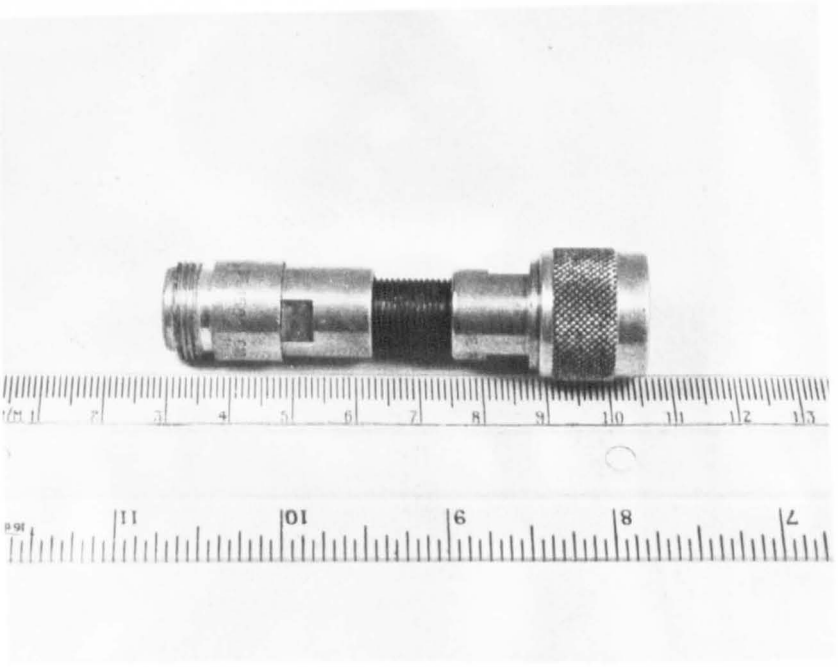

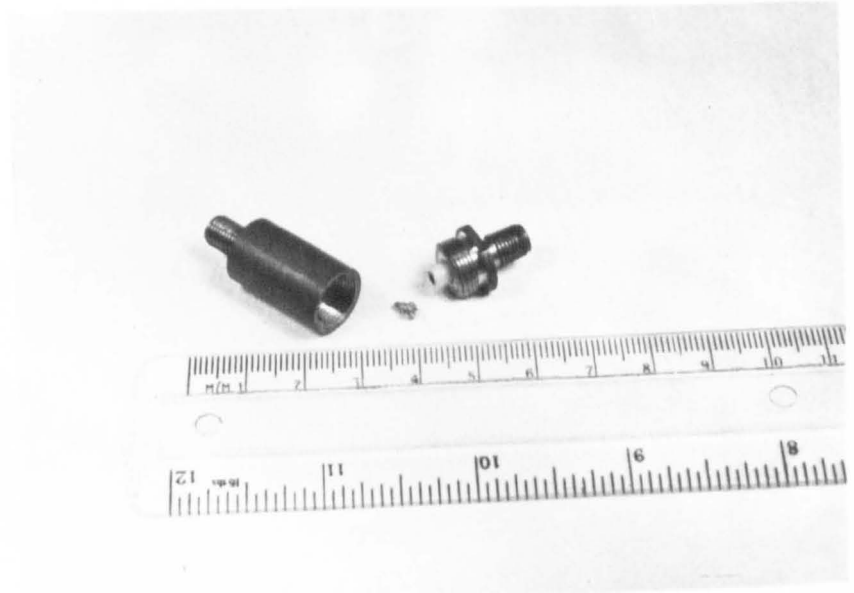

6.6 Microwave Spectral Assessment. The Practical Results

6.6.1 Schottky Barrier Mixer diodes H/P 2800 Series

The spectral output of three diodes at a fairly high power level is shown in fig. (6.6.1). The very low harmonic outputs, particularly from the 2800 and 2833 types implied that very little rectification took place, although a bias circuit was provided and each harmonic optimised. The 2811 showed a biassed rectifier type of harmonic spectrum, of very low amplitude but having the characteristic hump. Comparisons were made with figs. A6.3.5-10 making allowance for the difference between the voltage and power plots. It appeared that the rectifier had very little bias, as the third harmonic output was low. However, some fifth harmonic was present, possibly due to a very small degree of step-recovery at the frequency used, which was much greater than the intended operating range of the device.

6.6.2 Step-Recovery Frequency Multiplying Diode - HP 5082-0386

The diode which was chosen as the basis of the frequency multiplier construction was the 0386 type, which offered the fastest risetime available, consistent with reasonable charge storage. A complete spectral assessment of a particular diode was made over a very wide range of input amplitudes (50 mW - 1400 mW). The mount 2 was used. Power was matched into the diode with a 3-stub tuner (fig. 6.6.6) and the output was fed to a 50 Ω load. The input frequency was 1.56 GHz.

The results are tabulated in fig. A(6.6.2) and plotted in figs. (6.6.3) and (6.6.4). Bias current was allowed to flow through a pencilled resistor of about 50K; this was a broadly optimum figure.

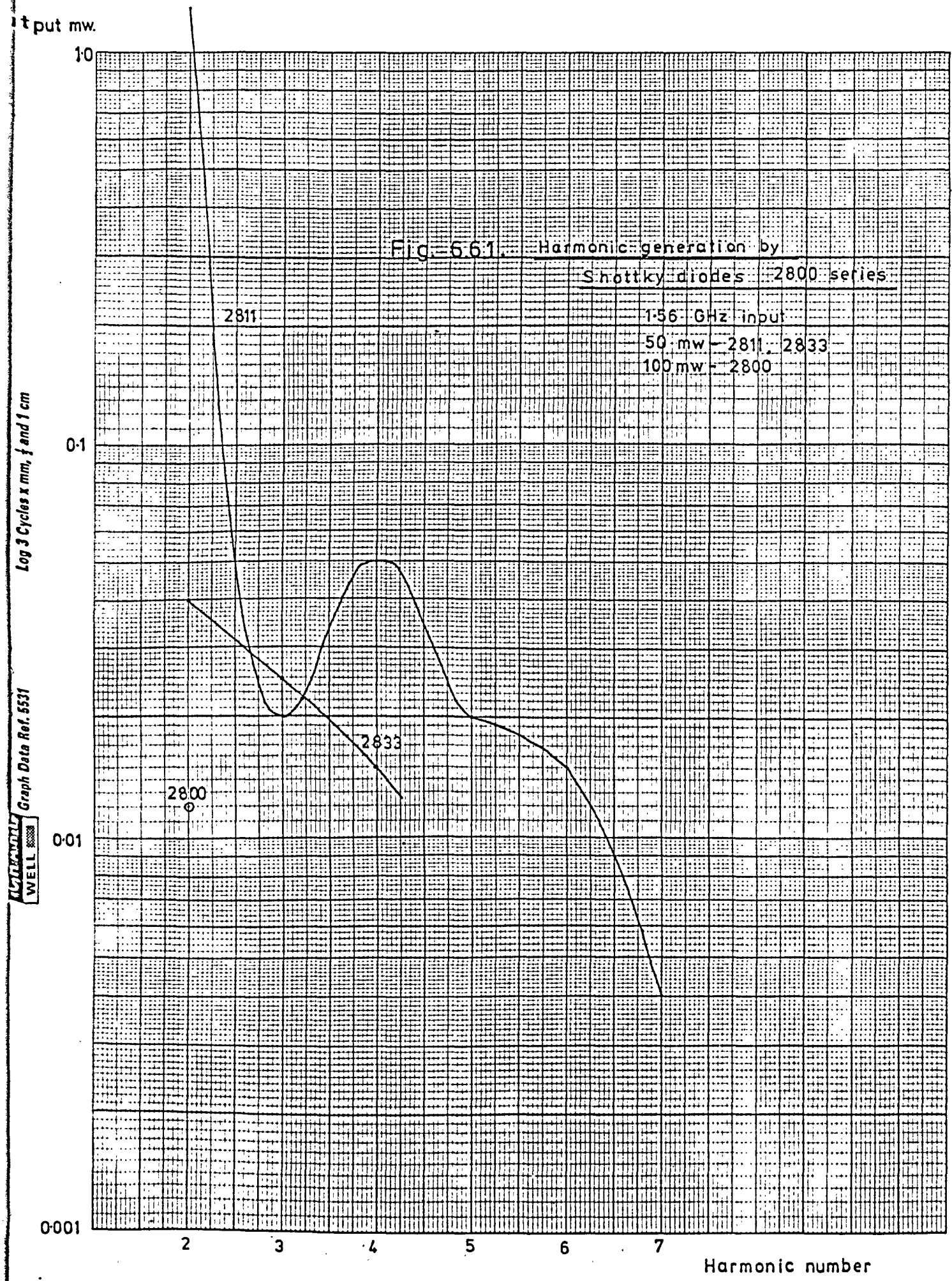

Fig. 5.6.1. Harmonic generation by Schottky diodes 2800 series

1·56 GHz input

50 mw – 2811, 2833

100 mw – 2800

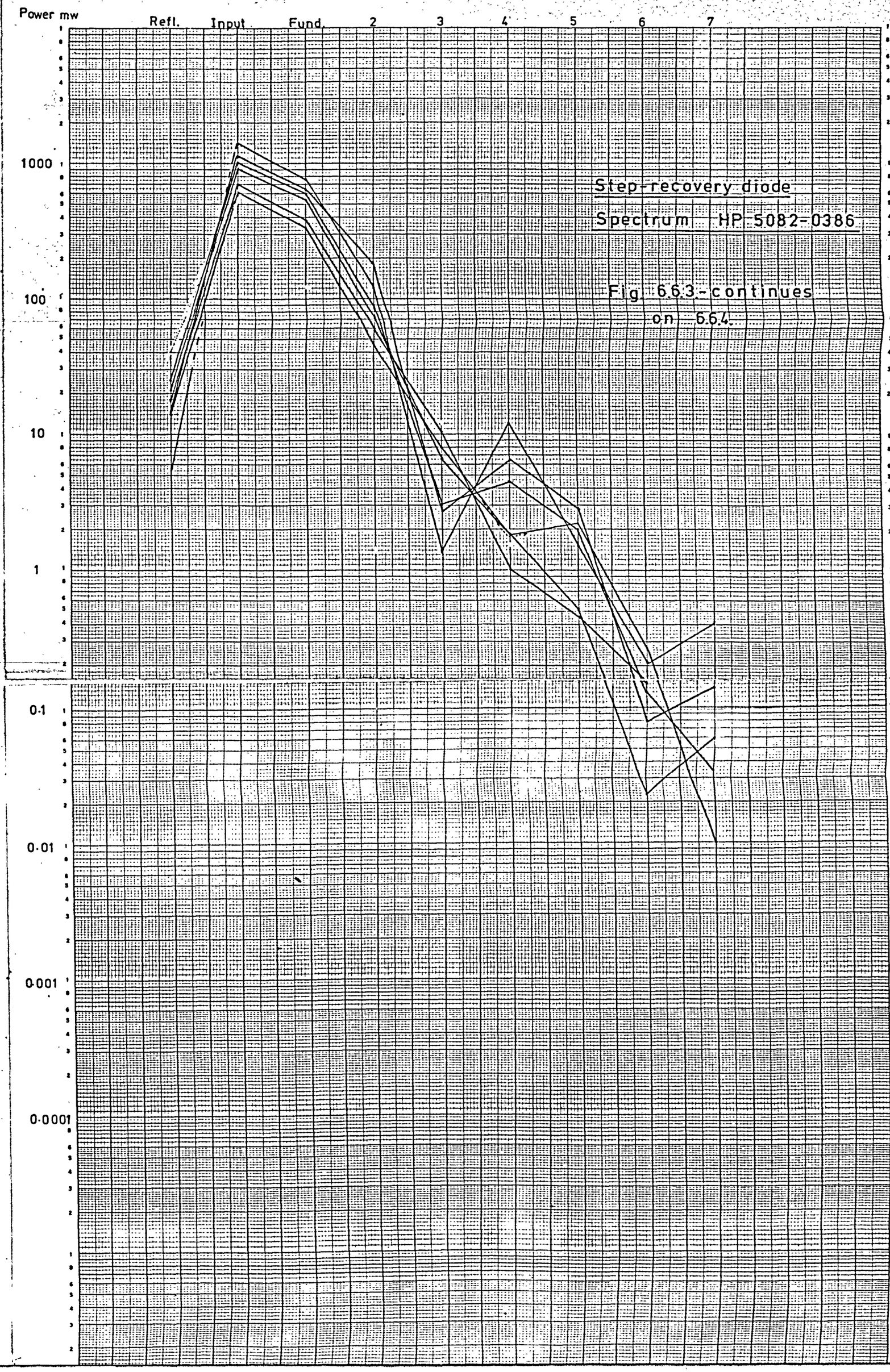
Power mw
Refl.
Input
Fund.
2
3
4
5
6
7
1000
100
10
1
0·1
0·01
0·001
0·0001
Step-recovery diode
Spectrum HP 5082-0386
Fig 6.63 - continues on 6.64.

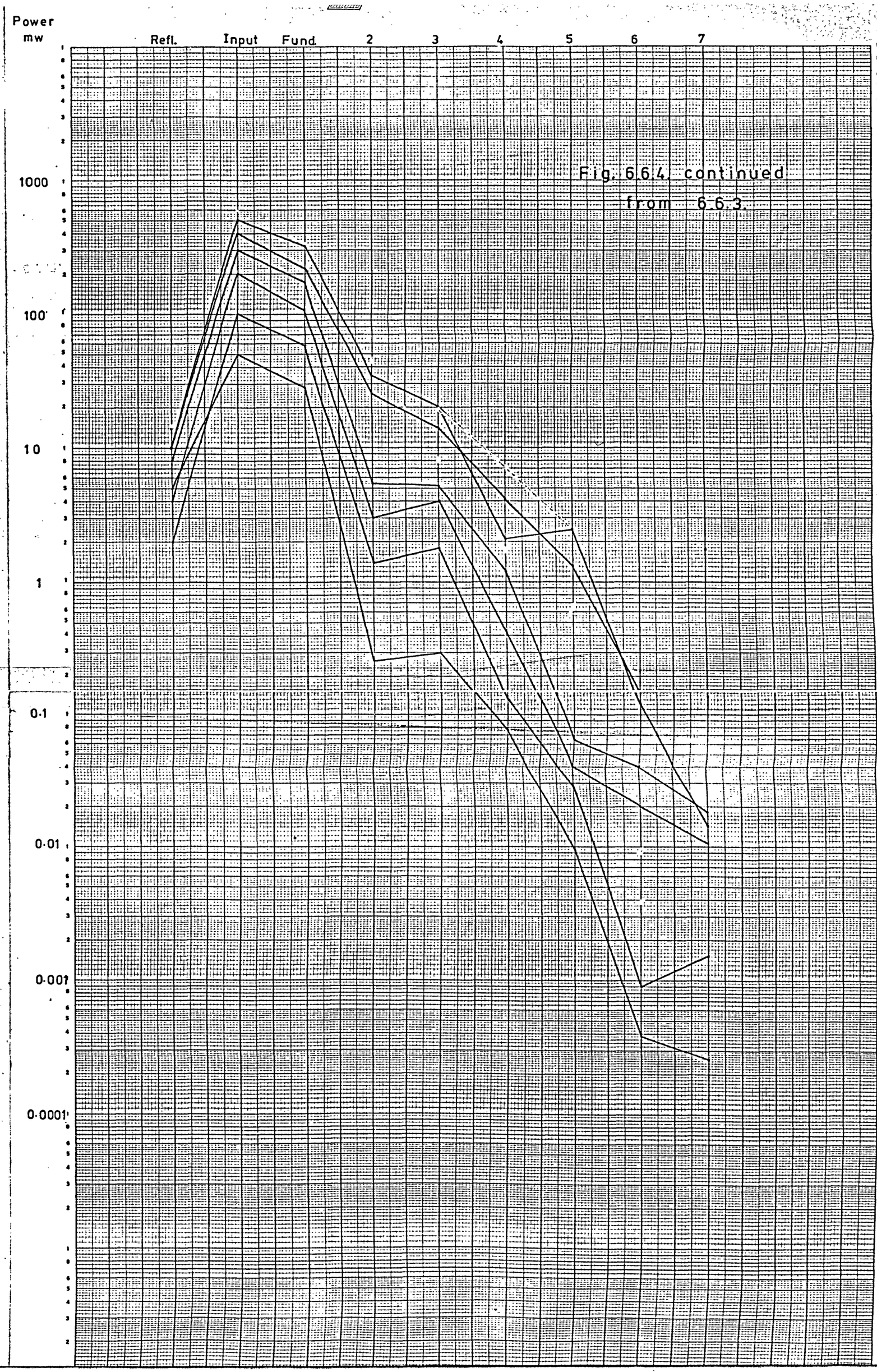

Fig. 6.6.4. continued
from 6.6.3.

The analysis of the results was performed graphically.

A series of predicted harmonic spectra were traced onto clear plastic sheets, similar in form to fig.6.6.5. (The figure referred to is representative but some of the data points are omitted for clarity.) The predicted spectra sheets were used as overlays on the measured output spectra(figs.66.3. and 6.6.4)

It was clear from the high amplitudes of the harmonics that the mechanism of the diode was not rectification. A curve fitting process was carried out on the measured spectra. The measurement technique provided only amplitude information, so the amplitude envelopes of the predicted spectra were plotted accordingly.

After several trials, the curve for N = 2, or t_p = 160 ps, was superimposed on fig. 6.6.3/4. The agreement in shape of the predicted and measured curves was excellent. It was concluded that the HP 5082-0386 operated as a very good step recovery diode in the frequency range under consideration. The transition time, t_p, was approximately 160 ps at the 1.4 watt drive level, and fell to 120 ps at the low levels (c.200 mW). These results were to be used later in the frequency multipliers constructed.

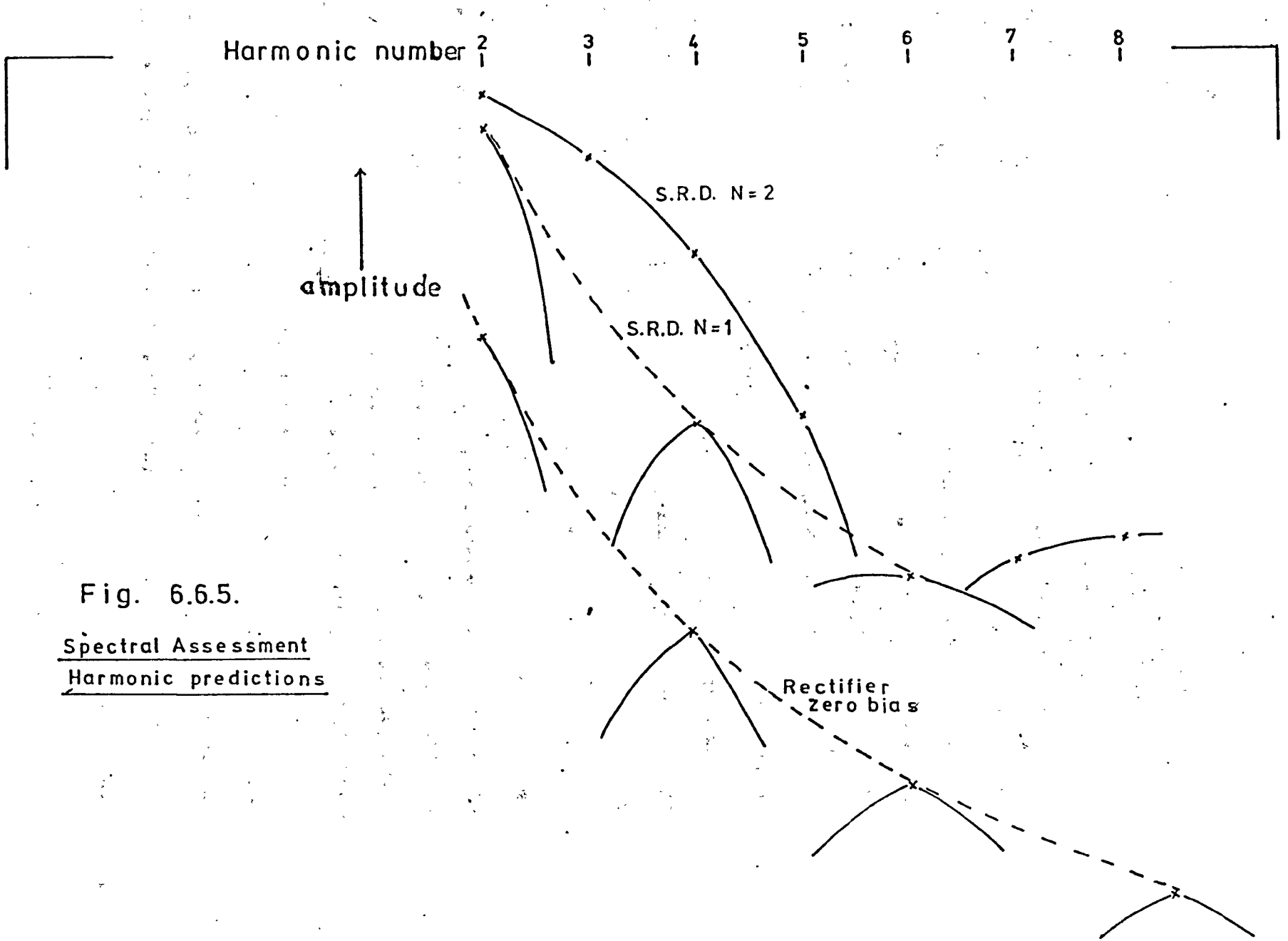

Fig. 6.6.5.

Spectral Assessment

Harmonic predictions

7. EXPERIMENTAL BROADBAND FREQUENCY MULTIPLIERS

7.1 Introduction

Several previous authors (Kotzebue & Matthaei, Redd & Kotzebue) have constructed multipliers which featured a balanced structure to eliminate certain harmonics. In this chapter it will be shown that bandwidths close to the theoretical maxima are possible, with low spurious output content, provided that certain generalized construction rules are obeyed. High-order harmonic generation presents no problems other than obtaining suitable diodes; of course, one must expect, and the theory confirms this, that the broadband power output is lower than that obtained under narrow band conditions.

The particular system chosen as an example of a typical multiplier design was a single-stage, two-diode quintupler, with a target bandwidth of 25% (theoretical maximum 33%). Secondary objectives were, small size and low cost. Efficiency was considered to be important, but, in this research effort, was traded where necessary for bandwidth.

One of the most significant advances in microwave techniques in recent years has been the introduction of microwave integrated circuits. This technique has not been applied previously to frequency multipliers, and it is believed that the multipliers to be described are the first to employ an integrated construction. It is necessary to be able to reproduce all the components in the circuit to a high degree of accuracy, but when this accuracy is achieved, the need for adjustable circuit elements such as trimmer capacitors is removed. Incidental advantages of the integrated structure are the small size and low cost required, and the possibility of large scale production of a successful design.

7.2.1

Diodes (SRD) and chip capacitors

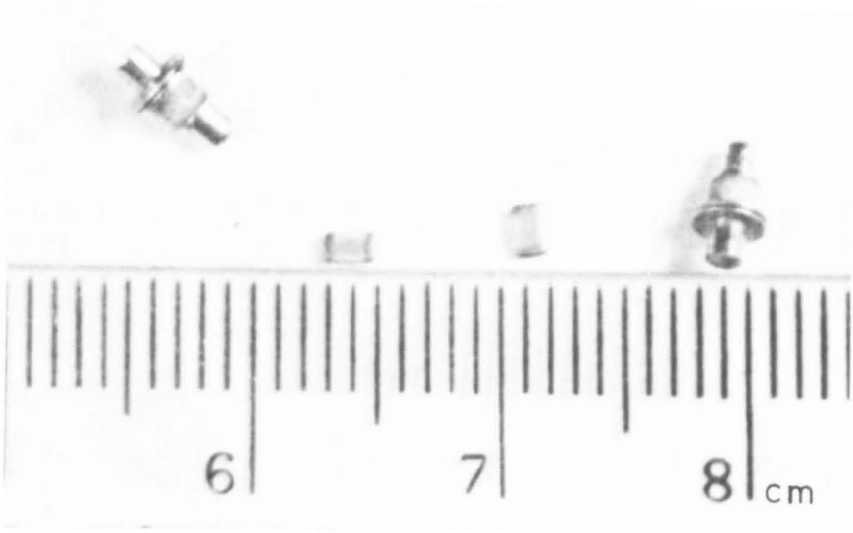

7.3.10

Transistors (DC 5502)

7.3.7

Oscillator

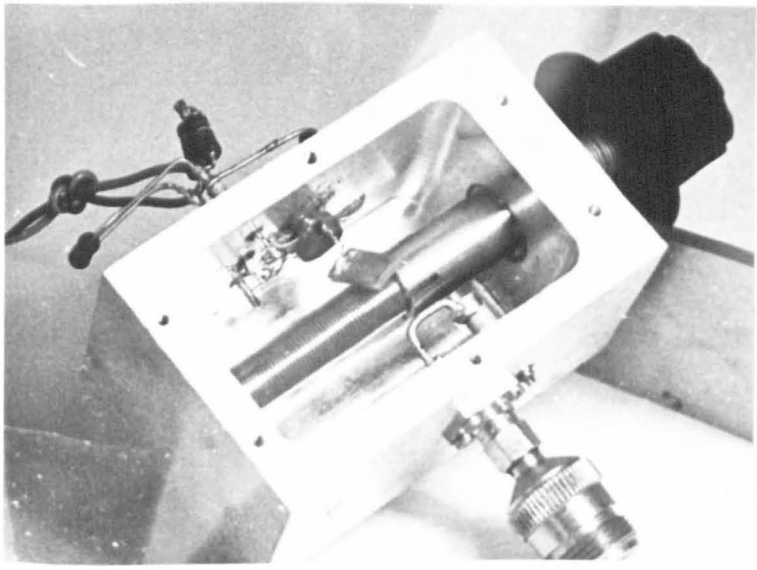

7.2 Design Consideration

7.2.1 Choice of Multiplying Factor and frequency

The purpose of this chapter is to describe the design procedure followed in the production of a class of broadband frequency multipliers and to report on their performance. The example chosen for discussion was evolved after careful consideration of a number of factors.

At the outset, only two high-powered microwave sources were available, both crystal-controlled, and separated in frequency by less than 1%. The frequency of one of them, 1.56 GHz, was chosen as the nominal centre frequency. An examination of manufacturers' data for a large number of S.R.D's indicated that the best devices available at the time were H.P. 5082 - 0386 (or 0335) (fig.7.2.1) It was never intended that the multiplier should be oversensitive to the choice of a device. The spectral evidence (Chapter 6) showed that only harmonics of 1.56 GHz below the seventh could be realistically considered. The theory of Chapter 5 is only directly applicable to the fourth harmonic or higher, so that extra terms must be inserted for the third. The achievement of a true 180° phase difference in the feed to the two diodes over a wide frequency range was acknowledged to be as an extremely difficult practical problem, so that even order harmonic generation was not favoured. Finally, as previous workers had concentrated on triplers it was decided to direct the effort to the generation of the fifth harmonic. Subsequent results justified this choice. The problem of a wide band variable oscillator for test purposes was overcome by the use of specially constructed transistor and valve circuits.(see appendix 7.3.3)

7.2.2 Filtering Requirements

The maximum theoretical bandwidth, as indicated in Chapter 5 is given by:

$$\theta = \frac{2}{n+1} = 33\%$$

Clearly, it would not be wise to aim directly at the theoretical limit. A compromise bandwidth of 25% was selected using the practical filter measurements as a guide.

The ultimate limitations on the bandpass filters are indicated in Fig. 7.2.2. The construction of this type of chart is considered to be an important step in frequency multiplier design, and will be described in some detail.

Harmonics of odd order only are considered, but the full bandwidth of the multiplier must be taken into account. The chart is a more detailed guide to the filters required than is the bandwidth formula above.

At the lowest input frequency, i.e.

(centre frequency) - $(B/2)$ = 1.3 GHz (B = Bandwidth in GHz)

the fifth harmonic (6.5 GHz) produces the lowest end of the output pass-band. The seventh harmonic (9.1 GHz) must not be allowed into the output circuit, hence the upper output limit is Δ F below 9.1 GHz, where Δ F depends on the filter bandedge slope, and the acceptable purity of the output signal.

Turning to the upper input limit, (1.82 GHz), this is set by the equation for B at 1/5 of 9.10 GHz. Clearly, the seventh harmonic of 1.82 GHz is well into the output stopband. The third harmonic, 5.46 GHz, represents another limit to the output stopband. Finally, the frequency which is one third of the minimum output frequency has been plotted. In general, filters are designed to fit the minimum limits, i.e. 1.3 GHz to 1.82 GHz and 6.5 GHz to 9.1 GHz, but, should any discrepancy occur, then the two inner band edges are seen from the diagram to be less critical than

Filter Characteristics for a × 5 Multiplier Fig. 7.2.2.

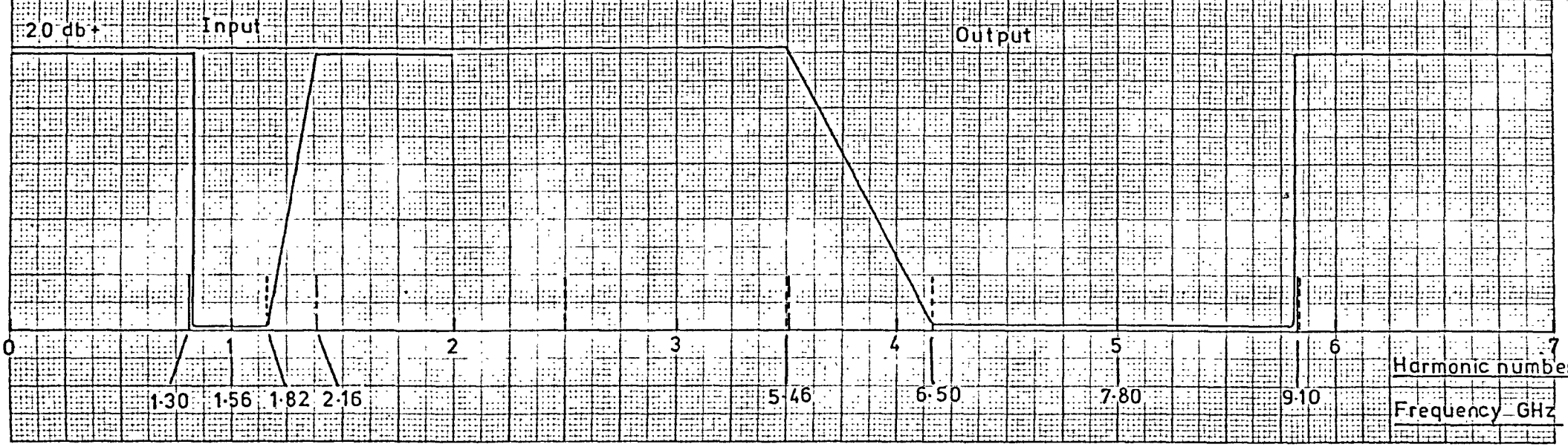

the outer band edges; on no account should frequencies outside these limits be allowed in the output. (On the input, a low pass filter is permissible provided the output circuit can eliminate the spurii involved).

It is usually convenient to make filters with symmetrical bandpass characteristics, so that a 25% bandwidth within the output range and slightly biassed towards the lower end, was chosen. This provided a high insertion loss at the critical frequency of 9.1(GHz, and a low loss over the passband.

Spectral evidence suggested that seventh harmonic generation with the diodes used in the frequency range selected was likely to be small, so that the filter requirement was slightly eased.

7.3 Filters and Bias Networks

7.3.1 Techniques

The techniques employed in the construction of the filter networks are described in appendix 7.3. The choice of the copper laminated Tetra-flouro-ethylene (TFE) system was dictated mainly by the economy and ease of processing. Secondary advantages of this system were a high degree of repeatability and the availability of accurate design information. Full use was made of several reference works on filter design (Zverev; Young, Matthaei and Jones) and certain research papers (Youla, Nicholson Young).

It is evident from Appendix 7.3 that the presence of a ground potential in the centres of the triplate structure is extremely undesirable. In general, the series L with the capacity to ground system is preferred, which leads to a low pass type of structure. In the input, this was not

Low pass

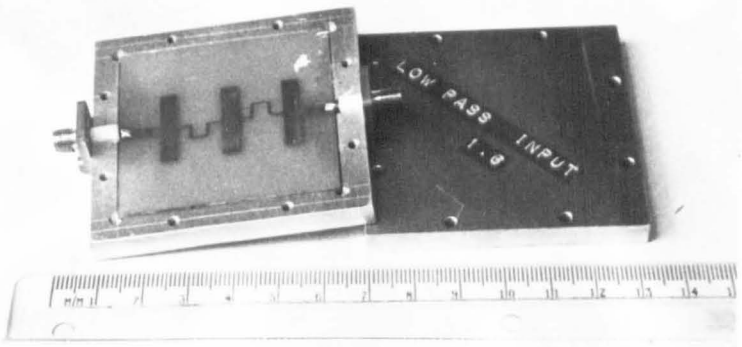

High pass

7.3.2.

Stripline filters

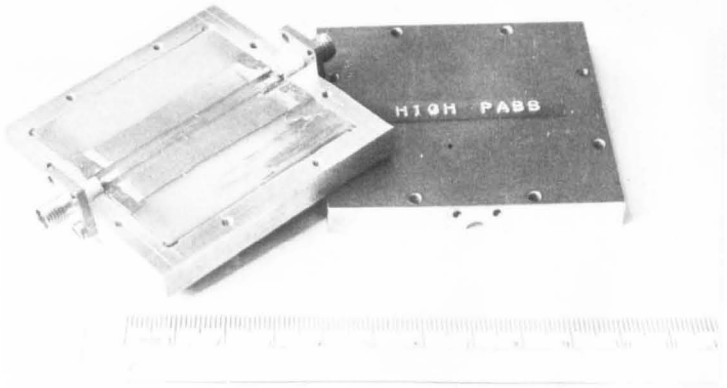

Band pass

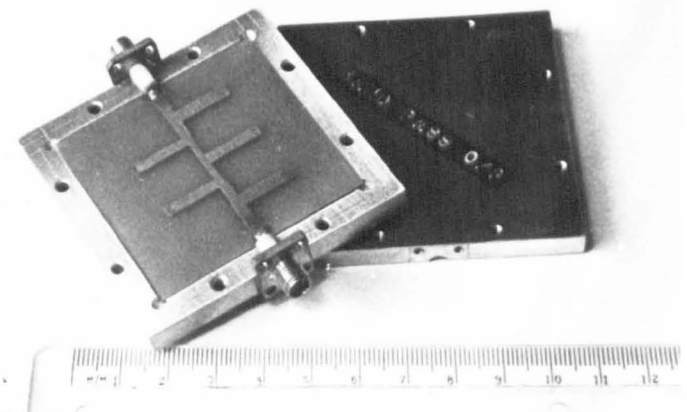

(centre)
directional
coupler

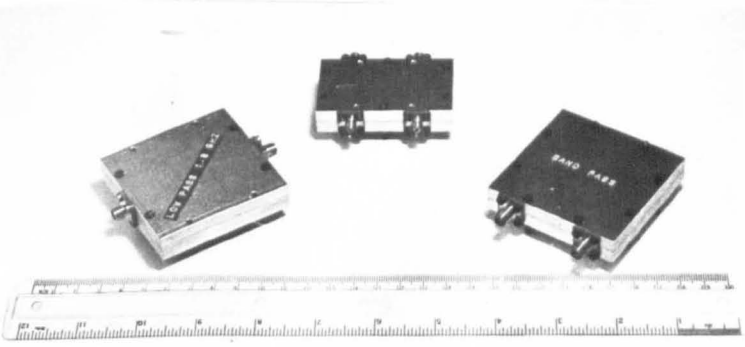

Multiplier assembly
(before integration)

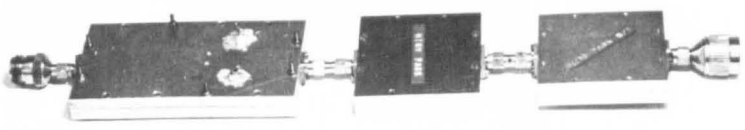

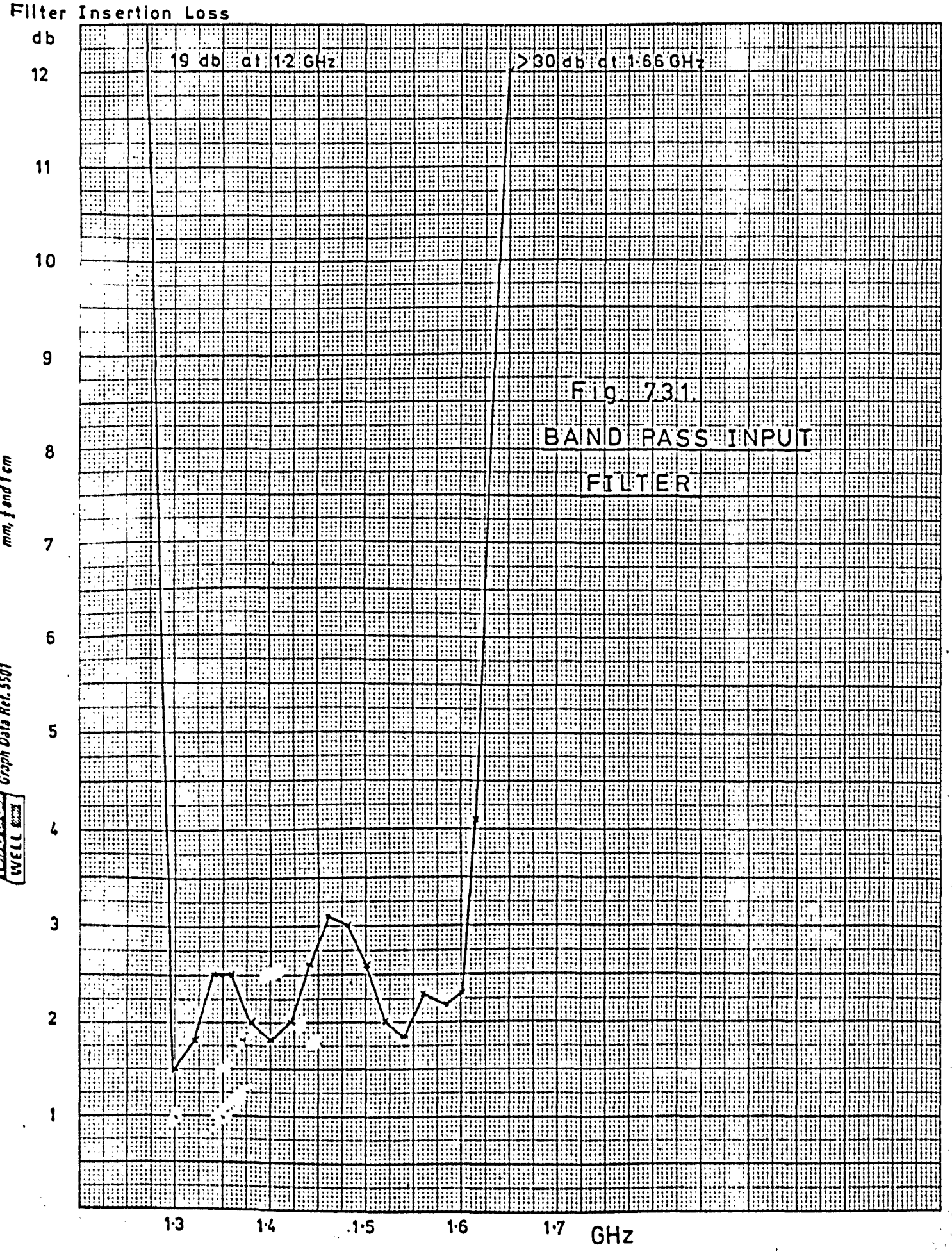
Filter Insertion Loss
db
12
11
10
9
8
7
6
5
4
3
2
1
19 db at 1·2 GHz
>30 db at 1·66 GHz
Fig. 7.3.1.
BAND PASS INPUT
FILTER
1·3
1·4
1·5
1·6
1·7
GHz
mm, ∫ and I cm
Graph Data Ref. 5501
WELL

a disadvantage as it was found in practice that this structure helped to reduce some of the spurii. (See also Parker). However, it was necessary to incorporate a band-pass section in the outputs to reduce the level of unwanted harmonics.

7.3.2 The Input Filters

Two input filters were constructed. The initial design consisted of a 7 section (9 - element) interdigitated filter, with a band-pass response. Several models were built with similar characteristics. Unfortunately, the tolerances on digit widths and gaps were not good enough to produce the predicted characteristic. The passband response is shown in fig. 7.3.1. The most remarkable feature of this filter was the high bandedge slopes (> 230 dB/octave).

After some consideration, the design shown in fig. 7.3.2 was adopted.

The low-pass input characteristic (fig. 7.3.3) had a low in-band insertion loss (< 1 db) with good out-of-band rejection (> 30 db). Some features of this design were thought to be unique, so a full description is included here.

It has been pointed out (6'clock, ref.40) that a very wide variation in the filter cut-off frequency can be achieved around a standard design, without seriously affecting the passband characteristics. The input filter was designed using lumped element techniques, taking 150 ohms as the highest practical line impedance.

According to the design tables, a five element filter would give a 0.1 db (Tchebyshev) ripple and 35 db rejection at the 2nd harmonic (of 1.8 GHz).

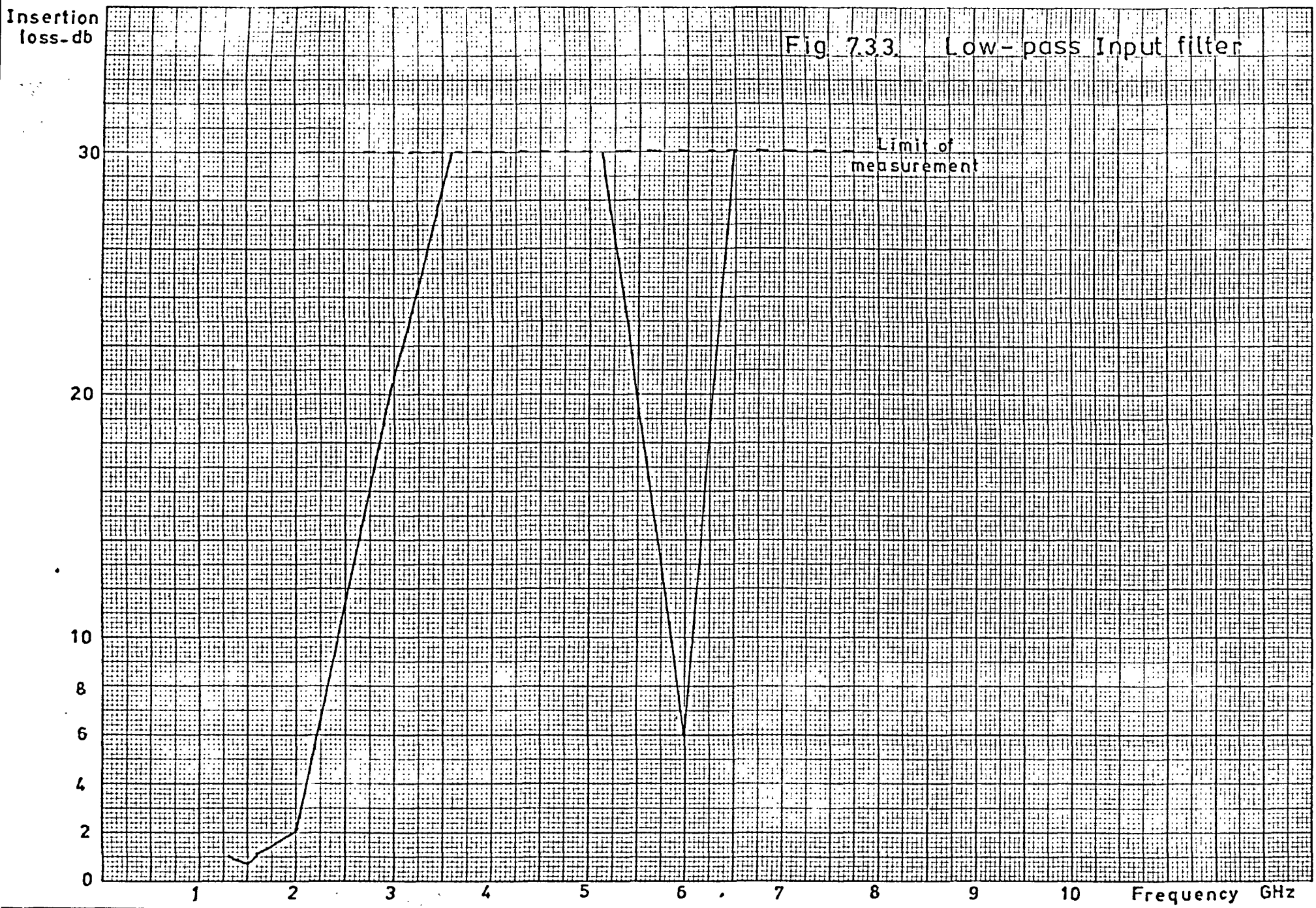

The lengths of the inductive lines proved to be inconveniently long, so that they were folded, as may be seen in the photograph. The corners were bevelled to reduce reflections. The low-impedance capacitive sections were deliberately made about 25% too wide (referred to the roll-over frequency of 1.8 GHz) and the filter was constructed in the usual way. It was found that the roll-over was 1.6 GHz. A simple modification of the mask using 'chartpak' tape moved the roll-off frequency to 1.8 GHz (fig. 7.3.3), accurately predictable from the first filter results. Several models were constructed as general-purpose laboratory filters. Only one spurious passband, around 6 GHz, was noted, where the high impedance lines were self-resonant. The aims were very nearly met ($\sim$ .2db) by most of the filters constructed; in particular, the stop-band insertion loss was better than 30 db, which is in itself remarkable for a microwave system.

7.3.3 The Output Filter

The requirements for the output filter were minimal passband loss, low ripple and a high stopband insertion loss, especially over the ranges of the third and seventh harmonics. The bandwidth was set at 25%, with a theoretical ripple of .25 db.

Examination of the filter design tables showed that one type was particularly suitable. Half wavelength open-circuit lines. with quarter-wavelength separations were to be used; a five-section Tchebyshev response was capable of .25 db ripple with a low in-band loss. The theoretical stopband loss for this type of filter was said to be infinite at 0.5 and 1.5 times the centre frequency which fitted in well with the third and seventh harmonic rejections. However, because the filter is a resonant element type,

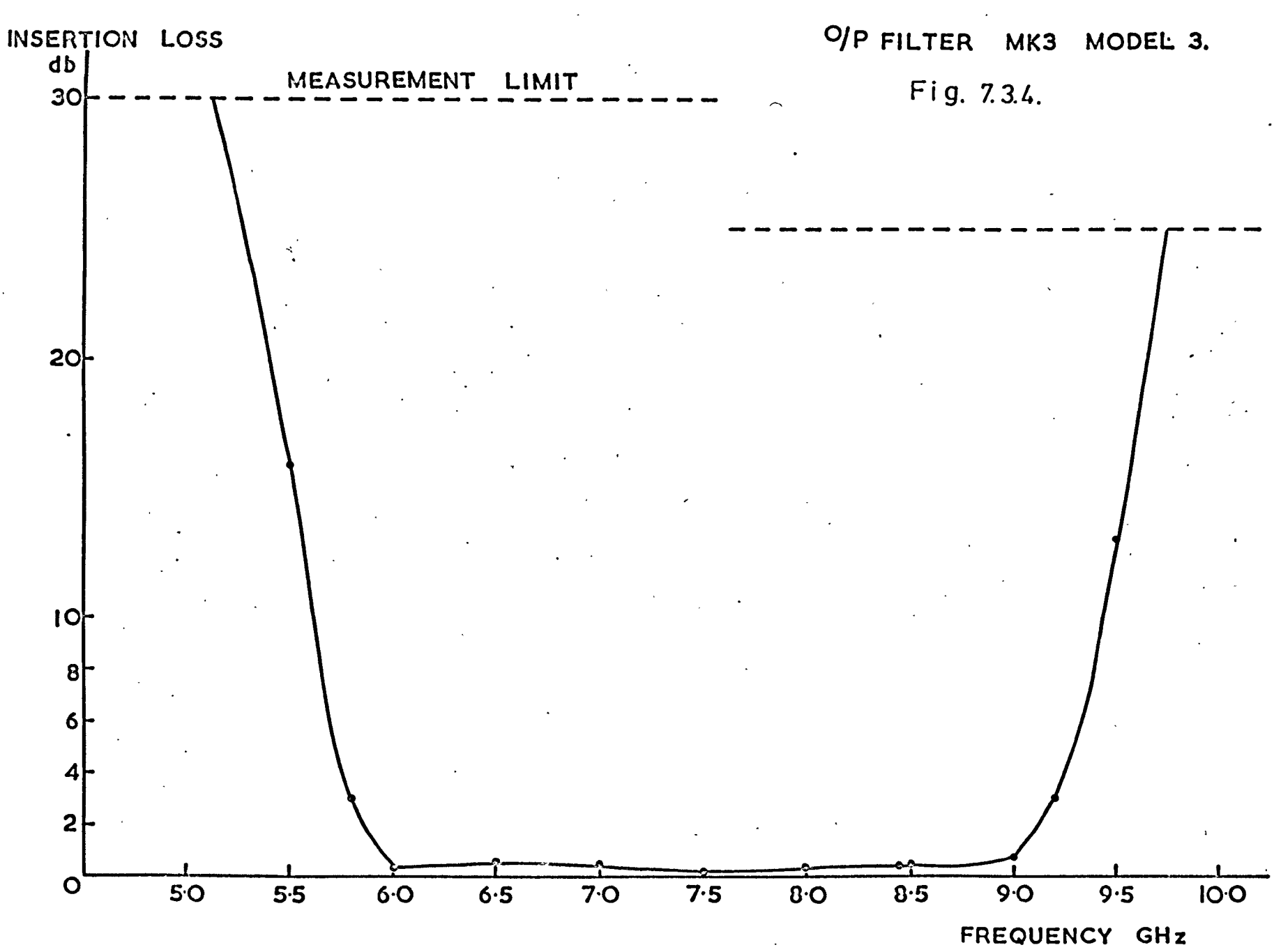

O/P FILTER MK3 MODEL 3.

Fig. 7.3.4.

a spurious passband occurred from d.c. to 3 GHz, so a high pass section was inserted to overcome this difficulty. The properties of this filter were not critical, the requirement being a low insertion loss above 4.5 GHz with a minimal ripple. A Butterworth design was chosen, consisting of two inductive short-circuited stubs and a capacitive coupling. Measurements indicated that the stop band insertion loss was too low, so one more section was included in the final multiplier. An excessive insertion loss near the pass band centre was traced to a resonance of the box in which the filter was mounted. The design was based on lumped elements, and it was considered to be very successful. Fig. 7.3.2. shows the individual filters prior to assembly. The filter passband characteristic is shown in fig. 7.3.4.

7.3.4 The Bias Networks

The bias networks were required to supply a d.c. current path through the diodes without allowing any R.F. to leak out of the circuit. Previous workers in this field have used R.F. chokes, external resistors, or miniature resistors inside cavities. It was found that pencil 'lead' lines across the ceramic diode packages provided adequate bias for single diode multipliers and this technique was used extensively. However, for the two diode multiplier, it was essential that the same current flowed through both devices. After several trials, it was found that symmetrical low pass networks gave suitable performance with an external (selected) resistor. The chosen roll-off frequency was 600 MHz, i.e. just below half of the minimum input frequency. Chokes were made from 42 s.w.g. tinned copper wire, and ceramic chip capacitors (fig. 7.2.1) were used for bypass.

base + diodes

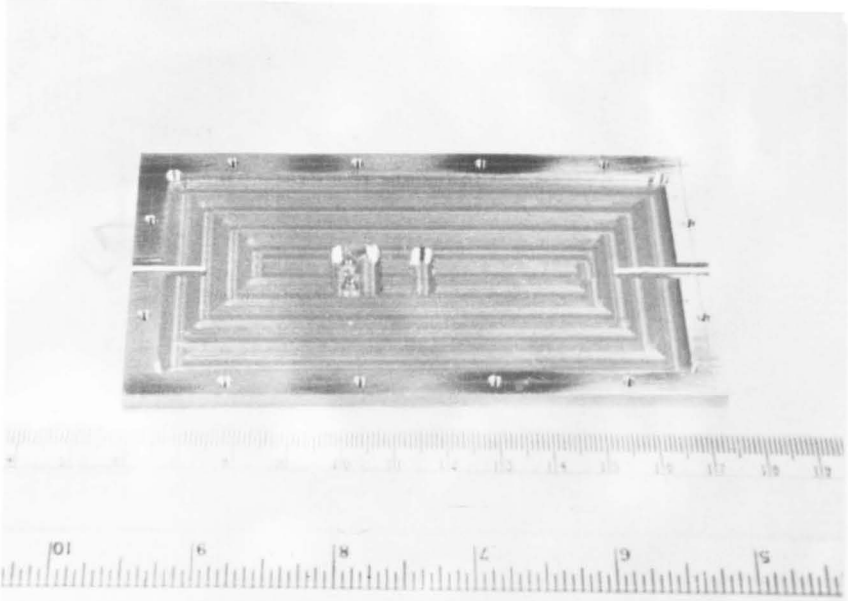

7.4.1.

The Integrated Multiplier

substrate

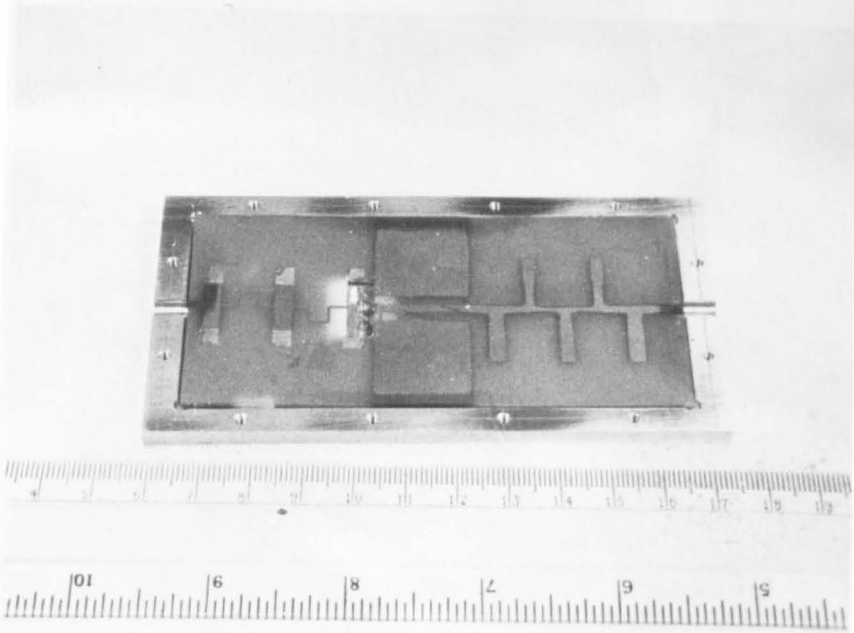

assembly

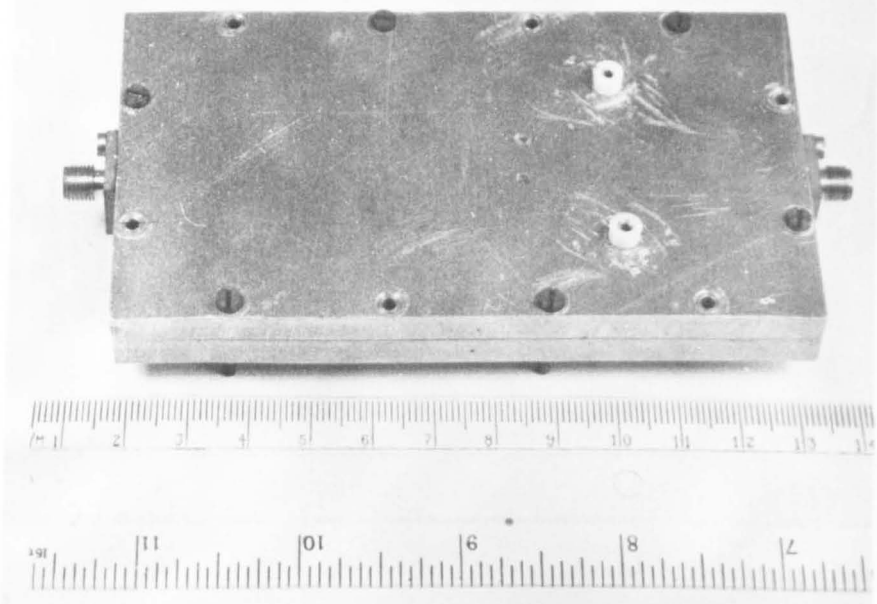

Copper foil plates provided the output capacitance. Leakage was negligible. The circuit shows how the diodes were arranged, so that bias could be automatic or external, with identical or separate current paths. (Figs. 7.3.5 and 7.3.6)

7.4 The Integrated Circuit

The fabrication of filters, bias networks and matching networks as individual components was carried out as a preliminary to the construction of a fully integrated unit. Each separate component was characterised, and with repeatability assured by the photo-etch process, the same characteristics could be confidently expected from the integrated unit.

Although the input low-pass, the output high-pass and the band-pass circuits have been discussed, no consideration of matching has been made. The impedance transformation has been used previously (Kotzebue and Mattaei) in the design of frequency multipliers. However, it was decided that, as filters are more easily constructed and characterised at 50 Ω , there were some advantages in operating all the system components at this impedance, and hence transformers were inserted in front of and after the diode assembly. Obviously, as the multiplier was intended only for experimental work, the drive level was likely to vary considerably, so that the predicted impedances could vary widely.

The theoretical work of chapter 5 indicated the values to be expected for input and output impedance under optimum conditions. The computed results for a x5 multiplier are shown in appendix 7.3

The input impedance was about 40Ω and the output impedance $\sim$10Ω . Three types of transformer were tried. A test jig was constructed for measuring insertion loss; two transformers were connected 'back-to-back' to maintain the 50 Ω measuring system. Distributed transformers, in the

THE 2-DIODE NETWORK

Fig. 7.3.5. Bias Circuit

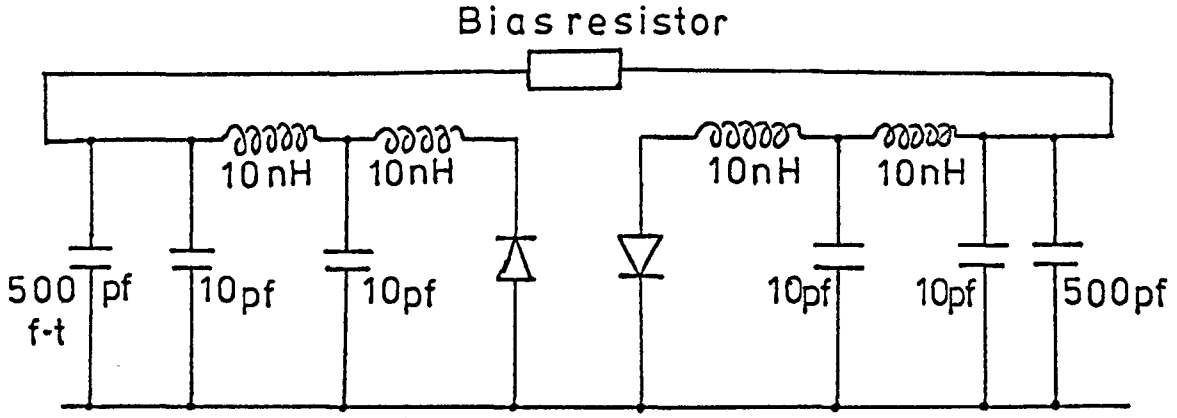

Fig. 7.3.6. R.F. Circuit

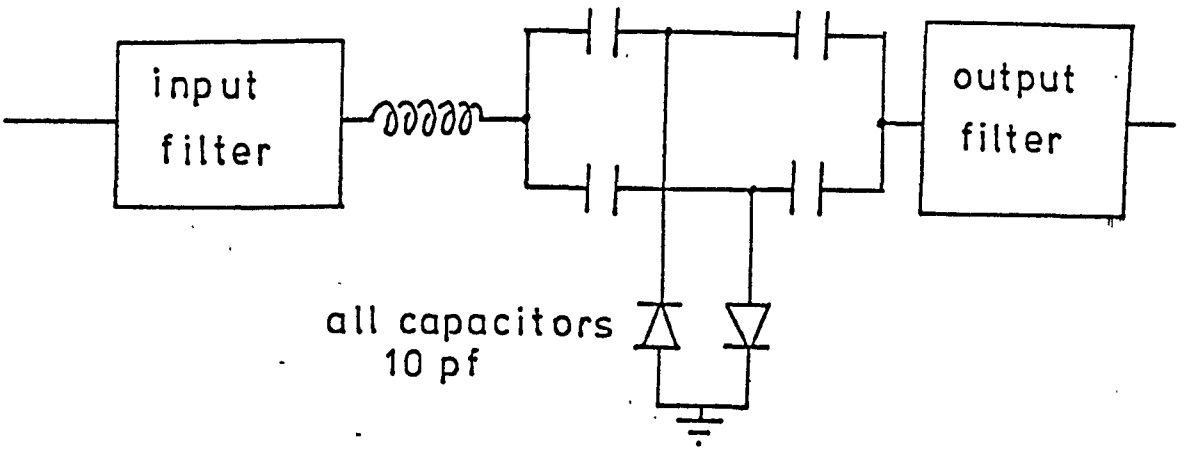

form of a 3 step $\lambda/4$ transformer, and a continuous taper transformer were tested. Although the reflections appeared small, the losses in the output transformer were unreasonably large. Calculations showed that a capacitive transformer would be fairly well matched to the output, and as capacitive isolation was required, this was the method used.

In the input, the final section of the input filter was formed by the diodes themselves, and this was found to be a very efficient circuit. The 40 Ω to 50 Ω mismatch was neglected, but the reflected power remained below half of the incident power at all levels.

The first tests on the multiplier were carried out using a partially integrated version shown on fig. 7.3.2. A very deep dip in the output was seen at the mid-band region. This was traced to a spurious resonance in the 2" x 2" case, and was quite repeatable between different substrates and cases. The fully integrated model is shown disassembled in fig. 7.4.1., excluding the chokes and decoupling components for clarity.

7.5 Power Output and Efficiency Measurements

The measurements were conducted using the comparison technique described in Chapter 5. Comparison measurements prevented the possibility of overloading and cross-modulation in the spectrum analyser.

The block diagram (fig. 7.5.1) indicates the technique used.

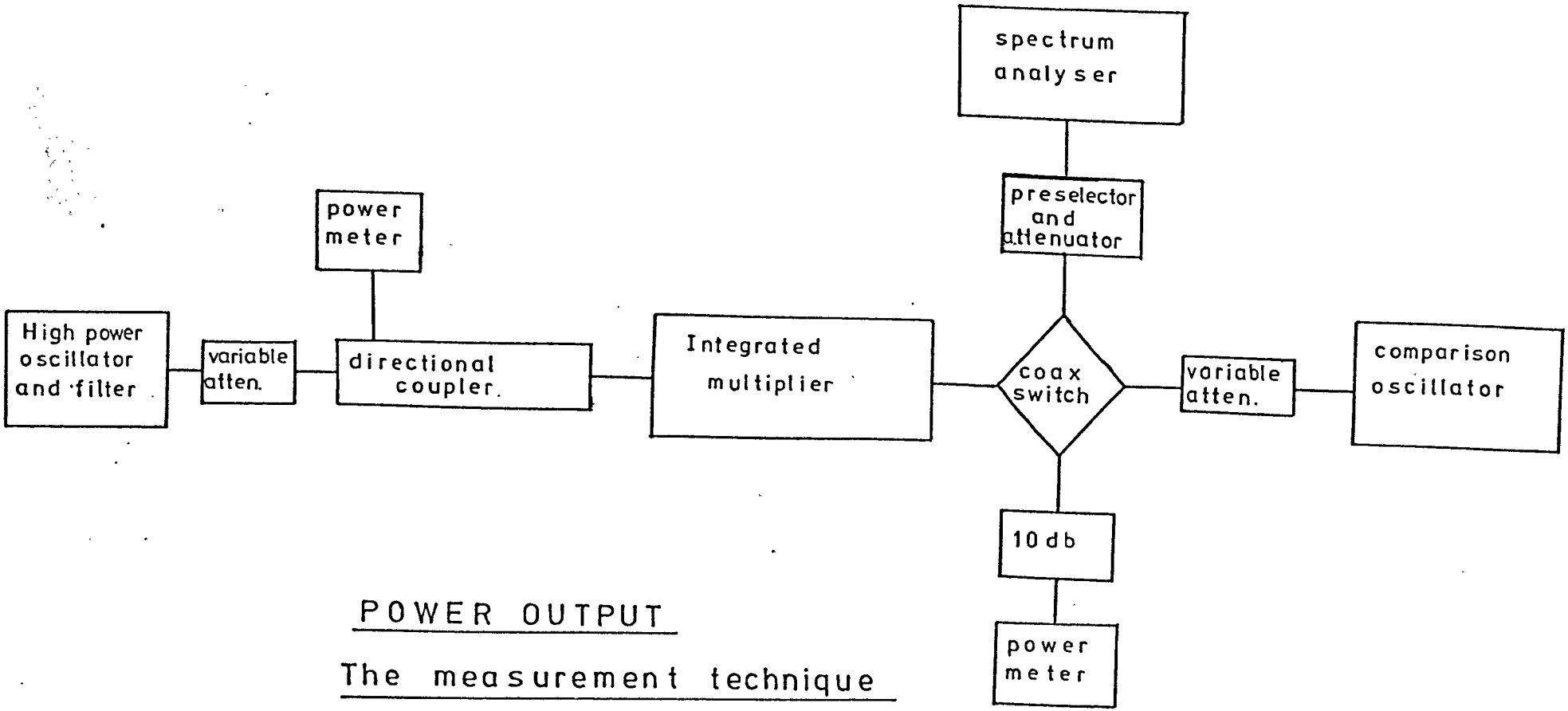

POWER OUTPUT

The measurement technique

Fig. 7.5.1.

A specific harmonic was selected on the analyser, and peaked with the tunable filter (fig. 7.5.2)

A signal derived from a monochromatic tunable source was then applied to the filter/analyser combination. Amplitudes were equalized, and then the power of the monochromatic source was measured. The only assumptions made were that the switch was symmetrical (fig. 7.5.3) and that the power meter was accurate. As both these instruments were nearly new, the assumptions were considered justifiable. A check of the meter against two others, one of a different type, showed no systematic errors.

The need for symmetry in this type of circuit has been commented on, previously. Although the diodes were closely matched some capacitance and thermal asymmetry was inevitable. However, the very low spurious output level indicated that these effects were small.

Measurement data from the three multipliers is included in figures (7.5.4/6) The output bandwidth closely followed the characteristic of the output filter, and the target figure of 25% was achieved. The optimum bias was set in each case at a frequency towards the top of the range, although the variations across the band were less than 10%.

A bias compensation network similar to that suggested by Corbey and Davies was considered but discarded since the output was found to be substantially level over the pass-band; the theory predicted that, in the operating region, only very small changes in efficiency would occur.

753

SWITCH

666

3 STUB TUNER

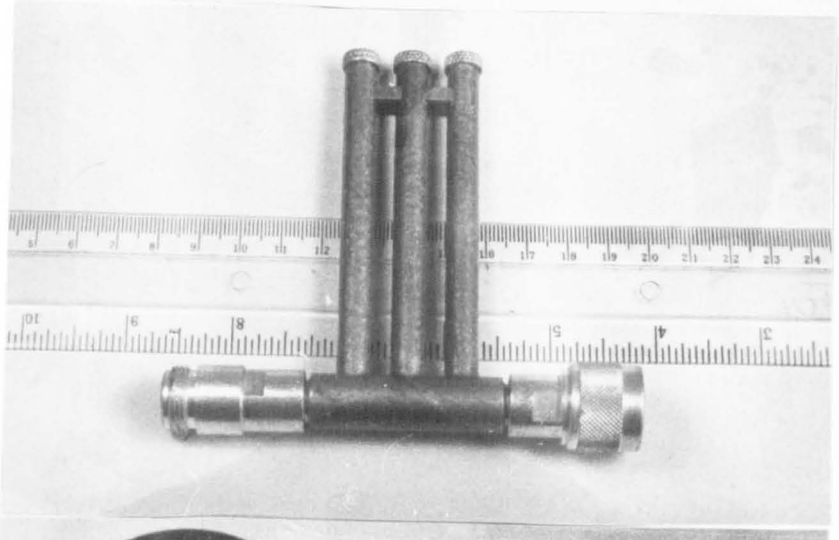

752

FILTERS

for preselection

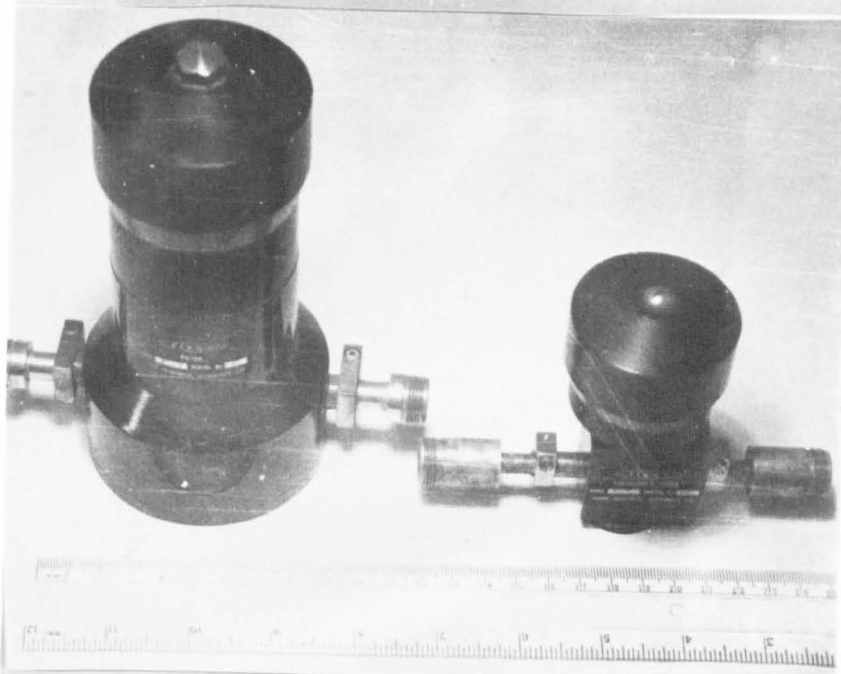

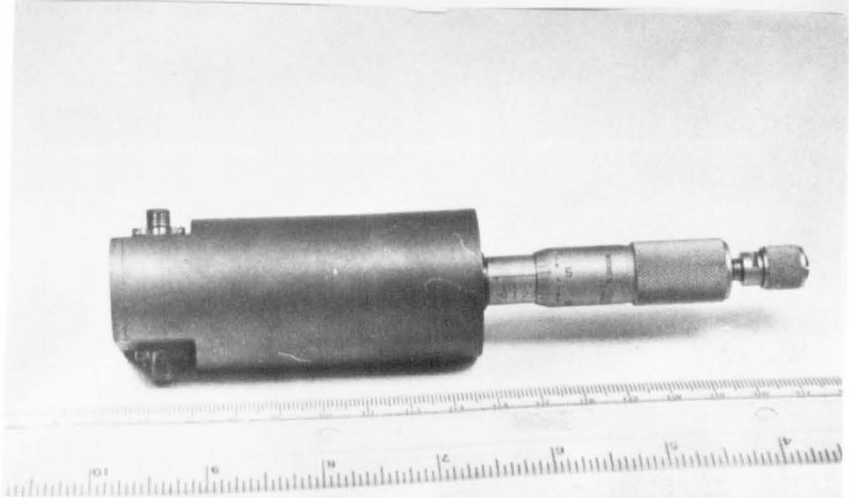

7.6 Results

The results are shown on figs.(7.5.4/6). The difference in performance between two multipliers (A and B) using the same type of diode (0386) was small and consistent with minor constructional variations. The third multiplier, C was fitted with higher performance devices, 5082-0335's, and gave a higher power output as predicted by the theory. The optimum efficiency figure, nearly 3% agreed well with theory; lower figures were recorded for the poorer diodes. It was evident that the capacitive transformer coupling worked well. The predicted bandwidth was achieved, with power output substantially level over the band. The spurious output rejection characteristics were very good. None of the broadband multipliers produced any non-harmonically related outputs, or half-multiple products, as can occur in some narrowband systems. The output filter removed well beyond the range of measurements any third or fifth harmonics; the only measurable spurious harmonics were the 2nd, 4th and 6th. The high pass section was intended to reduce the 2nd harmonic and the 4th and 6th were eliminated by circuit symmetry. The rejection figures for the even harmonics, in the appendix, show that the multiplier performance in this respect was as good as many commercial narrowband designs.

The impedances were predicted by the theory, and matched by the capacitive transformers; the efficiency agreed so well with the calculated figure that one must conclude that the theory was correct. The amount of power reflected at the input indicated that a good match was achieved, the power reflection ratio (P. forward, P reflected) was generally less than 0.2, and only reached 0.5 at the extreme band edges.

7.7 Comparison with theory and conclusions

The theoretical analysis of the SRD has been presented in section 5.4.2 and the associated appendix. The normalized results of the analysis were shown in figs. 5.5.1 and 5.5.2. The diode loss resistance for the diodes used initially was 0.65 Ω. The stored charge was 1400 pC and the 'ω' = 10^{10} Hz. The maximum voltage excursion was 2 x 26 volts, and therefore, using the results of chapter 5, the maximum theoretical output was 21 mW, and the efficiency 6%.

The output power/frequency plots show the results obtained (figs. 7.5.4 - 6). The efficiency was only 3%, but the filter losses accounted for the difference between the theoretical and practical results. The multiplier 'C' used better diodes, with a lower loss resistance and greater charge storage, so that the maximum output power was 30 mW, in good agreement with the theory.

The output power/frequency characteristics closely followed the characteristics of the bandpass output filters.

The spurious output were measured and tabulated in table 7.1. No output could be measured on the third and seventh harmonics, while the fundamental and the second, fourth and sixth harmonics were more than 10 db below the fifth harmonic.

In conclusion, the design of the frequency multiplier was proved to be successful. The balanced diode technique generated reasonably low levels of spurii, while operating over bandwidth at least three times greater than the widest previously report multipliers. The results achieved agreed well with the theory which predicted a low, but acceptable efficiency.

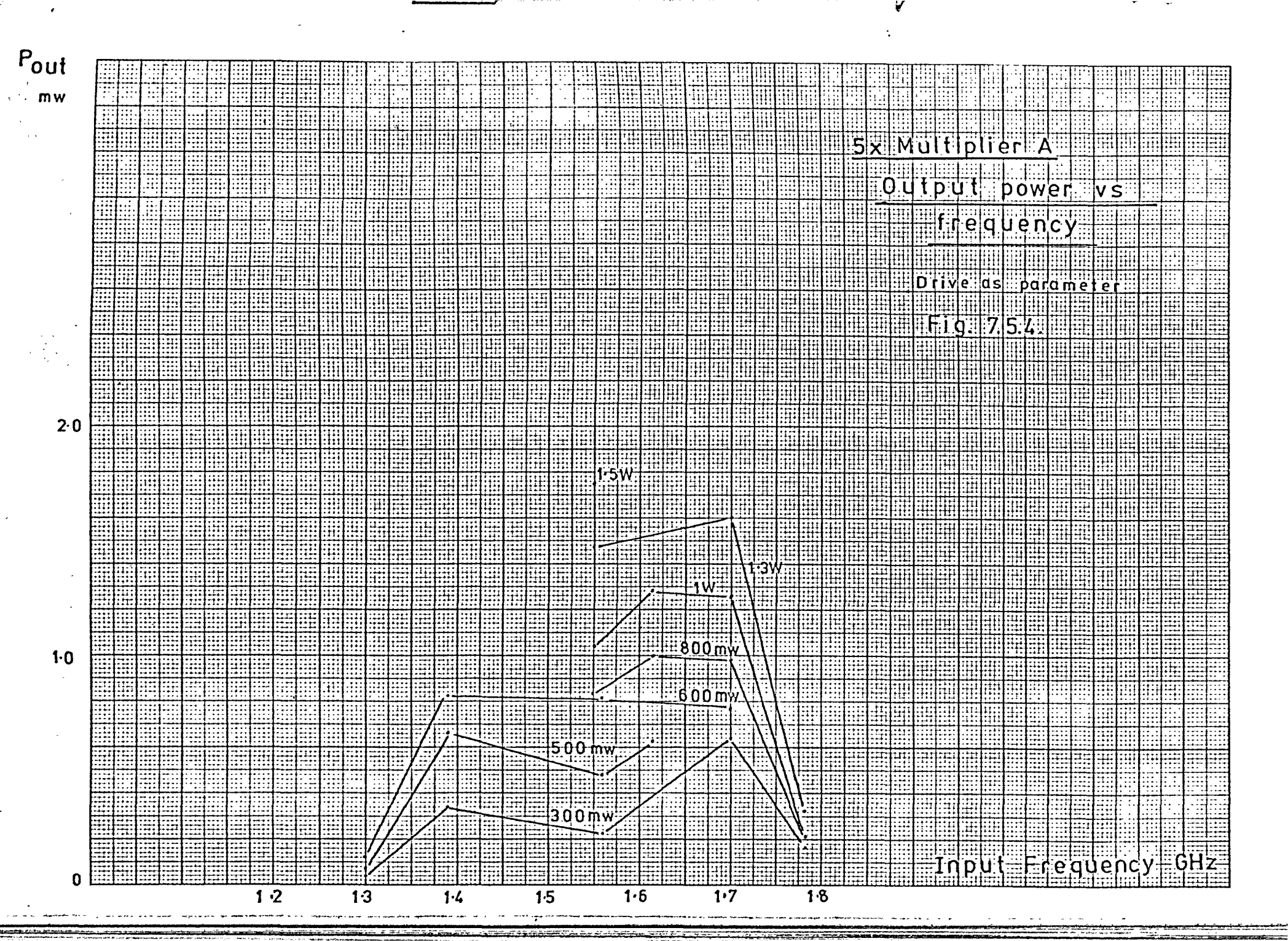
Pout
mw
5x Multiplier A
Output power vs
frequency
Drive as parameter
Fig. 7.5.4.
2·0
1·0
0
1·5W
1·3W
1W
800mw
600mw
500mw
300mw
1·2
1·3
1·4
1·5
1·6
1·7
1·8
Input Frequency GHz

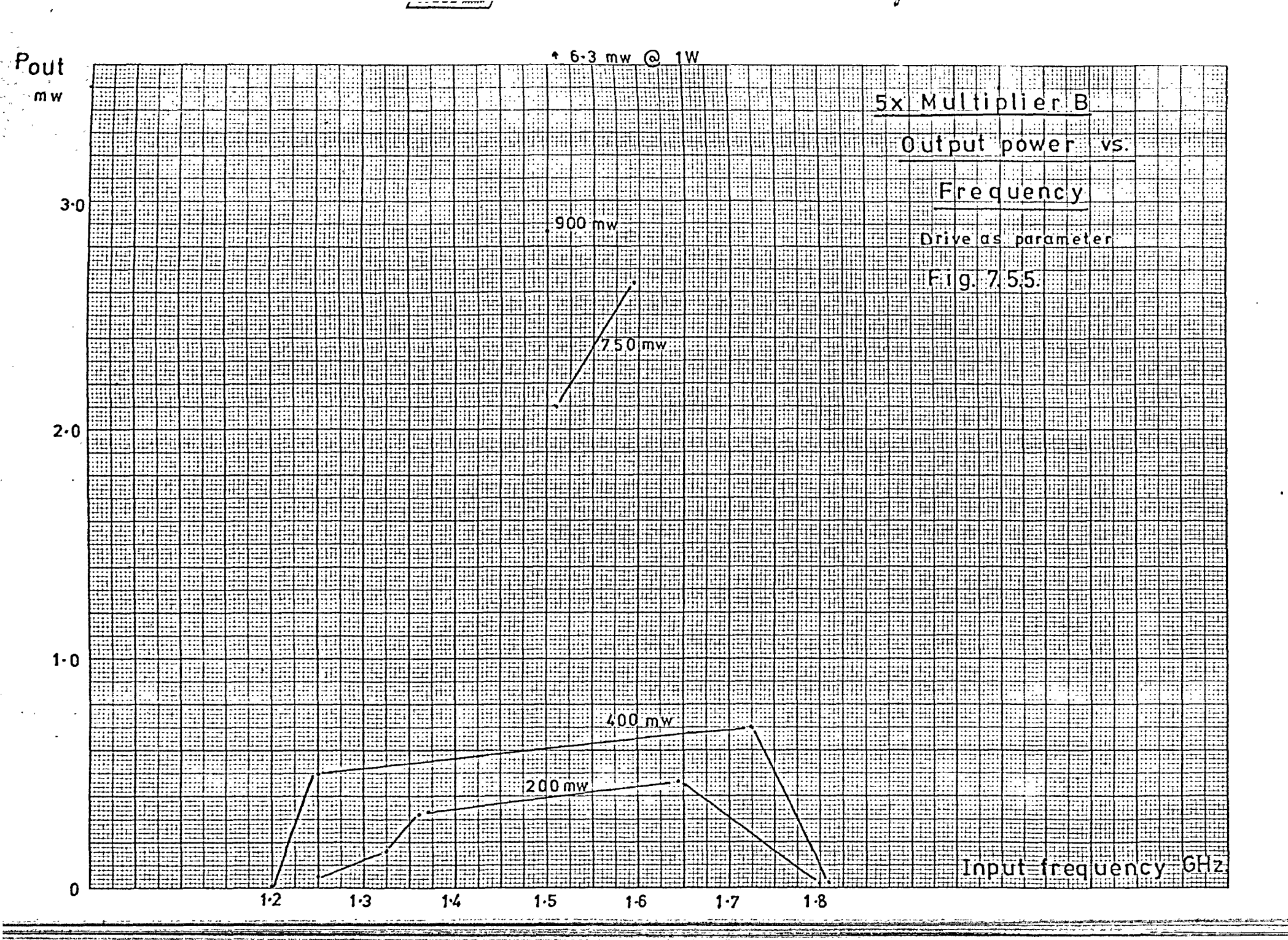
Pout
mw
6·3 mw @ 1W
5x Multiplier B
Output power vs.
Frequency
Drive as parameter
Fig. 7.55.
900 mw
750 mw
400 mw
200 mw
3·0
2·0
1·0
0
1·2
1·3
1·4
1·5
1·6
1·7
1·8
Input frequency GHz

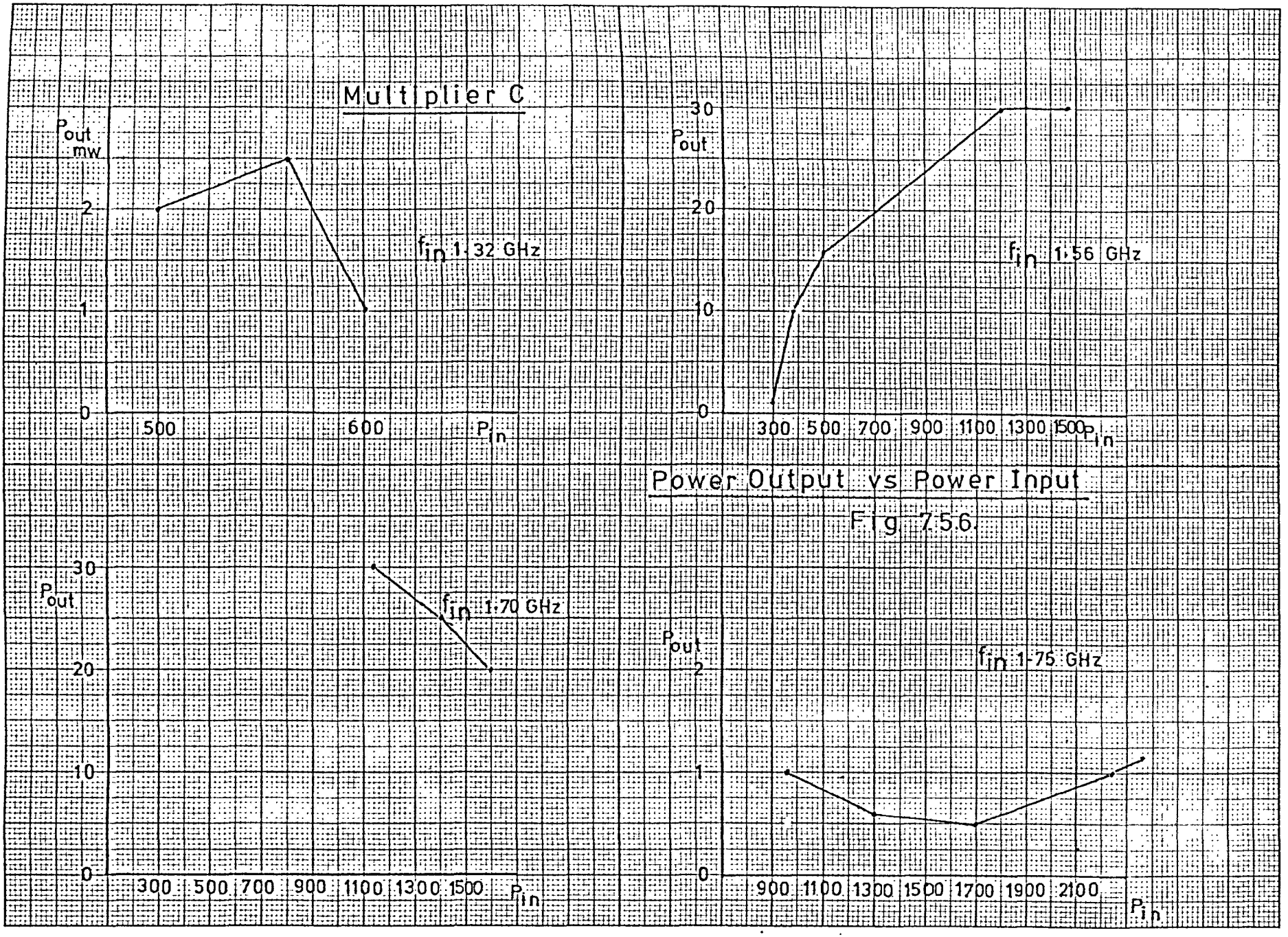
Multiplier C
Pout mw
2
1
0
500
600
Pin
fin 1.32 GHz
30
Pout
20
10
0
300 500 700 900 1100 1300 1500 Pin
fin 1.56 GHz
Power Output vs Power Input
Fig 7.5.6.
30
Pout
20
10
0
300 500 700 900 1100 1300 1500 Pin
fin 1.70 GHz
Pout
2
1
0
900 1100 1300 1500 1700 1900 2100
Pin
fin 1.75 GHz

CHAPTER 8 - CONCLUSIONS

8.1 The Relevance of Frequency Multiplying Systems

A chart recently published in a technical journal (Electronics, Sept 1972), showed that the electromagnetic spectrum from the S.L.F. up to the infrared is almost totally allocated. Every frequency band lower than the shortest millimetre wavelengths is used for some practical purpose. Only at the top end of the range were there gaps in the allocations.

Radar, both military and civil, in aircraft, ships and land vehicles, occupies a number of bands in the microwave spectrum, and was largely responsible for the early growth in this area.

Communications, the largest and possibly the most important user of the electromagnetic spectrum, covers the range from the lowest radio frequencies right into microwaves.

The services provided include radio and television, which as first comers in the field were allocated the most suitable frequencies and telephone, video, and data long-haul links. Police, fire, ambulance and taxi services operate in the VHF and UHF bands, while interaircraft and ground-control systems are currently using the L and S bands. Communications satellites primarily using the microwave bands, are providing many more channels for intercontinental links and making possible geological discoveries of prime importance.

As a result of the increasing importance and volume of communications there is a world-wide demand for communications equipment, particularly in the microwave region, where relatively large information bandwidths are available. In particular there is a need for microwave frequency sources of extremely high frequency stability, such as can only be crystal-derived, but, simultaneously,

variable frequency, or multi-channel, operation must be available.

The broadband frequency multiplier which has been described is proposed as a fundamental system building block. The bandwidth is, by a large margin, wider than other multipliers reported to date, the cost of fabrication low, and repeatability easily achieved. Spurious outputs have been minimized using filter techniques and a symmetrical arrangement of variable capacitance diodes. The availability of such broadband frequency multipliers could, for example, make the design of a full microwave frequency synthesizer a possibility.

8.2 The Hyperabrupt Diode-Consequences of the Analysis

The analysis of a hyperabrupt variable capacitance diode was undertaken at a period when it was thought that they would become available. Some novel aspects of the operation of this device were predicted and it was unfortunate that the samples promised by a manufacturer were not made.

The work of Kulesza showed that an inherent low pass filtering effect may be present if a diode with a specific non linear law is available. However, it must be noted that, if the m ($= \frac{1}{1-\gamma}$) of the diode is not exactly an integer then harmonics with $n > m$ are produced. Kulesza's theory holds and has been verified experimentally with an approximately-abrupt junction device operating in a waveguide 'high-pass filter'. The output was predominantly at the second harmonic, although this could not be said to represent a conclusive test. The most significant property of the hyperabrupt devices is the possibility of higher impedance operation than with the conventional devices. It is, essentially, this property which forms the basis of the predictions of high efficiency and relatively high power.

The starting point of the analysis was the construction of a set of equations for the voltages and currents in the circuit. In their general form, these basic equations are similar to those of Scanlan and Laybourne. The first major departure from that standard form was the introduction of the limiting curve conditions. This concept was originally due to Penfield and Rafuse, but its inclusion here in the general equations is thought to be unique. The new equation:-

$$\tan(n\Theta + \phi) = -n \tan\Theta \qquad \Theta = \text{phase angle at which limiting curve is tangential.}$$

was introduced. This equation has been shown to apply generally to any voltage or current limited operating conditions.

The limiting curve equation above was inserted back into the power series to obtain the values of input and output currents and voltages. Predictions were then made of the efficiency, bias point, and input and output impedances. It became evident that the efficiency tended to 100% for the diodes with $\gamma = 1$ This had been hinted at by previous authors on this subject (Kulesza, Markard and Yuan). It was shown that this was not an anomaly; although the efficiency at $\gamma = 1$ was a predicted 100%, the input and output impedances were infinite, and the power transferred was identically zero.

The existence of a peak in the power transfer curve was demonstrated. It was found that the optimum γ to generate the 'nth' harmonic obeyed the law

$$\gamma = \left(1 - \frac{2}{3n}\right) \quad \text{or more simply,} \quad m = 3/2\,n.$$

This was in exact agreement with the findings of Leonard for the doubler case; the result here is generalized. One important practical consequence from

this result is in varactor-tuning applications. If varactors having $\gamma \simeq 1$ were manufactured, one would expect reasonably wide tuning range with very little harmonic generation. The devices would therefore be less susceptible to interfering signals.

In frequency multipliers, the varactor diode should be chosen according to the application. Power output and efficiency can be selected if γ is closely controlled. Graphs such as fig. 4.3.1. should be constructed to aid in the selection of a suitable diode.

Finally, Kannam has reported very low coefficients of capacitance change with temperature over very wide ranges for implanted devices. This is a very significant property, as it means that the properties of a hyperabrupt frequency multiplier should be almost independent of the operating temperature.

8.3 The Step-Recovery Diode Analysis

The significance of the recombination and transition times has been explained in the analysis. It has been shown that, ideally, the diodes selected should operate at a point between these two extremes. When the devices are designed, the operating frequency should be included in selection of parameters. Charge stored, loss resistance, dynamic impedance and breakdown voltage are the other main parameters so that the selection of devices becomes complicated. Hence, the spectral assessment of diodes suggested in chapter 6 could be significant in the selection of devices and for matching.

The limiting curve expression first derived in chapter 4 was used with an extension to the 'single-sided' limiting condition i.e. the only voltage limit was the reverse breakdown. The mathematical model used was based on the exponential

capacitance first proposed by Shockley. A similar model has been successfully used by Jungmeister and Schmidt.

i.e.

$$C_s = C_o \exp\left(\frac{v_c}{V_{co}}\right) + C_c$$

C_c = residual capacitance

$V_{co} = KT/q$

The assumptions in the analysis were that:-

1. The exponential model for the capacitance was valid.
2. No appreciable power was lost in rectification.
3. Q_n^2 was small.
4. Some generalizations are allowed to simplify the output expressions.

The analysis produced algebraic expressions for the Fourier coefficients a_1, b_1 (the input voltage terms) an, bn (the output voltage terms) and the input and output power terms.

The bias point was predicted by the analysis, but it was felt that practical devices might well have to be operated in regions other than the ideal, when self-biassed. The main differences due to non-ideal bias would be in the available voltage swing and the power handled.

Curves have been drawn which predict the efficiency versus loss resistance for practical diodes. Later comparisons with the measured results suggested that the theoretical work was justified.

For generality, all the equations were worked in normalized terms. Denormalization was based on the measured data from the practical devices. The step-time was found by spectral analysis. The charge storage and

dynamic loss resistance were taken from the manufacturer's data. It would have been more satisfactory to obtain direct measurements of the charge storage but the necessary equipment was not available.

The operation of the step-recovery diode was shown to be extremely complex, but explainable by a relatively straightforward theoretical model. Measurements from the spectral assessment helped to understand the results of the analysis. Eventually, the final multiplier was constructed using data derived from the analytical treatment of the general step-recovery multiplier.

8.4 Spectral Assessment

It is evident that one requires as much performance data on the devices used as is practically obtainable. A new technique in this field is the spectral assessment measurement. At first, static measurements of current-voltage and capacitance-voltage were made. The C-V measurement has proved to be an extremely useful tool in initial acceptance trials, and a file of diode types was assembled to assist identification of parameters. No useful hyperabrupt devices were available at the time of this work.

In a practical multiplier situation, three mechanisms of harmonic generation are possible, and in general may contribute to the output spectrum. The mechanisms are:-

1. Half-wave rectification.
2. 'Varactor' harmonic generation, i.e. by time varying capacitance.
3. Step-recovery, in which the capacitance change occurs over a relatively small change in voltage and is a dynamic effect.

Low frequency physical and mathematical models were required for the prediction and confirmation of the harmonic pulse spectra of various diodes. It was known that SRD's show very little change in capacitance, and the C-V plots confirmed this. Hence, the predominant effects to be observed at microwave frequencies were rectification and step-recovery. Relatively simple broadband pulse analytical methods were used (figs. 6.3.1 - 3), both for single and double diodes, and for SRD's and half-wave rectifiers. The diodes chosen as physical models gave very good results in both the quantitative and qualitative senses and clearly demonstrated the different harmonic spectra which are to be associated with particular diode types.

In particular, the series of oscilloscope photographs showing the progress of the SRD from a good rectifier, through step-recovery, to attenuation only is thought to be a novel feature of the experiment, and correlated well with the theoretical and practical measurements.

The double-diode arrangement provided highly satisfactory results, and clearly showed that odd harmonics were produced with reduced even harmonic output.

Measurements at microwave frequencies were naturally more restricted. No sampling oscilloscope was available, and the spectrum analyser had a useful range up to 12 GHz only. However, the sensitivity of the analyser formed the basis of an extremely accurate assessment of the devices used. Essentially, the sampling oscilloscope is a linear system; its resolution is only about 3% of 'full-scale'. The spectrum analyser can be used logarithmically, and hence with help from external filters, has a potential range of $>$ 100 db. To take advantage of this, the comparison technique was evolved, which maintained system errors below 1 db.

Using the comparison technique, microwave frequency measurements were performed on Schottky barrier and step-recovery devices. With the models derived in the low frequency work it was possible to examine the device behaviour in detail, and to note that for the SRD at 1.5 GHz input, the operation was predominantly step-recovery. This device was intended for higher frequency operation, so it was important to check that rectification was not taking place. In addition, it was found that the first spectral null occurred in the region of the seventh harmonic. Although this inferred that the fifth harmonic would not be efficiently generated (confirming the earlier theoretical work) it showed that suppression of the next troublesome harmonic would not be required to be great.

The spectral assessment technique was found to be relatively simple to apply, when the basic theory had been derived, and provided an extremely useful insight into diode operation. In particular, the low frequency model was found to be a surprisingly good guide to the operation of the high frequency devices and it is hoped that this work will continue.

8.5 The Practical Results

Chapter 7 was intended to give a detailed design procedure for the construction of a broadband step-recovery diode frequency multiplier, and to report the results on a practical design. The design considerations are:-

1. Bandwidth required.
2. Physical dimensions and weight.
3. Cost
4. Efficiency.
5. Power output
6. Number of stages (one stage should give results applicable to a chain).

Clearly these factors are closely interrelated. In general, the application requirement dictates the final compromises which must be reached. Cost is, increasingly, a significant factor as civilian applications move into the microwave range. This project was highly significant in that the end product was a fully integrated microwave circuit on a single substrate. Although microwave I.C's are now coming into production, units are usually subdivided into sections. This device was a complete circuit in one package.

The stripline-TFE structure has been commented on. It is probably the most economical means of producing M.I.C's, and is likely to remain so. The techniques are basically those used for high precision printed-circuit work, and as such are easily adaptable to conventional electronics laboratories. The alternative technique of gold deposited on alumina is still largely experimental, and requires a great deal of specialized (and expensive) equipment and highly skilled personnel. It was felt that the alumina technique could be profitably investigated thoroughly at a later date, although it seems likely that, because of the expense, it will be restricted to relatively cost-insensitive, performance-critical areas.

The only fundamental limit to the bandwidth of the double diode system is the presence of interfering harmonics. The general expression for the fractional bandwidth referred to the centre frequency is:-

$$\theta = \frac{2}{n+1}$$

Harmonic charts such as fig. 7.2.1 are useful in checking for possible filter problems. It is clearly not desirable to aim for the theoretical maximum bandwidth unless some appreciable spurii can be tolerated. The filter performance would give a good guide as to how near the band edges the

multiplier may be operated.

Filter synthesis represented a significant part of the practical work in the multiplier. In such a complex subject, it was thought necessary to consult several texts on the subject. The main reference was the book by Matthaei et al. with some additional information from Geffe, and Youla. Design parameters were selected fairly arbitrarily; a spurious suppression (third and seventh harmonics) of $>$ 20 db was desired, although in practice it proved convenient to put theoretically infinite rejection points in these regions.

The critical component of the final design was the output filter. It was designed in two stages, a bandpass network, which ultimately defined the output passband, and a low-ripple, high-pass filter which rejected the fundamental. The results of the measurements on the filters were regarded as good examples of the capability of the Copper-TEE system. The input filter was designed as a low-pass network, for ease of construction and to prevent subharmonic oscillations. It has been shown that rejection of low frequencies back into the multiplier can cause oscillations, particularly at half the fundamental frequency, due to the negative resistance of the diodes (Parker). A low pass network enables oscillations at these frequencies to pass into the buffer-isolator on the input. In practice, this was not a problem, as such oscillation was not detected. The input filter was designed as a general purpose unit, adjustable by mask modification to any frequency between 1.5 GHz and 2 GHz, while retaining approximately correct terminating impedances. A feature of all the filters was the close adherence to the design parameters; it was felt that the gold/ceramic system would have presented many more problems in this area.

The bias networks provided a severe design problem. In keeping with the general integrated circuit approach, it was necessary that they were simple, but effective. After several trials, the circuits shown in fig. (7.3.7.) were adopted. Construction by a reasonably skilled technician would be possible. The chip capacitors were difficult to handle, and were not really suitable for soldering, although, with care, this was achieved. Unfortunately, these components are not yet at the stage where all the behaviour is entirely repeatable, so screening of the devices before use is highly desirable. The parameters are actual capacitance, and self-resonant frequency. Ideally, the chips should maintain the balance of symmetry.

Ideally, diodes should be selected for the multiplier to be constructed according to the criteria suggested in chapter 7. However, very often, one must use the diodes available at the right price, so that the design must be a compromise. This was the case with the 5082-0386 devices, which were nominally identical to the more expensive .0335. The results showed conclusively that the latter devices were superior in performance. The design procedure used the device parameters measured in circuit to assess performance. The resulting multiplier was not sensitive to the type of the devices, provided they were a reasonably matched pair. Clearly however, better devices gave better results.

Although it was not at first intended to introduce significant mechanical improvements, this project produced a completely integrated multiplier, which, although not a new concept, was the first practically realized circuit of its kind. The power output and efficiency closely matched the theoretically

predicted values, as did the bandwidth. The spurious harmonic suppression was found to be equal or better than that from commercial narrow-band frequency multipliers.

Summary

It was felt that the research project achieved its goals as a training in research techniques and methods, and as a thorough theoretical and practial investigation of a particular topic. It is hoped that some of the theoretical observations, when published, will lead to a new understanding of the operation of non-linear capacitance active devices.

In the literature, the variable capacitance device as an harmonic generating circuit element, as distinct from a tuning function, is often neglected. While it is clear that a full understanding of non-linear resistive elements is of primary importance, non-linear capacitance is an inherent and inseparable part of every semiconductor junction and hence a knowledge of the operation of such elements is of vital importance.

Appendix 1

The Scanlan and Laybourne papers (q.v.), and later the chapter 'Analysis of Varactor Harmonic Generators' by Professor Scanlan in the book called 'Advances in Microwaves' were found to be very useful guides to the performance of the analysis. The final Scanlan analysis used a truncated power-series form to include some large signal effects, basically, the form

$$C(v) = \frac{C_0'}{(1 - v/\phi)^m}$$

was adopted. It is felt by the present author that the weakness of this analysis occurs when $v = \phi$; this region is avoided in the analysis. The main difference between Professor Scanlan's analysis and that to be presented in chapter 4 is in the charge equation. Prof. Scanlan constrains the charge to

$$Q = Q_B + Q_0 \cos \omega t$$

A more realistic approach would be

$$Q = Q_B + Q_1 \cos \omega t + Q_n \cos n\omega t$$

This equation has been used for both the hyperabrupt and the step-recovery diode analysis.

Appendix 2- Fourier Spectrum of a Part-Sinusoid Pulse

In certain cases the voltage pulse from a step-recovery diode may be approximated to a part-sinusoid i.e.

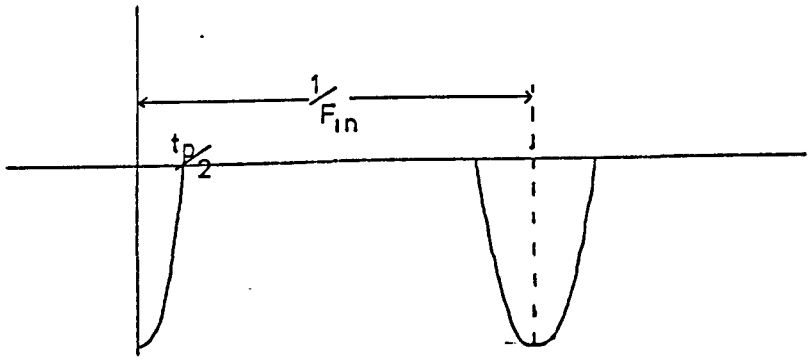

The input frequency is F_{IN}, and the pulse width tp

$$t_p \simeq \pi \sqrt{L C_{va}}$$

or modified by load, see appendix (A.3.1)

The Fourier series is an even function

$$F(x) = a_0 + \sum_{n=1}^{\infty} a_n \cdot \cos nx.$$

where

$$a_0 = \frac{1}{\pi} \int_0^{\pi} F(x) \cdot dx.$$

and

$$a_n = \frac{2}{\pi} \int_0^{\pi} F(x) \cdot \cos nx \cdot dx.$$

The assumption made about F(x) is

$$F(x) = 0 \qquad \text{for} \quad t_p/2 < x < (1/F_{in} - t_p/2)$$

$$F(x) = -\cos\left\{\frac{1}{2 t_p F_{IN}} \cdot x\right\} \quad \text{for} \quad 0 \leq x < t_p/2 \quad \text{and} \quad (1/F_{in} - t_p/2) < x < 1/F_{IN}$$

$$a_0 = \frac{1}{\pi} \int_0^{\pi} - \cos \left\{ \frac{1}{2 t_p F_{IN}} \cdot x \right\} \cdot dx$$

$$= -\frac{1}{\pi} \int_0^{t_p F_{IN} \pi} \cos \left\{ \frac{1}{2 t_p F_{IN}} \cdot x \right\} dx$$

$$= -\frac{1}{\pi} \left[2 t_p F_{IN} \cdot \operatorname{Sin} \left(\frac{1}{2 t_p F_{IN}} \cdot x \right) \right]_0^{t_p F_{IN} \pi}$$

$$= -\frac{1}{\pi} \cdot 2 \cdot t_p \cdot F_{IN} \cdot \operatorname{Sin} \frac{\pi}{2}$$

$$\therefore a_0 = -\frac{2}{\pi} \cdot t_p \cdot F_{IN}$$

or, let $\frac{1}{2 t_p F_{IN}} = N$

$$\therefore a_0 = -\frac{1}{\pi} : \frac{1}{N}$$

$$a_n = -\frac{2}{\pi} \int_0^{\frac{1}{N} \cdot \frac{\pi}{2}} \operatorname{Cos} \cdot Nx \cdot \operatorname{Cos} nx \cdot dx.$$

$$= -\frac{2}{\pi} \int_0^{\frac{1}{N} \cdot \frac{\pi}{2}} \frac{1}{2} \left\{ \cos (N+n)x + \cos (N-n)x \right\} \cdot dx.$$

$$= -\frac{1}{\pi} \cdot \left[\frac{1}{N+n} \cdot \sin (N+n)x + \frac{1}{N-n} \cdot \sin (N-n)x \right]_0^{\frac{1}{N} \cdot \frac{\pi}{2}}$$

$$= -\frac{1}{\pi} \cdot \left[\frac{1}{N+n} \cdot \sin \frac{\pi}{2} \left(1 + \frac{n}{N}\right) + \frac{1}{N-n} \sin \frac{\pi}{2} \left(1 - \frac{n}{N}\right) \right]$$

$$a_n = -\frac{1}{\pi} \left(\frac{2N}{N^2 - n^2} \cdot \operatorname{Cos} \left(\frac{\pi n}{2N} \right) \right)$$

Appendix 3.1

The Fourier coefficients of a part sine wave

(Section 3.2.1)

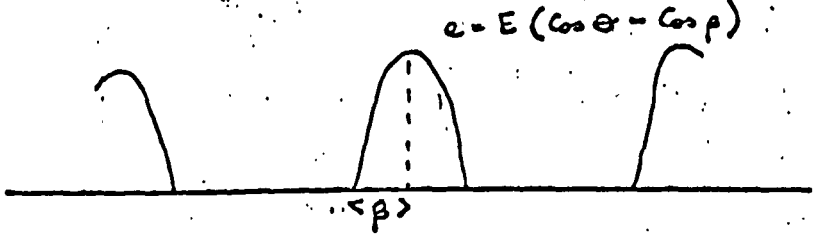

Fig. 3.2.1.

are, from tables,

$$a_0 = \frac{E}{\pi}\left(\sin\beta - \beta\cos\beta\right)$$

$$a_1 = \frac{E}{\pi}\left(\beta - \frac{\sin 2\beta}{2}\right)$$

$$a_n = \frac{2E}{\pi n(n^2-1)}\left(\sin n\beta.\cos\beta - n\cos n\beta.\sin\beta\right)$$

$$b_n = 0.$$

Inspection of the a_u coefficient shows that an optimum condition exists for any $n \geq 2$.

i.e.

$$\frac{d(a_n)}{d\beta} = \frac{2E}{\pi n(n^2-1)}\left[\begin{matrix} n.\cos n\beta.\cos\beta - \sin n\beta.\sin\beta \\ + n^2\sin n\beta.\sin\beta - n\cos n\beta.\cos\beta \end{matrix}\right]$$

$$= \frac{2E}{\pi n(n^2-1)}\left[(n^2-1).\sin n\beta.\sin\beta.\right]$$

$$\therefore \frac{da_n}{d\beta} = \frac{2E}{\pi n}\left[\sin n\beta.\sin\beta\right]$$

At a maximum, minimum, or inflexion,

$$\frac{da_n}{d\beta} = 0.$$

$$\therefore 0 = \sin n\beta.\sin\beta$$

$$\therefore \beta = 0 \text{ or } K\pi$$

$$\text{or } n\beta = 0 \text{ or } K\pi$$

} K = any integer.

$$\frac{d^2 a_n}{d\beta^2} = \frac{2E}{\pi n}\left[n \cos n\beta . \sin\beta + \sin n\beta . \cos\beta\right]$$

When $\beta = 0$

$$\frac{d^2 a_n}{d\beta^2} = 0 \quad \text{inflexion ;}$$

When $\beta = \frac{\pi}{n}$,

$$\frac{d^2 a_n}{d\beta^2} = \frac{2E}{\pi n}\left[-n \sin\frac{\pi}{n} + 0\right]$$

i.e. −ve maximum ;

Similarly at

$$\beta = \frac{2\pi}{n}$$

$$\frac{d^2 a_n}{d\beta^2} = +ve \qquad \text{minimum}$$

Alternate maxima and minima occur respectively at odd and even multiples of $\frac{\pi}{n}$

i.e. For maximum

$$\beta = \frac{(2K+1)\pi}{n}$$

Physically, the first solution is usually the best for efficient operation.

Efficiency in the ideal case may be calculated from

$$\eta = \frac{a_n^2}{a_o^2}$$

$$\text{i.e. } a_n^2 = \left[\frac{2E}{\pi n (n^2-1)}\left(-n \cos\left(n . \frac{\pi}{n}\right) . \sin\frac{\pi}{n}\right)\right]^2$$

$$= \left[\frac{2E}{\pi n (n^2-1)} . n \sin\frac{\pi}{n}\right]^2$$

$$a_o^2 = \left[\frac{E}{\pi} \left(\sin\frac{\pi}{n} - \frac{\pi}{n}\cos\frac{\pi}{n} \right) \right]^2$$

$$\therefore \eta = \left[\frac{\frac{2E}{\pi(n^2-1)} \sin\frac{\pi}{n}}{\frac{E}{\pi}\left(\sin\frac{\pi}{n} - \frac{\pi}{n}\cos\frac{\pi}{n}\right)} \right]^2$$

$$\eta = \frac{4}{(n^2-1)^2} \cdot \frac{\sin^2\frac{\pi}{n}}{\left(\sin\frac{\pi}{n} - \frac{\pi}{n}\cos\frac{\pi}{n}\right)^2} \qquad (1)$$

This is the efficiency of conversion of the D.C. supply to the nth harmonic and neglecting device non-linearity and signal input power. Clearly, the efficiency falls rapidly with n. The possibility of high efficiencies if the denominator has zero value, i.e.

$$\sin\frac{\pi}{n} = \frac{\pi}{n}\cos\pi/n$$

may be disregarded; it leads to the equation

$$\tan\pi/n = \pi/n$$

i.e. $$\pi/n \rightarrow 0$$

Than a_n tends to 0

and a_1 " " 0

The efficiency is indeterminate; no d.c. input gives no harmonic output.

Equation (1) above is general for any device which produces the waveform described. The main application is to the 'class-C' amplifier to be described in the next chapter.

APPENDIX - Filtering Limitations on Frequency Multipliers
3.2

1. General System - All harmonics possible

Conditions must be imposed on any harmonic generating system which prevent oscillations at harmonics other than the desired from entering the output port. The input and output passbands must be such that, in the limits, the next nearest possible harmonics are just prohibited. For an 'nth' harmonic generator, this means that the upper limit is the (n + 1)th harmonic of the lowest input frequency. The lower limit is necessarily symmetrically placed with respect to the centre frequency. The conditions may be summarized algebraically:

System centre frequency f

Bandwidth δ

Fractional bandwidth ϕ

Upper limit of output $= (n+1)\left\{f - \delta/2\right\}$

Lower limit of output $= nf - n\delta/2$

From the first equation it may be seen that

$$n\left(\frac{\delta}{2} + f\right) = (n+1)\left\{f - \frac{\delta}{2}\right\}$$

$$\therefore n.\frac{\delta}{2} + (n+1)\frac{\delta}{2} = (n+1)f - nf$$

$$\frac{2n+1}{2}.\delta = f$$

$$\therefore \quad \delta = \frac{2f}{2n+1}$$

$$\text{or,} \quad \phi = \frac{2}{2n+1}$$

The lower limit of the output may be derived from the input

$$\text{i.e.} \quad nf - n\delta/2 = n\left(f - \delta/2\right)$$

2. Cancelling System – odd or even harmonics only

Systems are available which cancel out, by balancing or waveshaping, the even or odd harmonic components in the available spectrum. In the above example, the nearest interfering harmonics are shifted to (n + 2) and (n – 2).

Hence, the upper limit of the output is

$$\text{Upperbound} = (n+2)\left\{f - \delta/2\right\}$$

and therefore

$$n\left(f + \frac{\delta}{2}\right) = (n+2).\left(f - \frac{\delta}{2}\right)$$

$$\therefore n.\frac{\delta}{2} + (n+2).\frac{\delta}{2} = 2f$$

$$\therefore \quad \delta = \frac{4f}{2n+2}$$

$$\delta = \frac{2f}{(n+1)}$$

$$\text{or,} \quad \underline{\delta = \frac{2}{n+1}}$$

Clearly, a substantial improvement in bandwidth is brought about by a cancelling system.

Comparative bandwidths are:

FRACTIONAL BANDWIDTHS (MAX. THEORETICAL)

n	All	evens only	odds only
2	.400	.667	
3	.286		.500
4	.222	.400	
5	.182		.333
6	.153	.286	
7	.133		.250
8	.118	.222	
9	.105		.200
10	.095	.182	

As n tends to infinity, the advantage of the balanced system tends to 2 : 1.

Methods have been suggested (Scanlan) which cancel the odd order harmonics and the fourth harmonic, in a doubler. The bandwidth available is, derived by the method above, i.e.

$$\phi = \frac{10}{2n+5} = .667$$ i.e. as above

No intrinsic advantage is gained in terms of bandwidth, although the practical construction of the filters may be eased.

Appendix 4.1.1

Many of the analyses presented before about 1965 made small signal approximations. Although many variations have been made, the equations derived below cover most such approaches.

The general C-V expression is:-

$$C(v) = \frac{C_o}{(1 + v'(t))^{\gamma}}$$

where

$$v'(t) = \frac{v(t)}{v_o + \phi}$$

The charge is defined by

$$Q = \int C(v).dv.$$

$$\therefore \quad Q = C_o.(v_o + \phi).\frac{1}{1-\gamma}.[1 + v'(t)]^{1-\gamma}$$

When $v'(t) = 0$, $Q = Q_o$

$$\therefore \quad Q_o = \frac{C_o(v_o + \phi)}{(1-\gamma)}$$

And $$Q = Q_o.(1 + v'(t))^{1-\gamma}$$

Or, let $Q = Q_o + Q_{ac}$

$$\therefore \quad (1 + v'(t)) = \left(1 + \frac{Q_{ac}}{Q_o}\right)^{\frac{1}{1-\gamma}}$$

Two alternative circuit assumptions are available; the current-driven shunt, and the voltage driven series. The expansions of the above equations are respectively:

$$\frac{Q}{Q_o} = 1 + \frac{Q_{ac}}{Q_o} = 1 + (1-\gamma)v'(t) + \frac{(1-\gamma).(-\gamma).(v't)^2}{2!}$$

$$+ \frac{(1-\gamma).(-\gamma).(-\gamma-1).[v'(t)]^3}{3!} \quad \ldots\ldots$$

general coefficient

$$A_{n_1} = \frac{1}{n!}.(1-\gamma).(-\gamma) \cdots\cdots (1-\gamma-n+1)$$

and

$$1+v'(t) = 1 + m Q_{ac}' + \frac{1}{2!}.m.(m-1).Q_{ac}'^{2} \cdots\cdots$$

$$\therefore A_{n_2} = \frac{1}{n!}.(m).(m-1) \cdots\cdots (m-n+1) \quad \text{where } m = \left(\frac{1}{1-\gamma}\right)$$

The zeroes of the An are the first guide to the properties of the hyperabrupt frequency multiplier. The current driven shunt multiplier has

$$A_n = \frac{1}{n!}..m.(m-1) \cdots\cdots (m-n+1)$$

Clearly, the zeros occur when:-

$$m = \text{integer}$$

and the series terminates when:-

$$m = n$$

Hence, to generate the 'nth' harmonic, a particular varactor should have

$$m \geq n$$

The first zero occurs when

$$(m-1) = 0 \quad \text{(Hence } n = 2\text{)}$$

$$\therefore \frac{1}{1-\gamma} - 1 = 0$$

$$\therefore \gamma = 0$$

i.e. the device is not a variable capacitance, so no harmonics are generated.

The first true zero is

$$(m - 2) = 0$$

i.e. $n = 3$

$$\gamma = 0.5$$

This zero repeats for all higher n values. Higher terms are calculated in a similar way. Finally, the curves of fig. 4.1.2 may be constructed for any n. The curves are drawn with respect to $A(\gamma)$, the voltage coefficient described above, but a dual set (with different zeroes) could be constructed for the voltage driven multiplier.

The conclusion is that to generate a harmonic 'n', it is preferable to have $\gamma \geqslant \frac{n-1}{n}$

although non-integral 'm' values will produce some harmonic output for any n.

Appendix 4.2.1 Solution of Power Integrals.

The integrals equations 4.2.14 and 4.2.15 are

$$P_\alpha = -\frac{n\omega}{2\pi}\sum_{K=0}^{m}\binom{m}{K}\cdot Q_1'^{K}\cdot Q_n'\int_{-\pi}^{\pi}(\cos\omega t)^K\cdot\sin(n\omega t+\phi)\cdot d\omega t$$

$$P_\beta = -\frac{n\omega}{2\pi}\sum_{K=0}^{m}\binom{m}{K}\cdot Q_1'^{K-1}\cdot Q_n'^{2}\cdot\frac{K}{2}\int_{-\pi}^{\pi}(\cos\omega t)^{K-1}\cdot\sin(2n\omega t+\phi)\cdot d\omega t.$$

In the interval $-\pi$ to π , all time variables average to zero. Only the cross-products which result in D.C. terms need be considered. In the expansion of $(\cos \omega t)^K$, $(\cos n\omega t)$ occurs for $K \geqslant n$, in alternate terms. The coefficients of the terms are derived from the binomial expression for $(\cos \omega t)^K$, i.e. a Pascal's Triangle.

Substituting values of K in the above expressions,

for P_α , $K \geqslant n$

$$P_\alpha = -\frac{n\omega}{2\pi}\left\{\binom{m}{n}\cdot Q_1'^{n}\cdot Q_n'\int_{-\pi}^{\pi}\frac{\sin(n\omega t+\phi)}{2^{n-1}}\cdot\cos n\omega t\cdot d\omega t\right.$$

$$+\binom{m}{n+2}\cdot Q_1'^{n+2}\cdot Q_n'\int_{-\pi}^{\pi}\frac{(n+2)}{2^{n+1}}\cdot\sin(n\omega t+\phi)\cdot\cos n\omega t\cdot d\omega t$$

$$+\binom{m}{n+4}\cdot Q_1'^{n+4}\cdot Q_n'\int_{-\pi}^{\pi}\frac{(n+4)\cdot(n+3)}{2^{n+3}\cdot 2!}\cdot\sin(n\omega t+\phi)\cdot\cos n\omega t\cdot d\omega t$$

$$\left.+\binom{m}{n+6}\cdot Q_1'^{n+6}\cdot Q_n'\int_{-\pi}^{\pi}\frac{(n+6)(n+5)(n+4)}{2^{n+5}\cdot 3!}\cdot\sin(n\omega t+\phi)\cdot\cos n\omega t\cdot d\omega t\right.$$

— — et. seq. — — — —

In general

$$P_\alpha = -\frac{n\omega}{2\pi}\left[\sum_{j=0}^{\frac{1}{2}(m-n)}\binom{m}{n+2j}\cdot\frac{(n+2j)!}{(n+j)!}\cdot\frac{Q_1'^{n+2j}\cdot Q_n'}{2^{n+2j-1}}\cdot\frac{1}{j!}\cdot\int_{-\pi}^{\pi}\frac{\sin\phi\,d\omega t}{2}\right]$$

$$\therefore\quad P_\alpha = -\frac{n\omega}{2}\left\{\sum_{j=0}^{\frac{1}{2}m-n}\binom{m}{n+2j}\cdot\frac{(n+2j)!}{(n+j)!}\cdot\frac{Q_1'^{n+2j}\cdot Q_n'}{2^{n+2j-1}}\cdot\frac{1}{j!}\cdot\sin\phi\right\}$$

Similarly, P_β is non-zero only if $m > (2n+1)$

The solution is

$$P_\beta = -\frac{n\omega}{2}\sum_{i=0}^{\frac{1}{2}(m-(2n+1))}\binom{m}{2n+2i+1}\cdot\left(\frac{2n+2i+1}{2}\right)\cdot\left(\frac{(2n+2i+1)!}{(2n+i+1)!}\right)\cdot\frac{1}{i!}$$
$$\times\frac{Q_1'^{2n+2i}\cdot Q_n'^{2}}{2^{2n+2i-1}}\cdot\sin\phi$$

i, j are integers

Examination of the coefficients indicates that P_α is the dominant term, when $m > (2n+1)$, and, of course, the only term for $m < (2n+1)$.

The next term in the series, which has been so far ignored, is

$$P_\psi = -\frac{n\omega}{2\pi}\sum_{K=0}^{m}\binom{m}{K}\cdot\left\{Q_1'^{K-2}\cdot Q_n'^{2}\cdot\frac{K(K-1)}{2!}\int_{-\pi}^{\pi}(\cos\omega t)^{K-2}\cdot(\cos n\omega t+\phi)^{2}\cdot(\sin n\omega t+\phi)^{2}\cdot d\omega t\right\}$$

Provided $Q_n'^{2}$ is negligible, this term can be ignored.

Appendix 4.3.1. Maximum Power Transfer

The equation 4.3.1d is

$$\frac{Q_n'}{Q_1'} = \frac{\sin\theta}{n.\sin(n\theta+\phi)} \qquad \text{A.4.3.1}$$

A further differentiation is necessary at this stage to optimise the output conditions. In conventional analyses, this type of differentiation is performed at the end of the work, with a loss of generality. Introduction of the differential at this stage gives a clear insight into the working of the mathematical model of the varactor.

Several possible approaches are available. Differentiation must be w.r.t. θ, but the dependent variable may be Q_1', Q_n', (Q_n'/Q_1') or

$$\left(\frac{Q_1'^2 + Q_n'^2}{Q_1'.Q_n'}\right),$$

a term on which the total power dissipated in the loss resistance depends. It can be shown that all these are identically equivalent equations, and indeed lead to the same result. Intuitively, therefore, we take the ratio of the currents Q_n'/Q_1' as the parameter to maximise.

$$\left.\begin{aligned} \frac{Q_n'}{Q_1'} &= \frac{\sin\theta}{n.\sin(n\theta+\phi)} \\ \frac{d}{d\theta}(Q_n'/Q_1') &= \frac{n\sin(n\theta+\phi).\cos\theta - \sin\theta.n^2.\cos(n\theta+\phi)}{n^2\sin^2(n\theta+\phi)} \end{aligned}\right\} \qquad \text{A.4.3.2}$$

at the maxima and minima,

$$\frac{d}{d\theta} = 0$$

$$\therefore \sin(n\theta+\phi).\cos\theta = +n.\sin\theta.\cos(n\theta+\phi)$$

$$\therefore \underline{\tan(n\theta+\phi) = +n.\tan\theta} \qquad \text{A.4.3.3}$$

This equation is readily solved. The worst case value of ϕ is 0, and therefore

$$\tan n\theta = n \tan\theta \qquad \text{A.4.3.4}$$

$$\therefore \quad \theta = 0 \text{ or } \pi \text{ etc.}$$

However, differentiating equation A.4.3.2 a second time shows that $\frac{d^2(Q_n'/Q_1')}{d\theta^2}$ is identically zero when $\theta = 0, \pi$ etc. and these points are only inflexions. Consideration of the primary equation 4.3.1b in chapter 4 shows that any solution found must be a four-quadrant solution i.e. the solution must be equally valid for θ and $-\theta$ simultaneously. Hence equation A.4.3.3 may be written in the alternative forms.

$$\tan(-n\theta+\phi) = n\tan\theta \qquad \text{A.4.3.5}$$

$$\tan(-n\theta+\phi) = -n\tan\theta \qquad \text{A.4.3.6}$$

$$\tan(n\theta+\phi) = -n\tan\theta \qquad \text{A.4.3.7}$$

Equations A.4.3.6 differs from A.4.3.3 only in the sign of ϕ ; these are further inflexions. Equations A.4.3.5 and A.4.3.7 are true solutions of the equation A.4.3.1 and contain maxima and minima.

The differentiation has been checked with the alternative parameters.

From section 4.2 it is evident that if, under the assumptions made, P_α is the dominant term, then

$$P_\alpha \text{ proportional to } -\sin\phi \qquad \text{A.4.3.8}$$

Normally, one is concerned with operation at the maximum power point (although this may not coincide with maximum efficiency) and hence

$$\phi = \frac{3\pi}{2}, \frac{7\pi}{2} \text{ ----} \qquad \text{A.4.3.9}$$

The solution of the general equation

$$\tan(n\theta+\phi) = -n\tan\theta \qquad \text{A.4.3.10}$$

may proceed.

Rewriting A.4.3.10, with the solution for ϕ,

$$\cot n\theta = n\tan\theta$$

The first solution of this equation for any n lies between 0° and $\pi/2n$. Solutions may be worked by trial, by hand or computer, but an analytical solution may be considered more appropriate.

$$\cot n\theta = \frac{i.(e^{in\theta}+e^{-in\theta})}{(e^{in\theta}-e^{-in\theta})}$$

and

$$n\tan\theta = \frac{n}{i}.\frac{(e^{i\theta}-e^{-i\theta})}{(e^{i\theta}+e^{-i\theta})}$$

$$\therefore \; i.\frac{(e^{in\theta}+e^{-in\theta})}{(e^{in\theta}-e^{-in\theta})} = \frac{n}{i}.\frac{(e^{i\theta}-e^{-i\theta})}{(e^{i\theta}+e^{-i\theta})}$$

and

$$\therefore \quad (e^{in\theta} + e^{-in\theta})(e^{i\theta} + e^{-i\theta}) = -n.(e^{i\theta} - e^{-i\theta})(e^{in\theta} - e^{-in\theta})$$

$$\therefore \quad 0 = (n+1)\left[e^{i\theta(n+1)} + e^{-i\theta(n+1)}\right] - (n-1)\left[e^{i\theta(n-1)} + e^{-i\theta(n-1)}\right]$$

Hence

$$\underline{(n+1)\,\mathrm{Cos}(n+1).\theta = (n-1).\mathrm{Cos}(n-1)\,\theta}$$

$$Q_o = \frac{m.V_B.C_o}{2^m - 1} \qquad \text{for any 'n'}$$

Solutions to the equations have been found by computation.

n	θ	nθ°	Q_n'/Q_1'	nQ_n'/Q_1'
2	24.095	48.19	.3060	.6120
3	16.268	48.805	.1417	.4251
4	12.251	49.005	.0703	.2812
5	9.822	49.110	.0450	.2250
6	8.198	49.190	.0314	.1884
7	7.029	49.205	.0231	.1617
8	6.153	49.225	.0177	.1416
9	5.471	49.240	.0140	.1260
10	4.925	49.250	.0113	.1130

Now

$$Q_1'\,\mathrm{Cos}\theta - Q_n'\,\mathrm{Sin}\,n\theta = 1$$

$$\text{and} \quad \frac{Q_n'}{Q_1'} = \frac{-\mathrm{Sin}\,\theta}{n\,\mathrm{Cos}\,n\theta}$$

$$\therefore Q_1'\mathrm{Cos}\theta + Q_1'\frac{\mathrm{Sin}\,n\theta.\mathrm{Sin}\theta}{n\,\mathrm{Cos}\,n\theta} = 1$$

$$\therefore Q_1' = \frac{n\,\mathrm{Cos}\,n\theta}{n\,\mathrm{Cos}\,n\theta.\mathrm{Cos}\,\theta + \mathrm{Sin}\,n\theta.\mathrm{Sin}\theta}$$

Hence, from appendix 4.3.3. , it may be shown that the maximum power transfer conditions occur when

$$\underline{m = 3/2\ n}$$

Fig. 4.3.3.

$$Q_o = \frac{m.V_B.C_o}{(2^m - 1)}$$

m	$\left(\frac{m}{2^m-1}\right)$ to power 2 - Denormalization factor (Q_o^2)	
2	.666666	.44444
3	.428571	.18367
4	.266666	.07111
5	.161290	.02601
6	.095238	.00907
7	.054687	.00299
8	.031249	.00098
9	.017612	.00031
10	.009775	.00010

The multiplying factor V_B Co.ω appears in every denormalized charge term. At an input frequency in the 1GHz to 10GHz range, a typical device might be such that V_BCo ω has unity value. This is particularly convenient in calculations of examples, although in a practical case the actual values must be inserted.

4.3.3 Solutions of Hyperabrupt diode Equations

The equation $\cot n\theta = n \cdot \tan\theta$

The computed solutions are:-

n	θ	$n\theta$	Q_n'/Q_1'	nQ_n'/Q_1'	Q_1'	Q_n'	nQ_n'
2	24.095	48.190	.3060	.6120	.8765	.2682	.5364
3	16.268	48.805	.1417	.4251	.9375	.1328	.3984
4	12.251	49.005	.0703	.2812	.9632	.06771	.2708
5	9.822	49.110	.0450	.2250	.9759	.04392	.2196
6	8.198	49.190	.0314	.1884	.9831	.03087	.1852
7	7.029	49.205	.0231	.1617	.9874	.02281	.1596
8	6.153	49.225	.0177	.1416	.9904	.01753	.1402
9	5.471	49.240	.0140	.1260	.9924	.01389	.1250
10	4.925	49.250	.0113	.1130	.9938	.01123	.1123

The power levels in the varactor are calculated from the expression for P_j' i.e.

$$P' = \frac{n\omega}{2} \sum_{j=0}^{k(m-n)} \binom{m}{n+2j} \cdot \frac{(n+2j)!}{(n+j)!} \cdot \frac{Q_1'^{n+2j} \cdot Q_n'}{2^{n+2j-1}} \cdot \frac{1}{j!} \qquad (kP' = P_\alpha)$$

For a doubler, n = 2, the results are tabulated below

m	$P'_{algebraic}$	$= \omega \times P'$	P denormalized
2	$\omega \cdot \left(\frac{Q_1'^2 Q_n'}{2}\right)$	.103022	.045787
3	$\omega \left(\frac{3}{2} \frac{Q_1'^2 Q_n'}{2}\right)$	.309066	.056766
4	$\omega \left\{\frac{Q_1'^4 Q_n'}{2} + 3 \cdot Q_1'^2 \cdot Q_n'\right\}$	.697282	.049583
5	$\omega \left\{\frac{5}{2} \cdot Q_1'^4 Q_n' + 5 \cdot Q_1'^2 Q_n'\right\}$	1.425960	.037089
6	$\omega \left\{\frac{15}{32} \cdot Q_1'^6 Q_n' + \frac{15}{2} Q_1'^4 Q_n' + \frac{15}{2} Q_1'^2 Q_n'\right\}$	2.789549	.025301

For $n = 5$,

m	$P'_{algebaic}$	P'	P denormalized
5	$\omega \cdot \left\{ \frac{5}{2} \cdot \frac{Q_1'^5 Q_n'}{2^4} \right\}$	ω_x .006073	ω_x .000157
6	$\omega \left\{ \frac{5}{2} \cdot 6 \cdot \frac{Q_1'^5 Q_n}{2^4} \right\}$	ω_x .036435	ω_x .000330
7	$\omega \left\{ \frac{5}{2} \cdot \frac{7 Q_1'^7 Q_n'}{2^6} + \frac{5}{2} \frac{Q_1'^5 Q_n'}{2^4} \right\}$	ω_x .137640	ω_x .000410
8	$\omega \left\{ \frac{5}{2} \cdot \frac{56 Q_1'^7 Q_n'}{2^6} + \frac{5}{2} \cdot \frac{56 \cdot Q_1'^5 Q_n'}{2^4} \right\}$	ω_x .421025	ω_x .000412
9	$\omega \left\{ \frac{5}{2} \cdot \frac{72 \cdot Q_1'^9 Q_n'}{2^9} + \frac{5}{2} \frac{252 Q_1'^7 Q_n'}{2^6} + \frac{5}{2} \cdot 126 \cdot \frac{Q_1'^5 \cdot Q_n'}{2^4} \right\}$	ω_x 1.141870	ω_x .000352
10	$\omega \left\{ \frac{5}{2} \cdot \frac{720 \cdot Q_1'^9 Q_n'}{2^8} \frac{1}{2} + \frac{5}{2} \cdot 840 \cdot \frac{Q_1'^7 \cdot Q_n'}{2^6} + 5/2 \cdot 252 \cdot \frac{Q_1'^5 \cdot Q_n'}{2^4} \right\}$	ω_x 2.868688	ω_x .000285

The actual values of P denorm in the real case must take into account the value of $\omega . V_B . C_o$. In the examples below, this will be assumed to have unit value, a reasonable approximation for a varactor in the 1 GHz to 10 GHz region.

The most important parameters in a frequency multiplier are generally the power handled and the efficiency. It is usually helpful to know the input and output impedances, but often these can be matched over quite a wide range by the external circuit.

The power handled by the varactor is

$$\frac{\omega . V_B C_o \quad P \text{ denorm}}{} \qquad (P \text{ denorm includes the } \omega \text{ term})$$

For a given value of $\omega . V_B C_o$, the power handled by the varactor in each case considered (n = 2 and n = 5) passes through a peak. Respectively, the peaks occur at m = 3 and m = 7 or 8. Similar plots of other 'n' multipliers indicate that the optimum value of m for the best power handling conditions is

$$m = \frac{3}{2} n$$

The efficiency is given by:

$$\eta = \frac{P - P_{\text{Loss output}}}{P + P_{\text{Loss input}}}$$

This formula is intuitive from the power flow conditions

Hence

$$\eta = \frac{P' - r_s . n^2 \left(\frac{Q_n'^2}{2}\right)}{P' + r_s . \left(\frac{Q_i'^2}{2}\right)}$$

The denormalization factor (Q_b^2) has been cancelled from this equation. If r_s is set equal to say, 1 ohm, the respective efficiency figures are:

Doubler - n = 2

Output Power loss	$r_s . n^2 \left(\frac{Q_n'^2}{2}\right)$	= 1x 0.14386
Input Power loss	$r_s . \left(\frac{Q_i'^2}{2}\right)$	= 1x 0.38412

The efficiency values are tabulated:-

$\frac{1}{1-\delta}$	P'	η	
2	.103022	-	(the matched condition is not possible with the r_s and $V_B C_o w$ conditions imposed)
3	.309066	.23832	
4	.697282	.51176	
5	1.425960	.70831	
6	2.789549	.83363	

2. X5 Multiplier $n = 5$

Output Power loss $r_s \cdot n^2 \left(\frac{Q_1'}{2}\right)^2 = 1. \quad .02411$

Input Power loss $r_s \cdot \left(\frac{Q_1'}{2}\right)^2 = 1. \quad .47619$

$\frac{1}{1-\delta}$	P'	η	
5	.006073	-	(matching conditions not possible under assumed values of r_s, w $V_B C_o$)
6	.036435	.0204	
7	.137640	.1849	
8	.421025	.4423	
9	1.141870	.6908	
10	2.868688	.8504	

'Single-Sided' Limiting Conditions - Section 5.3.1

In some circumstances it may be possible to operate the SRD assuming only the limitation of reverse breakdown voltage. This is usually the case when the recombination time is long compared to the pulse-width generated. We define a Q_0, the d.c. charge level on the varactor.

Let the alternating components of charge be

$Q_1' \cos \omega t$ at frequency ω

$Q_n' \cos(n\omega t + \phi)$ " " $n\omega$

(ϕ is the phase angle relative to the fundamental)

In the reverse charged state, the total charge must correspond at the maximum to the maximum reverse voltage, V_R, which may be the breakdown voltage.

Hence,

$$\left[Q_1' \cos \omega t - Q_n' \cos(n\omega t + \phi) \right] < 1.$$

This condition is similar to that for the general two-limit case. However, it may be seen that more freedom exists in choice of Qo and ϕ.

Suppose there exists an angle θ such that

$$Q_1' \cos\theta - Q_n' \cos(n\theta + \phi) = 1$$

and, as this is a maximum,

$$Q_1' \sin\theta - n Q_n' \sin(n\theta + \phi) = 0$$

$$\therefore \frac{Q_n'}{Q_1'} = \frac{\sin\theta}{n \sin(n\theta + \phi)}$$

and, as described in appendix 4.3.1 this leads to the fundamental equation:

$$\underline{\tan(n\theta + \phi) = -n \tan\theta}$$

When the hyperabrupt varactor was examined, it was found that $\phi = \frac{3\pi}{2}$ was the optimum condition. Solutions for Q_1', Q_n' etc. were found by computation.

It is interesting to consider alternative values of ϕ

e.g. $\phi = 0$ or $+\pi$

$\phi = 0$

$$\frac{Q_n'}{Q_1'} = \frac{\sin\theta}{n\sin(n\theta+0)}$$

$\phi = \pi$

$$\frac{Q_n'}{Q_1'} = \frac{\sin\theta}{n.\sin(n\theta+\pi)}$$

Solution = $\theta \to 0$

Expressions are indeterminate; by the usual rule,

$$\frac{Q_n'}{Q_1'} = \lim_{\theta\to 0} \frac{\cos\theta}{n^2\cos n\theta}$$

$$\frac{Q_n'}{Q_1'} = \frac{1}{n^2}$$

$$\frac{Q_n'}{Q_1'} = \lim_{\theta\to 0} \frac{\cos\theta}{n^2\cos(n\theta+\pi)}$$

$$\frac{Q_n'}{Q_1'} = -\frac{1}{n^2}$$

Similarly,

$$Q_1' = \frac{n\sin\theta}{n\cos\theta.\sin n\theta - \sin\theta.\cos n\theta}$$

In the limit as $\theta \to 0$

$$Q_1' = \lim_{\theta\to 0} \frac{n^2\cos n\theta}{\left(n^2\cos\theta.\cos n\theta - n\sin\theta.\sin n\theta + n\sin\theta.\sin n\theta - \cos\theta.\cos n\theta\right)}$$

$$\therefore \quad Q_1' = \frac{n^2}{n^2-1}$$

$$Q_n' = \frac{1}{n^2-1}$$

$$Q_1' = \frac{-n\sin n\theta}{n\cos\theta.\sin n\theta + \sin\theta.\cos n\theta}$$

In lim $\theta\to 0$

$$Q_1' = \lim_{\theta\to 0} \frac{-n^2\cos n\theta}{\left(n^2\cos\theta.\cos n\theta - n\sin\theta.\sin n\theta - n\sin\theta.\sin n\theta + \cos\theta.\cos n\theta\right)}$$

$$\therefore Q_1' = -\frac{n^2}{n^2+1}$$

$$Q_n' = \frac{1}{n^2+1}$$

Hence, for any phase angle ϕ, the current conditions for any varactor may be defined; the solutions for $\pm \pi/2$ and $0, \pi$ have been carried through.

Appendix 5.4.2 The Analysis of The Step-Recovery Diode

From Section 5.4.2.,

$$\frac{v_c'}{V_{co}'} = \sum_{K=1}^{\infty} (-1)^{K+1} \cdot \frac{1}{K} \left\{ (Q_1' \cos \omega t)^K - (Q_1' \cos \omega t)^{K-1} \cdot (Q_n' \cos (n\omega t + \phi_n)) \right\}$$

and

$$v_n' = a_n \cos n\omega t + b_n \sin n\omega t$$
$$v_1' = a_1 \cos \omega t + b_1 \sin \omega t$$

where

$$a_1 = \frac{1}{\pi} \int_{-\pi}^{\pi} \left(\frac{v_c'}{V_{co}'} \right) \cdot \cos \omega t \cdot d(\omega t)$$

$$b_1 = \frac{1}{\pi} \int_{-\pi}^{\pi} \left(\frac{v_c'}{V_{co}'} \right) \cdot \sin \omega t \cdot d(\omega t)$$

and

$$a_n = \frac{1}{\pi} \int_{-\pi}^{\pi} \left(\frac{v_c'}{V_{co}'} \right) \cdot \cos n\omega t \cdot d(\omega t)$$

$$b = \frac{1}{\pi} \int_{-\pi}^{\pi} \left(\frac{v_c'}{V_{co}'} \right) \cdot \sin n\omega t \cdot d(\omega t)$$

The derivations of the a_n, b_n etc. are:-

$$a_n = \frac{1}{\pi} \int_{-\pi}^{\pi} \sum_{K=1}^{\infty} \frac{(-1)^{K+1}}{K} \left\{ Q_1'^K \cdot \cos^K \omega t \cdot \cos n\omega t + \frac{1}{2} \cdot Q_1'^{K-1} \cdot Q_n' \cos^{K-1} \omega t \cdot \cos (2n\omega t + \phi) \right.$$
$$\left. + \frac{1}{2} Q_1'^{K-1} \cdot Q_n' \cdot \cos^{K-1} \omega t \cdot \cos \phi \right.$$

Selecting only the relevant cross-product terms:-

$$a_n = \frac{1}{\pi} \int_{-\pi}^{\pi} \left[\begin{array}{l} \frac{(-1)^{n+1}}{n} \cdot \frac{1}{2^{n-1}} \cdot Q_1'^n \cdot \cos^2 n\omega t \cdot \\ + \frac{(-1)^{n+3}}{n+2} \cdot \frac{1}{2^{n+1}} \cdot Q_1'^{n+2} \cdot \cos^2 n\omega t \cdot (n+2) \\ + \frac{(-1)^{n+5}}{n+4} \cdot \frac{1}{2^{n+3}} \cdot Q_1'^{n+4} \cdot \cos^2 n\omega t \cdot \frac{(n+4)(n+3)}{2!} \\ \vdots \quad \vdots \quad \vdots \quad \vdots \quad \vdots \end{array} \right] = a_n$$

$$+\frac{1}{2}Q_n'\left[\begin{array}{l}\dfrac{(-1)^{2n+2}}{2n+1}\cdot Q_1'^{2n}\cdot\dfrac{1}{2^{2n-1}}\cdot\cos 2n\omega t\cdot\cos(2n\omega t+\phi)\\ +\dfrac{(-1)^{2n+4}}{2n+3}\cdot Q_1'^{2n+2}\cdot\dfrac{1}{2^{2n+2-1}}\cdot(2n+2)\cdot\cos 2n\omega t\cdot\cos(2n\omega t+\phi)\\ +\dfrac{(-1)^{2n+6}}{2n+5}\cdot Q_1'^{2n+4}\cdot\dfrac{1}{2^{2n+4-1}}\cdot\dfrac{(2n+4)(2n+3)}{2!}\cdot\cos 2n\omega t\cdot\cos(2n\omega t+\phi)\\ \vdots\qquad\qquad\vdots\qquad\qquad\vdots\end{array}\right]=a_{n2}$$

$$+\frac{1}{2}Q_n'\left[\begin{array}{l}Q_1'^{K-1}\cdot\cos^{K-1}\omega t\cdot\cos\phi\\ \text{(odd terms only)}\end{array}\right]\cdot d\omega t=a_{n3}$$

The third term occurs in other parts of the expansion, and will be solved first.

$$a_{n3}=\frac{1}{2\pi}\int_{-\pi}^{\pi}\sum_{K=1}^{\infty}\frac{(-1)^{K+1}}{K}\cdot Q_1'^{K-1}\cdot Q_n'\cdot\cos^{K-1}\omega t\cdot\cos\phi\cdot d\omega t.$$

The non-zero terms occur for $(K-1)$ even.

i.e.
$$\frac{1}{2\pi}\int_{-\pi}^{\pi}\frac{(-1)^2}{1}\cdot Q_1'^{0}\cdot Q_n'\cdot\cos\phi\cdot d\omega t$$
$$+\frac{1}{2\pi}\int_{-\pi}^{\pi}\frac{(-1)^4}{3}\cdot Q_1'^{2}\cdot Q_n'\cdot\frac{1}{2}\cdot\cos\phi\cdot d\omega t$$
$$+\frac{1}{2\pi}\int_{-\pi}^{\pi}\frac{(-1)^6}{5}\cdot Q_1'^{4}\cdot Q_n'\cdot\frac{3}{8}\cdot\cos\phi\cdot d\omega t$$
$$\vdots\qquad\qquad\vdots$$
$$=\cos\phi\cdot\sum_{l=0}^{\infty}\left(\frac{1}{1+2l}\right)\cdot Q_1'^{2l}\cdot Q_n'\cdot\frac{1}{2^{2l}}\cdot\frac{(2l)!}{l!\,l!}$$

Similarly the a_{n1} and a_{n2} are solved and

$$a_n = \sum_{l=0}^{\infty} \left\{ \frac{(-1)^{n+2l+1}}{(n+2l)} \cdot \frac{(n+2l)!}{(n+l)!} \cdot \frac{1}{1!} \cdot \frac{1}{2^{n+2l}} \cdot Q_1'^{\,n+2l} \right\}$$

$$+ \sum_{l=0}^{\infty} \left\{ \frac{1}{2} \cdot Q_n' \cdot \frac{1}{2n+2l+1} \cdot \frac{(2n+2l)!}{(2n+l)!} \cdot \frac{1}{1!} \cdot \frac{1}{2^{2n+2l}} \cdot Q_1'^{\,2n+2l} \right\} \cdot \cos\phi$$

$$+ \sum_{l=0}^{\infty} \left\{ \frac{1}{(1+2l)} \cdot \frac{(2l)!}{1!\,l!} \cdot \frac{1}{2^{2l}} \cdot Q_1'^{\,2l} \cdot Q_n' \right\} \cdot \cos\phi$$

The derivation of the b_n coefficient is similar to the a_n but simplified by the general rule:-

$$\int_{-\pi}^{\pi} (\cos \omega t)^K \cdot \sin n\omega t = 0$$

In general, therefore,

$$b_n = \frac{1}{\pi} \int_{-\pi}^{\pi} \sum_{K=1}^{\infty} \frac{(-1)^{K+1}}{K} \left\{ (Q_1' \cos\omega t)^K + (Q_1' \cos\omega t)^{K-1} (Q_n' \cos(n\omega t + \phi)) \right\} \cdot \sin n\omega t \cdot dt$$

Using the rule stated above,

$$b_n = \frac{1}{\pi} \int_{-\pi}^{\pi} \sum_{K=1}^{\infty} \frac{(-1)^{K+1}}{K} \cdot Q_n' (Q_n' \cos\omega t)^{K-1} \cdot \frac{1}{2} \left[\sin(2n\omega t + \phi) + \sin(-\phi) \right] \cdot d\omega t$$

The sin $(-\phi)$ has a coefficient corresponding to the a_{n3} term, so the working for this will be omitted. Only the $(2n\omega t)$ terms contribute to the b_n coefficient, so

$$b_n = \frac{1}{\pi} \int_{-\pi}^{\pi} \cos 2n\omega t \cdot \sin(2n\omega t + \phi) \cdot \left[\frac{(-1)^{2n+2}}{2n+1} \cdot Q_1'^{\,2n} \cdot \frac{Q_n'}{2} \cdot \frac{1}{2^{2n+1}} \right.$$

$$+ \frac{(-1)^{2n+4}}{2n+3} \cdot Q_1'^{\,2n+2} \cdot \frac{Q_n'}{2} \cdot \frac{1}{2^{2n+3}} \cdot \frac{(2n+2)}{1!}$$

$$\left. \frac{(-1)^{2n+6}}{2n+5} \cdot Q_1'^{\,2n+4} \cdot \frac{Q_n'}{2} \cdot \frac{1}{2^{2n+5}} \cdot \frac{(2n+4)(2n+2)}{2!} \right]$$

$$\vdots \qquad \vdots$$

+ a $\sin(-\phi)$ term.

Summarising,

$$b_n = \sin\phi \left[\sum_{l=0}^{\infty} \frac{1}{2n+2l+1} \cdot Q_1'^{2n+2l} \cdot Q_n' \cdot \frac{1}{2^{2n+2l+1}} \cdot \frac{(2n+2l)!}{(2n+l)!} \cdot \frac{1}{l!} \right]$$

$$+ \sin(-\phi) \left[\sum_{l=0}^{\infty} \frac{1}{2l+1} \cdot Q_1'^{2l} \cdot Q_n' \cdot \frac{1}{2^{2l}} \cdot \frac{(2l)!}{l!\ l!} \right]$$

It is noteworthy at this point that the assumptions made to derive a_n and b_n are that $(Q_n')^2$ is small (i.e. $n \geq 4$) and that the diode non-linearity is as described. Forward conduction can be corrected for in the values of Q_1' and Q_n' substituted into the equations.

The power converted by the device is closely related to a_n and b_n. The current at the nth harmonic is

$$I_n = -n\omega Q_n' \sin(n\omega t + \phi)$$

Let P = Power handled by the device

$$P = \frac{-n\omega Q_n'}{\pi} \int_{-\pi}^{\pi} \sum_{K=1}^{\infty} \frac{(-1)^{K-1}}{K} \left(Q_1'^{K} \cdot \cos^K \omega t \cdot \sin(n\omega t+\phi) + (Q_1' \cos\omega t)^{K-1} \cdot Q_n' \cos n\omega t \cdot \sin(n\omega t+\phi) \right) \cdot d\omega t.$$

The solution of this equation is performed by comparison with the a_n and b_n terms, one pair of which cancel, and shows that:

$$P = -n\omega Q_n' \left[\sin\phi \sum_{l=0}^{\infty} \frac{(-1)^{n+2l-1}}{n+2l} \cdot \frac{(n+2l)!}{(n+l)!} \cdot \frac{1}{l!} \cdot \frac{1}{2^{n+2l}} \cdot Q_1'^{n+2l} \right.$$
$$\left. + \sin 2\phi \sum_{l=0}^{\infty} \frac{1}{2n+2l+1} \cdot \frac{(2n+2l)!}{(2n+l)!} \cdot \frac{1}{l!} \cdot \frac{1}{2^{2n+2l}} Q_1'^{2n+2l} \cdot Q_n' \right]$$

The intuitive choice of the phase angle, as described in chapter 4 is

$$\phi = \pi/2 \quad \text{or} \quad 3\pi/2$$

The expression derived for P seems to bear this out, for, if we select (for consistency of sign)

$$\phi = 3\pi/2 \qquad \text{(or } \pi/2 \text{ as appropriate)}$$

Then

$$P = n\omega Q_n' \left[\sum_{l=0}^{\infty} \frac{1}{n+2l} \cdot \frac{(n+2l)!}{(n+l)!} \cdot \frac{1}{l!} \cdot \frac{1}{2^{n+2l}} \cdot Q_1'^{n+2l} \right]$$

The remaining terms in a_n and b_n are

$$a_n = \sum_{l=0}^{\infty} \frac{1}{n+2l} \cdot \frac{(n+2l)!}{(n+l)!} \cdot \frac{1}{l!} \cdot \frac{1}{2^{n+2l-1}} \cdot Q_1'^{n+2l}$$

and

$$b_n = -\sum_{l=0}^{\infty} \frac{1}{2l+1} \cdot \frac{(2l)!}{l!\,l!} \cdot \frac{1}{2^{2l}} \cdot Q_1'^{2l} \cdot Q_n'$$

(In most cases the second term in b_n is small)

i.e.
$$+ \sum_{l=0}^{\infty} \frac{1}{2n+2l+1} \cdot \frac{(2n+2l)!}{(2n+l)!} \cdot \frac{1}{l!} \cdot \frac{1}{2^{2n+2l+1}} \cdot Q_1'^{2n+2l} \cdot Q_n'$$

In 'real and imaginary' terms, b_n is the real coefficient, a_n is the imaginary.

The techniques used for a_n and b_n can be applied to a_1 and b_1; when these are known, the complete specification of the step-recovery diode can be written down.

$$V_1' = a_1 \cos \omega t + b_1 \sin \omega t$$

$$I_1 = \omega . Q_1' . \sin \omega t$$

and

$$a_1 = \frac{1}{\pi} \int_{-\pi}^{\pi} \frac{v_c'}{V_{co}'} . \cos \omega t . d\omega t$$

$$b_1 = \frac{1}{\pi} \int_{-\pi}^{\pi} \frac{v_c'}{V_{co}'} . \sin \omega t . d\omega t$$

We have

$$\frac{v_c'}{V_{co}'} = \sum_{K=1}^{\infty} (-1)^{K+1} . \frac{1}{K} \left[(Q_1' \cos \omega t)^K + (Q_1' \cos \omega t)^{K-1} . (Q_n' \cos n\omega t + \phi) \right]$$

$$\therefore \quad a_1 = \frac{1}{\pi} \int_{-\pi}^{\pi} \sum_{K=1}^{\infty} \frac{(-1)^{K+1}}{K} \left[(Q_1' \cos \omega t)^{K+1} + Q_1'^{K-1} . \cos^n \omega t . Q_n' . \cos (n\omega t + \phi) \right] d\omega t$$

These terms will be solved separately with the identifiers a_{11} and a_{12} respectively:

$$a_{11} = \frac{1}{\pi} \int_{-\pi}^{\pi} \sum_{K=1}^{\infty} \frac{(-1)^{K+1}}{K} . Q_1'^{K+1} . (\cos \omega t)^{K+1} . d\omega t.$$

The non-zero terms in the integral occur for $(K - 1)$ even.

$$\therefore \quad a_{11} = \frac{1}{\pi} \int_{-\pi}^{\pi} \frac{(-1)^2}{1} . Q_1'^2 . \frac{1}{2} . d\omega t.$$

$$+ \frac{1}{\pi} \int_{-\pi}^{\pi} \frac{(-1)^4}{3} . Q_1'^4 . \frac{3}{8} . d\omega t.$$

$$\therefore\ a_{11} = \frac{1}{\pi}\int_{-\pi}^{\pi}\sum_{l=0}^{\infty}\frac{1}{2l+1}\cdot Q_1'^{2l+2}\cdot\frac{1}{2^{2l+2}}\cdot\frac{(2l+2)!}{(l+1)!(l+1)!}\cdot d\omega t$$

$$\therefore\ a_{11} = \sum_{l=0}^{\infty}\frac{1}{2l+1}\cdot\frac{1}{2^{2l+1}}\cdot\frac{(2l+2)!}{(l+1)!\,(l+1)!}\cdot Q_1'^{2l+2}$$

$$a_{12} = \frac{1}{\pi}\int_{-\pi}^{\pi}\sum_{K=1}^{\infty}\frac{(-1)^{K+1}}{K}\cdot Q_1'^{K-1}\cdot Q_n'\cdot \cos^K\omega t\cdot\cos(n\omega t+\phi)\cdot d\omega t.$$

$$= \frac{1}{\pi}\int_{-\pi}^{\pi} Q_n'\cos n\omega t\cdot\cos(n\omega t+\phi)\left[\begin{array}{l}\dfrac{Q_1'^{n}}{2^{n-1}}\cdot\dfrac{1}{n}\\ +(n+2)\dfrac{Q_1'^{n+2}}{2^{n+1}}\cdot\dfrac{1}{n+2}\\ +\dfrac{(n+4)(n+3)}{2}\cdot\dfrac{Q_1'^{n+4}}{2^{n+3}}\cdot\dfrac{1}{n+4}\\ \quad\vdots\qquad\qquad\vdots\end{array}\right]$$

$$a_{12} = \cos\phi\sum_{l=0}^{\infty}(-1)^{n+2l+1}\cdot\frac{1}{(n+2l)}\cdot Q_1'^{n+2l-1}\cdot Q_n'\cdot\frac{1}{2^{n+2l}}\cdot\frac{(n+2l)!}{(n+l)!\,l!}$$

Similarly,

$$b_1 = \frac{1}{\pi}\int_{-\pi}^{\pi}\frac{v_c'}{V_{co}'}\cdot\sin\omega t\cdot d\omega t.$$

$$= \frac{1}{\pi}\int_{-\pi}^{\pi}\sum_{K=1}^{\infty}\frac{(-1)^{K+1}}{K}\cdot\left[(Q_1'\cos\omega t)^K+(Q_1'\cos\omega t)^{K-1}(Q_n'\cos(n\omega t+\phi))\right]\cdot\sin\omega t\,d\omega t.$$

The first term is, by the usual rule, zero. The second term must be resolved into components suitable for application of the standard method used earlier.

i.e. $$b_1 = \frac{1}{\pi}\int_{-\pi}^{\pi} \sum_{K=1}^{\infty} \frac{(-1)^{K+1}}{K} \cdot Q_n' \cdot Q_1'^{K-1} \cdot (\cos\omega t)^{K+1} \cdot \frac{1}{2} \cdot \left(\sin(n+1)\omega t + \phi + \sin(n-1)\omega t + \phi\right)$$

The usual method of solution is applied, the terms being derived together and the (n + 1) for (m - 1) substitution made.

$$b_1 = \frac{1}{\pi}\int_{-\pi}^{\pi} \frac{(-1)^{n+1}}{n} \cdot Q_n' \cdot Q_1'^{n-1} \cdot \frac{1}{2^{n-2}} \cdot \frac{1}{2} \cdot \sin\phi$$

$$+ \frac{(-1)^{n+3}}{n+2} \cdot Q_n' \cdot Q_1'^{n+1} \cdot \frac{1}{2^n} \cdot \frac{1}{2} \cdot \sin\phi \cdot (n+2)$$

$$+ \frac{(-1)^{n+5}}{n+4} \cdot Q_n' \cdot Q_1'^{n+3} \cdot \frac{1}{2^{n+2}} \cdot \frac{1}{2} \cdot \sin\phi \cdot \frac{(n+4)(n+3)}{2!}$$

$$\vdots \qquad\qquad \vdots \qquad\qquad \vdots$$

$$b_1 = \sum_{l=0}^{\infty} \frac{(-1)^{n+2l+1}}{(n+2l)} \cdot Q_n' \cdot Q_1'^{n-1+2l} \cdot \frac{1}{2^{n+2l-2}} \cdot \frac{(n+2l)!}{(n+l)!} \cdot \frac{1}{l!} \cdot \sin\phi \cdot \qquad \text{---}(n+1)\text{ terms.}$$

$$+ \sum_{l=0}^{\infty} \frac{(-1)^{n+2l+3}}{(n+2l+2)} \cdot Q_n' \cdot Q_1'^{n+1+2l} \cdot \frac{1}{2^{n+2l}} \cdot \frac{(n+2l+2)!}{(n+l+2)!} \cdot \frac{1}{l!} \cdot \sin\phi.$$

A rearrangement, with some simplification, gives

$$b_1 = \sum_{l=0}^{\infty} (-1)^{n+1} \cdot Q_n' \cdot Q_1'^{n+2l-1} \cdot \frac{1}{2^{n+2l-2}} \cdot \frac{1}{l!}$$

$$\times \left[\frac{(n+2l-1)!\,(n+l+2)(n+l+1) + \frac{Q_1'^2}{4}(n+2l+1)!}{(n+l+2)!}\right] \cdot \sin\phi.$$

If we now refer to the output conditions, and take the obvious choice of $\sin \phi = 1$ then $\cos \phi = 0$, so that:

$$a_1 = \sum_{l=0}^{\infty} \frac{1}{2l+1} \cdot \frac{1}{2^{2l+1}} \cdot \frac{(2l+2)!}{(l+1)!(l+1)!} \cdot Q_1'^{2l+2}$$

and

$$b_1 = \sum_{l=0}^{\infty} (-1)^{n+1} \cdot Q_n' \cdot Q_1'^{n+2l-1} \cdot \frac{\sin \phi}{2^{n+2l-1}} \cdot \frac{1}{l!} \left[\frac{(n+2l-1)!(n+l+2)(n+l+1) + \frac{Q_1'^2}{4}(n+2l+1)!}{(n+l+2)!} \right]$$

The justification for assuming $\sin \phi = 1$ can be questioned. From the harmonic voltage plots it seems the intuitive choice. Similarly, the output conditions indicate mathematically that the value must be unity or at least very close to it. However, in some cases, especially where other harmonics are allowed to flow, this choice of phase angle may not be optimum; from previous papers on the subject, and in the light of experimental results in this project it is considered that the value of sin ϕ should not substantially deviate from unity.

The major results of this part of the analysis, assuming sin $\phi = 1$, are:-

$$P = n\omega Q_n' \sum_{l=0}^{\infty} \frac{(-1)^{n+1}}{(n+2l)} \cdot \frac{(n+2l)!}{(n+l)!} \cdot \frac{1}{l!} \cdot \frac{1}{2^{n+2l}} \cdot Q_1'^{n+2l}$$

$$a_n = \sum_{l=0}^{\infty} \frac{1}{(n+2l)} \cdot \frac{(n+2l)!}{(n+l)!} \cdot \frac{1}{l!} \cdot \frac{1}{2^{n+2l-1}} \cdot Q_1'^{n+2l}$$

$$b_n = -\sum_{l=0}^{\infty} \frac{1}{(2l+1)} \cdot \frac{(2l)!}{l!\,l!} \cdot \frac{1}{2^{2l}} \cdot Q_1'^{2l} \cdot Q_n'$$

$$a_1 = \sum_{l=0}^{\infty} \frac{1}{(2l+1)} \cdot \frac{1}{2^{2l+1}} \cdot \frac{(2l+2)!}{(l+1)!(l+1)!} \cdot Q_1'^{2l+2}$$

$$b_1 = -\sum_{l=0}^{\infty} \cdot Q_n' \cdot Q_1'^{n+2l-1} \frac{1}{2^{n+2l-2}} \cdot \frac{1}{l!} \left[\frac{(n+2l-1)!(n+l+2)(n+l+1) + \frac{Q_1'^2}{4}(n+2l+1)!}{(n+l+2)!} \right]$$

The input power to the diode, when the loss resistances are considered separately, is equal to the output power.

An assessment of the series derived is difficult. The coefficients tend ultimately, with large 'l', to unit value, so that the only convergent term is $Q_1'^{2l}$, which occurs in each series. Precise values for any 'n' selected can be obtained by computer, which would be programmed with suitable step instructions. However, by making a simplification which will be stated below a general expression for the series, which is not seriously in error for $n \geqslant 4$, can be found.

The expression for P will be taken as an example of the approximation.

$$P = n\omega Q_n' \sum_{l=0}^{\infty} \frac{(n+2l-1)!}{(n+l)!\, l!} \cdot \frac{1}{2^{n+2l}} \cdot Q_1'^{\,n+2l}$$

The first term of the series ($l = 0$) is

$$n\omega Q_n' \cdot \frac{1}{n} \cdot \frac{1}{2^n} \cdot Q_1'^{\,n}$$

and the 'K'th term (not related to the previous K) is

$$n\omega Q_n' \frac{(n+2K-1)!}{(n+K)!\, K!} \cdot \frac{1}{2^{n+2K}} \cdot Q_1'^{\,n+2K}$$

The (K - 1)th term is

$$n\omega Q_n' \frac{(n+2K-3)!}{(n+K-1)!\,(K-1)!} \cdot \frac{1}{2^{n+2K-2}} \cdot Q_1'^{\,n+2K-1}$$

Basically the procedure follows the D'alembert ratio test:

$$\frac{K\text{th term}}{(K-1)\text{th term}} = \frac{(n+2K-1)\cdot(n+2K-2)\cdot Q_1'^{2}}{(n+K)\cdot K\cdot 4}$$

The multiplier $\dfrac{(n+2K-1)(n+2K-2)}{(n+K)(K)\cdot 4}$

tends to unity as $K \to \infty$. However, the product term $Q_1'^{2}$ has a constant fractional value, so that the series is unconditionally convergent.

The sum of the series is,

$$n\omega Q_n' \cdot \frac{1}{n} \cdot \frac{1}{2^n} \cdot Q_1'^{2} \left(1 + Q_1'^{2} + Q_1'^{4} \ldots\ldots\right) \times A$$

where A is a correction factor derived from the multiplier above. A good approximation for A is the value of the multiplier term at K = n.

hence

$$P = n\omega Q_n' \cdot \frac{1}{n} \cdot \frac{1}{2^n} \cdot \frac{Q_1'^{n}}{(1-Q_1'^{2})} \cdot A.$$

In the same way,

$$a_n = \frac{1}{n} \cdot \frac{1}{2^{n-1}} \cdot \frac{Q_1'^{n}}{(1-Q_1'^{2})} \cdot A_1$$

$$b_1 = -Q_n' \cdot Q_1'^{\,n-1} \cdot \frac{1}{2^{n-2}} \left(\frac{1}{n} + \frac{Q_1'^{2}}{4} \cdot \frac{1}{n+2}\right) \cdot \frac{Q_1'^{n}}{(1-Q_1'^{2})} \cdot A_2$$

The value of A_2 is a complicated term from the multiplier; in practice it is similar to A_1

The b_n and a_1 terms cannot be safely approximated in this way, as the first few terms fluctuate wildly; in practice again, however, the first N terms of the series give a very good approximation to the answer.

Up to this point, the approximations made for the step-recovery diode are:

1. The exponential capacitance model
2. No forward conduction in current terms; if conduction does occur it can be introduced as a correction factor.
3. $Q_n'^2$ small; this is proved for $n \geq 4$.
4. Certain simplifications in the series in order to obtain general results; comparison with accurate values for examples shows that the errors are small.

Making these assumptions, we have arrived at a complete description of the step-recovery multiplier in terms of input and output voltages and currents. Any other parameters, i.e. input and output impedances can be derived from these parameters in a quite general way.

Appendix 5.5

The Step-Recovery Diode: Exponential 2-Current Model

5.5.1 Summary

Power Handled

$$P = \omega \cdot Q_n' \cdot \frac{1}{2^n} \cdot \frac{Q_1'^n}{(1 - Q_1'^2)} \cdot A$$ See Appendix 5.3.2

Output voltage - Imaginary coefficient

$$a_n = \frac{1}{n} \cdot \frac{1}{2^{n-1}} \cdot \frac{Q_1'^n}{(1 - Q_1'^2)} \cdot A$$

- real coefficient

$$b_n = -\sum_{l=0}^{\infty} \frac{1}{2l+1} \cdot \frac{(2l)!}{l!\, l!} \cdot \frac{1}{2^{2l}} \cdot Q_1'^{2l} \cdot Q_n'$$

Input voltage - real coefficient

$$a_1 = \sum_{l=0}^{\infty} \frac{1}{2l+1} \cdot \frac{1}{2^{2l+1}} \cdot \frac{(2l+2)!}{(l+1)!(l+1)!} \cdot Q_1'^{2l+2}$$

- imaginary coefficient

$$b_1 = -\sum_{l=0}^{\infty} \frac{Q_n' Q_1'^{n+2l-1}}{2^{n+2l-2}} \cdot \frac{1}{l!} \left[\frac{(n+2l-1)!\,(n+l+2)(n+l+1) + \frac{Q_1'^2}{4}(n+2l+1)!}{(n+l+2)!} \right.$$

The phase angle, ϕ, has been shown to have the value $\pi/2$ or $3\pi/2$ as appropriate. The solutions for Q_1' and Q_n' are identical to those for the hyperabrupt junction.

Appendix 6.2 Analysis of the Capacitance-Voltage Plots

The operation of the instrument is described in App. 6.1. For permanent records, slow scanning and an X-Y recorder were preferred to oscilloscope photographs. Remarks on the plots are tabulated below.

1. BA141/2

This television band tuning varactor was near the γ range required for hyperabrupt 'optimum efficiency' multiplication, and could make a good doubler. The C-V data has been transposed from linear to logarithmic coordinates to find the γ value; in, general, this was the best technique, avoiding the expense and possible errors of logarithmic amplifiers for the C-V plotter.

2. MV1403 (from manufacturer's data)

The only production hyperabrupt diode available at the time of the experiment , the design purpose of this diode was wide range tuning. The γ was around 3.5 for a useful range, but the diode was not suitable for multipliers.

3. A Germanium point-contact diode. The main features were a low capacitance, mainly package, with a very short capacitance ramp at turn-on.

4. IN914.

A silicon junction signal diode, to be found in circuits generally similar to (3). The junction area showed a higher capacitance, and, by the shape and length of the turn-on capacitance ramp, it may be seen that the junction represented a larger fraction of the total capacitance than (3).

5. HP 5082-2800, 2811, 2833.

A series of 'economy' wire-ended Schottky barrier diodes intended for mixing, modulation, or detection up to 1.5 GHz. Surprisingly, the normally faster diodes showed higher capacitances than the high-voltage but relatively low-speed 2800. This was confirmed in a microwave mixer circuit built concurrently by Mr. J. Gregory, using diodes from the same batch; the performance of the 2800 group was found to be superior. This was possibly due to a batch marking error. The diodes featured highly repeatable characteristics between examples of the same type and batch. The turn-on capacitance ramp was small, corresponding to the low turn-on voltage with a very sharp increase in forward current. Ripple on the characteristics was due to an instrument fault.

6. DC4000.

A microwave tuning varactor made by AEI. The useful tuning range was very limited (approx. 1.4:1) and was not specified by the manufacturer (this was an early X-band type). The use would probably be in AFC loops or narrow-range tuning of solid state oscillators. The characteristic was similar to the IN914, although

the diodes were very dissimilar in purpose; this was the characteristic of silicon junction diodes.

7. BXY27

A 'varactor displaying step-recovery characteristics' made by Mullard. Very little capacitance change occurredbefore the turn-on ramp. This diode proved to be a highly successful multiplier, obviously working in a primarily step-recovery mode. Later observations showed that this type of characteristic in silicon varactors could be correlated with frequency multiplier performance.

8. IN5155.

A diode listed by Ferranti as a step-recovery for medium power operation. The capacitance was more than twice that of the other SRDs measured, although the series loss resistance was about the same. As expected, the performance was reasonable in a 4.5 GHz output narrow band tripler, but tests up to 9 GHz showed poor results. The structure of the diode was a diffused junction, without an intermediate 'i' layer.

9. HP5082-0386. (Pair)

The type of diodes used in the broadband multiplier. This pair showed excellent matching of reverse bias capacitance and reverse voltage breakdown; the differences were within the range of zeroing errors. The turn on ramp was short and had the characteristic spike shape of the SRD. The manufacturers statedthat the structure was p-i-n.

10. 5082-0386 (Pair) The plot showed the detection of a 'reject' diode. The diodes were obtained as a pair from the manufacturer. The only external difference was in the size of the dots used for colour coding, although the code was correct. Diode 2 showed highly uncharacteristic behaviour, with high reverse capacitance, which had a negative shape towards breakdown, and an unexplained 'hump' in the curve at about 8 volts. This type of characteristic was similar to some zener or transistor base-emitter junctions. The devices were returned to the manufacturers, but no explanation was given by them.

11. 2N706. A small-signal transistor. The capacitance of the emitter-base and collector-base showed the same shapes, with a slight change in magnitude. A significant change in the slope of the curve at low reverse voltages was characteristic of many transistors of this class.

12. 2N3866. This medium-power, high-frequency device had the complex interdigital structure which is becoming popular at UHF and microwave frequencies. The collector-base diode showed characteristics close to the SRD type and, as may be expected, these devices are recommended as multipliers in a parametric mode. The emitter-base diode had a reverse slope near breakdown of large amplitude, due to the complex device structure, which to a first approximation was a 'pagoda' type similar to that reported by Chang et. al.

The C-V plots of many more devices could be made; one class omitted was the conventional abrupt tuning varactor. However, as a first step in device assessment a C-V plot can usually direct the researcher to the class to which a device belongs. The magnitude of the capacitance indicates, with the loss resistance, the useful frequency limit of the device, and the exact tuning law can be deduced.

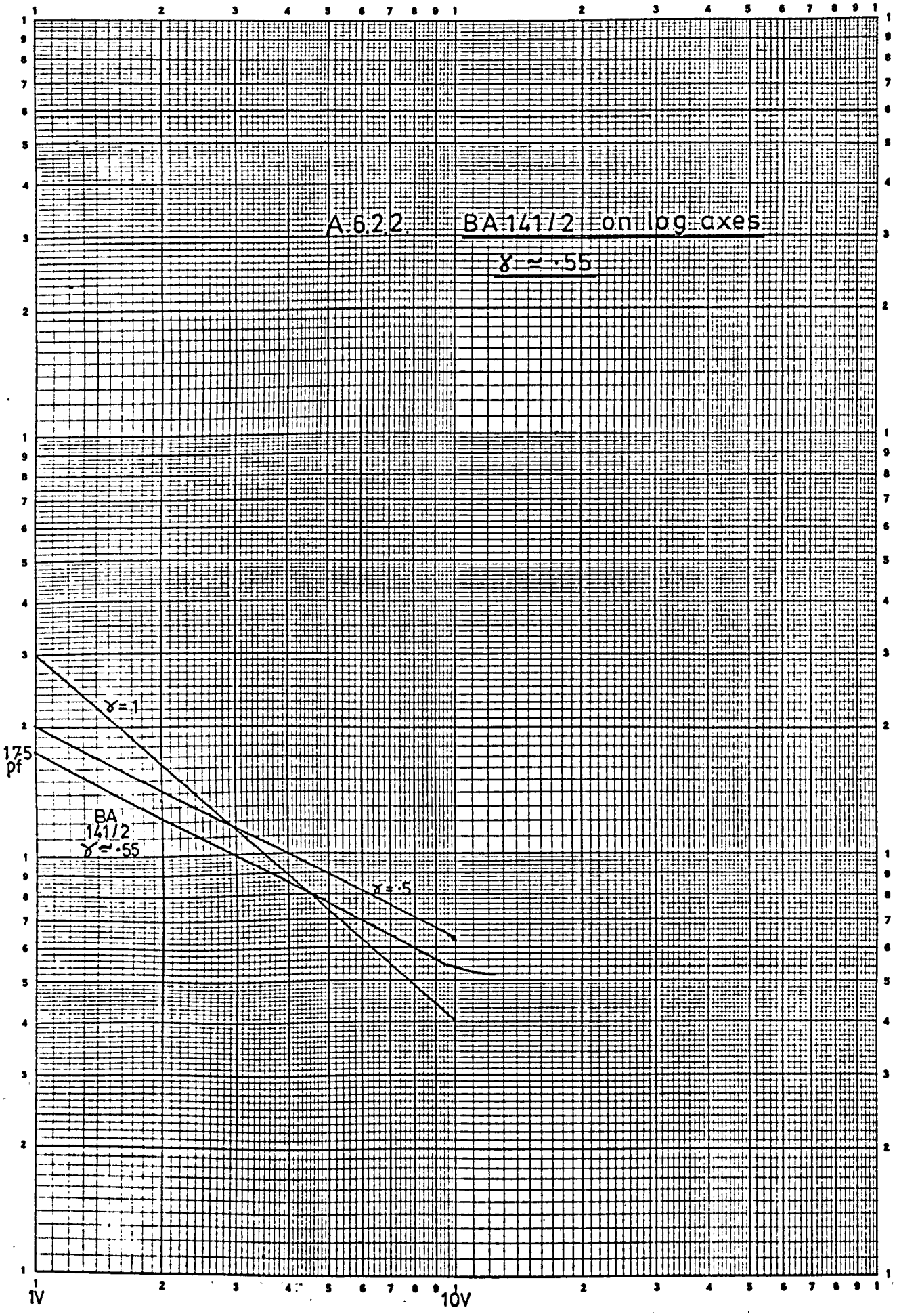

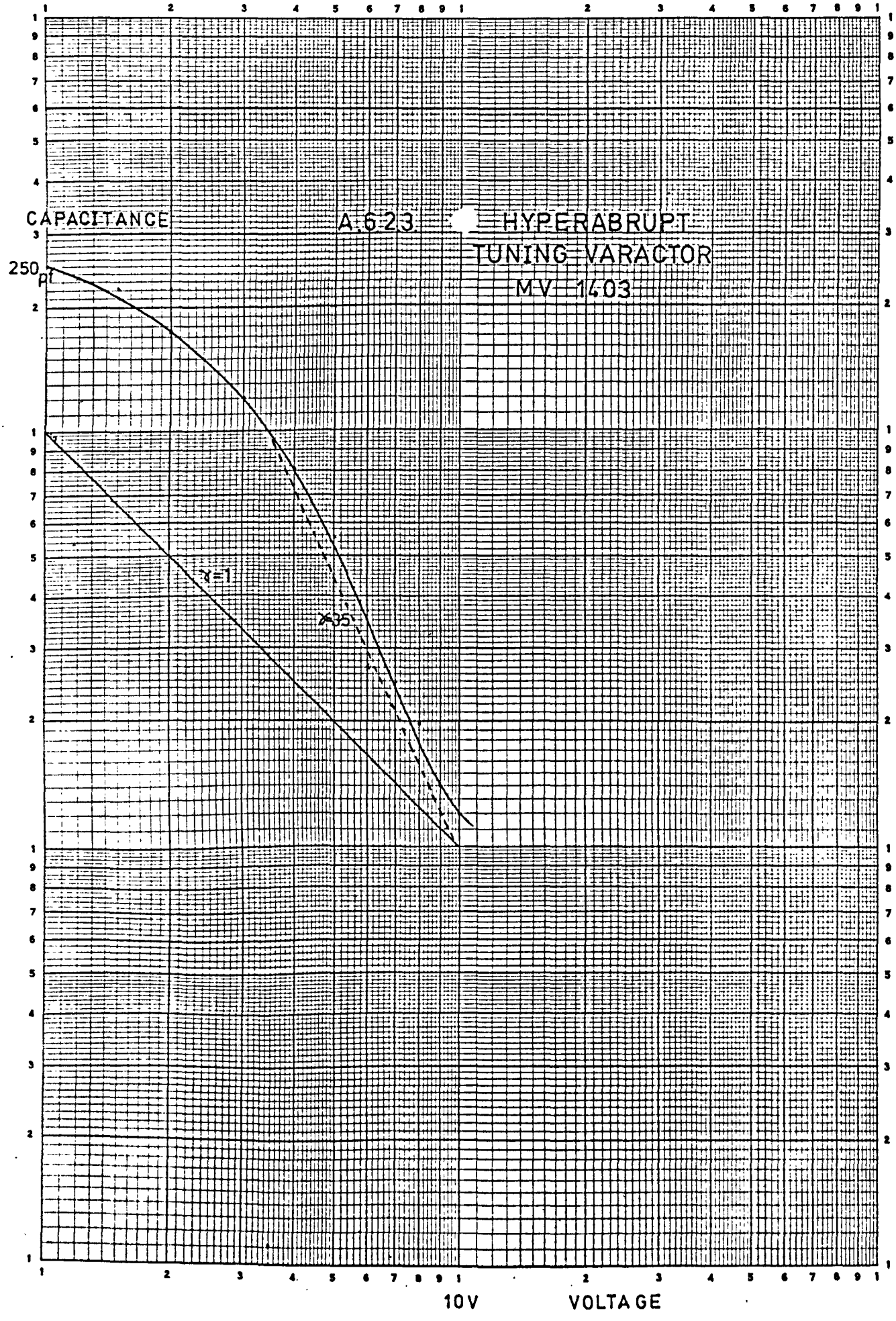
CAPACITANCE
A.623 HYPERABRUPT
TUNING VARACTOR
MV 1403
250 pf
γ=1
γ=3.5
10V
VOLTAGE
Log 3 Cycles x 2 Cycles
Graph Data Ref. 5932
WELL

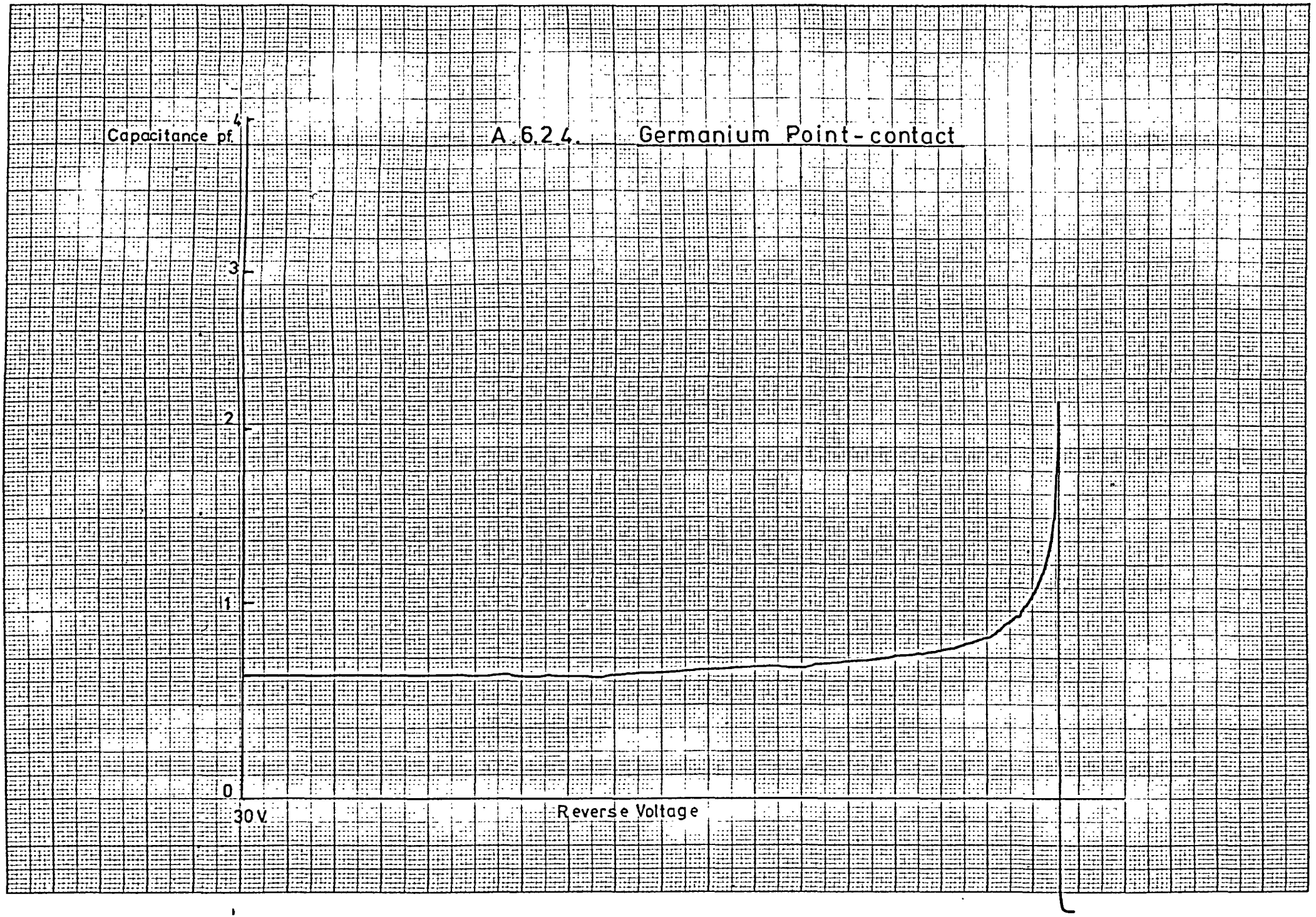
A.6.2.4. Germanium Point-contact
Capacitance pf.
4
3
2
1
0
30 V.
Reverse Voltage

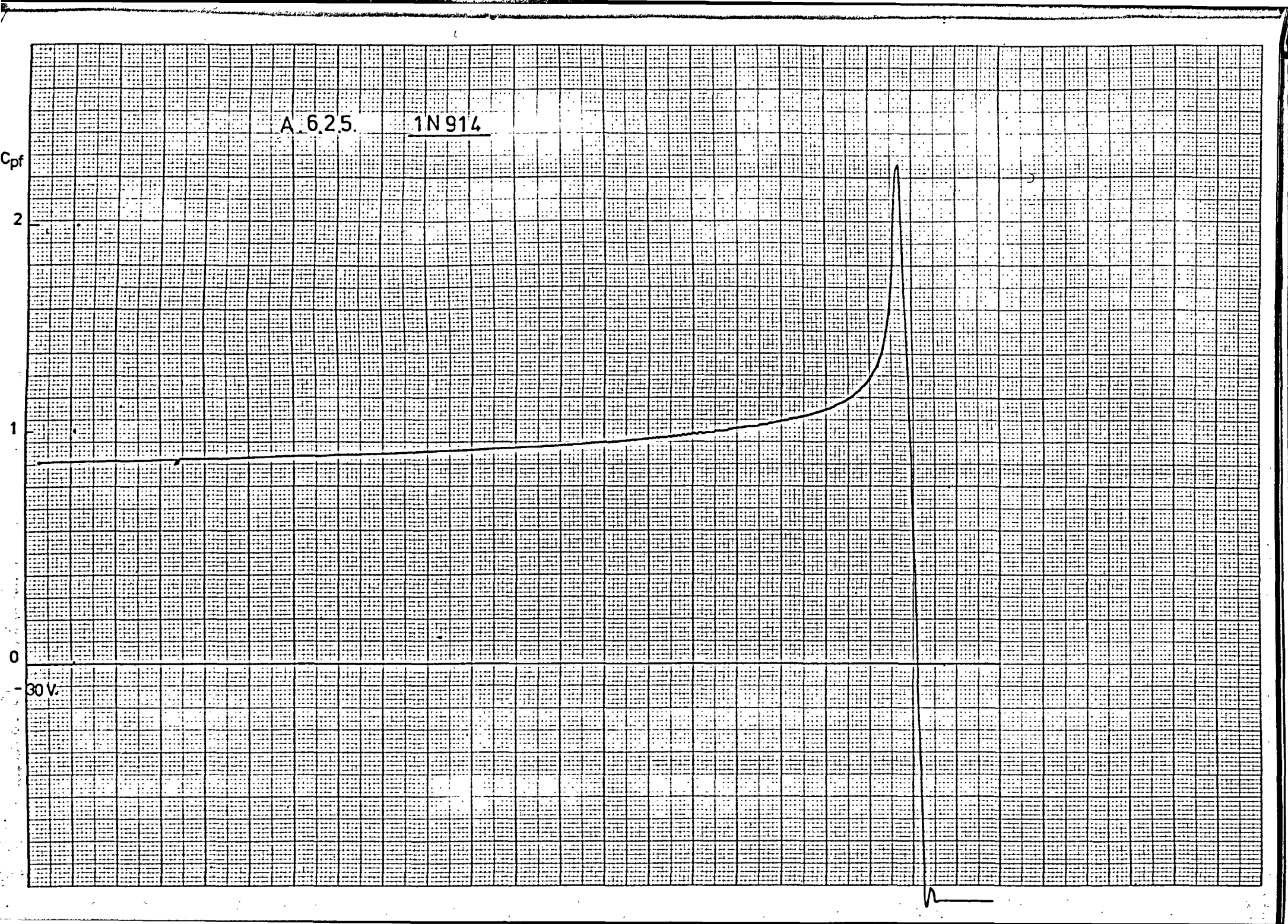
A.6.2.5. 1N914
Cpf
2
1
0
-30 V.

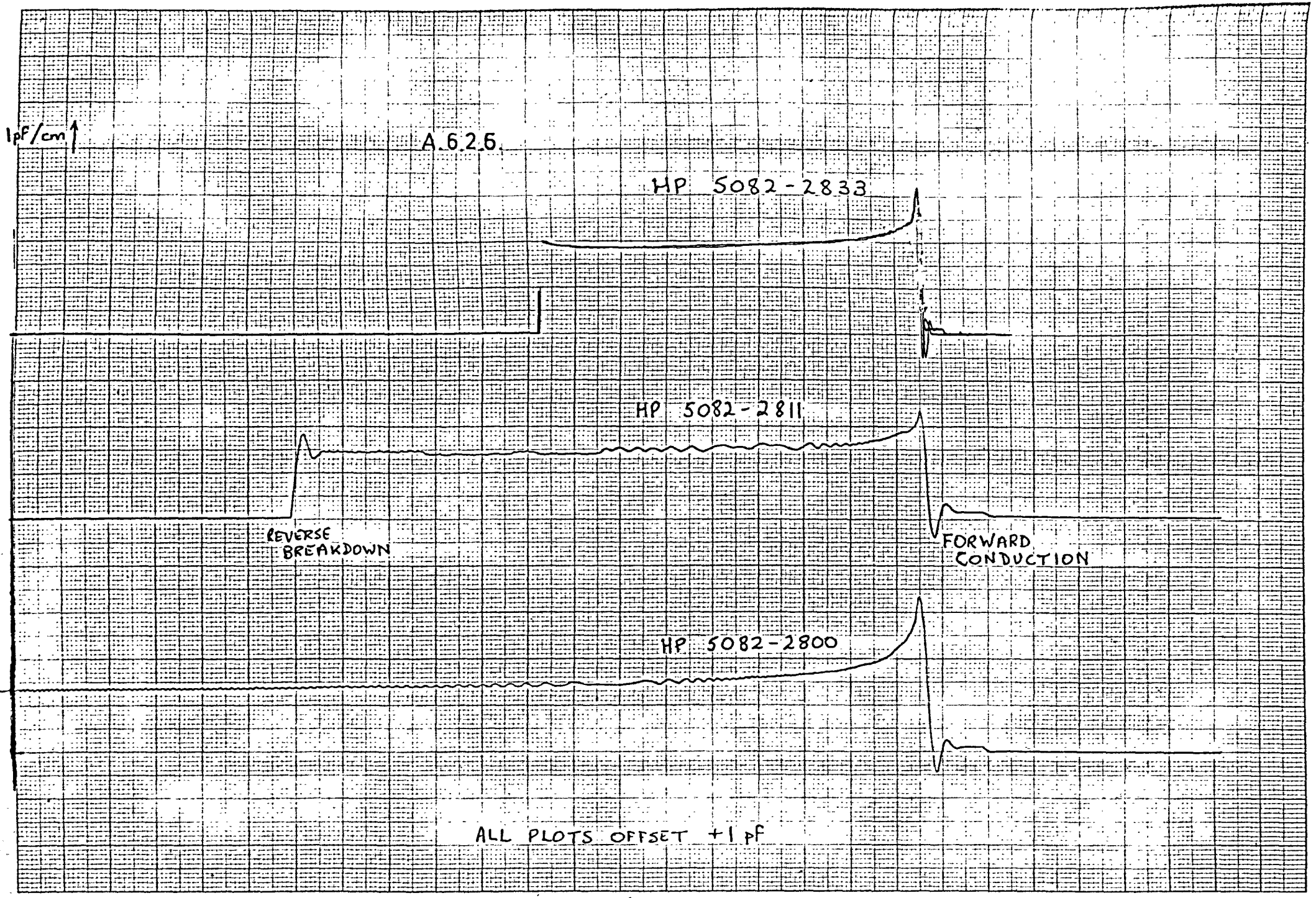
1pF/cm
A.6.2.6.
HP 5082-2833
HP 5082-2811
REVERSE BREAKDOWN
FORWARD CONDUCTION
HP 5082-2800
ALL PLOTS OFFSET +1 pF

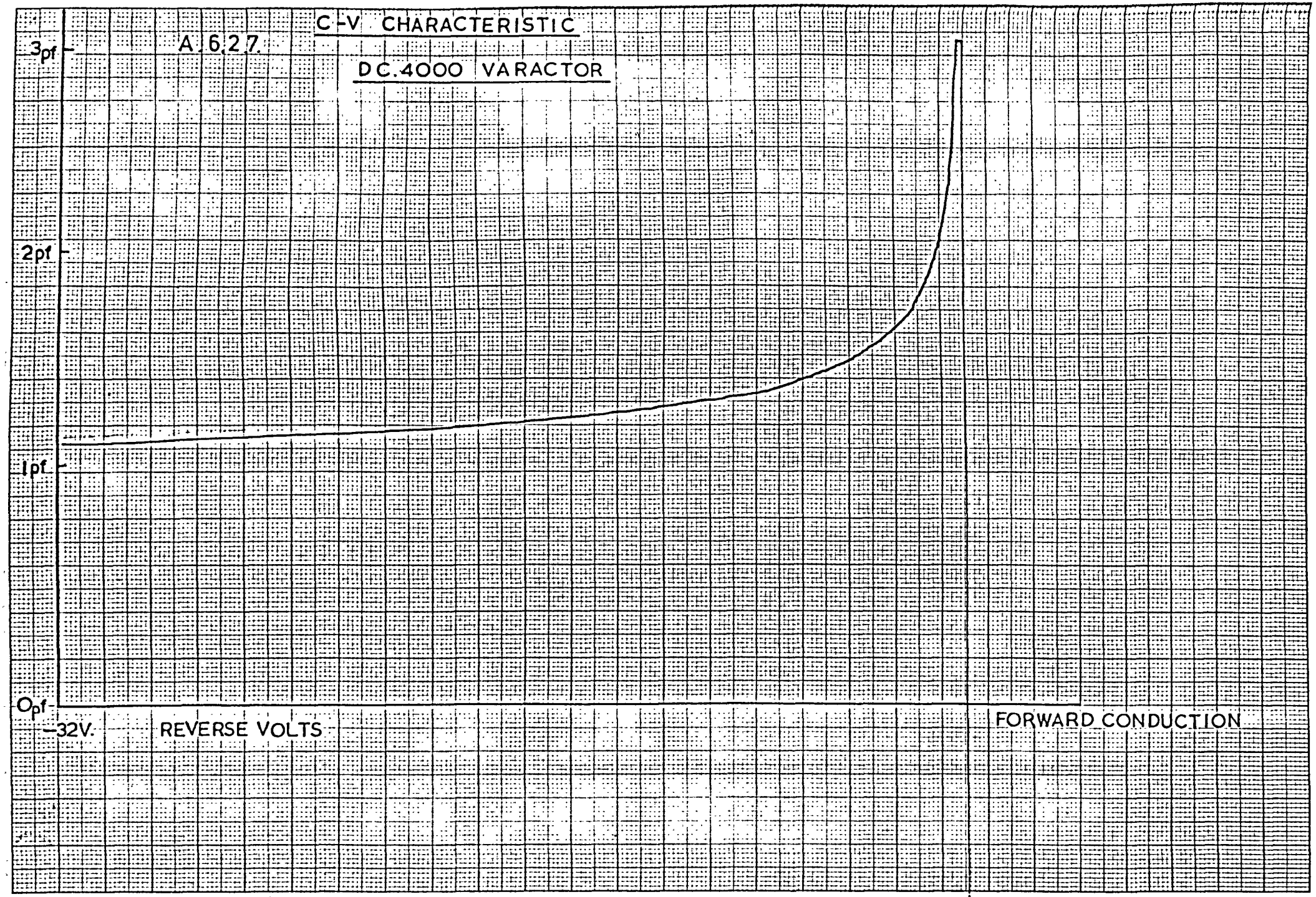
C-V CHARACTERISTIC
A.6.27.
DC.4000 VARACTOR
3pf
2pf
1pf
Opf
-32V.
REVERSE VOLTS
FORWARD CONDUCTION

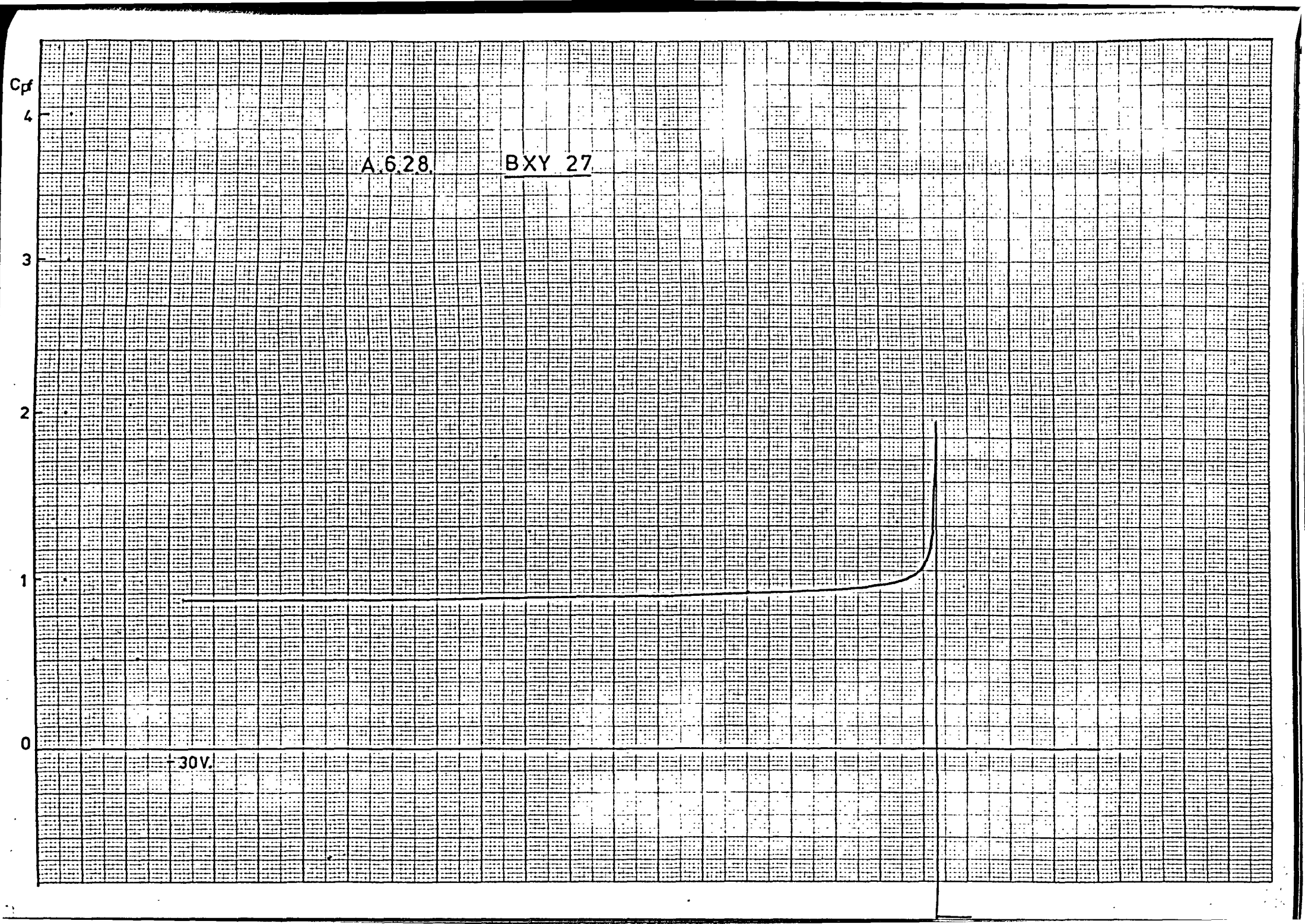
Cpf
4
3
2
1
0
A.6.28.
BXY 27
-30V.

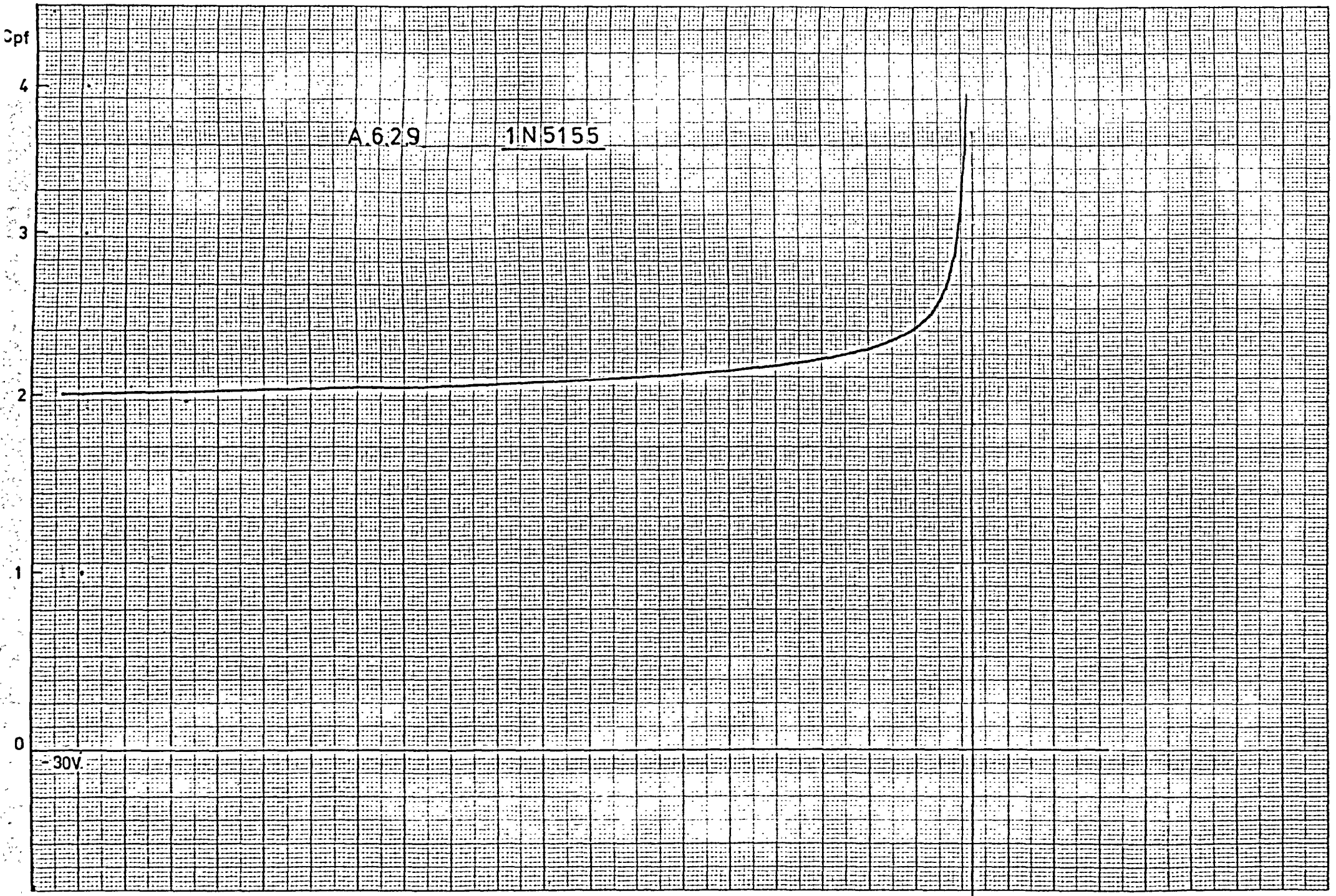
Cpf
4
3
2
1
0
A 629
1N5155
-30V.

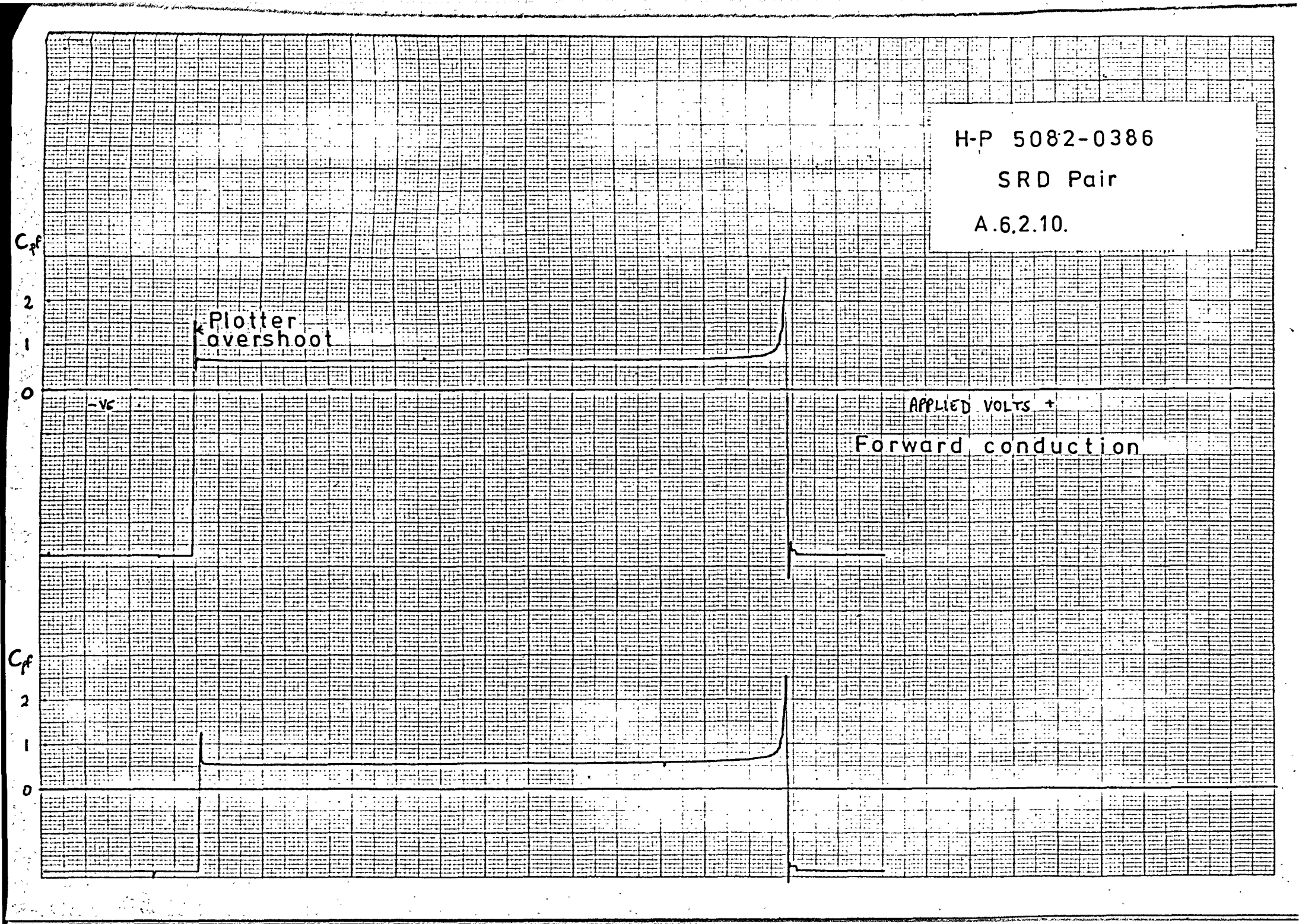
H-P 5082-0386
SRD Pair
A.6.2.10.
C_{pf}
2
1
0
Plotter overshoot
-Vc
APPLIED VOLTS +
Forward conduction
C_{pf}
2
1
0

H.P. STEP RECOVERY 5082-0386

C-V PLOTS

A.6.2.11.

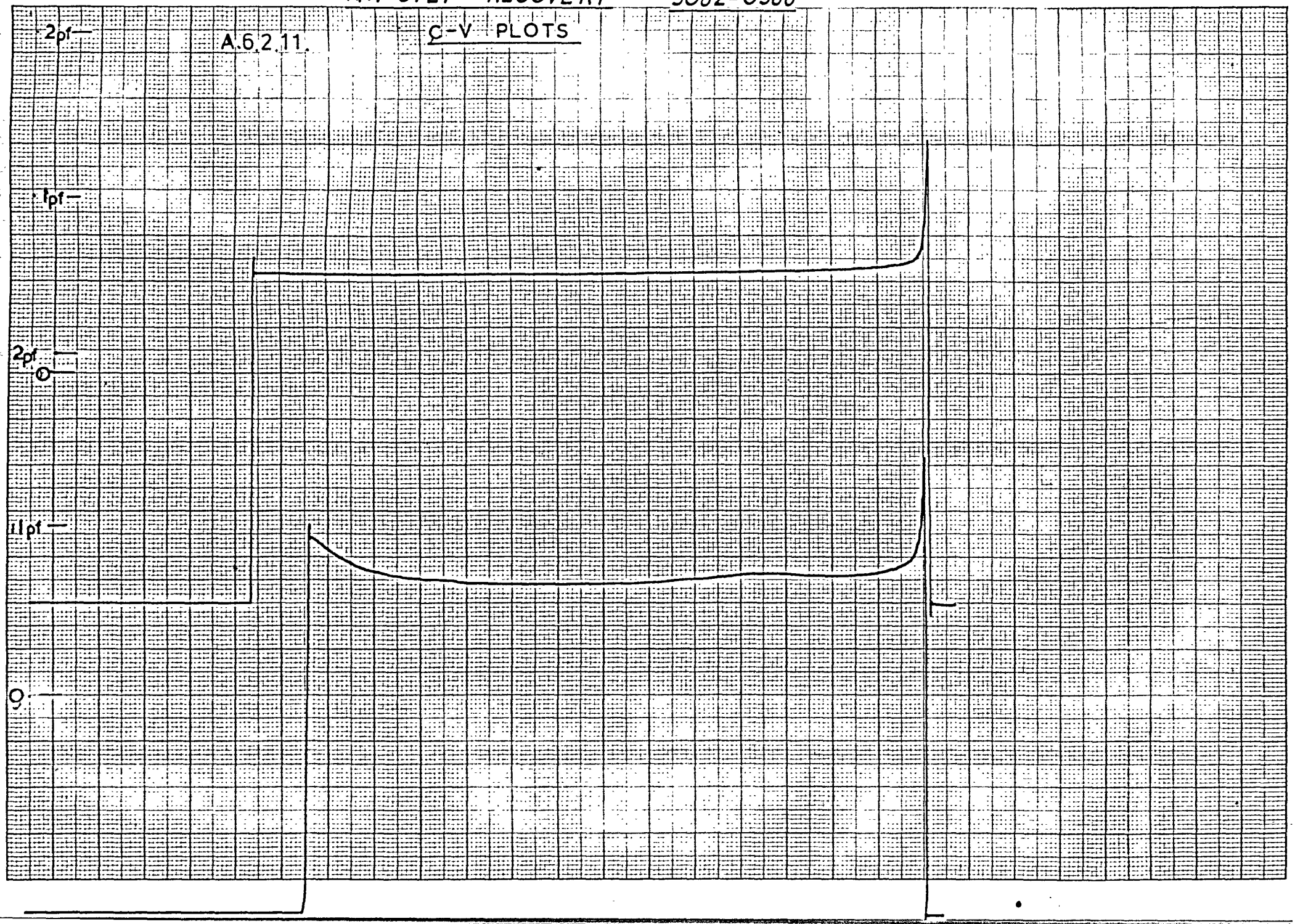

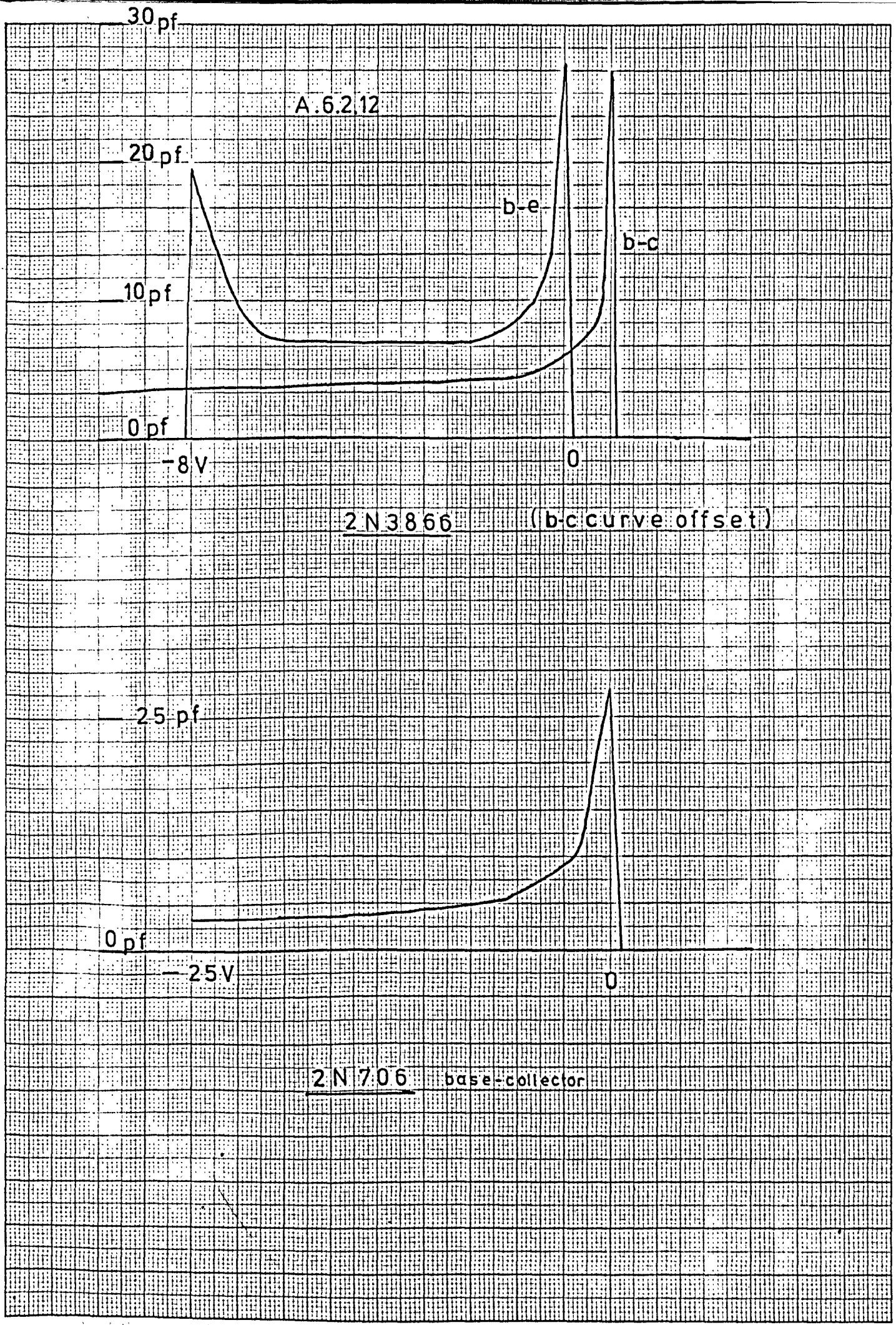
30 pf
A.6.2.12
20 pf
b-e
b-c
10 pf
0 pf
-8 V
0
2N3866 (b-c curve offset)
25 pf
0 pf
-25 V
0
2N706 base-collector

Appendix 6.2 The Capacitance - Voltage Plotter

At the time of construction of this instrument, no commercial dynamic C-V plotters were available. Recently, a very expensive commercial equipment has been put on the market, but it is considered by the author to make a basically faulty assumption i.e. that all diodes are abrupt junctions. The apparatus constructed made no such assumptions, but the output consisted of a straight forward C-V plot, from which deductions of the diode non-linearity could be made. The addition of logarithmic amplifiers was contemplated, but the complexity of setting up and use would have been too great to justify this step.

A similar instrument had been constructed by another member of the department, and some of the circuitry involved was copied, with necessary alterations, from that equipment.

The block diagram of the instrument is shown in fig. (A.6.1). It was decided that the precision timebase in the oscilloscope would be used, to save time and expense in construction. The fundamental characteristics were laid out in the design data table below.

Parameter	Required better than	Achieved
Resolution	0.2 pF	0.1 pF
Accuracy	± 0.2 pF	±0.1 pF *
Voltage range	- 80 to + 15	specification
VAC at diode under test	(as small as possible)	(about 25 mV) ((adequate))
Linearity	better than 10% per decade	estimated about 8% per decade

(* - with reasonable precautions)

Fig. A.6.1. C-V PLOTTER BLOCK SCHEMATIC

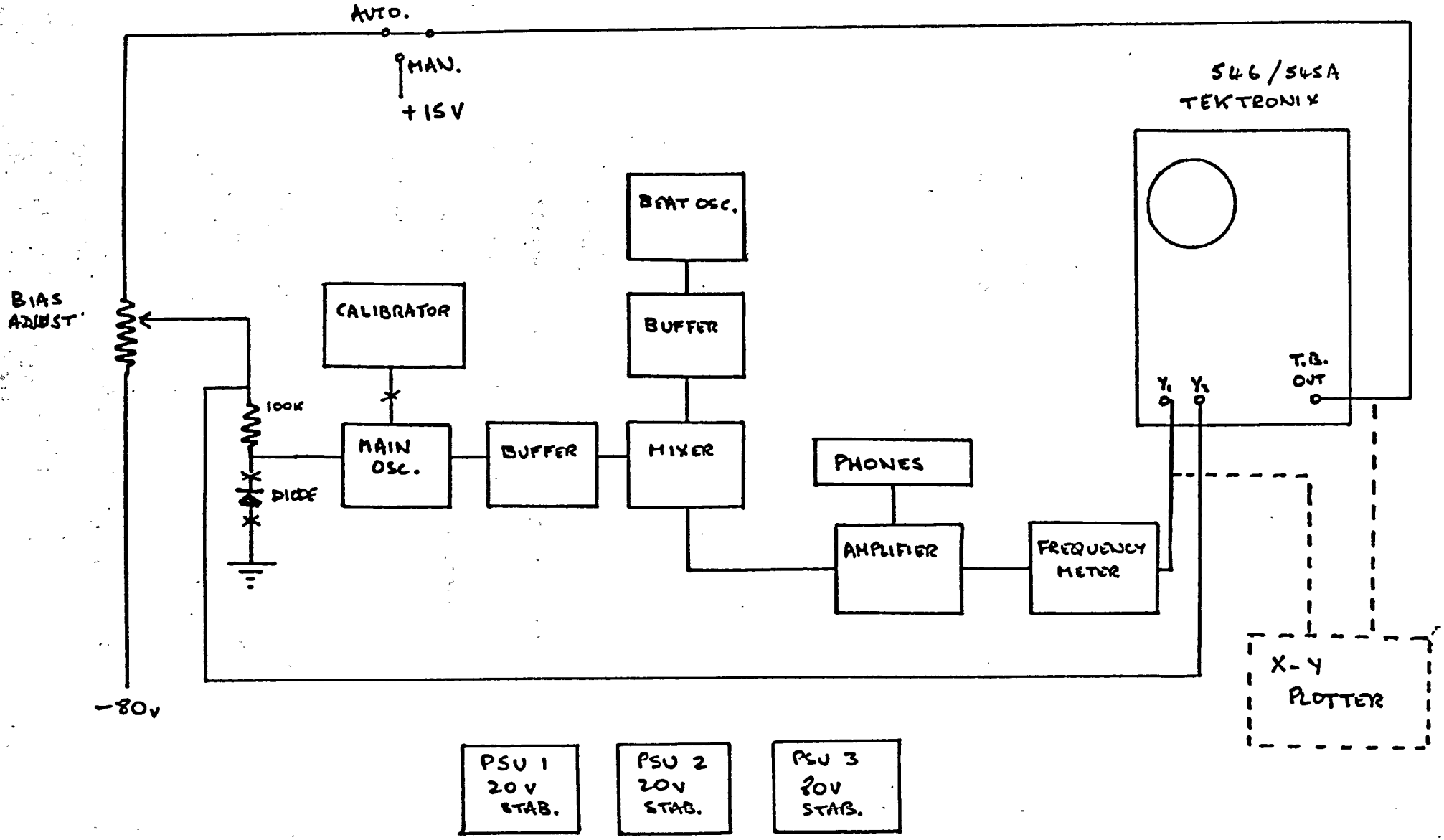

Normal operation was carried out using the oscilloscope display at about 1 sweep per second. High-precision plots were performed on a Bryans X-Y plotter.

Circuit Description

The circuit block diagram and the essential individual circuits are shown in figs.(A.6.2/4.). Manually or automatically swept bias was provided to the diode. The frequency of the main oscillator depended on three capacitors, the main tuning gang, the calibrator (when in circuit) and the diode reverse bias capacitance. Signals were provided at the mixer from the main (variable) oscillator and the fixed reference (beat) oscillator. The low frequency productwas filtered, amplified, clipped and counted in an analogue circuit. An output voltage, proportional to the difference frequency, was applied to the oscillscope or X-Y recorder.

Main Osc/Buffer

The main oscillator used two junction-gate F.E.T's in a Franklin circuit. Heavy padding capacitance across the tuned circuit was available to swamp large varactor capacitance when needed; only relatively small frequency changes were desirable. A single transistor emitter follower provided the low output impedance to the mixer, a simple two diode type.

Beat Osc.

The beat oscillator, an RC Wien bridge, was of a very common type. Control of R and C was provided, to increase the versatility of the instrument.

Fig. A.6.2.

WIEN-BRIDGE BEAT OSCILLATOR

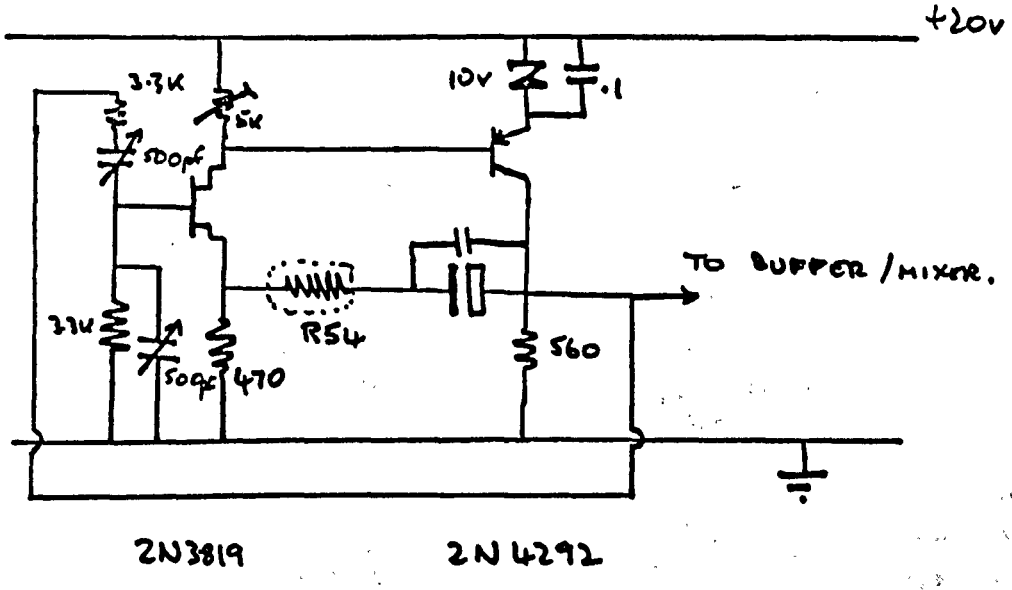

P.S.U.'s 1 AND 2.

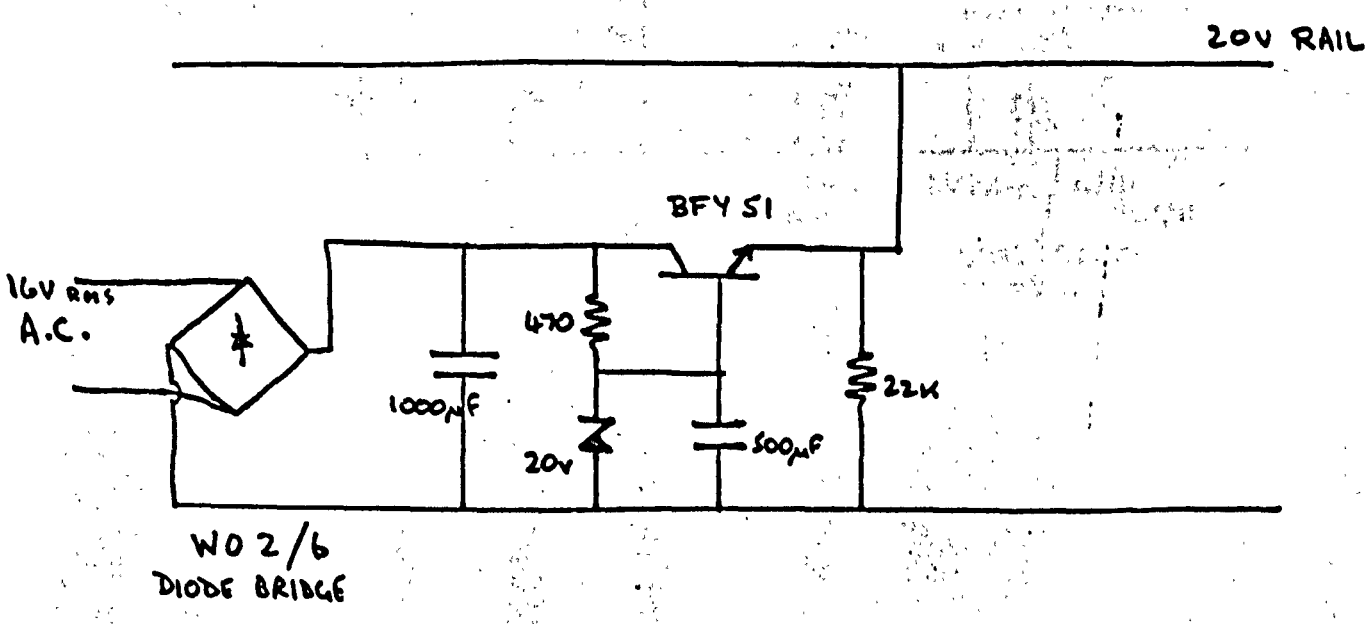

64V A.C. P.S.U. 3: WO 6 100μF 3x27V ZENERS 50μF MJE 340 150K

Fig. A.6.3,4.

AMPLIFIER

FREQUENCY METER

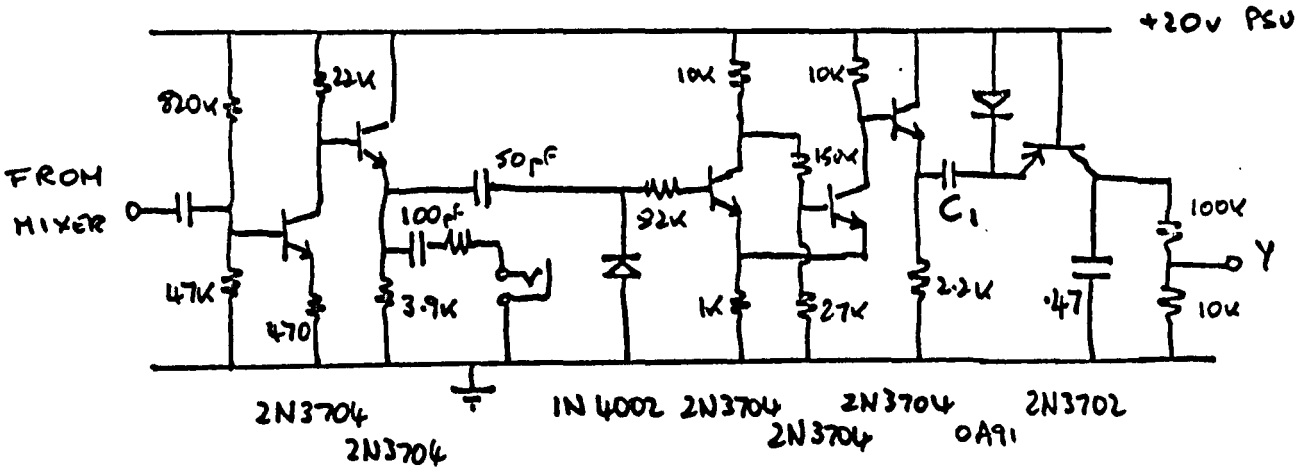

C1 depends on frequency and slew rate; approx 150pF. for 1 MHz, 1 sweep/sec

MAIN OSCILLATOR AND BUFFER/MIXER

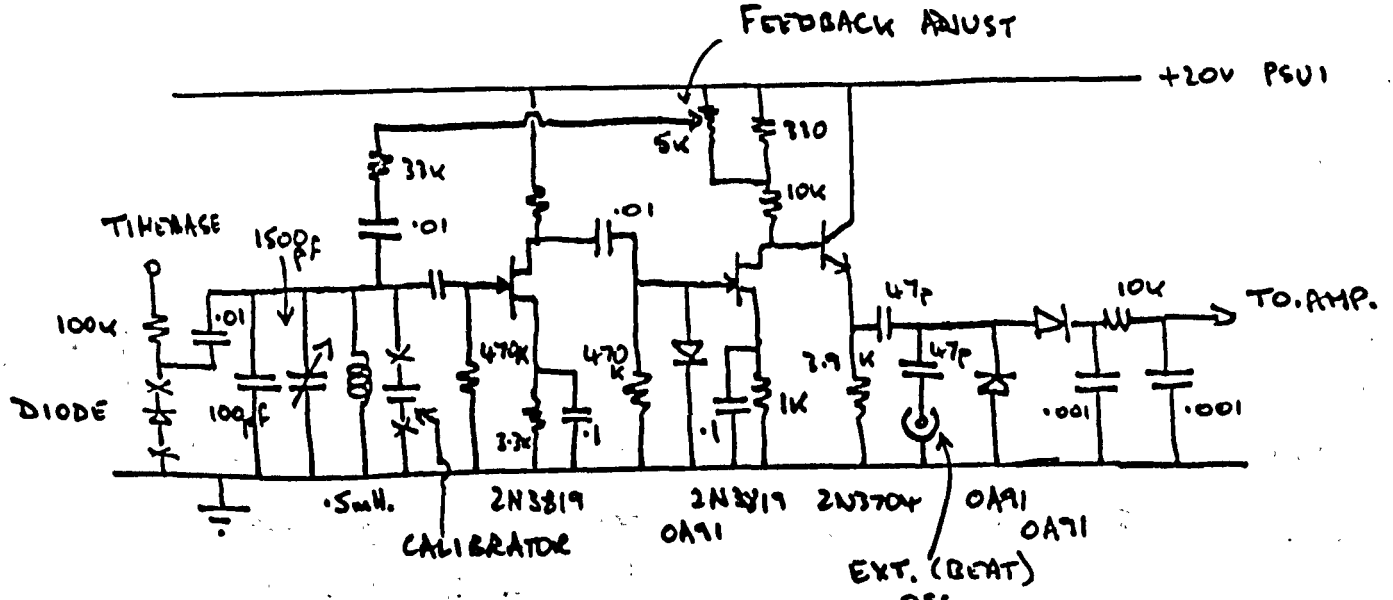

In practice, however, a reference frequency of about 1 MHz was found most useful. It was necessary to include an emitter follower 'buffer', and a separate, and heavily decoupled, power supply for the beat oscillator, to prevent frequency locking of the oscillators at a low beat frequency. Full screening of the beat oscillator was employed, and an external calibrator for the main oscillator was also found necessary.

Amplifier/Frequency Meter

The low-frequency beat note was filtered after the mixer and amplified in the conventional two stage circuit. An outlet for high impedance phones helped in searching for zero beat. The a.c. waveform was heavily clipped and fed to a diode-transistor pump type frequency meter, which depended on C_1 for its operation. The maximum usuable operating frequency (i.e. the highest beat note) was approximately 15 KHz, for the reference frequency of 1 MHz and slow-rate of 1 sweep per sec.

Power Supplies

The power supplies were simple series transistor stabilisers. Component values were adjusted to suit the output voltage.

Operation

The method of operation was tabulated.

1. Connect the instrument to the oscilloscope and select a suitable sweep speed. 1 Hz (10 cm/sec) was used for screen displays, .05Hz for X-Y plots.
2. Select reference frequency. 1 MHz was used.
3. Select Manual/Auto sweep.

4. Set to zero beat using phones.

5. Operate calibrator switch to obtain scale calibrations and adjust oscilloscope/plotter gains for convenient deflections.

6. Connect diode observing polarity for consistency of plots.

7. After test re-check calibration or often during series of measurements.

The operation allowed both absolute and comparitive measurements, with adjustable sensitivity, achieved by changing the padding capacitor, from 4 pF max. to 100 pF max.

Performance

The overall performance of the instrument, after initial difficulties, was well up to expectation. Samples of the output are shown in sections (6.2) The calibrator proved useful in making exact capacitances measurable to a degree of accuracy comparable to the capacity standards in the box. In practice these were trimmers adjusted on a 1% bridge.

Fig.A.6.3.1.

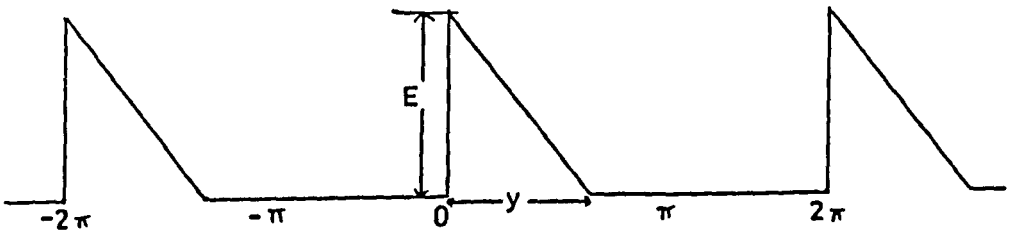

With Origin $\theta = 0$

$$a_0 = \frac{Ey}{4\pi}$$

$$a_n = \frac{E}{n^2 \pi y} \cdot (1 - \text{Cos } ny)$$

$$b_n = \frac{E}{n^2 \pi y} (ny - \text{Sin } ny)$$

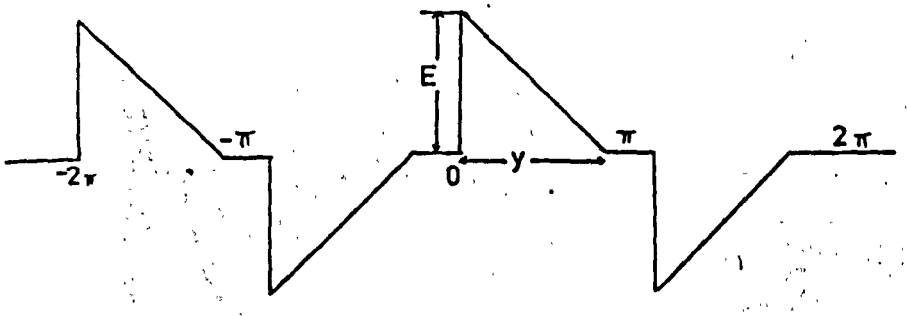

$$a_0 = 0$$

$$a_n = \frac{2E}{n^2 \pi y} \cdot (1 - \text{Cos } ny)$$

$$b_n = \frac{2E}{n^2 \pi y} \cdot (ny - \text{Sin } ny)$$

for n odd,

$a_n = b_n = 0$ for n even

Fig.A6.3.2.

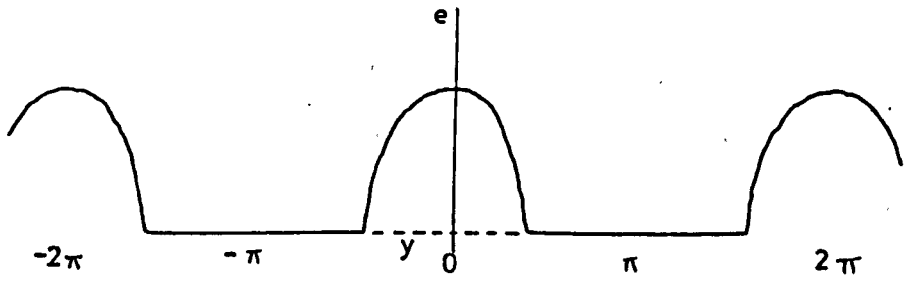

Function $e = E(\cos\theta - \cos y)$

$$a_o = \frac{E}{\pi}.(\sin y - y\cos y)$$

$$a_1 = \frac{E}{\pi}.\left(y - \frac{\sin 2y}{2}\right)$$

$$a_n = \frac{2E}{\pi n(n^2-1)}\ (\sin ny.\cos y - n\cos ny.\sin y)$$

$$b_n = 0$$

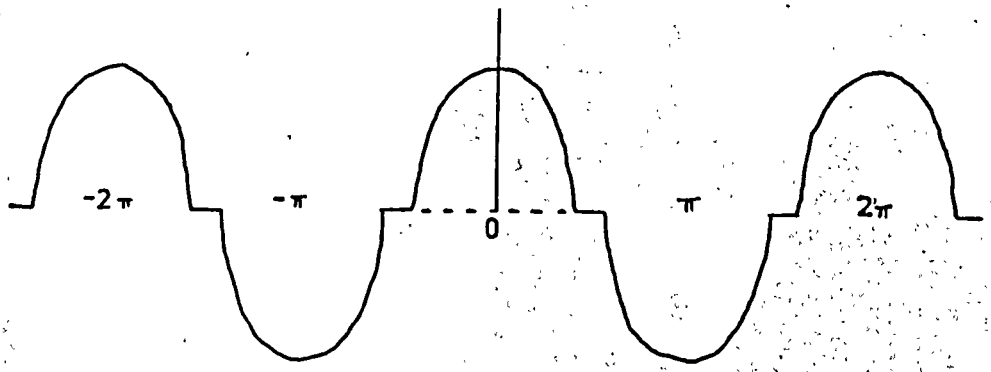

Function $e = E(\cos\theta - \cos y)$

$$a_o = 0$$

$$a_1 = \frac{E}{\pi}$$

$a_n = 0$ for n even

$$a_n = \frac{4E}{\pi n(n^2-1)}.(\sin ny.\cos y - \cos ny.\sin y.n)$$ n odd

$b_n = 0$ all n

Fig A6.3.3.

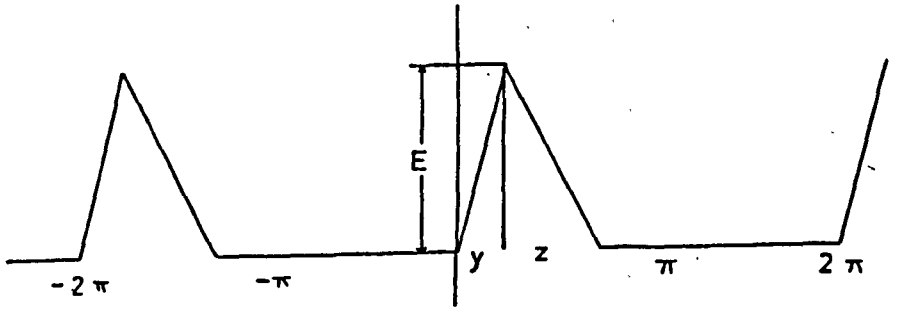

$$a_0 = \frac{E(y+z)}{4\pi}$$

$$a_n = \frac{E}{\pi n^2 yz}.[(y+z)\cos ny - z - y\cos(y+z)]$$

$$b_n = \frac{E}{\pi n^2 yz}.[(y+z)\sin ny - y\sin n(y+z)]$$

For all n

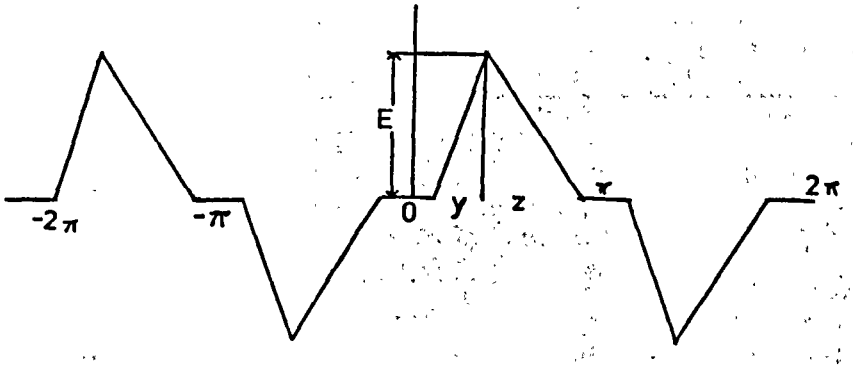

$$a_0 = 0$$

$$a_n = \frac{2E}{\pi n^2 yz}.[(y+z)\cos ny - z - y\cos(y+z)]$$

$$b_n = \frac{2E}{\pi n^2 yz}.[(y+z)\sin ny - y\sin n(y+z)]$$

For n odd,

$a_n = b_n = 0$ For n even

FigA6.3.4. The Half-wave Rectifier
a_n coefficients

Conduction half-angle	$\theta' =$	$\pi/2$	$\pi/3$	$\pi/4$	$\pi/5$	$\pi/6$
Voltage Coeff.	$a_n =$					
	2	·21220	·9607	·07502	·04311	·02653
	3		·03978	·05305	·03485	·02299
	4	−·04244	·02444	·03001	·02524	·01856
	5		·07047	·01061	·01556	·01378
	6	·01818	−·01575	−·00216	·00722	·00909
	7		−·05885	−·00756	·00093	·00491
	8	−·01010	−·00041	−·00714	−·00281	·00157
	9		·00397	−·00353	−·00420	−·00076
	10	·00642	·00477	·00045	−·00317	−·00209

Fig A6.3.5. The half-wave Rectifier - predicted spectra

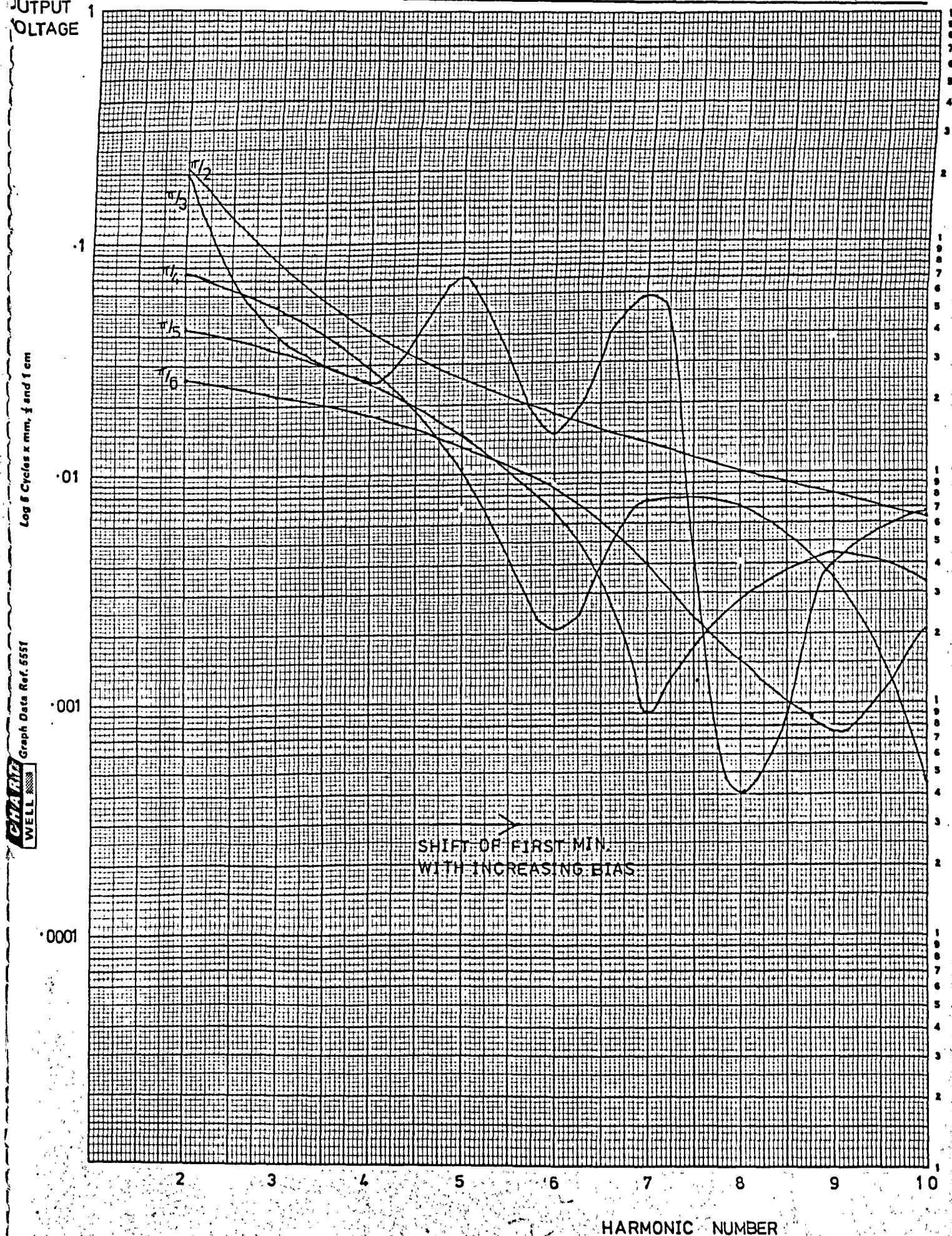

Fig A.6.3.6. Practical Rectifier 1N4002 1·5 KHz Input 50 ohm load

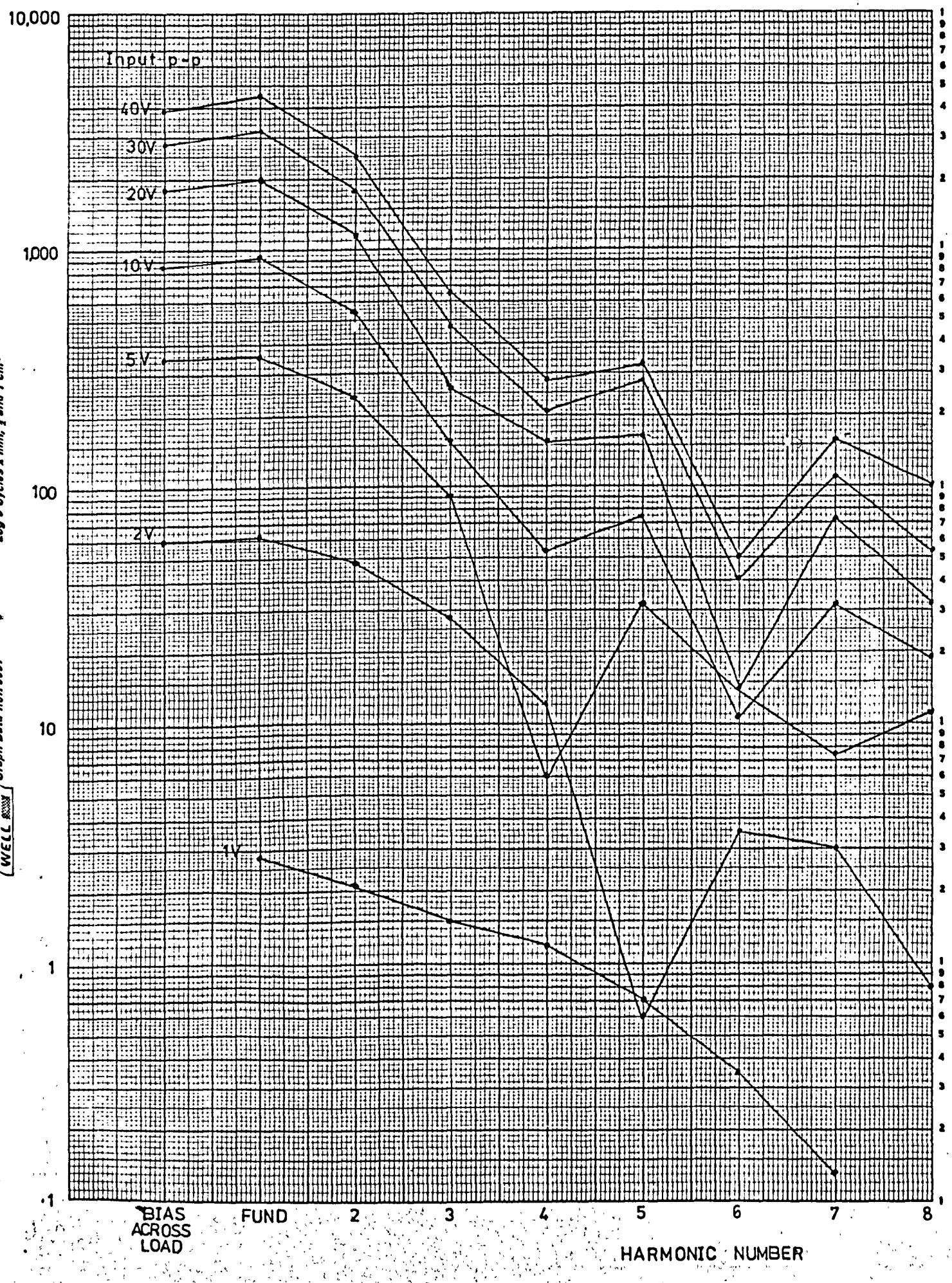

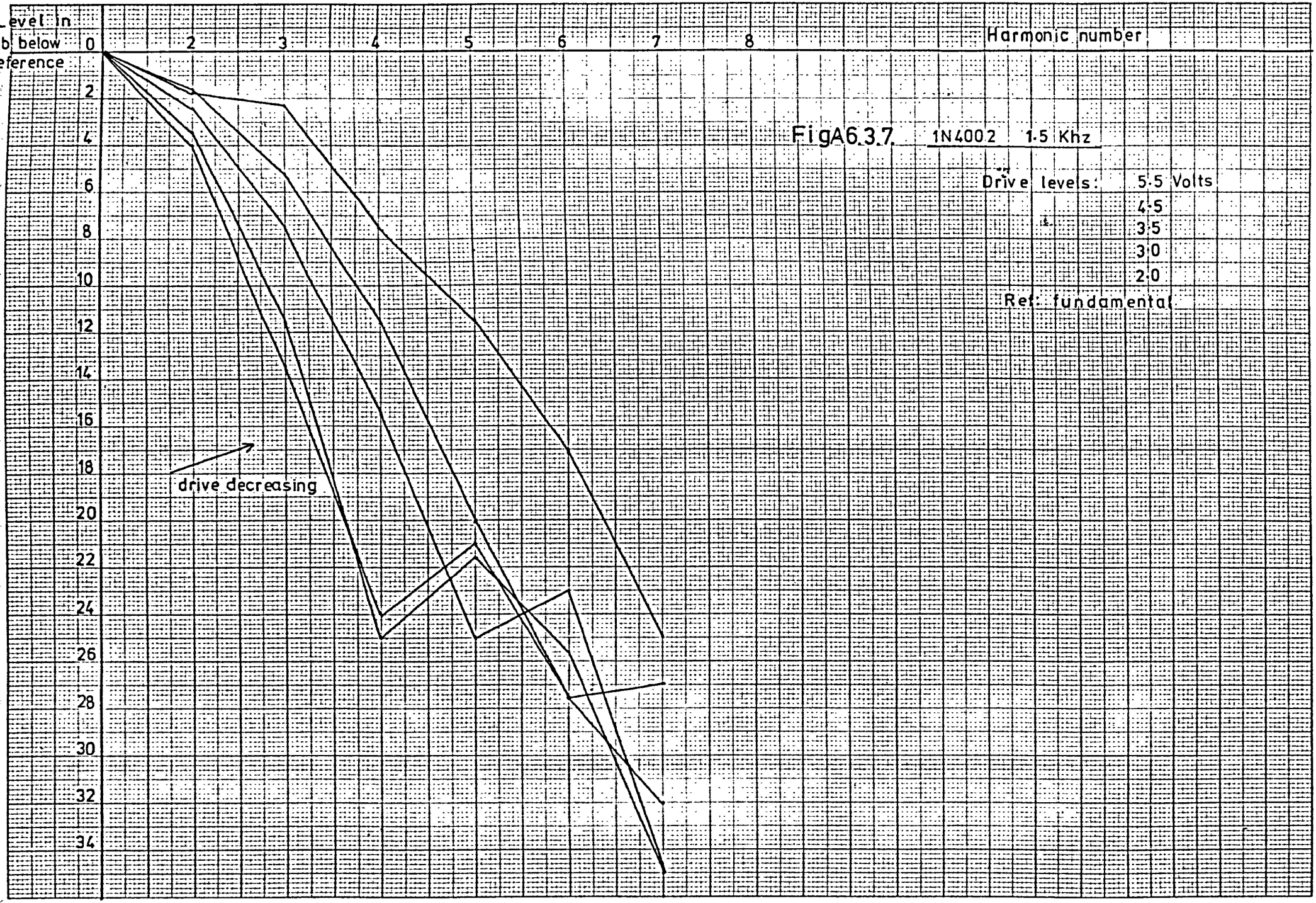

Fig A6.3.7 1N4002 1.5 Khz

Drive levels: 5.5 Volts
4.5
3.5
3.0
2.0

Ref: fundamental

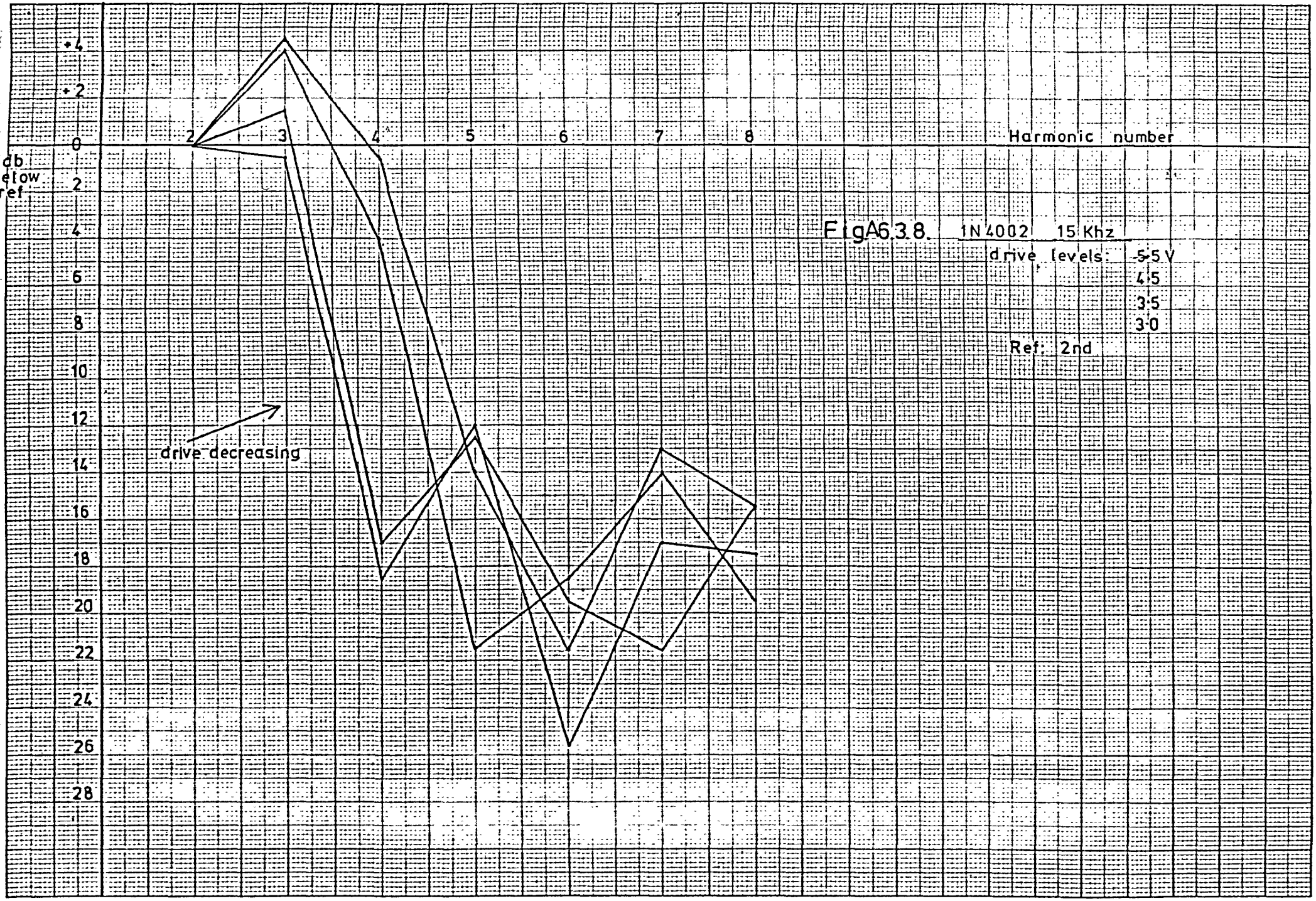

Fig A6.3.8. 1N4002 15 Khz

drive levels: 5·5 V
4·5
3·5
3·0

Ref: 2nd

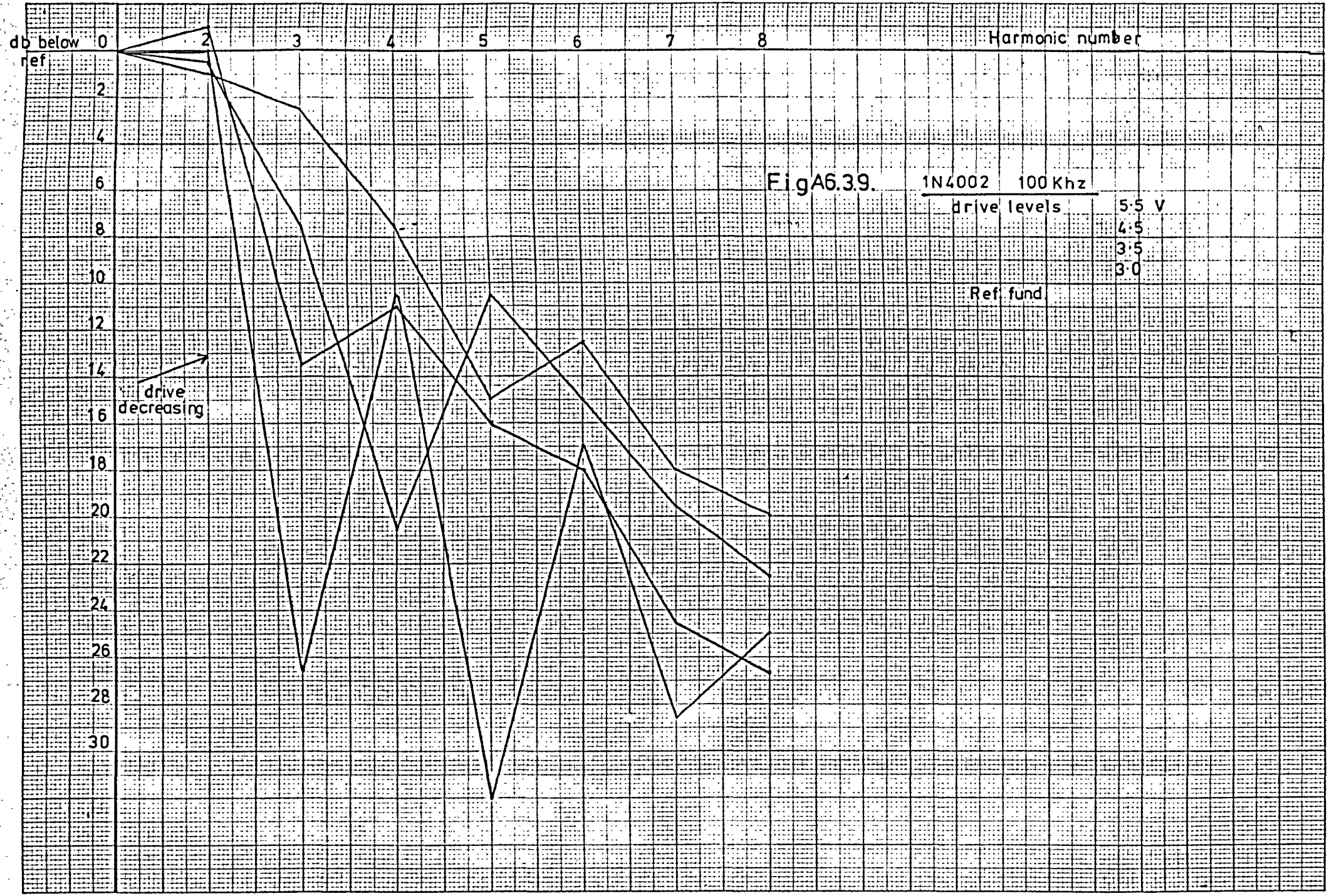
db below ref
0
2
4
6
8
10
12
14
16
18
20
22
24
26
28
30
2
3
4
5
6
7
8
Harmonic number
drive decreasing
Fig A6.3.9.
1N4002 100 Khz
drive levels
5·5 V
4·5
3·5
3·0
Ref fund

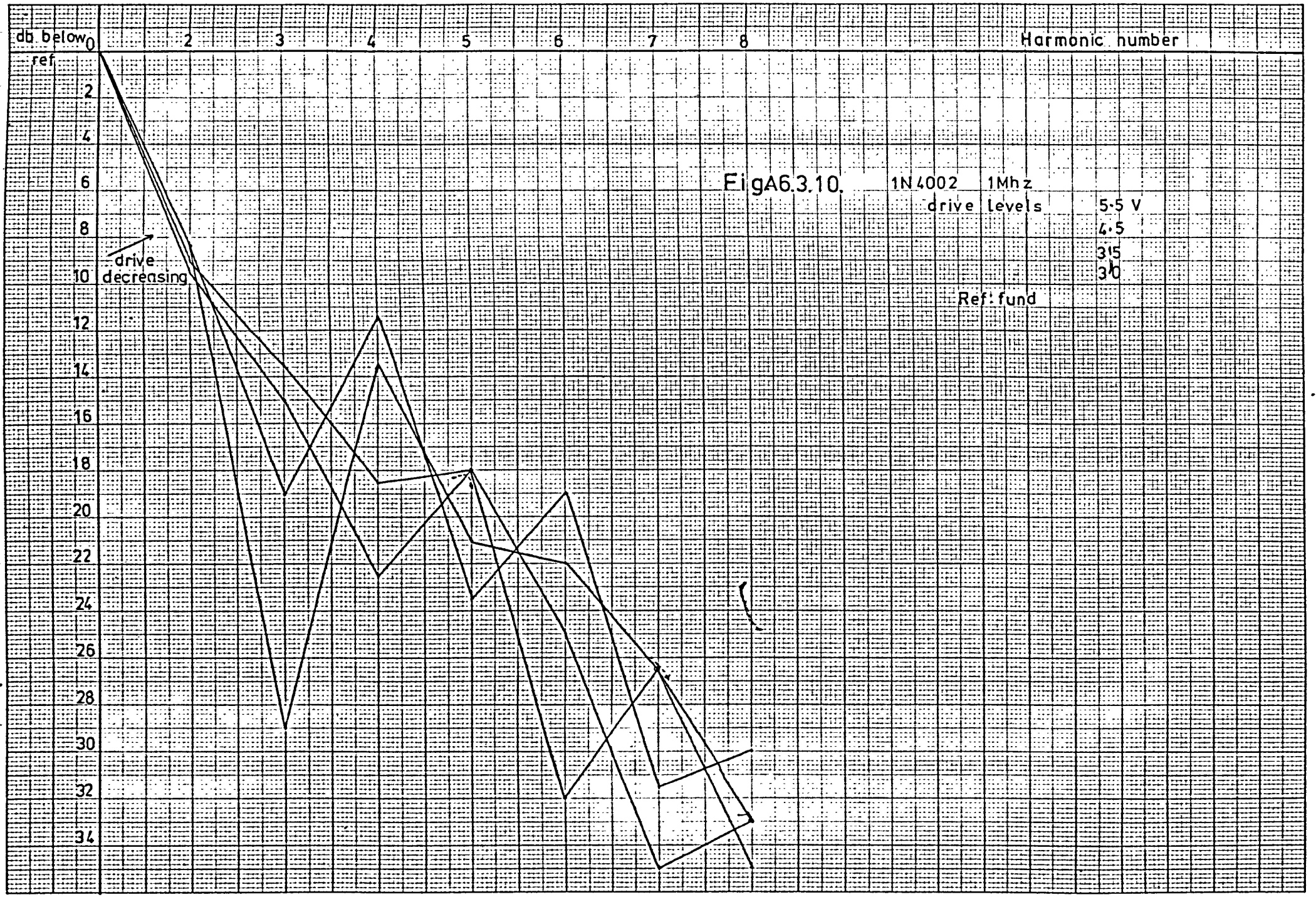
db below ref
0
2
4
6
8
10
12
14
16
18
20
22
24
26
28
30
32
34
1
2
3
4
5
6
7
8
Harmonic number
drive decreasing
FigA6.3.10.
1N4002 1Mhz
drive levels
5·5 V
4·5
3·5
3·0
Ref: fund

Appendix 6.4.1

The Step-Recovery diode in the Time Domain - An analysis of the Photographs

1. Single diode IN4719 1GHz - 40 KHs

   15Hz. The diode current showed half-wave rectification, offset by a small d.c. voltage. No d.c. was allowed in the load, so the voltage recorded was the alternating component.

2. 50Hz Carrier recombination at this frequency was virtually complete, so that the diode behaved as a good rectifier.

3. 100Hz Although the current distortion could be overlooked, significant voltage spikes were induced at the switching points.

4. 300Hz At the lower end of the step-recovery operating region, sufficient rectification took place to keep the charge stored relatively small, although the step could be seen in both current and voltage waveforms.

5. 1000Hz The reverse voltage spike had become a greater fraction of the operating cycle.

6. 3000Hz This frequency would have been the optimum operating region for this diode. Appreciable charge was stored, with a minimum of rectification, and a fast step.

7. 10 KHz This photograph, beyond the optimum range, illustrated the fall in voltage and current amplitude. The step time was comparable to the inverse drive frequency.

8. 20 KHz) The current step had degraded to a small perturbation of the
9. 30 KHz) d.c. level.
10. 40 KHz) The voltage consisted mainly of fundamental frequency feedthrough.

The overall interpretation of the series was that, for a given diode, an optimum operating frequency range existed. This was the circuit effect of the limiting parameters of recombination time Ts and transition time tt. The optimum appeared to be broad, and it may be desirable to place the input and output frequencies on each side of it.

The second series demonstrated the two-diode SRD array. The step effect was emphasised by the cancellation, between the diodes, of the rectifier-switching components, which were essentially even order terms, while odd-order terms were added to produce the quite spectacular voltage spikes. The measurement was for 2 x 1N4719.

1. 50 Hz

Two rectifiers connected in reverse-polarity parallel produced only a 'cross-over' distortion in the current.

2. 100 Hz Voltage spikes appeared at a very low level.

3. 300 Hz) As the switching time was reduced, the step recovery
4. 1000 Hz) effect increased.

5. 3000 Hz The optimum input frequency. The voltage spikes were symmetrical, and corresponded to small current cross-overs between the diodes.

6. 10 KHz

The timing of the current and voltage spikes was most evident at this point. The shape of the voltage pulse was characteristic of a wide-band system. The step in current produced the simultaneous fast leading edge of the spike, while the finite (i.e. non-zero) reverse bias capacitance slowed the trailing edge; this corresponded to the round of the pulse tail in a tuned system (Chapter 2).

7. 20 KHz, 30 KHz The switching time became comparable with the transition time so that the harmonic content of the output was much reduced compared to the lower input frequencies.

In all the oscilloscope photographs, a 50 MHz (7 nS risetime) instrument was used, in the 'chop' mode to maintain phase coherence between the traces.

The low frequency diode model showed the type of waveforms to be expected in a completely broadband system. The existence of an optimum input frequency for multiplication has been demonstrated; to reverse the argument, for a given operating frequency, diodes could be made with the right compromise between recombination and transition times for optimum operation. Chapter 5 did not in general, consider recombination, so that the optimum could not be predicted. A purely mathematical model to take this factor into account would be unnecessarily complex, and finally, the decision was made to construct a semi-emperical theoretical model from the practical results of measurements on the devices. It is hoped that this work will continue in the research group at Durham, and may lead to a new type of manufacturer's specification.

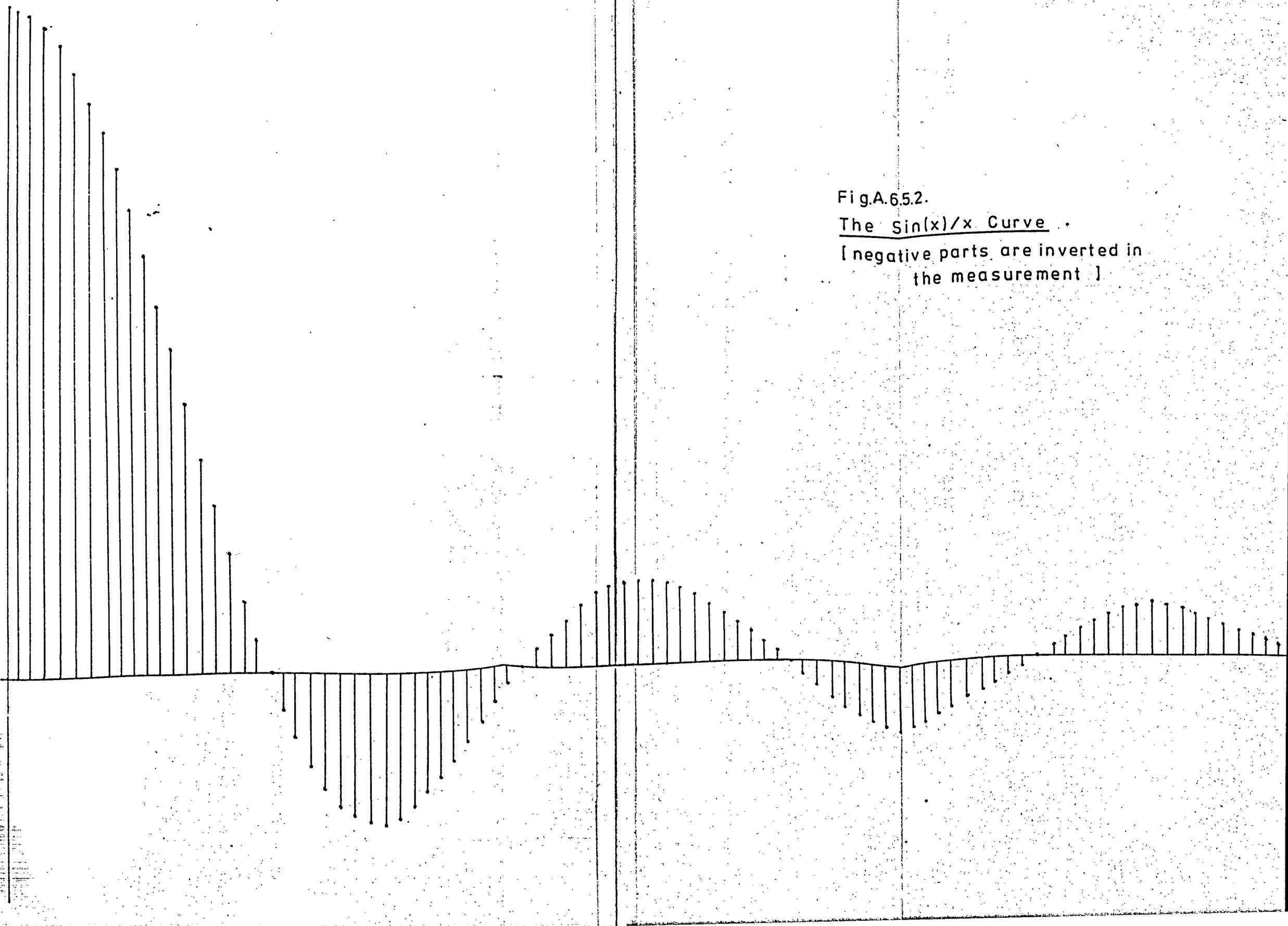

Fig.A.6.5.2.
The Sin(x)/x Curve .
[negative parts are inverted in the measurement]

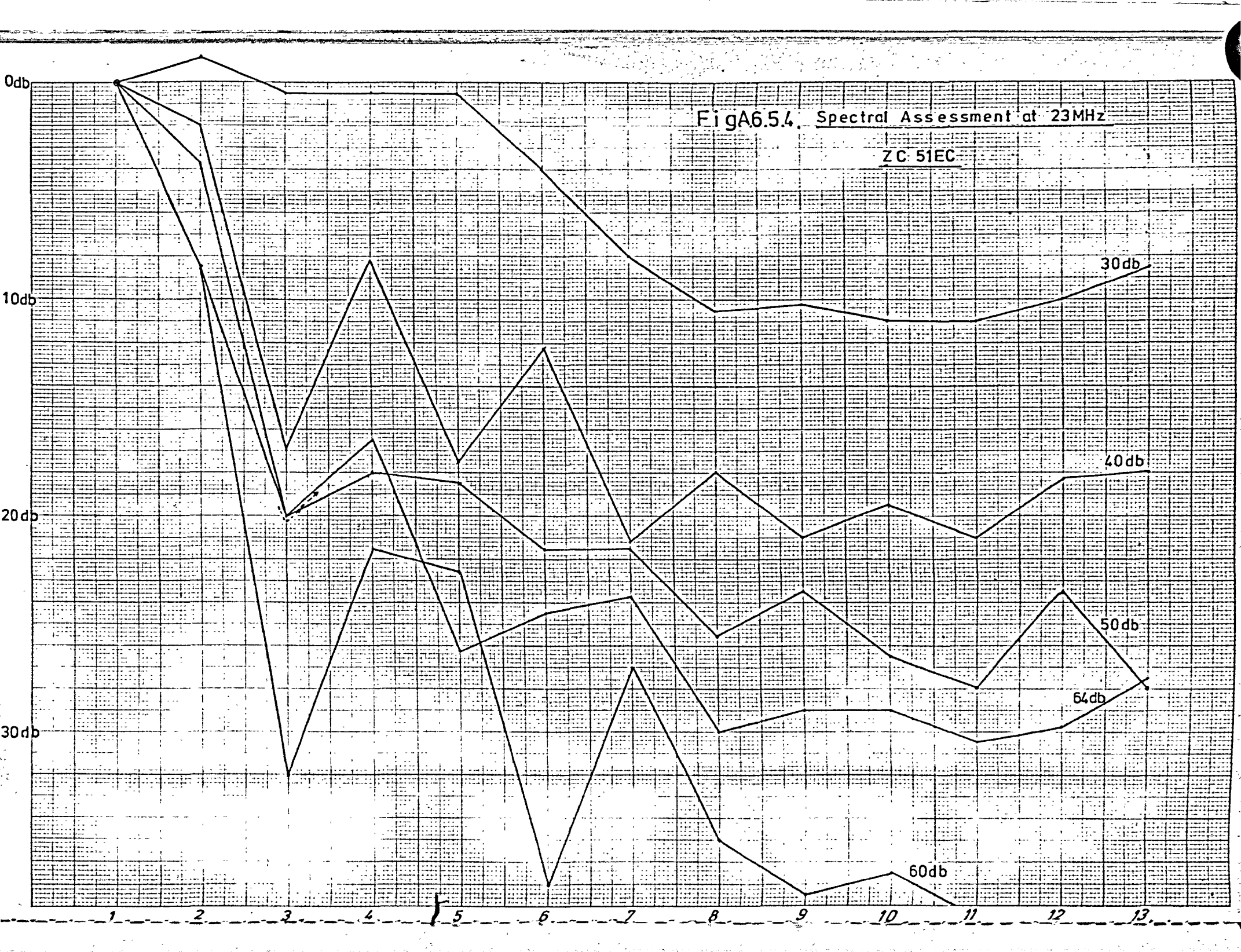
Fig A6.5.4. Spectral Assessment at 23MHz
ZC 51EC
0db
10db
20db
30db
30db
40db
50db
64db
60db
1
2
3
4
5
6
7
8
9
10
11
12
13

Power in mw.

Input power	Reflected power	Output fundamental	2	3	4	5	6	7
50	5·0	28·2	·26	·3	·075	·0095	·00039	·00026
100	2·0	58·0	1·4	1·8	·13	·028	·0009	·0015
200	4·0	108	3·0	4·0	·41	·04	·02	·011
300	8·0	171	5·4	5·2	1·2	·064	·04	·018
400	10	219	25·2	14·0	4·1	1·3	·15	1·86
500	10	309	34	20·0	2·1	2·5	·12	·014
600	14	334	45·1	8·0	1·8	2·2	·27	·01
700	18	382	47·8	10·2	1·0	·45	·15	-
900	21	516	70·3	5·6	1·8	·42	·023	·060
1000	24	570	85·6	3·0	4·6	2·0	·13	·034
1100	14	630	180	2·8	6·4	2·7	·078	·14
1400	5·8	760	119·9	1·4	11·9	1·6	·21	·41

Spectral assessment of

the step recovery diode

5082-0386

Fig.A.662 Data

Appendix 7.3

Constructional Techniques Employed

i. Cavity

Most of the early work on the project consisted of coaxial cavities of some type, generally milled from a solid. The materials were brass and aluminium, for ease of machining; no significant differences in performance were noted. The milled-from-solid technique can be extended to extremely complex filters, and is versatile in the types of filter which can be constructed. However, the equipment tends to become large and heavy, and is not readily adjustable; a few percent frequency error can mean a whole filter is useless. Generally for reasons of size, weight and repeatability, it was decided to aim for an integrated circuit stripline approach.

ii. The Stripline Technique

For economy and repeatability, the triplate stripline structure, using commercially available copper-TFE laminate was chosen. The other viable alternative was the gold-ceramic microstrip system, which has gained popularity recently, but it was considered that the technology involved was not sufficiently advanced to yield predictable and repeatable results. Recent talks with workers in this field suggest that this is still true especially as to repeatability. In addition, design data for components in microstrip have yet to be formulated on a thorough basis. In addition the cost of the gold-ceramic technology is much higher than that of the copper- TFE system; when costs become more reasonable and yields higher, there seems little doubt that the microstrip gold-ceramic technology will become very popular.

A technique was evolved for the production of M.I.C's on 'Polyguide' laminate. Two standard sizes were used, 2" x 4" and 2" x 2". Eventually it was found possible to construct the whole multiplier in the larger of the two boxes.

iii. The Photo-Etch Process

The process has been described in detail in a departmental memorandum, and is adapted from conventional precision printed circuit techniques. A brief description is given below.

a. Preparation of the 'Polyguide'

The polyguide material was cut to the required size and cleaned. A thin layer of Kodak KPCR photoresist was applied, and allowed to dry.

b. Preparation of the Mask

A scale model of the mask, in 'Chart pak ' tape on a drawing paper background, was made. The model was photographed in such a way that the negative was exactly the size of the final pattern, i.e. the negative was the mask for the exposure of the photoresist. Modifications to the scale could easily be made by changing the reduction ratio.

c. Exposure and Etch

The negative was clamped flat on the photo-resist surface of the polyguide, and the whole exposed to Ultra-violet light. Unaffected photo-resist was washed away in the developer and the dried substrate put in a Ferric Chloride etch bath. Finally, the etched pattern was cleaned, mounted and tested.

c. Errors

A programme of investigation of error was carried out. Errors were of the order of 2% in line and gap dimensions, comparable with the expected error in the original. Narrow lines and gaps, of course, showed larger fractional errors. It was concluded that the minimum gap between adjacent lines which could be made accurately (better than $\pm$ 10%) and reproducably, was 0.2 mm (8 thou). Narrow linewidths down to 0.05 mm (2 thou) were just possible with extreme care. Practical filters compared well with theory.

iv Microstrip and Thin film elements

Using the same technology as the stripline a few experiments in microstrip were undertaken, particularly for the centre section of the multiplier. Generally, the conductors themselves behaved reasonably well, but the transitions from stripline to microstrip were unavoidably abrupt, which led to reflections, so the technique was not applied further.

In an attempt to improve the coupling capacitors to the diodes, some thin film work was carried out. The substrate chosen was mica, which could be cleaved into very thin (0.5 thou) sheets. Silver conductors were vacuum deposited through a milled brass mask. Accurate performance checks were not possible, but it appeared that excess capacitance to ground impaired the diode operation quite severely. Eventually, contact to the diodes was made by ceramic chip capacitors and thin wire (soldered) leads.

v. Results

Examples of the filters produced are shown in Figs. 7.3.2 and 7.4.1. The characteristic responses are shown in Figs. 7.3.1, 7.3.3 and 7.3.4. A directional coupler was built using the same techniques for a passband of 4 - 8 GHz and achieved a passband ripple of $\pm$ .75 db (design $\pm$ .5 db) despite dimensional difficulties (Fig. 7.3.10).

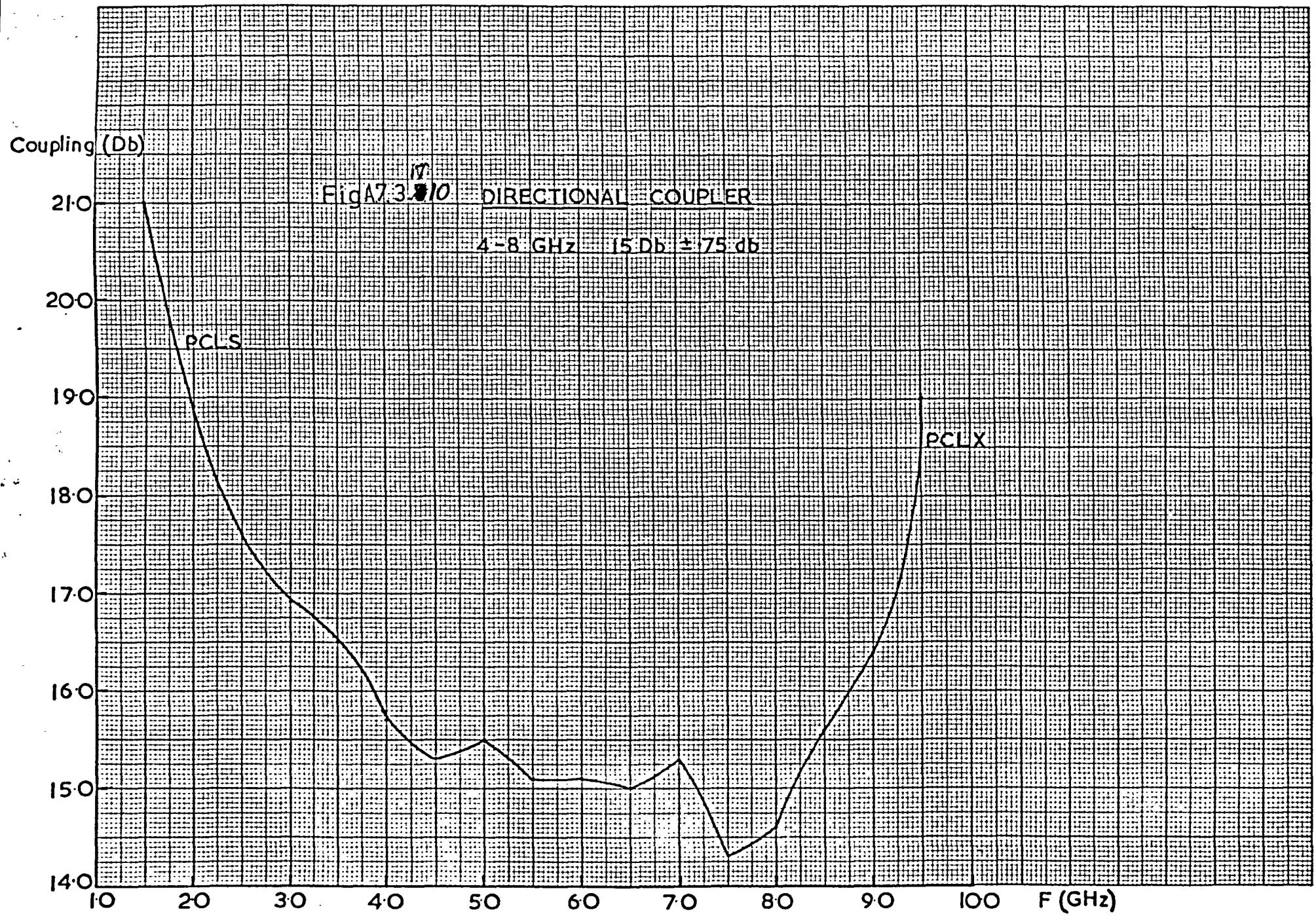

Fig A7.3 #10 DIRECTIONAL COUPLER

4 - 8 GHz 15 Db ± .75 db

Appendix 7.3.2

For generality and the ease of calculation, all the theoretical work was performed using normalized quantities. The important quantities to be denormalized are power, voltage and current, and hence impedance. Clearly, the denormalization of voltage and current is sufficient.

By the usual rule:-

Charge Q = Current x time

i.e.

$Q = 2\pi I$ x period of pulse (for a 'square' pulse)

It has been shown in chapter 6 that the diodes employed had a pulse length such that the first minimum in the Fourier spectrum occurred at the seventh harmonic of 1.56 GHz.

$$\therefore \text{ Period } = \frac{3}{2} \cdot \frac{1}{1.56 \times 7 \times 10^9}$$

However, the pulse is typically triangular so that the effective charge is halved.

$$\text{Hence } Q = \frac{1}{2} \cdot I \cdot \frac{3}{14 \times 1.56 \times 10^9} \cdot 2\pi$$

The manufacturers' data provides for values of Q up to 700 pC per diode or 1400 pC for the pair, with a small increase in the transition time at the higher powers. The transition time in circuit was approximately twice that claimed by the manufacturer under ideal conditions.

At the input centre frequency of 1.56 GHz the power is related to the

(I x V) per Hz as

$$P = I_{\text{per Hz}} \times V$$

Clearly, a very good estimate of the charge shared between the diodes can be deducedfrom the net input power less the calculated loss in the input filter. Hence, the charge induced may be calculated when it is known, and then the denormalization factor may be easily found

i.e.

$$I \text{ denormalization factor} = \frac{Q}{2\pi . \text{ period}}$$

When assessing the diodes, it was found that the breakdown (indicated by a noisy spectrum) occurred for a single diode at 1.6 watts (this is somewhat dependent on the thermal conditions) even when properly matched by a three-stub tuner (fig.6.6.6).

The total voltage excursion between the breakdown and the forward charge storage is approximately 26 volts ($\phi \sim 1$ volt).

In the exponential model assumed, the capacitance is proportional to

$$C \propto e^{V}$$

or

$$Q \propto V . e^{V}$$

V measured from V_{BR}

If the normalized maximum voltage swing is V',

$$Q_{BIAS} \propto \tfrac{1}{2} . V' . e^{V'}$$

and $\tfrac{1}{2} . V' . e^{V'} = V . e^{V}$

From tables

$$\therefore \quad V \simeq 0.7\, V'$$

In the case considered, $V' = 26$ volts and hence

$$V = V_{BR} + 0.7 \times V'$$
$$= -25 + 18$$
$$V = -7 \text{ VOLTS}$$

We are now in a position to fit values to the denormalization coefficient for impedance, i.e.

$$R_{DENORM} = R' \times \frac{7}{Q/(2\pi \times \text{period})}$$

The bias voltage is very nearly proportional to the charge of the diodes and hence, at 1.56 GHz, the denormalization factor is:

$$R_{DENORM} = 28.2 \text{ OHM.}$$

From section 5.5 and 5.6, the normalized input and output voltages

Output voltage coefficients

$A_n = .2114$

$b_n = 1.1927$

Input voltage coefficients

$a_1 = 1.282$

$b_1 = .2583$

and hence the impedances are:-

Input: $35.2\,\Omega + 7.25\,\Omega$ capacitive

Output: $6\,\Omega + 33.4\,\Omega$ capacitive

In practice, only the resistive parts of these impedances are likely to be reasonably matched, and the capacitive parts are more likely to be defined by the circuit constraints.

APPENDIX 7.3.3

Microwave Oscillators

Several microwave oscillators were constructed to supplement the crystal controlled source as drivers for the multiplier. A solid-state oscillator was naturally preferred, and the circuit used for the earlier oscillators was modified to suit the higher frequencies and greater powers (fig. 7.3.7). Several versions were constructed (by 7.3.8 a, b, c, d) and the power output measured. Generally, the results were not identically repeatable with different transistors, as the manufacturer's specifications at these frequencies (1.3 GHz - 1.8 GHz) are very wide. A typical output power vs. frequency graph is shown in fig. 7.3.9. The devices used were A.E.I. DC 5501/DC5502 types (fig. 7.3.10). The circuit was a modified Clapp oscillator, which proved fairly reliable, and gave an adequate tuning range, although the power output dropped rapidly with increasing frequency. A second version, with a lower inductance/capacitance combination proved no better, so it was concluded that the transistor dominated the frequency response. Some dual-moding of the oscillator was noted, due to the cavity resonance taking over from the tuned stub.

It was found necessary to protect the transistors by including an overcurrent trip-short on the power supply.

When R.F. power transistor technology becomes sufficiently advanced, it will be possible to cover the full required range with a single oscillator. However, it was found necessary for this project to construct a valve oscillator using a disc-seal triode. (2C39A). A two-cavity arrangement was used, with variable tuning and feedback. This gave ample power, but was not sufficiently developed for reliable operation.

It must be said that the signal sources left a great deal to be desired, and consequently full-range measurements were difficult to obtain.

7.3.8.abcd

Cavity Oscillators

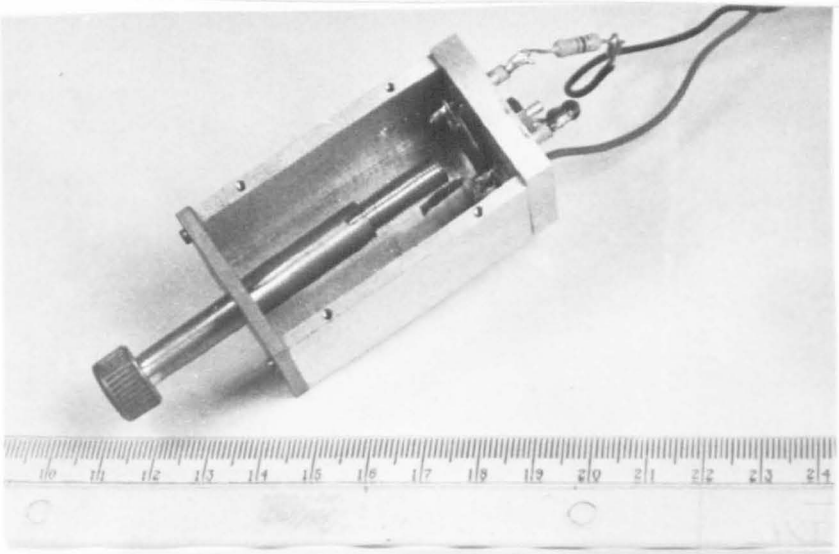

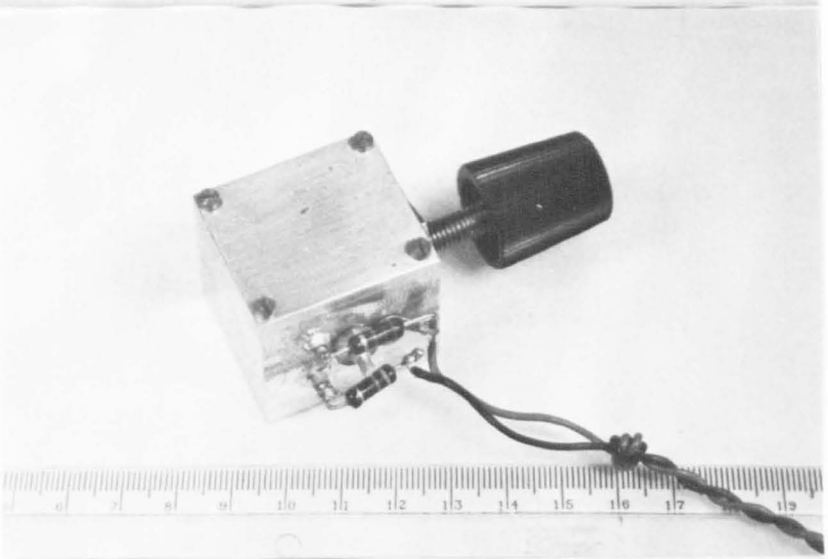

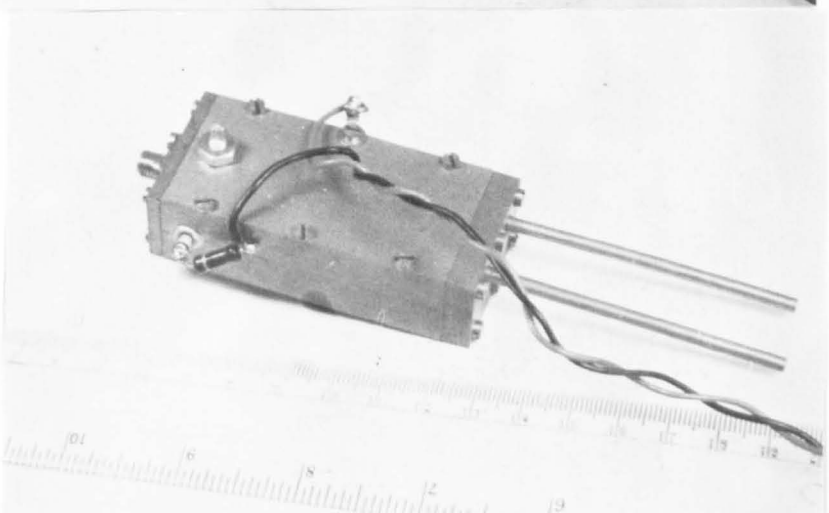

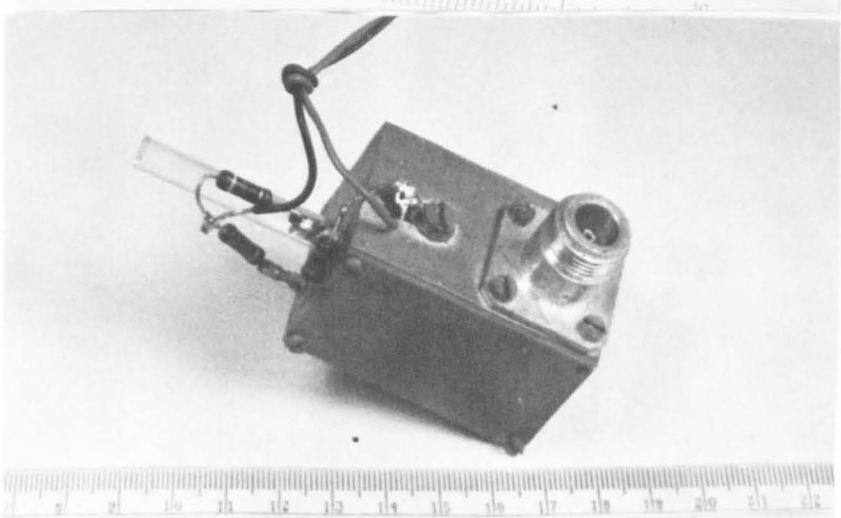

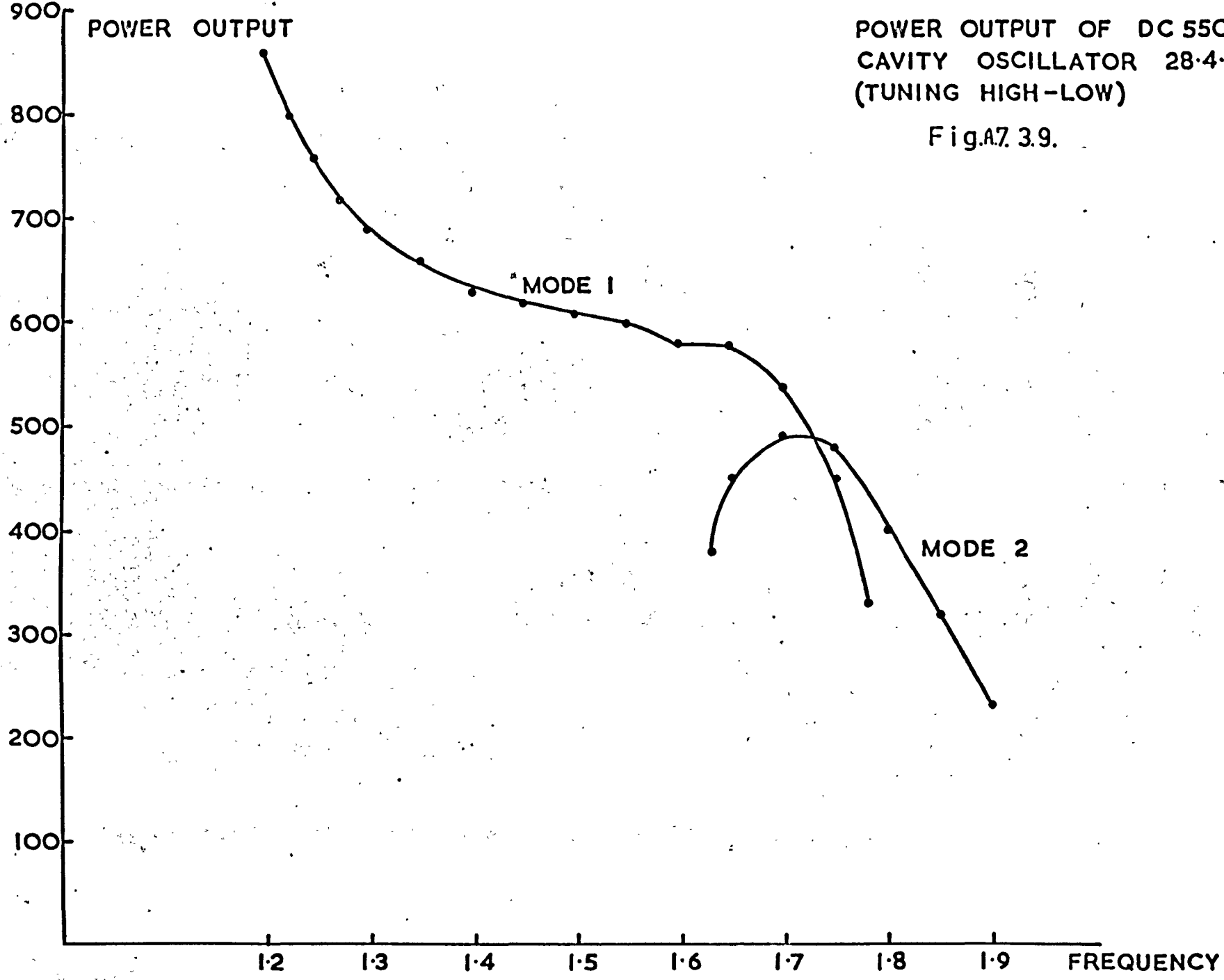

POWER OUTPUT OF DC 5502
CAVITY OSCILLATOR 28·4·72
(TUNING HIGH-LOW)

Fig.A7.3.9.

Spurious Even Harmonic Rejection — Table 7.1

The third and seventh harmonics were always > 30 db down.

Multiplier A.

			Rejection – db below output		
1.25 GHz	P_{input} (mW)	P_{out} (mW)	Harmonic 2nd	4th	6th
	200	.05	12	14	> 25
	400	.25	12	18	> 25
1.32 GHz	200	.19	18	15	> 25
1.56 GHz	800	2.2	15	10	> 25
	1000	6.3	15	16	> 25
1.72	400	.7	14	20	> 25

Multiplier B.

1.30	300	.03	13	10	> 25
	500	.06	15	11	
	600	.11	13	9	
1.38	300	.31	18	20	
	500	.64	15	12	
	600	.81	15	12	

Multiplier B (cont)

1.56	300	.22	15	12	>25
	500	.49	18	16	
	600	.82	17	14	
	800	.84	20	16	
	1000	1.08	25	18	
	1300	1.47	25	28	
	1500	1.78	25	22	
1.70	300	.63	14	12	
	600	.79	14	14	
	800	.97	14	12	
	1000	1.25	15	13	
	1300	1.6	18	14	
1.78 GHz	300	.16	12	10	
	800	.20	12	6	
	1000	.20	11	8	
	1300	.32	12	7	

Multiplier C

1.32 GHz	600	1.0	20	25	15
1.56	800	15.8	17	13	28
	1200	31.6	18	8	30
	1300	31.6	18	8	32
	1400	31.6	18	8	32
1.70	1200	31.6	22	15	> 25
	1400	25.1	21	24	> 25
	1600	20.0	20	20	> 25
1.75	900	1	20	25	>25
	1300	.56	18	7	>25
	1700	.5	17	10	>25

REFERENCES

1. Bakanowski, A.E.; Cranna, N.G.; Uhlir, A. IRE, ED-6, 4, Oct. 1959.
Diffused Silicon Non-linear Capacitors.

2. Bardeen, J.; Bell Syst. Tech. Journ. July, 1949.
On the theory of the A.C. Impedance of a Contact Rectifier.

3. Bozic, S.M. and Stinchcombe R.J. Int. J. Electronics 1969. Vol. 26 No. 2.
Circuit Models of the Step-recovery Diode.

4. Brand, F.A. Microwave Journal 15-2. Feb. 1972. Solid State Sources.

5. Burckhardt, C.B. Bell Syst. Tech. Journ. April 1965.
Analysis of Varactor Frequency Multipliers for Arbitrary Capacitance Variation and Drive Level.

6. Chang, J.J.; Forster, J.H.; Ryder, R.M. I.E.E.E. - ED. July 1963.
Semiconductor Junction Varactors with High Voltage Sensitivity.

7. Coerver, L.E.; I.E.E.E. - ED. May 1970.
Note on the Interpretation of C.V. Data in Semiconductor Junctions.

8. Constant, E; Allamands, E. Proc. I.E.E.E. 58-3 March 1970.
Transit-time Operation of an Avalanche Diode Driven by a Subharmonic Signal.

9. Corbey, C.D.; Davies, R. Electronics Letters. 8 April 1971. Vol. 7, No. 7
Amplitude Stabilization of a Varactor Frequency Multiplier using Self-bias Resistance Compensation.

10. Dickens, L.E. I.E.E.E. M.T.T. -15, 2., Feb. 1967.
Spreading Resistance as a Function of Frequency.

11. Eng, S.T. I.R.E. M.T.T. - 9, 1, Jan. 1961.
Characterization of Microwave Variable Capacitance Diodes.

12. Erikson, B.K. Proc. I.E.E.E. Sept. 1969.
A conjugate Matched Multiplier Having Minimum Thermal Resistance.

13. Furukawa, S; Nakagami, T. Proc. I.E.E.E. March, 1967.
Power Performance of a Self-excited Frequency Multiplier.

14. Furukawa, S; Nakagami, T. I.E.E.E. Sc.-5, 3, June 1970.
Design Theory of a Self-excited Frequency Multiplying Oscillator.

15. Gibbons, L.H.; Lamorte, M.F; Widner A.E. R.C.A. Rev. June 1963.
High Cut off Frequency GaAs Diffused Junction Varactor Diodes.

16. Grayzel, A.I. I.E.E.E. CT-13 No. 1 March 1966.
The Bandwidth of the Abrupt-junction Varactor Frequency Doubler.

17. Hedderley, D.L. I.R.E. ED-9 No. 6 Nov. 1962.
An Analysis of a Circuit for the Generation of High-order Harmonics using an Ideal Non-linear Capacitance.

18. Hyltin, T.M.; Kotzebue, K.L. I.R.E. M.T.T.-9 No. 1 Jan. 1961.
A Solid State Microwave Source from Reactance Diode Harmonic Generators.

19. Isobe, T.; Miyakawa, T.; Proc. I.E.E.E. April 1965.
Frequency Multipliers Consisting of NC and NR elements.

20. Johnson, K.M. I.E.E.E. SC-5, 3, June 1970.
Recent Advances in Microwave Integrated-Circuit Solid-State Source Design.

21. Johnston, R.H.; Boothroyd, A.R. Proc. I.E.E.E. 56-2 Feb. 1968.
Charge Storage Frequency Multipliers.

22. Judd, S.V. Radio Electronic Engineer July 1967.
High Order Multipliers without Idlers.

23. Jungmeister, H.G.; Schmidt, D. I.E.E.E. SC-5, 4, Aug. 1970.
High-speed Pulse Circuits obtained by Computer Aided Non-linear Analysis of Step-recovery Diodes.

24. Kannam, P.J.; Ponczak, S.; Olmstead, J.A. I.E.E.E. ED. Feb. 1971.
Design Considerations of Hyperabrupt Varactor Diodes.

25. Kotzebue, K.L. Proc. I.E.E.E. Dec. 1965.
A Circuit Model of the Step-Recovery Diode.

26. Kotzebue, K.L.; Matthei, G.L. I.E.E.E. M.T.T.-17, 12, Dec. 1969.
The Design of Broadband Frequency Doublers using Charge Storage Diodes.

27. Kulesza, B.L.J. Electronic Communicator. July 1966.
Highly Efficient Harmonic Generation using Varactor Diodes with Hyperabrupt Junctions.

28. Leenov, D.; Uhlie, A. Proc. I.R.E. 47 Oct. 1959.
Generation of Harmonics and Subharmonics at Microwave Frequencies with p-n Junction Diodes.

29. Leeson, D.B.; Weinreb, S. Proc. I.R.E. 47-12 Dec. 1959.
Frequency Multiplication with Non-linear Capacitors.

30. Leeson, D.B. Proc. I.R.E. 50-8 Aug. 1962.
Capacitance and Charge Coefficients for Varactor Diodes.

31. Leonard, T.C. Proc. I.E.E.E. Aug. 1963.
Prediction of Power and Efficiency of Frequency Doublers using Varactors Exhibiting a General Non-linearity.

32. Manley, J.M.; Rowe, H.E. Proc. I.R.E. 44-7, July 1956.
Some General Properties of Non-linear Elements.

33. Manley, J.M.; Rowe, H.E. Proc. I.R.E. 46-5 May 1958.
General Energy Relations in Non-linear Reactances.

34. Markard, E.; Yuan, S. R.C.A. Review 1964.
High Efficiency, High Order Idlerless Frequency Multipliers using Hyperabrupt Varactors.

35. McConnell, J.W.; Stegemaller, J.L. I.E.E.E. SC. Sept. 1968.
A Parametric Frequency Divider using Hyperabrupt Junction Diode Capacitance.

36. Maline, R.A.; Foxhall, G.F. I.E.E.E. ED-19 No. 2 Feb. 1972.
Ion-implanted Hyperabrupt Junction Voltage Variable Capacitors.

37. Mall, J.L; Hamilton, S.A. Proc. I.E.E.E. 57-7 July 1969.
Physical Modelling of the Step-recovery Diode for Pulse and Harmonic Generation Circuits.

38. Newcomb, R.W.; Seriki, O.A. Electronics Letters 7, No. 16.
Non-linear Capacitor Simulation.

39. Nicholson, B.F. Radio and Electronic Engineer, July 1967.
The Practical Design of Interdigital and Comb-line Filters.

40. O'Clock, G.D. I.E.E.E. M.T.T. - 20, 3, March 1972.
Tunable Frequency Range and Mismatch Adjustment for Comb-line Bandpass Filters.

41. Opdorp, C. van. Phys. Stat. Vol. 32.81 (1969)
Capacitance - Voltage Relations of Schottley and p-n Diodes.

42. Page, CH. Proc. I.R.E. Oct. 1958.
Harmonic Generation with Ideal Rectifiers.

43. Parker, D. I.E.E.E. SC-7 No. 1 Feb. 1972.
Conditions for Spurious Oscillations in a Frequency Doubler Circuit.

44. Parker, A.R. Solid State Electronics 13 - 1970.
The Measurement of Doping Profiles in Thick Epitaxial Layers of Ga-P using Schottley Barrier C-V Data.

45. Poon, H.C.; Gummel, H.K. Proc. I.E.E.E. Dec. 1969.
Modelling of Emitter Capacitance.

46. Redd, J.C.; Kotzebue, K.L. Electronics Letters 29. Oct. 1970.
Broadband High-Efficiency Frequency Tripler.

47. Roulston, D.J.
Frequency Multiplication using the Charge Storage Effect.

48. Rowe, H.E. Proc. I.R.E. 46-5 May 1958.
Some General Properties of Non-linear Elements; Part II.

49. Saito, Y. Electrical Engineering in Japan, 89-3, 1969.
Analysis of High-Order Harmonic Generator without Idlers.

50. Scandura, A.M. Telecommunications. Aug. 1971.
Frequency Multipliers for Communication Systems.

51. Scanlan, J.O.; Laybourn, P.J.R. Proc. I.E.E. 112-8 Aug. 1965.
Large Signal Analysis of Varactor Harmonic Generators without Idlers.

52. Scanlan, J.O.; Laybourn P.J.R. Radio and Electronic Engineer, June 1966.
Analysis of Varactor Multipliers with Idlers.

53. Scanlan, J. O.; Laybourn, P.J.R. Proc. I.E.E. 114-7 July 1967.
Bandwidth in Varactor Harmonic Generators.

54. Scanlan, J.O.; Laybourn, P.J.R. Proc. I.E.E. 114-11 Nov. 1967.
Analysis of Varactor Harmonic Generators with Arbitrary Drive Levels

55. Schneider, M.K.; Snell, W.W. Proc. I.E.E.E. 58-9 Sept. 1970.
Hybrid Integrated Frequency Multiplier from 10 to 30 GHz.

56. Shimizu, A; Nishizawa, J. I.R.E. ED.-8 No. 5 Sept. 1961.
Alloy-diffused Variable Capacitance Diode with Large Figure-of-merit.

57. Shockley, W. Bell. System. Tech. J. July 1949.
The Theory of p-n Junctions in Semiconductors and p-n Junction Transistors.

58. Steele, E.L. J. Appl. Phys. July 1954 Vol. 25. No. 7.
Charge Storage in Junction Diodes.

59. Sukegawa, T; Fujikawa, K.; Nishizawa, J. Solid State Electronics Jan.'63
Silicon Alloy - diffused Variable Capacitance Diode.

60. Sukegawa, T.; Sakurai, T.; Nishizawa, J. I.E.E.E. ED-13 No. 12 Dec. '66
A Design Method for Variable Capacitance Diodes with an mth power characteristic for a Wide Voltage Range.

61. Sukegawa, T.; Sakurai, T.; Nishizawa, J. R.I.E.C. Tech. Report.
A design Theory of Variable Capacitance Diodes for Large Amplitude Operation.

62. Wardrop, B. Electronics Letters. Aug. 6th 1970.
Electrical Lengths of Stripline Bends.

63. Young, L. Microwave Journal. April 1968.
Reflections on Microwave Filters and Couplers.

64. Young, L. editor. 'Advances in Microwaves'. Academic Press. N.Y.
(Analysis of Varactor Harmonic Generators - Scanlan, J.O.)

65. Ziel, A. vander. J. App. Phys. 19-11 Nov. 1948.
On the Mixing Properties of Non-linear Condensers.

66. Penfield, P. and Rafuse, R.P. Varactor Applications. M.I.T. Press 1962.